FRANK LABORATORY OF NEUTRON PHYSICS
JOINT INSTITUTE FOR NUCLEAR RESEARCH

# ANNUAL REPORT 2005

**Cover illustration**
Dismantling the IBR-30 core.

**Contacts:** FRANK LABORATORY OF NEUTRON PHYSICS
JOINT INSTITUTE FOR NUCLEAR RESEARCH
141980 Dubna Moscow region, Russia
Fax: (+7) 49621-65085
E-mail: khitrov@nf.jinr.ru
http:/nfdfn.jinr.ru

**Editors:** A.V.Belushkin, V.A.Khitrov

**Translated from Russian:** T.V.Avdeeva, E.V.Lokhmatova

**Typesetting:** V.S.Rumyantseva

**Cover:** I.N.Guseva

**Photography:** Yu.A.Tumanov

# FRANK LABORATORY OF NEUTRON PHYSICS OF THE JOINT INSTITUTE FOR NUCLEAR RESEARCH

The Joint Institute for Nuclear Research (JINR) is an international centre for experimental and theoretical investigations in the fields of elementary particle physics, nuclear and neutron physics, condensed matter research and related topics.

The JINR structure is determined by the fact that it is governed internationally and has many research specializations. Current scientific and financial affairs of the Institute's Laboratories, common services as well as the work of specialized departments are guided by the Institute Directorate.

The Frank Laboratory of Neutron Physics is one of the eight JINR Laboratories. It was established in 1956, soon after the foundation of JINR.

In 1960 a principally new source of neutrons - the IBR fast pulsed reactor of periodic operation - was created at FLNP under the leadership of Prof. D.I.Blokhintsev (11.01.1908 - 24.01.1979). The birth of this reactor gave rise to a new direction in the development of research neutron sources.

An extended scientific program with this reactor was initiated under the leadership of Nobel Prize Winner and Laboratory Director Prof. I.M.Frank (23.10.1908 - 22.06.1990) and Deputy Director Prof. F.L.Shapiro (06.04.1915 - 30.01.1973). Since 1960, a whole family of unique pulsed neutron sources for nuclear physics and condensed matter physics has been developed and constructed. The latest in the family, the IBR-2 high flux pulsed reactor, was commissioned in February 1984. The Laboratory was named after Prof. I.M.Frank in 1992. In the same year, in JINR the I.M.Frank Prize for Neutron Physics was established.

At present, the scientific activity of the Laboratory focuses on two fields of physics, namely nuclear physics and condensed matter physics. The first involves investigations of the neutron as an elementary particle and studies of compound states in neutron induced reactions. The second investigates pressing problems in the physics and chemistry of solid states, surfaces and liquids, and in molecular biology. Applied investigations are also carried out using nuclear physics methods.

# PREFACE

We would like to offer the readers the report on the scientific activity of the Frank Laboratory of Neutron Physics for 2005. The first part presents a brief review of the experimental and theoretical results achieved in the main scientific directions – condensed matter physics, neutron nuclear physics and applied research. The second part includes the reports on the operation of the IBR-2 pulsed reactor and realization of the IREN project. The third part is concerned with the development and creation of elements of neutron spectrometers for condensed matter investigations. The fourth part presents the experimental reports that cover the main scientific directions in greater detail. The report completes with the list of publications for 2005.

In 2005 the IBR-2 reactor operated ~ 1831 hours for physical experiments. Main results of the IBR-2 modernization in 2005: (1) New fuel charge – works to create a working site for assembling fuel elements into a fuel rod array were completed. The working site was approved to be put into service by a commission of representatives of JINR, GSPI, VNIINM, NIKIET. At present, the procedure of obtaining license for assembling fuel elements is under way. (2) Main equipment of the IBR-2M reactor – in NIKIET the manufacturing of a new reactor jacket continued. The manufacturing of an intra-jacket fuel-handling machine was completed. (3) In JINR EW the haulage equipment to place moderators for the IBR-2M reactor was manufactured. (4) CSS of IBR-2M. – in NIKIET the development of the design documentation of the AES actuating mechanism was completed. A prototype of an actuating mechanism for an automatic controller was manufactured in JINR EW. In SNIIP-SYSTEMATOM the development of ACSS was completed, the manufacturing of a prototype is under way. Works to create a system to control technological parameters were started (INEUM). (5) Complex of IBR-2M moderators – prototype works on transportation of $C_9H_{12}$ balls. In NIKIET work on the preliminary design of the IBR-2M moderator complex started. In HeliumMash works to manufacture CHF-700/15 continued.

The IREN project. In 2005 the main efforts and funds were focused on the completion of preparation and carrying out of works to dismantle the IBR-30 reactor. The major part of the reactor activated equipment was disassembled and transported to bldg. 117/b for temporary storage. By the middle of November the drilling-out of uranium inserts from the moveable parts of the IBR-30 core was completed. The removed fuel was evacuated for storage in DRFM JINR. On the $14^{th}$ of December at 11-45 an entry in the IBR-30 reactor logbook was made: «The last spent fuel assembly was taken out from the reactor core and placed in the container for transportation to storage». Thus, the more-than-forty-year history of the world's first pulsed reactor of periodic operation IBR came to its close. To the end the IBR reactor was one of the most powerful neutron sources for nuclear physics. This is a great success of the FLNP technical departments.

In view of real financial possibilities of the Institute, the JINR Directorate has taken a decision to realize a simplified variant of the IREN facility. Namely: to start up the first stage of the IREN facility including an electron accelerator for 100 MeV and a non-multiplying neutron-producing target with a test bench for applied investigations.

At the IBR-2 neutron spectrometers a number of interesting experiments were carried out. In particular, neutron diffraction studies of manganites $R_{0.5}Sr_{0.5}MnO_3$ (R=Sm, $Nd_{0.772}Tb_{0.228}$ and $Nd_{0.544}Tb_{0.456}$) aimed at establishing microscopic reasons for a giant oxygen isotopic effect discovered recently in $Sm_{0.5}Sr_{0.5}MnO_3$ were conducted. At the DN-12 diffractometer the effect of high pressures of up to 5 GPa on the crystal and magnetic structure of hexagonal manganite $YMnO_3$ in a temperature range of 10 - 295 K was studied. At the YuMO spectrometer liquid dispersions of detonation nanodiamonds were studied by small-angle neutron scattering. At the REMUR spectrometer the phenomenon of coexistence of ferromagnetism and superconductivity in layered structures, which is of importance both from fundamental and practical points of view, was investigated. At the NERA inverted geometry spectrometer the comparison characteristics of substances-candidates for neutron cold moderators at IBR-2: methane, methanol, mesitylene and water, were studied. At the DIN-2PI spectrometer the neutron diffraction experiment to study the microstructure of Li–N melts with a concentration of nitrogen impurity of 1.3 and 3.5 at.% and at a temperature of 823 K was performed. The basic microstructural characteristic of the substance – the total structural factor *S(Q)*, as well as the partial structural factors $S_{\alpha\beta}(Q)$ of melt components and corresponding radial distribution functions $g_{\alpha\beta}(r)$ and $g_{CC}(r)$ were obtained. A series of works, which sum up almost a 20-year debate on one of the key problems of statistical physics – interaction of fluctuating random surfaces, were completed by the physicists of the small-angle neutron scattering group. For the first time the dynamics of a crystal lattice of the superionic conductor AgCuSe was studied by inelastic neutron scattering. In a low-temperature phase the low-energy modes were detected, which are most likely of acoustic phonon nature.

In 2005 the technical works to modernize the IBR-2 spectrometers complex continued. For the most part, they concerned the detector systems of the spectrometers. In particular, at the FSD Fourier specialized diffractometer work to construct the detector system continued (6 out of 14 detector modules are ready), test filling of two-dimensional detector for YuMO was carried out and one-dimensional PSD with resolution of 1.8 mm was tested in actual operating conditions.

During the reported year a number of works were carried out and some interesting results were obtained in the field of nuclear physics: in the framework of the experiments to search for neutral currents in nucleon-nucleon interactions and to determine a weak π-meson coupling constant at the PF1B cold polarized neutron beam (ILL, Grenoble) a regular 48-day run of measurements of P-odd asymmetry ($\boldsymbol{\sigma}_n\mathbf{p}_t$) of triton escape in the reaction $^6Li(n,\alpha)^3H$ was conducted.

The works to test the equipment of the PF12 channel of the LANSCE neutron source (Los-Alamos) and the equipment for the experiment to measure P-odd asymmetry of γ-quanta in the reaction $np \rightarrow d\gamma$ aimed at determining a weak π-meson coupling constant were performed by the NPDG collaboration together with the FLNP specialists. In the framework of the preparation of the experiment of direct measurement of neutron-neutron scattering cross-section, the works to calibrate the neutron detectors used in the test experiments at the YAGUAR reactor (VNIITF, Snezhinsk) were carried out and the obtained data were refined. Using a new method of extracting the n,e-scattering length $b_{ne}$ from data of neutron diffraction by noble gases, the data obtained in Grenoble were processed for different states of gaseous $^{36}Ar$ and liquefied Kr. During 2005 the experimental data in the framework of the nTOF collaboration — study of the nature of vibrational resonances in neutron-induced fission and obtaining of fission cross-sections to solve problems of ADS-systems and radioactive waste incineration — were processed. The data on level densities and force functions of primary gamma-transitions for the nucleus excitation energy interval from ~5 to ~9 MeV were derived from the intensities of two-step quantum cascades measured by now in 51 nuclei ($27<A<201$) between the neutron resonance and the low-lying levels of the compound nucleus. At the PF1B and PF2 beams of the ILL reactor (Grenoble) the studies of cold neutron scattering from nanodiamond powder samples and from the structure of weakly bound nanoparticles $D_2O$ and $D_2$ in superfluid helium (gel) were carried out. A new experiment to observe a neutron energy change in passing through the accelerated substance was carried out. The neutron energy change was detected by the UCN gravitational spectrometer (ILL, Grenoble) with interference filters in phase with the movement of the sample and was of the order of $2 \cdot 10^{-10}$ eV.

In 2005 work to study atmospheric depositions of heavy metals using biomonitoring, NAA and GIS technologies on the territory of Russia and a number of other countries continued. New results of NAA to determine chrome in bacterial samples of *Arthrobacter oxidans* granted by the biochemists of the Institute of Physics of the Georgian AS were obtained. The analysis of 50 archeological samples of ceramics (early Neolithic age) from burial mounds of the Smolensk region and from the Maikop burial mound in the Northern Caucasus was performed for the State Hermitage (Saint-Petersburg). Works to study the effect of fission-spectrum neutrons on physical properties of fine-grained diamonds obtained in the Institute of Solid State and Semiconductor Physics NASB (Minsk) continued.

In 2005 the unification of all measuring equipment of DAQ and experiment automation systems and its accommodation at the spectrometers in the IBR-2 experimental halls was completed. The software was unified as well. Automation systems for spectrometers are composed of standardized hardware and software modules. An experiment can be controlled from any computer of the local area network. A serious technological basis (clean room, gas and test

benches) has been created, 1D and 2D MWPC-based position-sensitive neutron detectors have been developed and tested. Much progress in the development of scintillation detectors with ZnS(Ag)$^{6}$LiF glasses for neutron diffractometry and in the creation of helium cryostats for a temperature range of 6-300K has been achieved.

In summary it might be well to point out that the increasing interest of the JINR Member States is observed to the works in the field of neutron investigations. It is also of importance that in the last few years a lot of young people have come to the Laboratory. All these facts confirm that the Laboratory continues to develop successfully and dynamically, carrying out investigations in the interests of the JINR Member States.

***A.V. Belushkin***
***Director***

*March 9, 2006*

# 1. SCIENTIFIC RESEARCH

## 1.1. CONDENSED MATTER PHYSICS

The problem under study and the main objective of investigations within the theme was the application of neutron physics methods to study the structure and dynamics of condensed matter, the obtaining of new data on microscopic properties of systems under study, experimental verification of theoretical predictions and models and the revealing of new laws. Correspondingly, work in the framework of the theme was carried out in two main directions: conducting of experimental investigations at the IBR-2 spectrometers and of routine technical work aimed at modernizing the available spectrometers and creating new instruments at IBR-2. This work was performed by the specialists of the FLNP Department of Neutron Investigations of Condensed Matter (NICM) structurally organized in the form of sectors (including the teams responsible for the spectrometers) in basic research directions.

**Experimental equipment.** For the most part, the experiments were carried out at the FLNP basic facility – the IBR-2 reactor. In addition, the physicists of the NICM Department participated in a number of experiments in neutron centers of Europe. At the IBR-2 reactor the Department employees were in charge of operation and development of instruments and performance of physics experiments at 13 spectrometers: HRFD – High-Resolution Fourier Diffractometer, DN-2 – multipurpose diffractometer for experiments on poly- and single crystals, SKAT – diffractometer for texture investigations, EPSILON – diffractometer for internal stress investigations, FSD – Fourier diffractometer for internal stress studies, DN-12 – diffractometer for experiments at high external pressures, YuMO – small-angle scattering spectrometer, REMUR – polarized neutron spectrometer, REFLEX-P – polarized neutron reflectometer, DIN-2PI – direct geometry inelastic scattering spectrometer, NERA-PR – multi-crystal inelastic scattering spectrometer, KDSOG-M – inverted geometry inelastic scattering spectrometer. At all spectrometers, except for KDSOG-M, experiments are carried out in accordance with the user policy program. Below are the main scientific results obtained during the reported year.

**Main scientific results.** Neutron diffraction studies of manganites $R_{0.5}Sr_{0.5}MnO_3$ (R=Sm, $Nd_{0.772}Tb_{0.228}$ and $Nd_{0.544}Tb_{0.456}$) aimed at establishing microscopic reasons for a giant oxygen isotope effect discovered recently in $Sm_{0.5}Sr_{0.5}MnO_3$ have been conducted. It has been demonstrated that in all studied compositions at low temperatures there coexist two crystal phases with different types of Jahn-Teller distortions of oxygen octahedrons and different types of magnetic ordering. The diffraction data have made it possible to suggest the scenario of the observed phase transitions and to establish that the metal-insulator transition in the compositions with Sm upon $^{18}O$ for $^{16}O$ substitution has a percolation nature, i.e. the substitution of oxygen isotope results in a sharp decrease (from 65% down to 13%) in a ferromagnetic metal phase volume. This work can be considered to be final in a series of studies concerned with the reasons for a giant isotope effect in manganites — a change from low-temperature metal state to insulator state upon $^{18}O$ for $^{16}O$ substitution. It has been found that in compositions with a doping level of $x$=0.5, as well as in manganese oxides with $x$=0.3, the effect exists only if there is a phase-separated state on a mesoscopic scale. The main reason for equilibrium phase separation is the occurrence of a random stress field on incoherent boundaries of the coexisting phases.

At the DN-12 diffractometer the effect of high pressures of up to 5 GPa on the crystal and magnetic structure of hexagonal manganite $YMnO_3$ in a temperature range of 10 - 295 K has been studied (**Fig.1**). At normal pressures in this compound at $T \sim T_N$=70 K a spin liquid state is observed caused by magnetic frustration effects on a triangular lattice formed by Mn ions, whereas at $T<T_N$ an ordered triangular antiferromagnetic (AFM) state arises with a symmetry of irreducible representation $\Gamma_1$. As the pressure increases up to 5 GPa, a decrease in the value of the ordered magnetic moment of Mn ions from 3.27 down to 1.52 $\mu_B$ is observed at $T$=10 K and the

# 1.2. NEUTRON NUCLEAR PHYSICS

## Introduction

In the course of the year 2005 the main work in the field of neutron nuclear physics in FLNP JINR was carried out at the IBR-2 reactor, the EG-5 facility and on neutron beams in other nuclear centers of Russia, Bulgaria, Poland, Czech Republic, Germany, Republic of Korea, China, France, USA, and Japan. The studies were in traditional directions, such as the investigation of time and spatial parity violation processes in the interaction of neutrons with nuclei, studying of the quantum-mechanical characteristics and dynamics of the fission process, experimental and theoretical investigations of the electromagnetic properties and beta-decay of the neutron, gamma-spectroscopy of neutron-nuclear interactions, studies of atomic nucleus structure, obtaining of the new data for reactor applications and nuclear astrophysics, experiments with ultracold neutrons, and applied investigations.

## 1. Experimental investigations

### *1.1. Spatial and time parity violation in the interaction of neutrons with nuclei*

#### *1.1.1 Search for and investigation of the structure of subthreshold neutron p-resonances in lead isotopes by the combined correlation gamma spectroscopy method*

Works to search for and to study the structure of subthreshold neutron p-resonances in isotopes with mass number A = (80-130) by the high-resolution correlation gamma-spectroscopy method continued.

With the aim of testing the validity of the results obtained previously in the experiments to search for the negative neutron p-resonance in lead isotopes, the reconstruction of the gamma-spectrometer COCOS at channel №1 of the IBR-2 reactor has been carried out. As a result of installation of newly purchased semiconductor gamma-quantum detector GMX30-PLUS and specialized electronic blocks, the efficiency of the spectrometer has improved more than twice and its operation speed has increased.

At the reconstructed gamma-spectrometer the experiments to search for the negative neutron p-resonance in lead isotopes were carried out: two series of measurements with a natural mixture of lead isotopes were conducted.

#### *1.1.2. Preparation for investigations of T-noninvariance effects in neutron nuclear interactions*

In 2005 in the polarized target sector the works to study samples to verify T-noninvariance in nuclear interactions continued. Two single crystals of lanthanum aluminate $LaAlO_3$ with a paramagnetic impurity Nd3+: 0.3% and 0.08%, received from Japan, were studied. The amplified NMR signals were detected confidently on both crystals. A shift of the NMR lines of La and Al at rotation of crystals in a magnetic field was also observed. Unfortunately, it turned out to be impossible to observe thermo-equilibrium signals in a reasonable period of time. This is due to the fact that for nuclei of the crystal as compared to a hydrogen target their concentration is less by a factor of 2-3 and the difference of adjacent level population is less by a factor of 7 and 5, respectively.

At present, the modernization of Q-meter is in progress. The instrument sensitivity is expected to be improved by at least an order of magnitude.

### *1.1.3. Creation of the polarized proton target*

The creation of the polarized nuclear target was completed. To polarize nuclei of the target by the «brute force» method, a $^3$He in $^4$He dilution cryostat with a superconducting magnet was constructed. A bench test of the cryostat with a magnet was performed. The following parameters were obtained:

- minimal temperature on a sample T = 23 mK,
- magnetic field intensity H= 5.8 T at the homogeneity of a magnetic field in the center of the magnet $\Delta H/H= 10^{-4}$.

The polarized nuclear target was transported and installed on beam №1 of the IBR-2 reactor. Thus the creation of the «Kolkhida» setup intended to study the interaction of polarized neutrons with polarized nuclei was completed. For the setup a new software data acquisition system has been developed, which makes it possible to carry out measurements in an automatic mode for a number of points in the range of currents of the polarizing magnet; to perform necessary operations in an interactive operating mode; to visualize experimental data; to automatically control the quality of experimental data; to conduct necessary tests of the equipment and programs.

At present, the commissioning works at the «Kolkhida» setup on beam №1 of IBR-2 are under way. The beginning of nuclear precession (nuclear pseudomagnetism) experiments is scheduled for the first quarter of 2006.

### *1.1.4. Current status of the KaTRIn project. Nuclear pseudomagnetism measurement procedure*

In 2005 within the framework of cooperation with KEK (Japan) the prototype of a setup to study nuclear pseudomagnetism was created. Its schematic view is given in **Fig. 1**.

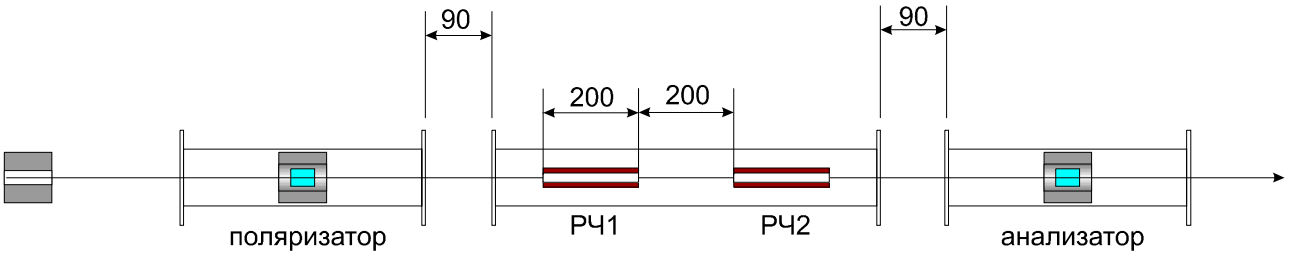


***Fig. 1.*** *The setup to study nuclear pseudomagnetism. Dimensions are in mm*

The setup was assembled on beam H-8 of the KENS source and includes a neutron polarizer and neutron polarization analyzer. Both devices are based on $^3$He cells with optical pumping. Between the polarizer and the analyzer a solenoid is positioned inside which there are two crossed radio-frequency coils spaced apart. On passing the polarizer, the neutron polarization $P_1$ is directed along the beam axis. Radio-frequency coils make it possible to turn the neutron polarization vector in an arbitrary direction and through an arbitrary angle.

If a guiding field in a big solenoid is $H_0$ and a coil creates an *oscillating* field $2H_1 \cos wt$, the effective field in the rotating coordinate system which "sees" the neutron is:

$$H = H_0 - w/\gamma + H_1,$$

where γ is the gyromagnetic ratio for the neutron. Then if we manage to choose RF field frequency to be equal to the Larmor frequency of the neutron in a field $H_0$, we obtain an optimal condition $H = H_1$. This means that in the passage through a coil in time $t_R$ to turn the neutron polarization vector through, say, $\pi/2$, it is necessary to fulfill a condition:

$$\gamma H_1 t_R = \pi/2 .$$

Of course, $t_R$ depends on neutron energy, but the amplitude $H_1$ can be modulated so that the condition is met for neutrons in a desirable energy range. On passing through the first coil, the neutron travels a distance between the coils in time $t_P$, the polarization vector rotates with Larmor frequency $w_0 = \gamma H_0$ and the corresponding angle of rotation in the plane perpendicular to the moving direction is $\phi = w_0 t_P$. Then if the operation of both coils is properly synchronized, it is possible to return the neutron polarization vector to its former direction along the beam axis as neutrons pass through the second coil: $P_2 = P_1$. If we place some material between coils, which creates an additional field along the beam axis, the phase that the neutron acquires when flying between coils, is no longer $w_0 t_P$. This means that upon passing through the second coil, the magnitude of neutron polarization will differ from that of the case considered above, i.e., $P_2 \neq P_1$. From the value and energy dependence of this deviation, the magnitude of an additional field created by this material may be determined.

The second realization of this technique is to use *a rotating* field instead of *oscillating* one, i.e., in place of one pair of turns in each coil to use crossed pairs to create orthogonal fields $H_1 \cos wt$ and $H_1 \sin wt$. The remainder of the consideration remains unchanged. The use *of* a *rotating* field makes it possible to reduce the amplitude of the RF-field by half, which lowers power requirements to RF-amplifiers.

Thus, the pseudomagnetism measurement procedure represents two consecutive measurements of neutron polarization when the substance under study is not polarized and polarized along the beam axis. The investigations of the parameters of the created setup and consecutive measurements of neutron time-of-flight spectra with the RF-coils in the "off" and "on" condition were carried out and their ratios were determined. **Figure 2** illustrates some examples of these ratios. Red lines – calculation (not fitting).

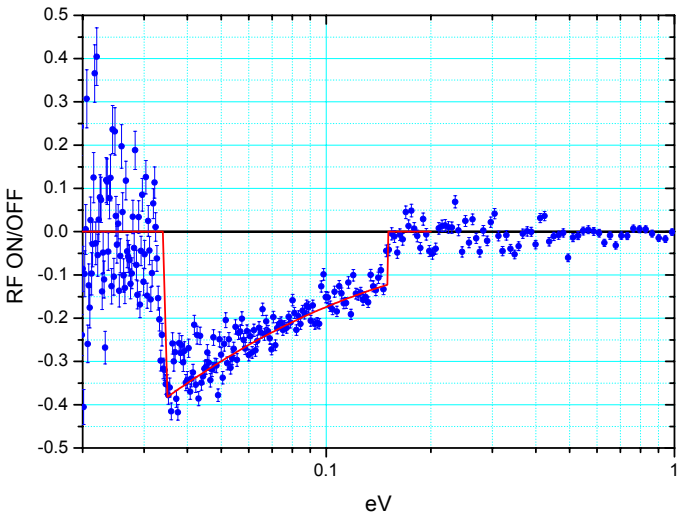


***Fig.2a.*** *The first RF-coil in the spin-flipper mode (180-degree turn of neutron polarization). The second coil is switched off. Rotating field*

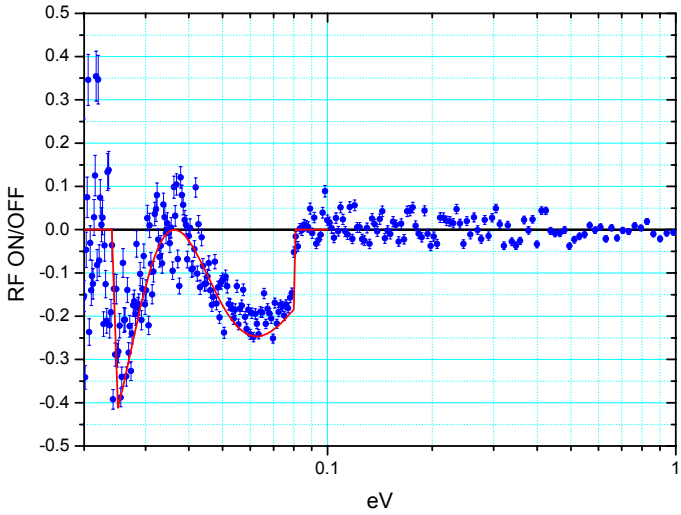


***Fig.2b.*** *Both coils are in the mode of 90-degree turn of neutron polarization. Field phase in the second coil is modulated from 0 to $2\pi$ in the range of 0.025-0.08 eV. Oscillating field*

Both coils consist of two pairs of crossed rings of 10 turns each. The RF-field amplitude is limited by the RF-amplifier output power and does not exceed 5 G. The magnitude of the big solenoid guiding field is 20 G, i.e. the working frequency is $w = w_0 \approx 60$ kHz.

Cells with $^3$He were under 2.8 atm each, the degree of $^3$He polarization was 54% for the polarizer and 24% for the analyzer. The $H_1$ amplitude was modulated by the law $1/t_R$ using programmable synthesizers (Arbitrary Waveform Generator). In the future we intend to place a small solenoid between the coils and to measure the ratios of time-of-flight spectra when this solenoid is off and on. In addition, we plan to manufacture somewhat smaller RF-coils and to enhance field $H_1$ by increasing the number of turns up to 15 in each crossed pair.

This procedure may also be used in the investigations of para- and ferromagnetic substances.

### *1.1.5. Investigations of parity violation in the systems with a small number of nucleons*

**Search for P-odd effect of triton escape in the reaction $^6$Li(n,α)$^3$H**

In the framework of the experiments to search for neutral currents in nucleon-nucleon interactions and to determine a weak π-meson coupling constant at the PF1B cold polarized neutron beam (ILL, Grenoble) a regular 48-day run of measurements of P-odd asymmetry ($\boldsymbol{\sigma}_n\mathbf{p}_t$) of triton escape in the reaction $^6$Li(n,α)$^3$H ($\boldsymbol{\sigma}_n$ – neutron spin, $\mathbf{p}_t$ – triton pulse) was conducted. A 48-section ionization chamber with 24 $^6$LiF targets absorbing more than 60% of neutron flux was used as a triton detector (**Fig.3**). An integral (current) method of event registration, a technique of compensation of reactor power fluctuations, as well as a technique with periodic switching of a guiding neutron spin magnetic field on samples to eliminate possible false effects were applied. The result with allowance made for corrections for neutron polarization and triton escape angle is $\alpha_t = -(9.3\pm2.5)\cdot10^{-8}$. A number of test experiments were also carried out. Judging from the sum of the results from three cycles, an obvious effect is observed in the main measurements $\alpha_t = -(8.6\pm2.0)\cdot10^{-8}$.

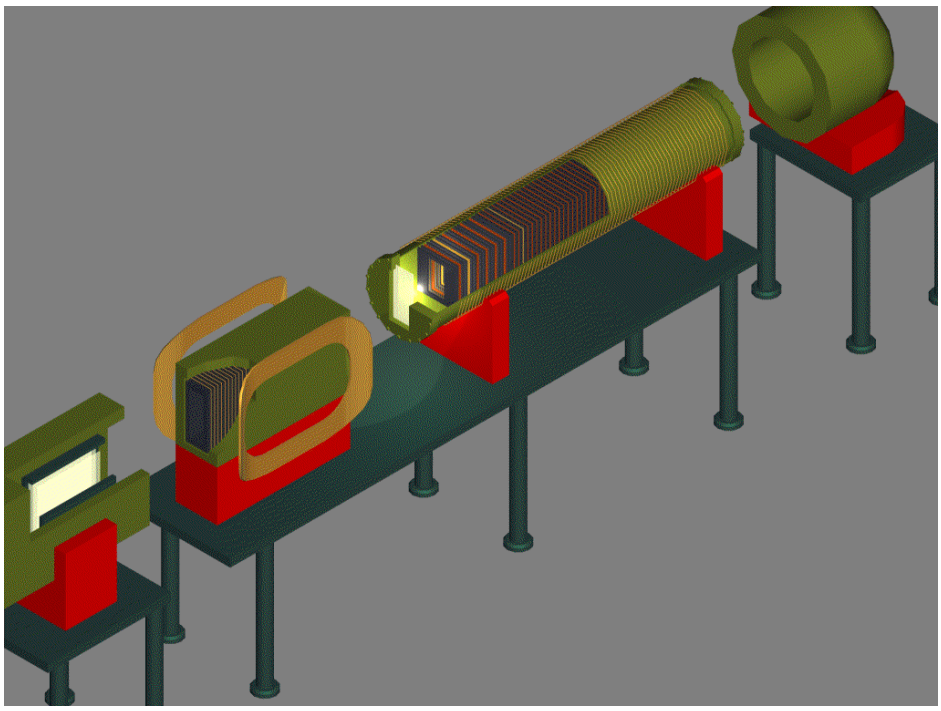

***Fig. 3.*** *Layout of the experiment: (from left to right) polarizer, RF-spin-flipper with coils of guiding field, multisectional ionization chamber, beam-stop.*

**Preparation for measurement of γ-quantum asymmetry in the reaction np→dγ**

The NPDG collaboration together with the FLNP specialists carried out the works to test the equipment of the PF12 channel of the LANSCE neutron source (Los-Alamos) and the equipment for the experiment to measure P-odd asymmetry of γ-quanta in the reaction np→dγ aimed at determining a weak π-meson coupling constant.

### *1.2 Induced and spontaneous fission*

#### *1.2.1 Measurement of delayed neutron yield at the IBR-2 reactor*

On channel №11-B of the IBR-2 reactor the modernization of the «Izomer» setup with the aim of development of works to obtain data on yields and decay constants of delayed neutron groups in minor actinide fission was completed. As a result of the modernization, the parameters of the setup were improved and its possibilities were enlarged. For the setup the following programs were developed: a program to control the movement of Cd-filter; a program of synchronization of data measurement process with changes of detection conditions; sorting of data files into groups according to detection conditions; calculations of exposition time, etc.

At the modernized setup the measurements were performed and the data on the delayed neutron yield in thermal neutron fission of $^{237}$Np isotopes were obtained.

#### *1.2.2 Measurement of neutron multiplicity in neutron-induced fission of $^{239}$Pu*

In 2005 experimental investigations of neutron-induced fission of $^{239}$Pu and $^{235}$U continued. The results of these investigations were reported at the International Conferences held in Russia, France and the USA in 2005.

The experiments on measurement of fluctuations of Total Kinetic Energy (TKE) in resonance neutron-induced fission of $^{235}$U were carried out in 1996-2000 at IBR-30. These

fluctuations were discovered in 1990 in Belgium at the GELINA setup and correlated well with the dependence of fluctuations of prompt fission neutron multiplicity on resonance neutron energy, which were revealed in the early seventies for uranium and plutonium nuclei. However, the statistical accuracy of the data obtained in Belgium was poor because of weak resonance neutron flux intensity, therefore independent verification of the results with better statistics was required. In the experiments conducted at IBR-30 the statistical accuracy of measurements was improved by more than 10 times and the obtained results coincided very closely with the results obtained in Belgium. In addition, the procedure of experimental data analysis was modified using more exact formulas to fit data obtained by Brosa, Muller and Grossman. The results obtained in Dubna have convincingly proved the presence of TKE fluctuations of fission fragments in resonance neutron energy region, which yet defied explanation within the framework of the available theoretical models of nuclear fission at low energies.

At the GELINA setup (IRMM, Belgium) the joint experiments to investigate the resonance neutron-induced fission of $^{239}$Pu nuclei, the fluctuations of prompt neutron multiplicity and the total kinetic energy of fission fragments are performed. This work is carried out using modern digital signal processing methods, when the form of pulses both from neutron detectors and from a fission chamber is converted into a digital sequence, which is stored and analyzed in an off-line mode. The obtained preliminary results show that the application of digital signal processing makes it possible to qualitatively change the procedure of measurements.

### *1.2.3 Investigation of mass-energy characteristics of binary and ternary fission products*

At the K-130 accelerator in Jyväskylä (Finland) in cooperation with the FLNP specialists the multiparameter experiment to measure mass-energy distributions of $^{238}$U $\alpha$-particle-induced fission fragments was carried out. The facility made it possible to detect time of flight and energy of each fragment that allowed us to determine their masses independently. Fission fragments were detected by two mosaics of silicon PiN-diodes located at a distance of about 0.5 m from the target. As a start detector a microchannel plate positioned in the immediate vicinity of the target was used. Data processing with the aim of searching for true ternary collinear decay in the fission is under way. Preparation for a similar experiment on neutron-induced fission measurement on beam 6b at the IBR-2 reactor with the use of "Mini-Phobos" detectors in cooperation with FLNR began.

Also, in Jyväskylä (Finland) an experiment to obtain total alpha-particle energy spectrum in ternary spontaneous fission of $^{252}$Cf was performed. As in the first experiment, mosaics of silicon PiN-diodes were used to detect light charged particles. The identification of particles was carried out by the TOF-E method. As a start detector also a microchannel plate responsive to one of fission fragments was used. To reduce background, an additional silicon detector registering the second fission fragment and synchronized with the start detector was employed. As the first result, the total $\alpha$-particle energy spectrum with the lower limit of ~1 MeV was obtained. The deviation of the spectrum shape from the Gauss distribution was observed in a low-energy region. Preliminary estimates show that this deviation cannot be entirely explained by the emission of $^{5}$He neutron-unstable nuclei, which upon decaying are identified as $\alpha$-particles.

### *1.2.4 Investigation of vibrational resonances in fission*

In the course of the year the experimental data processing was carried out within the framework of the nTOF collaboration program aimed at studying the nature of vibrational resonances in neutron-induced fission and at obtaining fission cross-sections to solve problems of ADS systems and of nuclear waste incineration.

### *1.3 Gamma-spectroscopy of neutron-nuclear interactions*

The data on level densities and strength functions of primary gamma-transitions have been derived from the intensities of two-step quantum cascades measured by now in 51 nuclei (27<A<201) between the neutron resonance and the low-lying levels of the compound nucleus. This has been done for the nucleus excitation energy interval from ~5 to ~9 MeV. These data have been obtained for the first time without resorting to any nuclear models or unverified hypotheses. The level densities and radiative strength functions obtained in this way have considerably fewer (practically by an order of magnitude) systematic errors than any available analogous data.

The improved accuracy has made it possible to observe strong effect of the structure of the nucleus on these main parameters of its cascade gamma-decay. So, the experimental values of level density both in spherical and deformed nuclei of any mass are well reproduced by the sum of partial level densities corresponding to the breakage of up to five Cooper pairs of nucleons and to the excitation of up to ten quasi-particles in a nucleus in combination with the excitations of vibrational type. The share of the latter in the region of half neutron binding energy exceeds the share of purely quasi-particle excitations by a factor of 10-20.

The obtained results open up new opportunities for experimental and theoretical studies of interaction and inter-transition of excitations of fermion and boson types in a nucleus. First of all there appeared a real possibility of practical determination of correlation functions of individual Cooper pairs of nucleons at various excitation energies of a nucleus. Great and principally unavoidable systematic errors in experimental determination of level densities eliminate the possibility of obtaining reliable information on the specified parameters of a nucleus using other techniques developed to date.

### *1.4 Investigation of (n,p) and (n,α) reactions*

**Angular correlations in (n,p) reaction**

Works to study angular correlations in the reaction $^{14}N(n,p)^{14}C$ continued. The theoretical estimation of asymmetry effects in the $^{14}N(n,p)^{14}C$ reaction was made within the framework of mixing compound-state model (**Fig.4**). The contribution of resonances into a neutron energy region of up to 1 MeV, as well as the effect of phases on the energy variation of asymmetry coefficients (forward-backward, left-right and parity violation) were analyzed. The calculations give values of forward-backward and left-right asymmetry coefficients of about $10^{-1}$ and $10^{-2}$, respectively. The obtained parity-violating correlation coefficient is several orders of magnitude less than the available experimental estimate.

For further experimental study of P-even asymmetry effects with unpolarized neutrons, a number of works were carried out to reequip the channel at EG-5. In particular, a rotary table was assembled making it possible to rotate the charged particle detector about its axis (to measure forward-backward coefficient) and to move the detector relative to the neutron target, taking it out of the direct neutron beam (to measure background).

At the EG-5 facility in FLNP the investigations of the $^{20}Ne(n,\alpha)^{17}O$ reaction were performed. Neutrons were produced in the $D(d,n)^3He$ reaction using a gas deuterium target at a deuteron energy Ed ≈ 2 MeV. The obtained neutron energy range En=3.7 – 4.1 MeV covered a group of neutron resonances of $^{20}Ne$. The detection and spectrometry of α-particles were carried out by means of a two-section grid ionization chamber and an electronic multidimensional data acquisition system. Gas Ne, filling the chamber, was the object of investigation. Some discrepancies between the obtained data and the resonance positions recommended for this reaction in neutron atlases were revealed. The investigations are planned to be continued using solid deuterium targets as a neutron source in order to reduce the scatter.

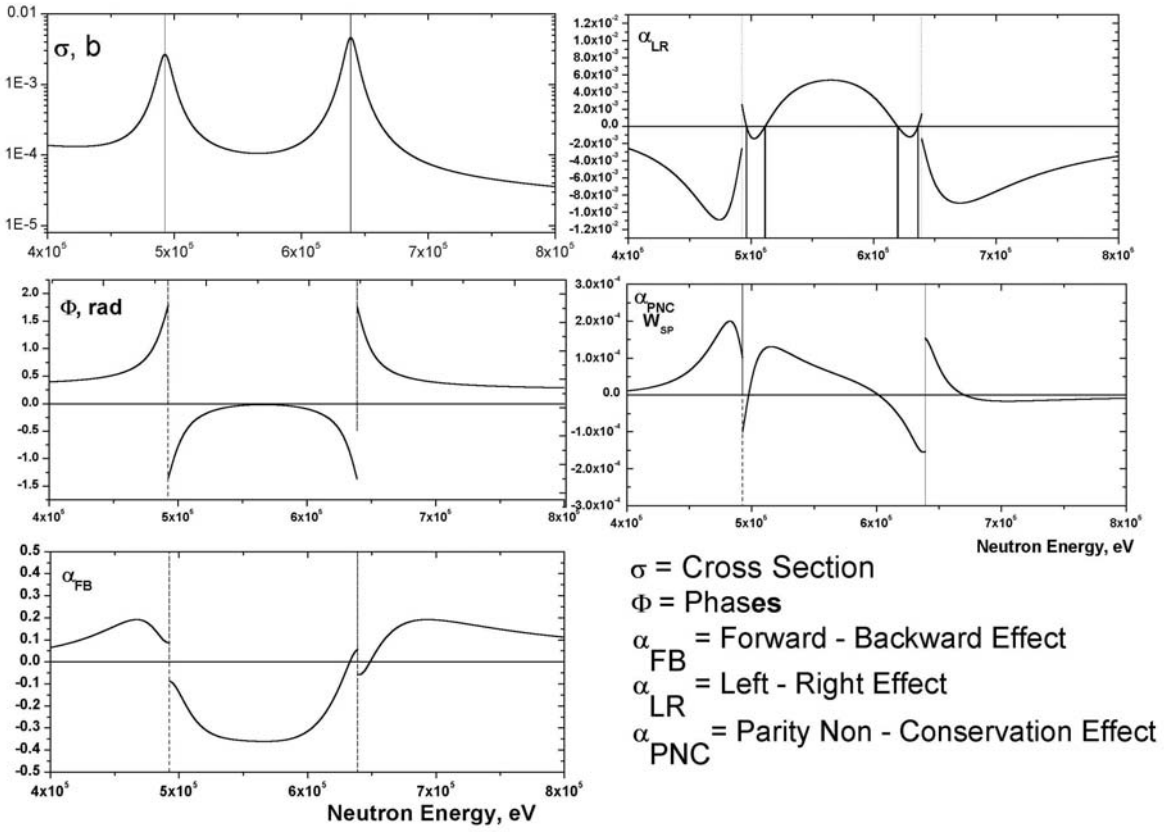


***Fig. 4***

Works to construct a new gas deuterium target, as well as to manufacture a lithium target and to purchase a tritium target are in progress. These targets are required to produce neutrons in a wide energy range at the EG-5 facility.

At the EG-4.5 in the Institute of Heavy Ion Physics, Peking University, China, measurements of cross sections of the $^{64}Zn(n,\alpha)^{61}Ni$ and $^{10}B(n,\alpha)^{7}Li$ reactions at neutron energies of 4, 5, 6 MeV were carried out. The neutron source was the $D(d,n)^{3}He$ reaction on a gas deuterium target. A two-section grid ionization chamber was used as an α-particle detector. The treatment of the obtained multidimensional data is under way.

### *1.5 Fundamental properties of the neutron*

#### *1.5.1. Investigation of n,e-scattering*

A new method developed in the Department of Nuclear Physics FLNP and described in three publications (2003–2005) to extract the n,e-scattering length $b_{ne}$ from data on neutron diffraction by noble gases was applied to process digital data on diffraction of neutrons with a wavelength of ~0,7Å. These data (obtained in Grenoble and sent to Dubna) contained sets of structural factors *S(q)* for a gaseous isotope $^{36}Ar$ of four different densities in the range of wave vector *q* of up to ~10 $Å^{-1}$ and for seven different states of liquefied Kr in the *q* range of up to ~16 $Å^{-1}$.

The experimental values of *S(q)* corrected by the authors for all kinds of distortion effects, except for the n,e-scattering, were described by a diffraction damped sinusoid with addition of monotonous *q* contribution from the n,e-interaction.

In the case of $^{36}Ar$, in principle, the result of a "zero-experiment" was obtained, since the n,e-scattering contribution is less than 0.2% of the nuclear contribution, whereas natural argon has

the n,e-contribution of ~1,9 %. Two mathematically different approaches to the solution of the multiparameter task gave the following results:

$$b_{ne} = -(1.33 \pm 0.28 \pm 0.57) \cdot 10^{-3}\ \text{Fm},$$

$$b_{ne} = -(2.15 \pm 0.49) \cdot 10^{-3}\ \text{Fm},$$

though of poor accuracy, but of significance.

The preliminary result of the data analysis for Kr, which is unfinished yet:

$$b_{ne} = -(1.36 \pm 0.14) \cdot 10^{-3}\ \text{Fm},$$

already approaches the level of the best (as to the accuracy) results.

In order to considerably improve the accuracy of determining the n,e-scattering length, a new experiment is being developed for the same setup in Grenoble, where the data on $^{36}$Ar and Kr have been obtained. The essence of the experiment is to conduct measurements with Ar, Kr and Xe in turn with the same measurements with $^{36}$Ar as «normalizing» ones.

The construction of the setup to measure $b_{ne}$ by scattering slow neutrons by gases Ar, Kr and Xe of low pressure (~1 atm.) using the time-of-flight method on neutron sources in Troitsk and at IREN-1 is in completion stage. It only remains to manufacture a rotating-positioning device.

### *1.5.2 Experiment of the direct measurement of neutron-neutron scattering cross-section*

Works on preparation of the experiment on the direct measurement of neutron-neutron scattering cross-section at the YAGUAR reactor (VNIITF, Snezhinsk) were continued. To verify the calculations and to choose an optimum variant of under-reactor shielding, in 2004 a test measurement was conducted.

In 2005 the works to calibrate the neutron detectors used in the test experiments at the YAGUAR reactor were carried out at the neutron setup of the Institute for Physics and Power Engineering (Obninsk). The performed calibrations allowed one to compare the results of background measurements with the calculations. The measurements were carried out in three different geometries of the collimation system. The measurement with geometry №3 is of particular interest. In this case the fast neutron background at the bottom of the shaft should be close to the background of a full-scale facility. The results of the calculations and measurements for the given case are presented in **Fig.5**.

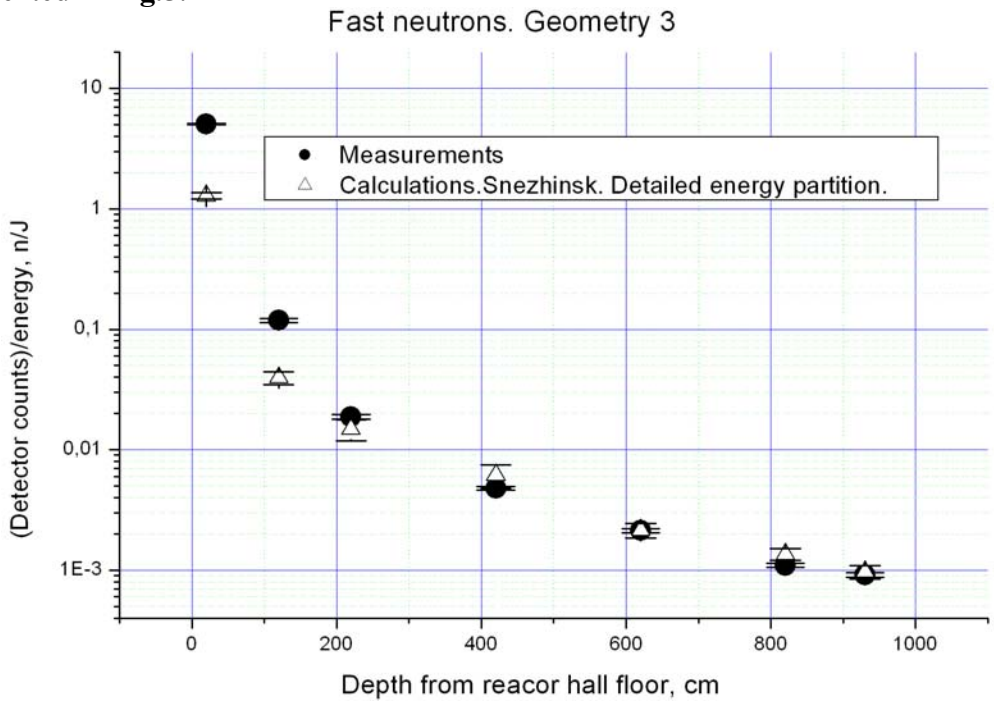


***Fig. 5.***

As may be seen in Fig. 5 the results of the calculations made by the group from Snezhinsk for a depth of more than 2 m are in complete agreement with the results of the measurements (deviation at small depths is connected with the accuracy of description of the shielding geometry at the level of the floor).

Thus, the test measurements demonstrate a high degree of reliability of the calculations made. The calculations of backgrounds in total geometry of the experiment have shown that the chosen geometry of the facility (**Fig.6**) will make it possible to carry out the nn-scattering cross-section measurements without a dominant role of background.

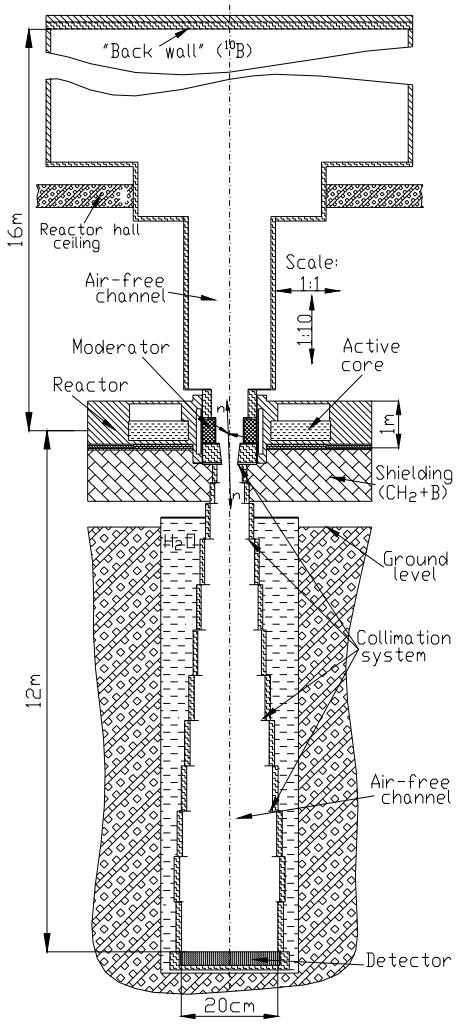


**Fig. 6**

**Fig. 7**

On the building of the YAGUAR reactor (Snezhinsk) the back flight base of the experimental facility (**Fig.7**) was installed.

The working draft of the whole experimental facility has been completed. In the FLNP experimental workshop the manufacturing of the lower part of the facility is in progress. The testing of the vacuum equipment is under way.

In 2006 it is planned to complete the manufacturing of the experimental facility, to conduct its assembling and adjustment at the YAGUAR reactor (Snezhinsk), to perform calibration measurements (neutron scattering by inert gases).

### *1.6 Ultracold neutron physics, neutron optics*

#### *1.6.1 Investigation of interaction of cold and very cold neutrons with nanostructures*

This study has been initiated by work [1] in which the idea of creation of a device for thermolysis of cold neutrons into the region of ultracold neutrons was proposed. For this purpose it was suggested that weakly bound nanoparticles in superfluid helium be used. The first step to experimental investigation of the possibility of realization of such a source should be the measurement of neutron scattering cross-section (double-differential scattering cross-section contains the greatest amount of information) with nanostructural objects.

To study the interaction of neutrons with nanostructures and to investigate the possibility of effective cooling of very cold and cold neutrons into the region of ultracold neutrons, the following experimental equipment was designed and manufactured: helium cryostat (manufactured in ISSP RAS, Chernogolovka), neutron velocity selector (to work with velocities of 30÷180 m/s) and 2π-detector of cold neutrons (manufactured in FLNP JINR, Dubna).

**Figure 8** presents the external appearance of the 2π-detector encircling a sample, and **Figure 9** displays the external appearance of the helium cryostat.

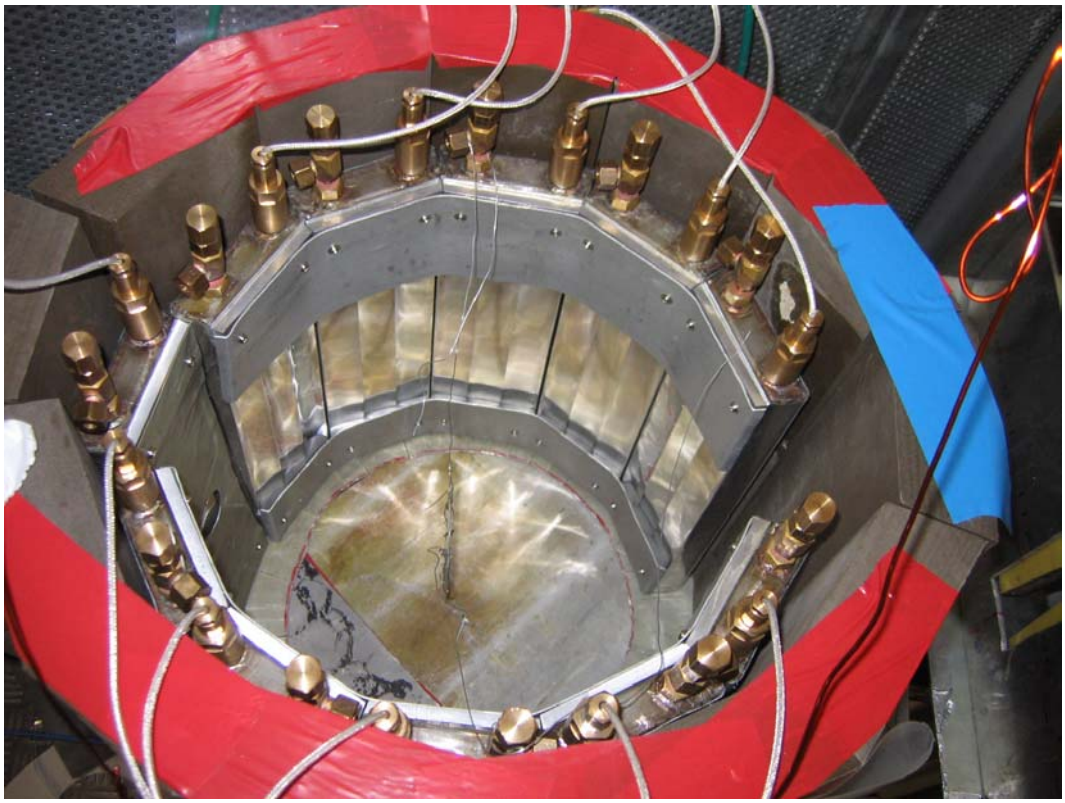

***Fig. 8***

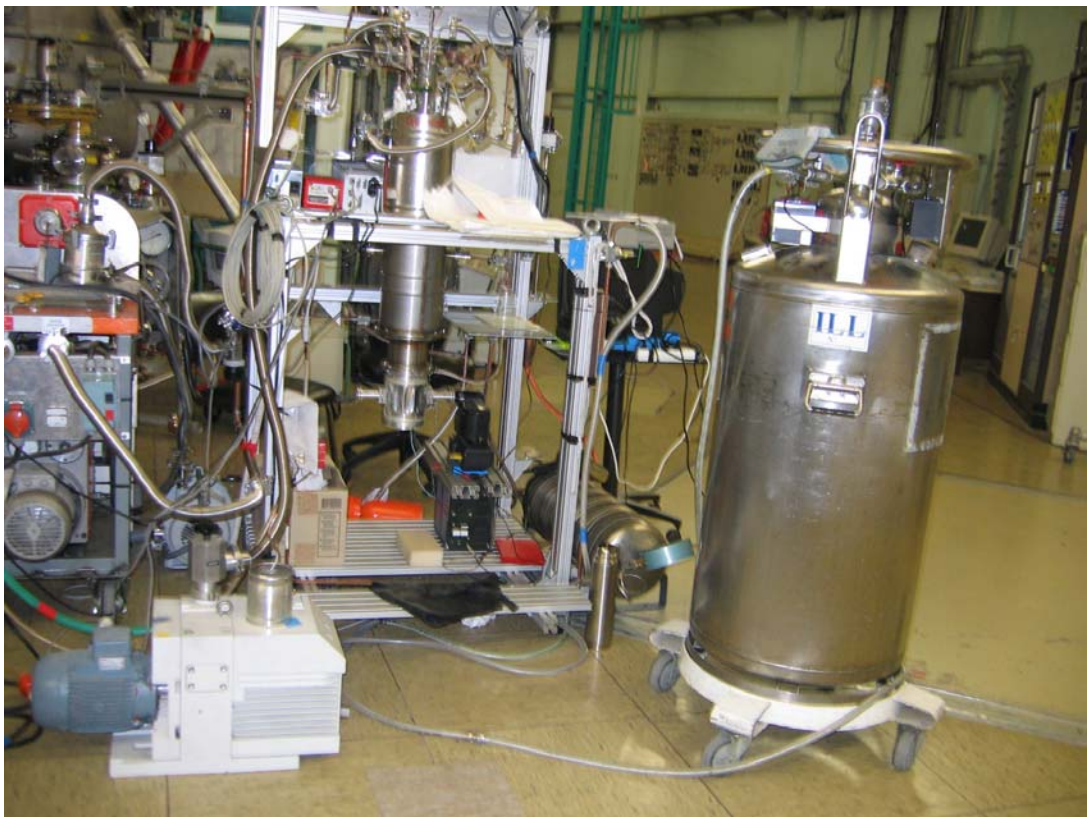


***Fig. 9***

The measurements were conducted on the PF1b and PF2 beams of the high flux reactor in ILL (Grenoble). The probability of scattering neutrons with velocities from 30 m/s to 1000 m/s depending on the scattering angle from the nanodiamond powder samples and on the structure of weakly bound nanoparticles $D_2O$ and $D_2$ in superfluid helium (jelly) was measured. The measurements with "jelly" samples show that the probability of neutron scattering from samples is rather high and if the processes of energy transfer from the neutron to the sample proceed rather intensively, than the jelly may be used for cooling very cold and cold neutrons into the ultracold neutron region. The obtained experimental data would suffice to test the validity of the theory of neutron diffusion in finely dispersed and nanodispersed media. The results also suggest that nanodispersed materials such as nanodiamond powders may be used as effective reflectors of cold and very cold neutrons when creating sources of these neutrons and in solving other experimental problems.

**Figure 10** demonstrates typical experimental dependences of counts of the $2\pi$-detector sections at various neutron energies and for various samples.

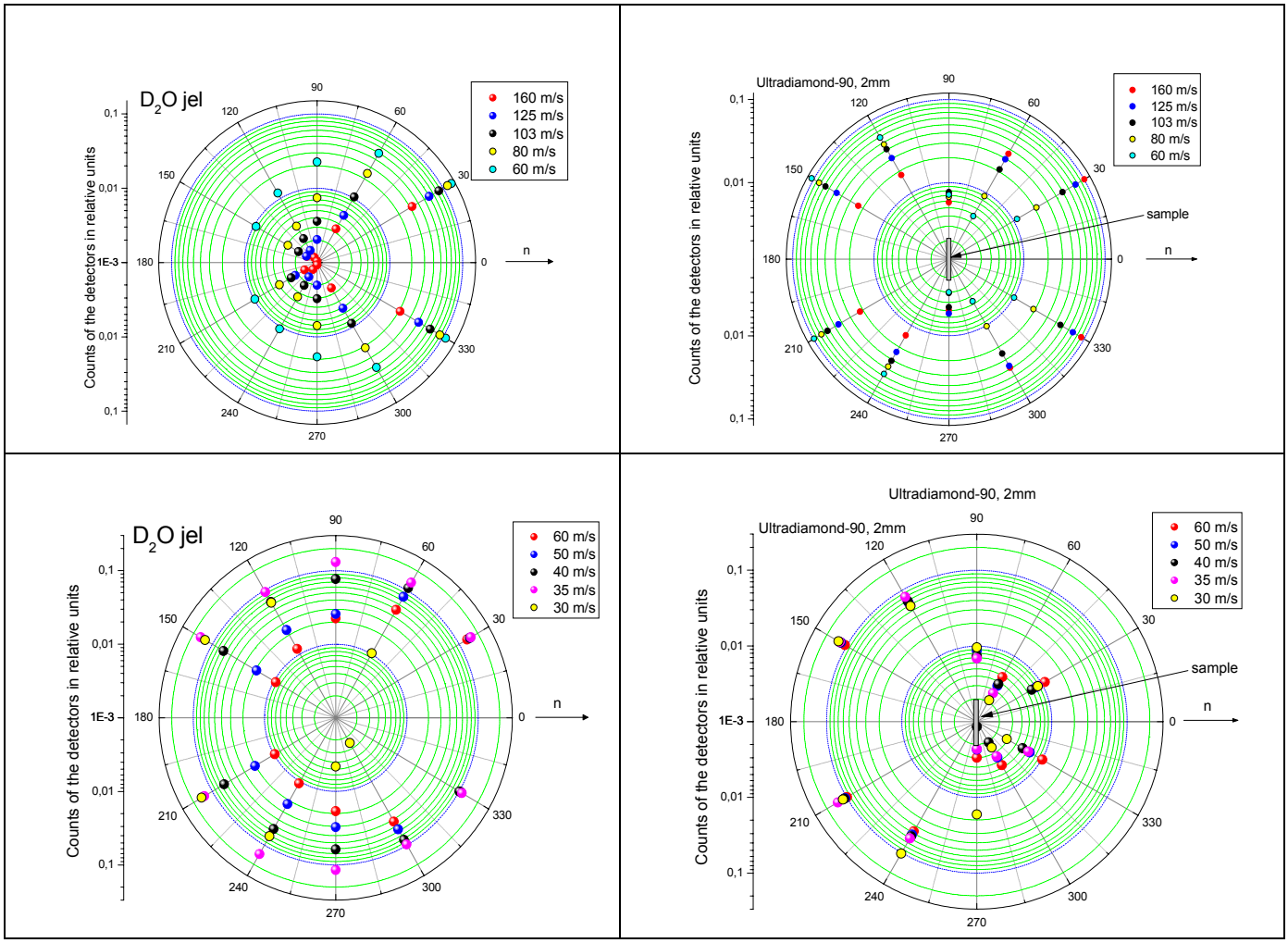


***Fig. 10***

### *1.6.2 Ultracold neutron optics*

A new experiment to observe a neutron energy change as neutrons pass through the accelerated substance was carried out. The existence of the effect follows from the validity of the equivalence principle and detailed neutron-optical calculations. The data treatment is unfinished yet, but it can be said with assurance that the specified effect was experimentally observed for the first time. To illustrate the complexity of the experiment it will suffice to mention that the neutron energy change detected in the experiment was of the order of $2 \cdot 10^{-10}$ eV. The sample (silicon plate) moved with sign-changing acceleration ranging up to 7.5g. A respective neutron energy change was detected by the UCN gravitational spectrometer with interference filters in phase with the sample motion.

A new experiment to test the validity of the 1/v law in the interaction of UCN with a sample of natural gadolinium (radiative capture cross-section is of the order of 25 Mbarn) was conducted. In the publication of 2003 it was reported that according to the obtained results the 1/v law is accurate in this case to no worse than 6% in the neutron velocity range from 4 to 120 m/s. In the new experiment the law 1/v was tested with an accuracy of the order of 0.1% but for the neutron velocity range from 4 to 35 m/s.

### *1.6.3 Investigation of weak heating and generation of UCN*

The total and differential cross-sections of very slow neutrons for liquid fluoropolymers at 80-300 K were measured to study the limits in UCN storage (experiment ILL 3-14-185). It is necessary (and planned) to carry out measurements at lower temperatures of these and other promising coatings for UCN storage.

The experiment (ILL 3-14-192) was conducted to study "weak heating" of UCN in the process of reflection from a solid surface. A considerable heating effect into the μeV energy region was revealed. These works are to be continued.

The experiment (in cooperation with PSI and ILL) on the direct measurement of UCN generation in gaseous, liquid and solid deuterium, oxygen and deuteromethane was performed in a temperature range of 8-100 K. The results are being treated and compared with the calculations, accurate in the incoherent approximation too. Measurements of density of states are planned at the inelastic scattering spectrometer.

Test works were carried out to start up a source for UCN generation in a cold solid-deuterium moderator at the pulsed reactor "TRIGA" (University of Mainz). The works are to be continued.

## 2. Theoretical investigations

A method of analytical description of neutron reflection from media with diffuse interfaces was developed to study magnetic field penetration and attenuation in high-temperature superconductors. Using this method, the experimental data on the measurement of a reflection curve of a particular multilayer system were processed. The analytical fitting was demonstrated to be 7 times faster than the standard numerical fitting.

The reflection of polarized neutrons from a magnetized mirror with a high coercive force in a weak external field whose direction varies with respect to the mirror magnetization was theoretically and experimentally investigated. The limiting energies of the mirror were demonstrated to follow the quantum rules and to be independent of the angle between the external and internal fields. The limiting energies were calculated for multilayer magnetic systems in which magnetizations of adjacent layers are directed at a specified angle to each other and the dependence of limiting energies on this angle was found as well.

A new method of calculating albedo neutron reflection from homogeneous and dispersive media has been developed. It has wider area of application than the standard diffusion method. With this method the efficiency of ultradispersed reflectors in neutron cold moderators has been studied.

In 2005 the investigation of radiative corrections to neutron beta-decay continued. In particular, it has been found that the application of current algebra cannot provide correct calculation of radiative corrections and their calculation should be made according to the modern Standard Model.

Next year it is suggested that electroweak processes be investigated within the framework of SM, in view of a sequential consideration of the hadron structure.

## 3. Applied research

### *3.1 Development of neutron detectors for space vehicles*

In collaboration with the Space Research Institute RAS the specialists of FLNP and LRB have developed a calibration technique for the detector LEND (Lunar Exploration Detector) intended to measure neutron fluxes from the lunar surface with high spatial resolution aboard the space vehicle LRO (Lunar Reconnaissance Orbiter) whose launching is scheduled for 2008. In FLNP the models of polyethylene collimators were made and in LRB the calculations of the

sensitivity of the laboratory model of the device were performed. The calibration of the laboratory model of the device was conducted.

### *3.2 Investigation of element compositions of various substances at the EG-5 accelerator*

Experimental investigations at the charged particle beams of the electrostatic generator EG-5 were carried out in close cooperation with the specialists of other JINR Laboratories as well as with the representatives of various Institutes of the JINR Member States.

In cooperation with the Institute of Physics of the Marie Curie-Sklodowska University (Lublin, Poland) the investigations of silicon oxide layers implanted with germanium ions were performed.

In cooperation with the Electrotechnical Institute SAS (Bratislava, Slovak Republic) the investigations of layered semiconductor structures Si/$HfO_2$/Ru annealed at various temperatures were carried out by the RBS method. The depth profiles of elements for 34 samples both in an initial state and upon annealing at temperatures of 800° C, 900° C and 1000° C were studied. By way of illustration **Figure 11** shows experimental (circles) and simulated (lines) spectra for the sample in the initial state and upon annealing at a temperature of 1000° C. The ruthenium layer in the initial state was 11 nm thick and the hafnium oxide layer was 3 nm with a layer of mixed composition 6 nm thick in between.

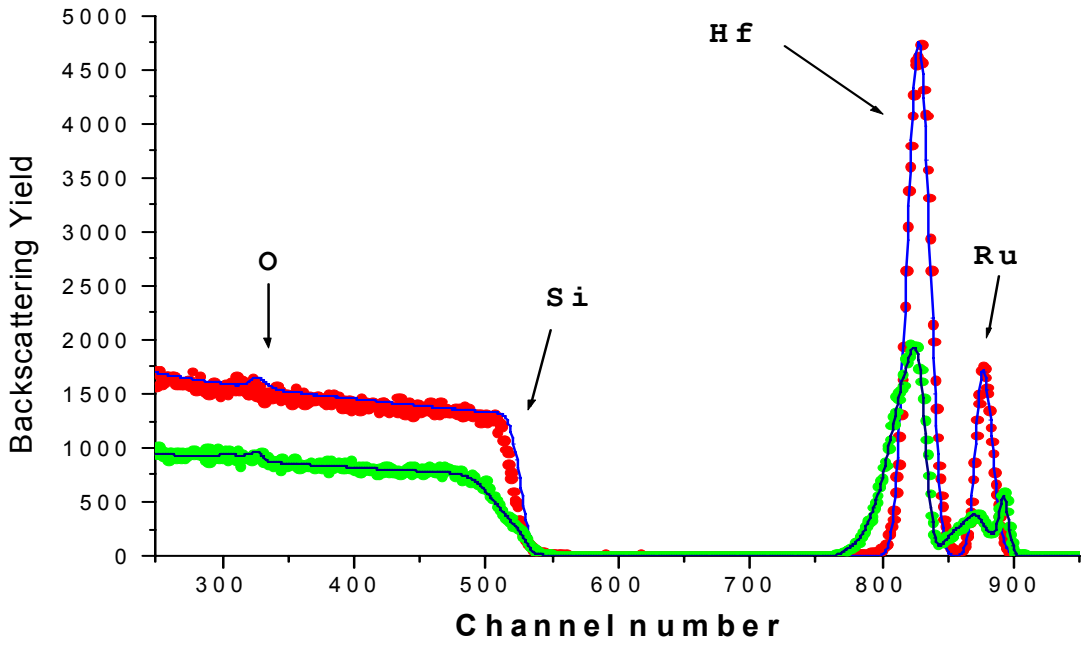


***Fig.11.*** *Rutherford backscattering spectra for the sample Si|$HfO_2$|Ru in the initial state and upon annealing at 1000 ℃*

In cooperation with the Electrotechnical Institute SAS (Bratislava, Slovak Republic) the silicon carbide amorphous layers doped with nitrogen were studied using the technique of "recoil protons" in combination with the RBS technique. The concentrations of silicon, hydrogen, carbon and nitrogen in micron-thick layers were determined.

The investigations of element compositions of aerosols in the air of Ulan-Bator were performed also using the PIXE and RBS techniques. The following trace elements were found in the samples: F, Na, Mg, Al, S, Cl, K, Ca, Ti, Mn, Fe, Cu, Zn, As, Sr, Zr, Ba.

The monitoring of the element composition of human teeth was conducted to control the population health. The samples of teeth were analyzed by the PIXE and RBS methods for 20 main

and trace elements. The concentration of Fe, Zn, Cr and Cu in the samples sometimes exceeds the control values more than 10 times. The monitoring strategy used in the present study identifies the health risk factors determined by environmental pollution, especially by industrial emissions. Heavy metal concentrations in human teeth reflect people exposure to certain atmospheric pollutants during their lives. Significant correlations between the pairs of heavy metal concentrations in human teeth point to the pollution sources typical for local industries and regional traffic networks.

### *3.3 Development of a setup for detection of hidden illicit substances*

The applied investigations aimed at creating a setup to detect hidden illicit substances using labeled fast neutrons were carried out. At present, a portable neutron generator with a built-in silicon 9-pixel alpha-detector developed in cooperation with the specialists of the All-Russian Research Institute of Automatics (Moscow) is used as a source of labeled neutrons. The neutron flux intensity of ING-27 is $2\times10^7$ $s^{-1}$.

The energy resolution of registration of characteristic nuclear γ-radiation generated on irradiation of the substance under study by the flux of labeled neutrons at $E_\gamma$ = 4.43 MeV averaged over all 9 beams of labeled neutrons is 5.5%. **Figure 12** gives the data on the measurement of temporal resolution of the whole system (velocity of a 14-MeV neutron is 5 cm/ns).

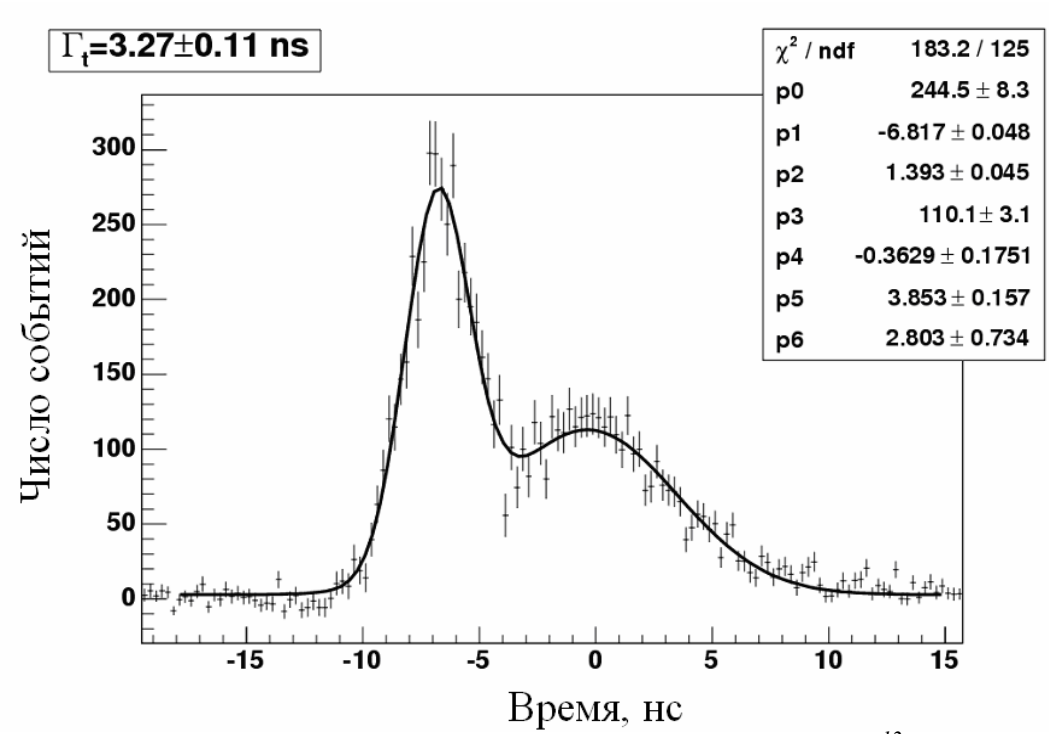


***Fig. 12.*** *Time spectrum of α-γ coincidences obtained on irradiation of $^{12}C$ sample measuring $10\times10\times10$ $cm^3$ by a neutron flux with an energy of 14.1 MeV. Solid line is the result of fitting*

The experiments on identification of melamine shielded by various substances (paper, wood, leather, steel) were conducted. The identification of melamine was carried out using the neural network technique.

## 4. Analytical studies at the IBR-2 reactor

**Methodical works**

In cooperation with the Czech Technical University in Prague (Czech Republic) neutron spectra were obtained at the pneumatic setup REGATA using multielement activation detectors.

## Ecology

*Biomonitoring*

In 2005 in connection with the carrying out of the regular European simultaneous collection of moss-biomonitors (moss-survey) the work to study atmospheric deposition of heavy metals using the biomonitoring, NAA and GIS technologies (REGATA Project) on the territory of Central Russia (Tula Region, Tver Region, Yaroslavl Region and southeast of Moscow Region), Bulgaria, Romania, Slovakia, Poland, Serbia and Macedonia, and also Armenia (Sevan), Mongolia and Vietnam was continued. The analysis of the samples collected in the summer of 2005 on the territory of Belarus will be made in early 2006. The comparative analysis of various biomonitors (lichens, bark) and soil from the area of the oil refinery in Constanta (Romania) was completed. The zone of environmental impact of this refinery on the Black Sea resort of Romania was determined.

The works in a new (for us) direction of active biomonitoring using pure mosses exposed in industrial areas with a high anthropogenic load attract increasing interest in the JINR Member and Non-Member States. Such studies were carried out in industrial areas of Baia Mare (Romania), Sofia (Bulgaria), Poznan (Poland) and Athens (Greece).

*Ecological assessment*

In cooperation with the National Institute of Physics and Nuclear Engineering (Bucharest) and the University of Bucharest the preparatory works to the analysis of the bottom sediment samples collected in the Danube delta were carried out. The analysis of the air filters from the territory of Slovakia simultaneously with the samples of pine needles and biological materials of animals (roe teeth) allowed us to make a better assessment of the degree of environmental impact of a number of large industrial plants of Slovakia, in particular, the aluminium factory in Ziar (Slovakia) on ecosystems of adjacent territories.

With the assistance of the Ecological Research Center of the Polish Academy of Sciences within the framework of the Grant of the Plenipotentiary of Poland the assessment of environmental impact of toxic elements on aquatic biota and humans in the area of the Mazur lakes (Poland) and the Rybinsk reservoir (Central Russia) was made using the nuclear-physical analytical methods.

*Foodstuff and human health*

In cooperation with the Institute of Geology RAS within the framework of the IAEA Coordination Program on technical cooperation the comparative analysis of element composition of a number of foodstuffs grown in industrially contaminated areas was conducted. The results of these works were reported at the IAEA Technical Cooperation Workshop (November 14-16, 2005, Dubna).

In 2005 the analysis of the Romanian ecological samples (soil, water and air filters) and human biosubstrata (hair, nails, teeth, etc.) was performed within the framework of the project «Monitoring of health of the personnel occupied in the production of phosphoric fertilizers at a number of factories in Russia, Uzbekistan, Poland and Romania» (European Program 5, Copernicus). The results of these studies made it possible to establish a link between levels of toxic element content in environmental objects and biosubstrata of personnel occupied in the production of phosphoric fertilizers in Turnu-Magurel (Romania).

The study of heavy metal content in edible unsaturated fats conducted in the framework of the Grant of the Plenipotentiary of Romania made it possible to experimentally establish a correlation between metal content and oxidizing ability of fats.

## Materials science

*Archeology*

The element analysis of 70 archeological samples of ceramics from burial mounds of the Smolensk region and the Northern Caucasus was performed in the framework of cooperation with the State Hermitage (Saint-Petersburg). The element composition of 65 samples of ceramics and 25

samples of Venetian glasses for the Historical Museum in Constanta (Romania) was determined within the framework of cooperation with the Ovidius University in Constanta.

*New materials*

In the framework of the Grant of the Plenipotentiary of Belarus the data analysis to study the effect of fission-spectrum neutrons on physical properties of fine-grained diamonds obtained in the Institute of Solid State and Semiconductor Physics of NAS of Belarus (Minsk) was completed.

amplification of diffuse scattering at temperatures near $T_N$ is also noted. The observed effects can be explained in the framework of the model of coexistence of an ordered antiferromagnetic phase and a spin liquid state without a long-range magnetic order, whose volume fraction rises with increasing pressure due to the enhancement of frustration effects. In addition, the exposure to high pressures results in spin reorientation of Mn magnetic moments and in a change in symmetry of AFM structure, which may be described by a combination of irreducible representations $\Gamma_1+\Gamma_2$.

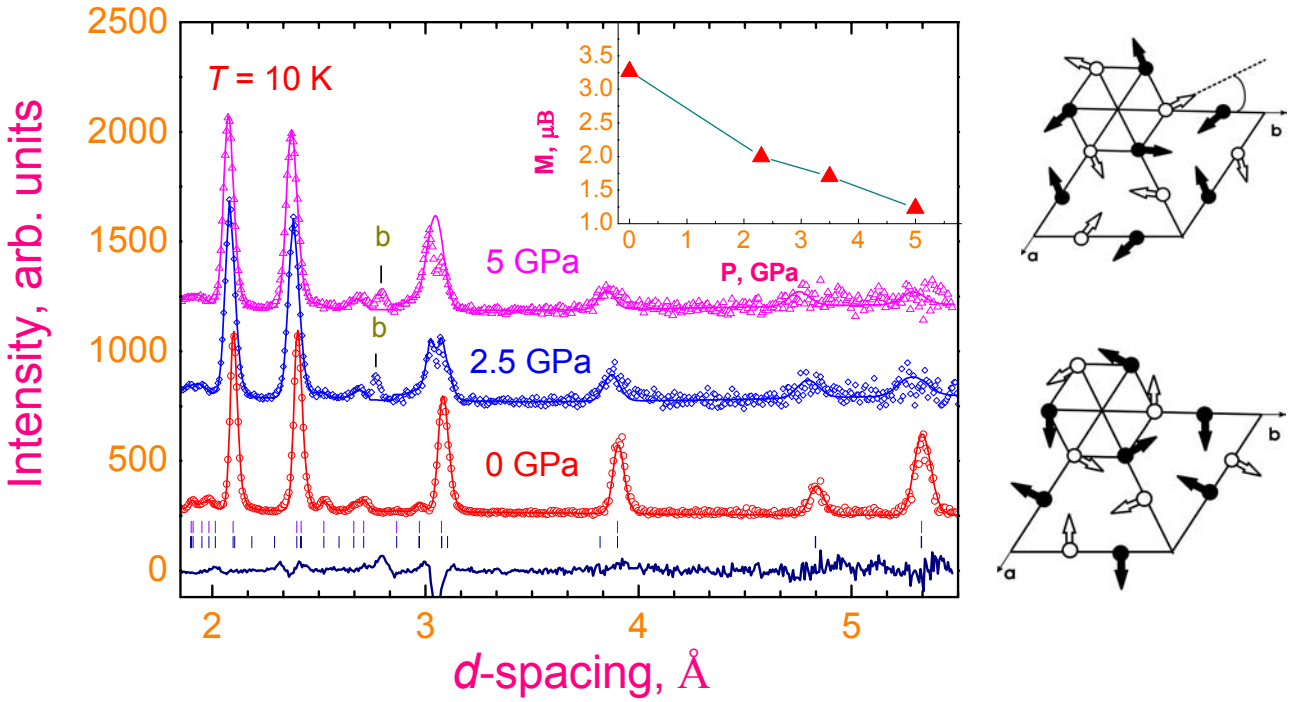


***Fig. 1.*** *Diffraction spectra of $YMnO_3$ obtained at pressures P = 0, 2.5 and 5 GPa at a temperature of 10 K at $2\theta$=90° and treated by the Rietveld method. The difference curve is shown for P=5 GPa. Tics indicate the calculated positions of structural (top row) and magnetic (lower row) diffraction peaks. The diffraction peak from a high pressure cell is marked by "b". In the upper inset: pressure dependence of manganese magnetic moment. The illustration at the right presents triangular AFM structures corresponding to the symmetry of irreducible representation $\Gamma_1$ and a combination of irreducible representations $\Gamma_1+\Gamma_2$. The orientation of Mn magnetic moments in neighbouring planes is shown in white and black colors.*

At the YuMO spectrometer liquid dispersions of detonation nanodiamonds have been studied by small-angle neutron scattering. Detonation nanodiamonds are formed as a result of explosion of oxygen-unbalanced explosives in the absence of any additional sources of carbon. The resulting nanodiamond crystals are extremely interesting and promising material for nanotechnologies. However, they are hard to free from explosion by-products. This is due to the formation of complex multilevel aggregation of nanodiamonds in the process of synthesis, which involves elements different from carbon. Disperse nanodiamond powders (prepared in zirconium mills) placed in various liquids form unusually stable colloidal solutions without addition of any surfactants. This phenomenon may be effectively used to study the internal structure of nanodiamond aggregates by small-angle neutron scattering. The obtained curves of scattering by nanodiamonds in various solvents show similar behavior (**Fig.2**). Nanodiamond particles (characteristic size of 5-6 nm) are organized in clusters structurally close to Gaussian polymers, with a size of more than 120 nm. The internal structure of clusters does not depend on their concentration in solution. The estimate of mean scattering density of clusters using contrast

variation in aqueous dispersions (light/heavy water) gives smaller value than the scattering density of a pure diamond. This points to the existence of a component different from diamonds in an elementary unit of aggregates. In particular, it can be a non-diamond shell which, on the one hand, is responsible for aggregation of particles during explosion and then provides stability of disperse particles due to interaction with a solvent.

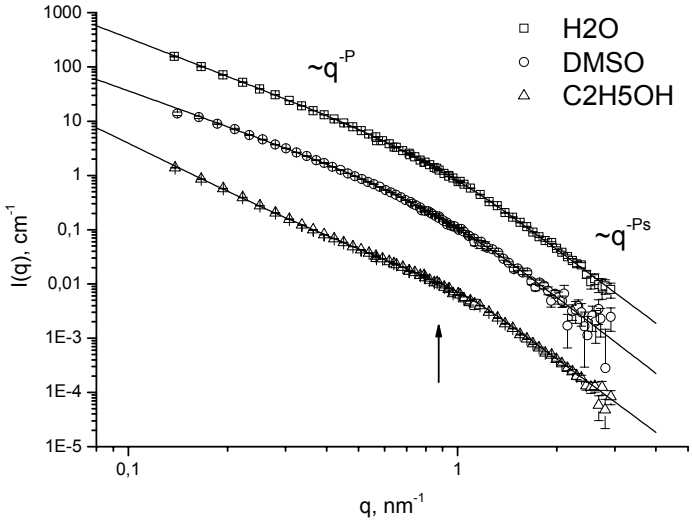


***Fig. 2.*** *Experimental curves of small-angle neutron scattering (circles) from detonation nanodiamonds dispersed in various liquids. For convenience sake the curves for DMSO and $C_2H_5OH$ are divided by 10 and 100, respectively. Parameter P reflects the fractal structure of nanodiamond clusters: 2.32 ($H_2O$); 2.16 (DMSO); 2.93 ($C_2H_5OH$). Parameter P corresponds to the diffuse surface of nanodiamonds: 4.52 ($H_2O$); 4.7 (DMSO); 4.49 ($C_2H_5OH$). The arrow points at the peculiarity of the scattering, by which the size of nanodiamonds is estimated: 5.6 nm ($H_2O$), 5.0 nm (DMSO), 6 nm ($C_2H_5OH$).*

At the REMUR spectrometer the phenomenon of coexistence of ferromagnetism and superconductivity in layered structures, which is of importance both from fundamental and practical points of view, has been investigated. It is well known that ferromagnetic and superconducting states cannot simultaneously coexist in homogeneous systems. But in inhomogeneous systems, which is the case for layered nanosystems, this coexistence is possible. These studies are of much practical importance, since they make it possible to develop essentially new nanodevices whose operation logic is determined simultaneously by changes in magnetic state and temperature within a small range. The experimental technique for studying this phenomenon is based on the generation of a neutron field of standing waves by reflecting a neutron wave from a periodic structure, and on a neutron polarization analysis and detection of specularly and diffusely reflected neutrons. Neutron investigations have been carried out on the structure Pd(2 nm)/V(33 nm)/Fe(3 nm)/ 20×[V(3 nm)/Fe(3 nm)]/MgO over a magnetic field intensity interval of 0.2÷4 kOe in a wide temperature range. It has been found that in the range 1.6÷3.5 K the superconducting state of the V(33 nm) layer changes the magnetic ordering in the periodic structure and the magnetization profile at the boundary between the Fe layer and the V(33 nm) layer. It has been also revealed that in the range 7÷30 K the magnetic state of periodic structures varies with temperature. The latter is associated with the ferromagnetism of interfaces. In a model diagram of magnetization distribution in nanostructures, the number of bilayers with antiferromagnetic ordering is $N_1$ without it – $N_2$ (**Fig.3**). The $N_1$ bilayers are immediately adjacent to a thick vanadium layer and are followed by the $N_2$ bilayers. The calculations show that $N_1$ is in the range 2÷8 and $N_2$ – in the range 18÷12. Thus, a thick vanadium layer changes the type of ordering in the nearest adjacent bilayers of the periodic structure.

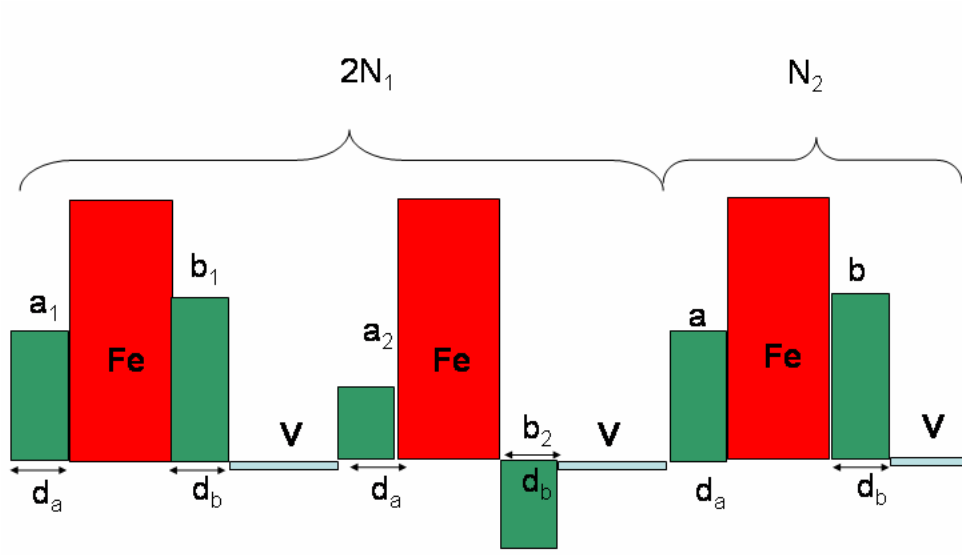


***Fig. 3.*** *Model diagram of the periodic structure describing the experimental data on the coexistence of ferromagnetism and superconductivity in layered structures obtained at the REMUR spectrometer. Interface areas comprised of a mixture of iron and vanadium atoms are shown in green.*

At the NERA inverted geometry spectrometer the comparison characteristics of substances-candidates for neutron cold moderators at IBR-2: methane, methanol, mesitylene and water, have been studied. The criteria were the amount of hydrogen in a substance, the appropriate density of phonon states and radiation resistance. Solid methane at $T$ <20 K is in a crystal phase II in a partially (~25 %) disordered state. At low temperatures methanol can be either in crystal or amorphous phases with either translational or orientational disorder. Mesitylene is a rather promising substance for use in cold moderators due to a high content of hydrogen, good moderating properties and radiation resistance. **Figure 4** illustrates the comparison of densities of phonon states obtained on the basis of single-phonon approximation from the incoherent inelastic scattering spectra for the specified substances. On the basis of these data as well as the results obtained in the course of the URAM-2 program, it may be concluded that mesitylene in glass-like state exhibits the best characteristics for moderating neutrons at helium temperatures.

At the DIN-2PI spectrometer the neutron diffraction experiment to study the microstructure of Li–N melts with a concentration of nitrogen impurity of 1.3 and 3.5 at.% and at a temperature of 823 K has been performed. The basic microstructural characteristic of the substance – the total structural factor $S(Q)$, as well as the partial structural factors $S_{\alpha\beta}(Q)$ of melt components and corresponding radial distribution functions $g_{\alpha\beta}(r)$ and $g_{CC}(r)$ (**Fig. 5**) have been obtained. It has been determined that at a concentration of impurity component less than 4 at.% the so-called "prepeak", which is an indicator of existence of clusters of particular size in melts, is missing from the structural factor of Li-N melts. The analysis of the partial structural characteristics of the melt suggests that nitrogen impurity is present in $Li_{0.987}N_{0.013}$ and $Li_{0.965}N_{0.035}$ melts as lithium nitride $Li_3N$.

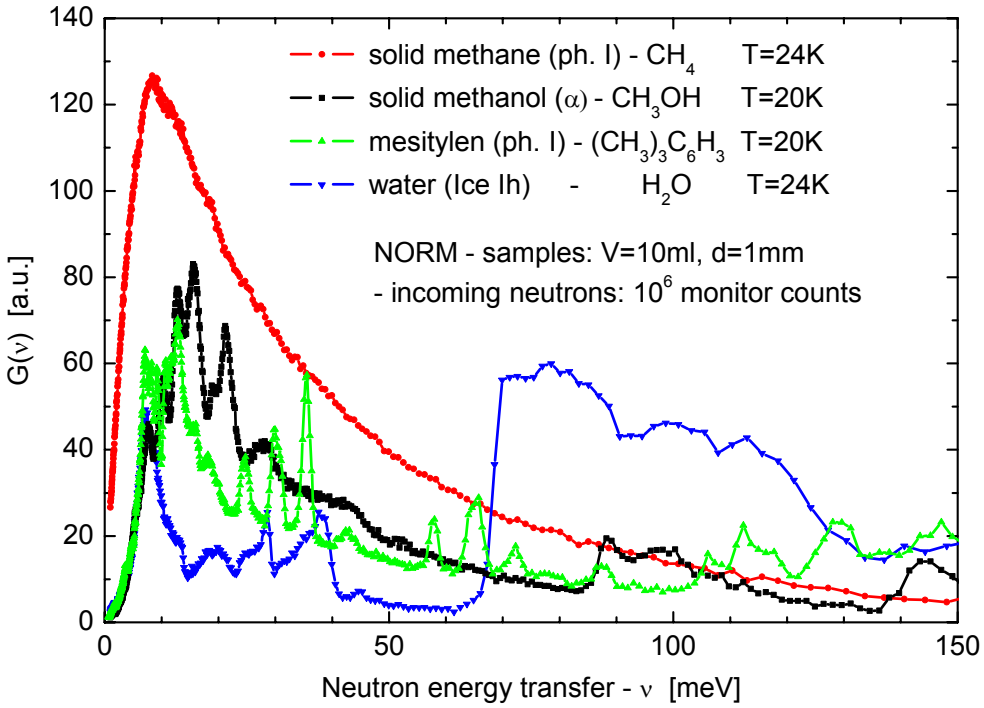


***Fig. 4***. *Comparison of densities of phonon states obtained on the basis of single-phonon approximation from the incoherent inelastic scattering spectra for methane, methanol, mesitylene and water.*

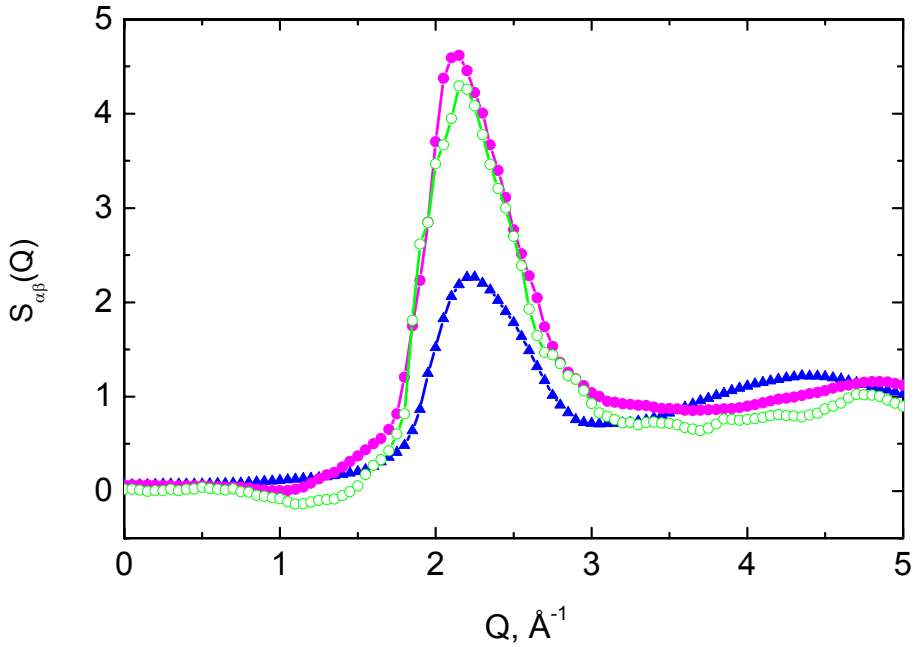


***Fig. 5.*** *Partial structural factors of liquid lithium and nitrogen for* $Li_{0.987}N_{0.013}$ *and* $Li_{0.965}N_{0.035}$ *melts. Triangles – structural factor of lithium* $S_{Li\ Li}(Q)$*, solid and open circles –* $S_{N\ N}(Q)$ *for concentrations of 1.3 and 3.5 at.%, respectively.*

A series of works, which sums up almost a 20-year debate on one of the key problems of statistical physics – interaction of fluctuating random surfaces, has been completed by the physicists of the small-angle neutron scattering group. A wide class of objects: from biological membranes to strings in the contemporary field theory belongs to random fluctuating surfaces. This is one of the reasons why the attention of contemporary theoretical physics is drawn to biological membranes, in particular, to lipid membranes. As a result, new approaches have been developed to study

intermembrane interactions and to detect a universal constant on the basis of investigation of temperature dependence of intermembrane interactions with the help of complementary use of small-angle neutron scattering and high-resolution diffraction on a synchrotron source. The value of the interaction constant has been obtained, which is $3\pi^2/256$ and agrees with the theoretically predicted one. It has been also shown that the transition from multilayer membranes to single ones proceeds in accordance with the theoretically predicted model of two states. In addition, it has been shown for the first time that the undulation forces make a significant contribution to the balance of intermembrane interactions and what is more, these forces become dominant at distances of more than 20 Å.

For the first time the dynamics of crystal lattice of the superionic conductor AgCuSe has been studied by inelastic neutron scattering. In a low-temperature phase the low-energy modes have been detected, which are most likely of acoustic phonon nature. The density of phonon states $G(\varepsilon)$ in $\alpha$- and $\beta$- AgCuSe is characterized by a non-Debye behavior. At the transition from $\beta$ to $\alpha$ phase the spreading of phonon state density spectrum and hardening of the spectrum as a whole are observed.

**Development activity**. In 2005 the technical works to modernize the IBR-2 spectrometers complex continued. For the most part, they concerned the detector systems of the spectrometers. In particular, at the Fourier specialized diffractometer FSD work to construct the detector system continued (6 out of 14 detector modules are ready), test filling of two-dimensional detector for YuMO was carried out and one-dimensional PSD with resolution of 1.8 mm was tested in actual operating conditions.

# 1. НАУЧНЫЕ ИССЛЕДОВАНИЯ

## 1.1. ФИЗИКА КОНДЕНСИРОВАННЫХ СРЕД

Основная цель - исследование методами нейтронной физики структуры и динамики конденсированных сред, получение новых данных о микроскопических свойствах исследуемых систем, экспериментальная проверка теоретических предсказаний и моделей, обнаружение новых закономерностей. Работа по теме строилась по двум основным направлениям: проведение экспериментальных исследований и текущая методическая работа, направленная на модернизацию действующих спектрометров и создание на ИБР-2 новых установок.

В основном эксперименты велись на базовой установке ЛНФ - реакторе ИБР-2, кроме того, сотрудники НЭО НИКС участвовали в выездных экспериментах в нейтронных центрах Европы. На реакторе ИБР-2 сотрудники отдела отвечали за эксплуатацию, развитие и проведение физических экспериментов на 13 спектрометрах: ФДВР - фурье-дифрактометр высокого разрешения, ДН-2 – многоцелевой дифрактометр для экспериментов на поли- и монокристаллах, СКАТ – дифрактометр для исследования текстур, ЭПСИЛОН – дифрактометр для исследования внутренних напряжений, ФСД – фурье-дифрактометр для исследования внутренних напряжений, ДН-12 - дифрактометр для экспериментов при высоких внешних давлениях, ЮМО - спектрометр малоуглового рассеяния, РЕМУР - спектрометр поляризованных нейтронов, РЕФЛЕКС-Р - рефлектометр на поляризованных нейтронах, ДИН-2ПИ - спектрометр неупругого рассеяния в прямой геометрии, НЕРА-ПР - многокристальный спектрометр неупругого рассеяния, КДСОГ-М - спектрометр неупругого рассеяния в обратной геометрии. На всех спектрометрах, кроме КДСОГ-М, проведение экспериментов регулируется программой пользователей. Ниже перечисляются, полученные в текущем году.

**Основные научные результаты.** Проведены нейтронные дифракционные исследования манганитов $R_{0.5}Sr_{0.5}MnO_3$ (R=Sm, $Nd_{0.772}Tb_{0.228}$ и $Nd_{0.544}Tb_{0.456}$), направленные на выявление микроскопических причин гигантского кислородного изотопического эффекта, недавно открытого в $Sm_{0.5}Sr_{0.5}MnO_3$. Показано, что во всех изученных составах при низкой температуре сосуществуют две кристаллические фазы с разным типом ян-теллеровских искажений кислородных октаэдров и с разным типом магнитного упорядочения. Дифракционные данные позволили предложить сценарий наблюдающихся фазовых переходов и установить, что переход из металлического состояния в диэлектрическое в составах с Sm при замене $^{16}O$ на $^{18}O$ является перколяционным, а именно, замена изотопа кислорода приводит к резкому (с 65% до 13%) уменьшению объема ферромагнитной металлической фазы. Эту работу можно считать итоговой по теме изучения причин гигантского изотопического эффекта в манганитах – смены низкотемпературного металлического состояния на диэлектрическое при замене $^{16}O$ на $^{18}O$. Установлено, что так же, как и в оксидах марганца с уровнем допирования $x$=0.3, в составах с $x$=0.5 эффект существует только при наличии фазово-расслоенного состояния на мезоскопическом масштабе размеров. Основной причиной равновесного фазового расслоения является возникновение случайного поля напряжений на некогерентных границах сосуществующих фаз.

На дифрактометре ДН-12 проведено исследование влияния высокого давления до 5 ГПа на кристаллическую и магнитную структуру гексагонального манганита $YMnO_3$ в температурном диапазоне 10 - 295 К **(Рис. 1).** При нормальном давлении в этом соединении при $T \sim T_N$=70 К наблюдается состояние спиновой жидкости, обусловленное эффектами магнитной фрустрации на треугольной решетке, сформированной ионами Mn, а при $T<T_N$ возникает упорядоченное треугольное антиферромагнитное (АФМ) состояние с симметрией

неприводимого представления $\Gamma_1$. При увеличении давления до 5 ГПа наблюдается уменьшение величины упорядоченного магнитного момента ионов Mn при $T$=10 К с 3.27 до 1.52 $\mu_B$, а также усиление диффузного рассеяния при температурах близких к $T_N$. Обнаруженные эффекты могут быть объяснены в модели сосуществования упорядоченной антиферромагнитной фазы и состояния спиновой жидкости без дальнего магнитного порядка, объемная доля которого возрастает при увеличении давления за счет усиления эффектов фрустрации. Воздействие высокого давления, кроме того, приводит к спиновой переориентации магнитных моментов Mn и изменению симметрии АФМ структуры, которая может быть описана комбинацией неприводимых представлений $\Gamma_1$+$\Gamma_2$.

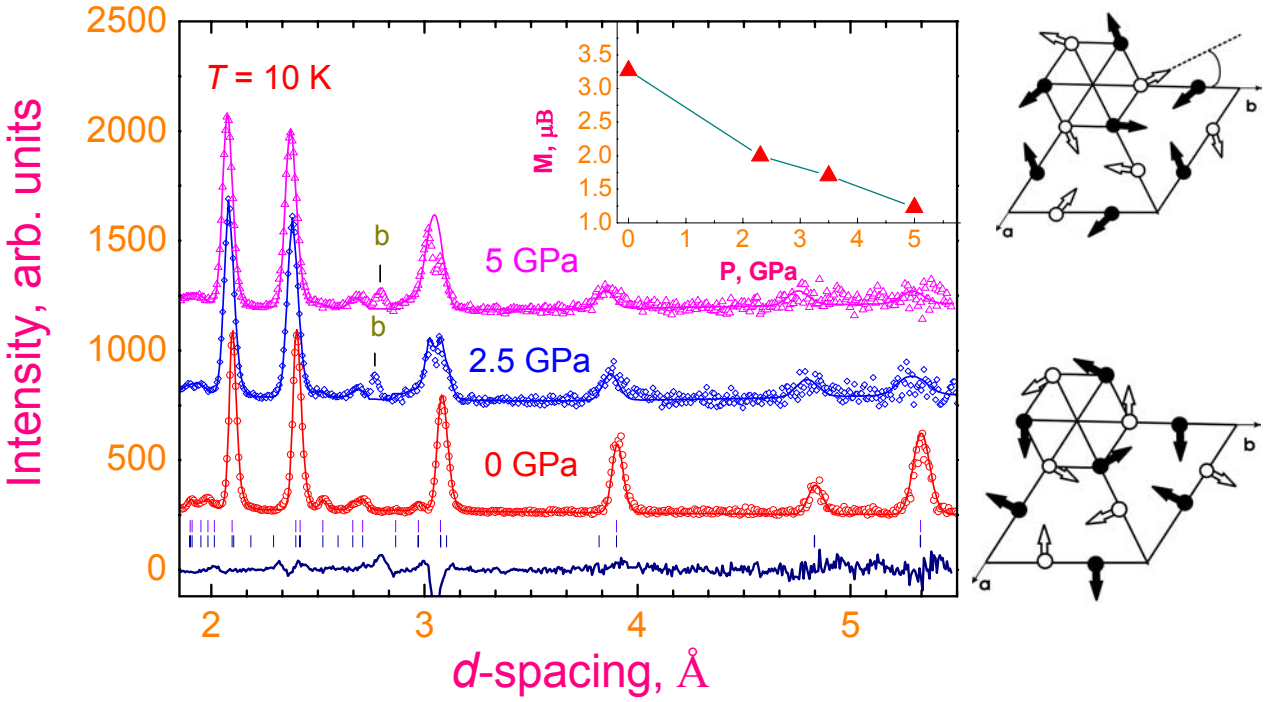


***Рис. 1.*** *Дифракционные спектры $YMnO_3$, измеренные при давлениях P = 0, 2.5 и 5 ГПа при температуре T=10 K при $2\theta=90^0$ и обработанные методом Ритвельда. Разностная кривая показана для P=5 ГПа. Штрихами указаны рассчитанные положения структурных (верхний ряд) и магнитных дифракционных пиков (нижний ряд). Дифракционный пик от камеры высокого давления отмечен буквой "b". На вставке: барическая зависимость магнитного момента марганца. Справа представлены треугольные АФМ структуры, соответствующие симметрии неприводимого представления $\Gamma_1$ и комбинации неприводимых представлений $\Gamma_1$+$\Gamma_2$. Белым и черным цветом показана ориентация магнитных моментов Mn в соседних плоскостях.*

Методом малоуглового рассеяния нейтронов исследованы жидкие дисперскии детонационных наноалмазов. Детонационные нанолмазы образуются в результате взрыва кислродо-несбалансированных взрывчатых веществ в отсутствие каких-либо дополнительных источников углерода. Образующиеся кристаллы наноалмазов являются крайне интересным и перспективным материалом для нанотехнологий. Однако, они трудноотделимы от побочных продуктов взрыва. Это связано с образованием сложной многоуровневой агрегации наноалмазов в момент синтеза, в которой участвуют элементы, отличные от углерода. Дисперсные наноалмазные порошки, приготовленные в циркониевых мельницах, помещенные в различные жидкости образуют необычно стабильные коллоидные растворы без каких-либо добавок поверхностно-активных веществ. Данное явление может быть эффективно использовано для исследования внутренней структуры агрегатов наноалмазов посредством малоуглового рассеяния нейтронов. Полученные кривые рассеяния на нанаолмазах в различных растворителях показывают сходное поведение **(Рис. 2).**

Частицы наноалмазов (характерный размер 5-6 нм) организованы в кластеры с размером более 120 нм, близкие по своей структуре к гауссовским полимерам. Внутренняя структура кластеров не зависит от их концентрации в растворе. Оценка средней рассеивающей плотности кластеров с помощью вариации контраста в водных дисперсиях (легкая/тяжелая вода) дает значение меньшее, чем рассеивающая плотность чистого алмаза. Это свидетельствует о существовании в элементарной единице агрегатов компоненты, отличной от алмазов. В частности, это может быть неалмазная оболочка, которая, с одной стороны, ответственна за агрегацию частиц во время взрыва, а затем, обеспечивает стабильность дисперсных частиц благодаря взаимодействию с растворителем.

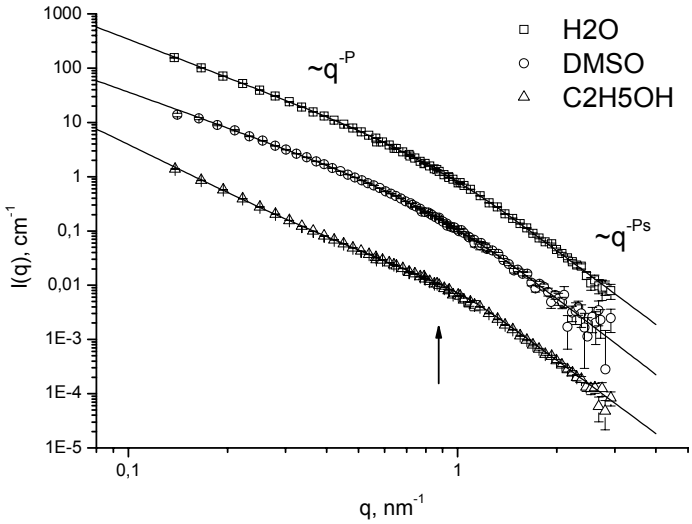


***Рис.2.*** *Экспериментальные кривые малоуглового рассеяния нейтронов (точки) на детонационных наноалмазах, диспергированных в различные жидкости. Для наглядности кривые для DMSO и $C_2H_5OH$ поделены, соответственно, на 10 и 100. Линии отвечают подгонке двухстепенной зависимостью. Параметр P отражает фрактальную структуру кластеров наноалмазов: 2.32 ($H_2O$); 2.16 (DMSO); 2.93 ($C_2H_5OH$). Параметр P соответствует диффузной поверхности наноалмазов: 4.52 ($H_2O$); 4.7 (DMSO); 4.49 ($C_2H_5OH$). Стрелка указывает на особенность рассеяния, по которой оценивается размер наноалмазов: 5.6 нм ($H_2O$), 5.0 нм (DMSO), 6 нм ($C_2H_5OH$).*

На спектрометре РЕМУР проведено исследование явления сосуществования ферромагнетизма и сверхпроводимости в слоистых структурах, важного как с фундаментальной, так и с практической точек зрения. Известно, что ферромагнитное и сверхпроводящее состояния не могут сосуществовать одновременно в однородной системе. Но в неоднородной системе, какой являются слоистые наносистемы, такое сосуществование возможно. Практическая важность этих исследований связана с возможностью разработки принципиально новых наноустройств, логика работы которых определяется одновременно изменением магнитного состояния и температуры в небольших пределах. В основе экспериментального метода исследования явления лежат генерация нейтронного поля стоячих волн путём отражения нейтронной волны от периодической структуры, поляризационный анализ нейтронов и регистрация зеркально и диффузно отражённых нейтронов. Нейтронные исследования были проведены на структуре Pd(2 нм)/V(33 нм)/Fe(3 нм)/20×[V(3 нм)/Fe(3 нм)]/MgO в интервале изменений напряжённости магнитного поля 0.2÷4 кОе в широком интервале температур. Обнаружено, что в интервале 1.6÷3.5 К сверхпроводящее состояние слоя V(33 нм) изменяет магнитное упорядочение в периодической структуре и профиль намагниченности на границе слоя железа со слоем V(33 нм). Было обнаружено также, что в диапазоне 7÷30 К изменяется магнитное состояние

периодической структуры в зависимости от температуры. Последнее связывается с ферромагнетизмом границ раздела. В модельной схеме распределения намагниченности в наноструктуре **(Рис. 3)** число бислоёв, в которых существует антиферромагнитное упорядочение равно $N_1$, а в которых оно отсутствует – $N_2$. При этом, $N_1$ бислои прилегают к толстому слою ванадия, а $N_2$ бислои следуют за $N_1$ бислоями. Расчёты показывают, что $N_1$ находится в диапазоне 2÷8, а $N_2$ – в диапазоне 18÷12. Таким образом, толстый слой ванадия изменяет тип упорядочения в ближайших прилегающих к нему бислоях периодической структуры.

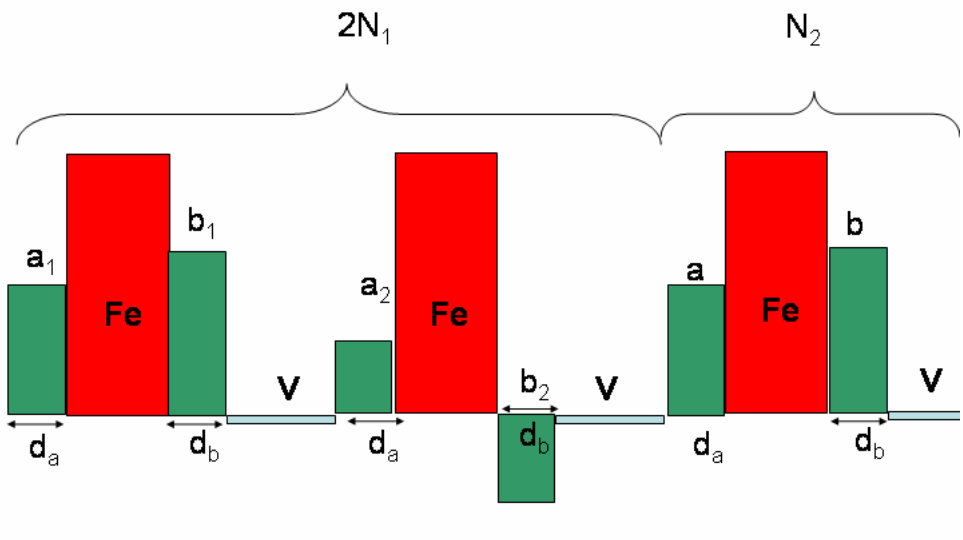


***Рис. 3.*** *Модельная схема периодической структуры, описывающая экспериментальные данные по сосуществованию ферромагнетизма и сверхпроводимости в слоистых структурах, полученные на спектрометре РЕМУР. Зелёным цветом показаны интерфейсные области, состоящие из смеси атомов железа и ванадия.*

На спектрометре обратной геометрии НЕРА выполнено изучение сравнительных характеристик веществ – кандидатов для холодных замедлителей нейтронов на ИБР-2: метана, метанола, мезителена и воды. Критериями являлись количество водорода в веществе, подходящая плотность фононных состояний и радиационная стойкость. Твердый метан при $T$ < 20 K находится в кристаллической фазе II в частично (~25%) разупорядоченном состоянии. Метанол при низкой температуре может находиться в кристаллической или аморфной фазах с трансляционным или ориентационным беспорядком. Мезитилен является весьма перспективным веществом для использования в холодных замедлителях благодаря высокому содержанию водорода, хорошим замедляющим свойствам и радиационной стойкостью. На **Рис. 4** сравниваются плотности фононных состояний, полученные на основе однофононного приближения из измеренных для указанных веществ спектров некогерентного неупругого рассеяния. Основываясь на этих данных, а также результатов, полученных в ходе программы УРАМ-2, можно придти к выводу, что для замедления нейтронов при гелиевых температурах наилучшими характеристиками обладает мезитилен в стеклоподобном состоянии.

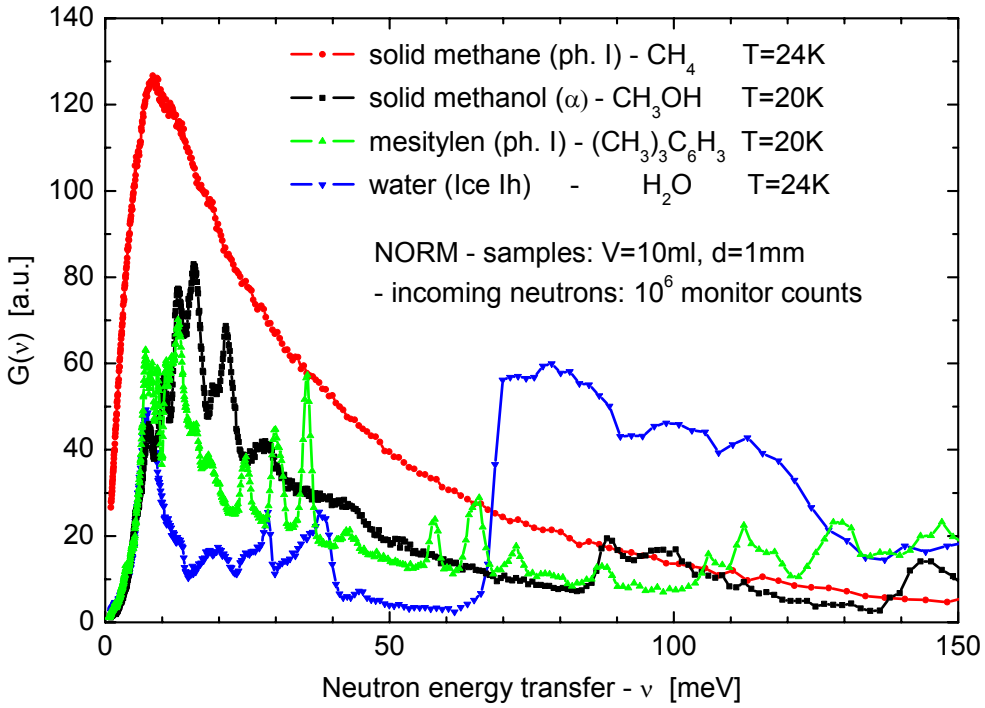


***Рис. 4***. *Сравнение плотностей фононных состояний, полученных на основе однофононного приближения из измеренных для метана, метанола, мезитилена и воды спектров некогерентного неупругого рассеяния.*

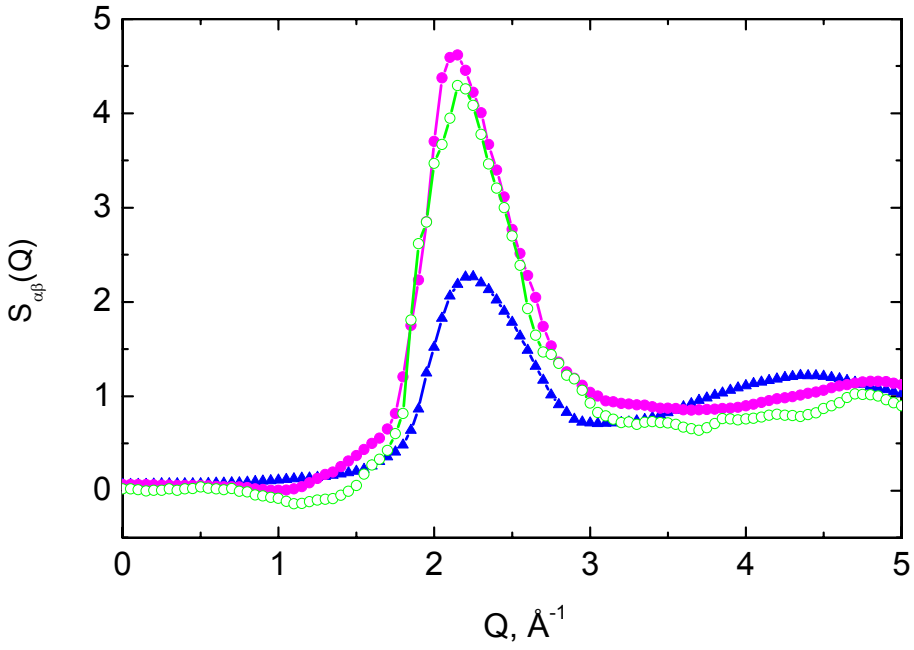


***Рис. 5***. *Парциальные структурные факторы жидкого лития и азота для расплавов* $Li_{0.987}N_{0.013}$ *и* $Li_{0.965}N_{0.035}$. *Треугольники – структурный фактор лития* $S_{Li\,Li}(Q)$, *заполненные и незаполненные кружочки -* $S_{N\,N}(Q)$ *для концентраций 1,3 и 3,5 ат.% соответственно.*

На спектрометре ДИН-2ПИ выполнен нейтрон-дифракционный эксперимент по исследованию микроструктуры расплавов Li–N с концентрацией примеси азота 1.3 и 3.5 ат.% и температуре 823 К. Получена основная микроструктурная характеристика вещества –

полный структурный фактор $S(Q)$, а также парциальные структурные факторы $S_{\alpha\beta}(Q)$ компонент расплава и соответствующие функции радиального распределения $g_{\alpha\beta}(r)$ и $g_{CC}(r)$ **(Рис. 5).** Установлено, что при концентрации примесного компонента менее 4 ат.% в структурном факторе расплавов Li–N отсутствует так называемый «предпик», который является признаком существования в расплаве кластеров определенного размера. Анализ парциальных структурных характеристик расплава дает основание предположить, что примесь азота присутствует в расплавах $Li_{0.987}N_{0.013}$ и $Li_{0.965}N_{0.035}$ в форме нитрида лития $Li_3N$.

Сотрудниками группы малоуглового рассеяния нейтронов завершен цикл работ, который подводит итог почти 20-летним дебатам по одной из ключевых проблем статистической физики - взаимодействию флуктуирующих случайных поверхностей. К случайным флуктуирующим поверхностям принадлежит широкий класс объектов: от биологических мембран до струн в современной теории поля. Это является одной из причин внимания современной теоретической физики к биологическим мембранам, в частности, к липидным мембранам. В результате были развиты новые подходы для исследования межмембранных взаимодействий и определения универсальной константы, основанные на исследовании температурной зависимости межмембранных взаимодействий с помощью комплементарного использования малоуглового рассеяния тепловых нейтронов и дифракции высокого разрешения на синхротронном источнике. Получено значение константы взаимодействия равное $3\pi^2/256$, совпадающее с теоретически предсказанным. Показано также, что переход от мультислойных к одиночным мембранам происходит в соответствии с теоретически предсказанной моделью двух состояний. Кроме того, впервые показано, какова истинная величина ондуляционных сил - они действительно вносят значительный вклад в баланс межмембранных взаимодействий и, более того, эти силы становятся доминирующими на расстояниях больше 20 Å.

Впервые исследована динамика кристаллической решетки суперионного проводника AgCuSe методом неупругого рассеяния нейтронов. В низкотемпературной фазе обнаружены низкоэнергетические моды, которые, по всей видимости, имеют природу акустических фононов. Плотность фононных состояний $G(\varepsilon)$ в $\alpha$- и $\beta$- AgCuSe характеризуется недебаевским поведением. При переходе от $\beta$ к $\alpha$ фазе наблюдается размытие спектра плотности фононных состояний и ужесточение спектра в целом.

**Главные методические результаты.** В 2005 г. продолжались методические работы по модернизации комплекса спектрометров реактора ИБР-2. В основном они затрагивали детекторные системы спектрометров. В частности, на специализированном фурье-дифрактометре ФСД продолжалась комплектация детекторной системы (готовы 6 из 14 детекторных модулей), проведены пробные заполнения двумерного детектора для ЮМО, испытан в реальных условиях однокоординатный ПЧД с разрешением 1.8 мм.

# 1.2. НЕЙТРОННАЯ ЯДЕРНАЯ ФИЗИКА

**Введение**

В течение 2005 основные работы в области нейтронной ядерной физики в ЛНФ им. И. М. Франка проводились на реакторе ИБР-2, установке ЭГ-5, на нейтронных пучках других ядерных центров России, Болгарии, Польши, Чехии, Германии, Республики Корея, Китая, Франции, США, и Японии. Исследования проводились в традиционных направлениях: изучение процессов нарушения пространственной и временной четности при взаимодействии нейтронов с ядрами; изучение квантово-механических характеристик, энергетики и динамики процесса деления; экспериментальное и теоретическое исследование электромагнитных свойств нейтрона и его бета-распада; гамма-спектроскопия нейтронно-ядерных взаимодействий; структура атомного ядра; получение новых данных для реакторных приложений и для ядерной астрофизики; эксперименты с ультрахолодными нейтронами; прикладные исследования.

**1. Экспериментальные исследования**

***1.1. Нарушение пространственной и временной четности при взаимодействии нейтронов с ядрами***

***1.1.1 Поиск и исследование структуры подпороговых нейтронных p-резонансов на изотопах свинца методом комбинированной корреляционной гамма-спектроскопии***

Были продолжены работы в направлении поиска и исследования структуры подпороговых нейтронных p-резонансов на изотопах с массовым числом A=(80-130) методом корреляционной гамма-спектроскопии высокого разрешения.

С целью проверки полученных ранее экспериментальных результатов по поиску отрицательного нейтронного p-резонанса изотопов свинца проведена реконструкция гамма-спектрометра COCOS на канале №1 реактора ИБР-2. В результате включения в состав спектрометра вновь приобретённого полупроводникового детектора гамма-квантов GMX30-PLUS и специализированных электронных блоков возросла эффективность спектрометра более чем в два раза, и увеличилось его быстродействие.

На реконструированном гамма-спектрометре проводились эксперименты по поиску отрицательного нейтронного p-резонанса у изотопов свинца: проведены две серии измерений на естественной смеси изотопов свинца.

***1.1.2. Подготовка к исследованию T-неинвариантных эффектов в нейтронно-ядерных взаимодействиях***

В 2005 году в секторе поляризованных мишеней продолжались работы по исследованию образцов для проверки T-неинвариантности в ядерных взаимодействиях. Исследовались два монокристалла алюмината лантана LaAlO3 с парамагнитной примесью Nd3+: 0.3% и 0.08% полученные из Японии. Уверенно наблюдались усиленные ЯМР сигналы на обоих кристаллах. Наблюдалось также перемещение ЯМР линий La и Al при вращении кристалла в магнитном поле. К сожалению, оказалось невозможным, с приемлемыми затратами времени, наблюдать терморавновесные сигналы. Это объясняется тем, что для ядер кристалла, по сравнению с водородной мишенью, их концентрация в два-три раза меньше и разность заселенности соседних уровней меньше в 7 и 5 раз, соответственно.

В настоящее время продолжается модернизация Q-метра. Ожидается улучшение аппаратурной чувствительности, по крайней мере, на порядок.

### *1.1.3. Создание поляризованной протонной мишени*

Завершено создание поляризованной ядерной мишени. Ядра поляризуются методом «грубой силы». Для этого был создан криостат растворения $^3$He в $^4$He со сверхпроводящим магнитом.

Проведено стендовое испытание криостата с магнитом. Получены следующие параметры:

- минимальная температура на образце T = 23 мК;
- напряженность магнитного поля H = 5,8 T при однородности поля в центре магнита $\Delta H/H = 10^{-4}$.

Завершена перевозка и монтаж поляризованной ядерной мишени на канале № 1 ИБР-2 и тем самым завершено создание установки «Колхида», предназначенной для исследования взаимодействия поляризованных нейтронов с поляризованными ядрами. Для установки разработана новая программная система регистрации данных, позволяющая выполнять: в автоматическом режиме измерения для ряда точек в диапазоне токов поляризующего магнита; необходимые операции в интерактивном режиме работы; визуализацию экспериментальных данных; автоматический контроль качества экспериментальных данных; необходимые тесты оборудования и программ.

В данный момент ведутся пусковые работы установки «Колхида» на канале № 1 ИБР-2. Начало экспериментов по ядерной прецессии (ядерному псевдомагнетизму) запланировано в первом квартале 2006 г.

### *1.1.4. Статус проекта KaTRIn. Методика измерения ядерного псевдомагнетизма*

В 2005 г. совместно с коллегами из КЕК (Япония) была создан прототип установки для исследования ядерного псевдомагнетизма. Схематически она показана на **рис.1**.

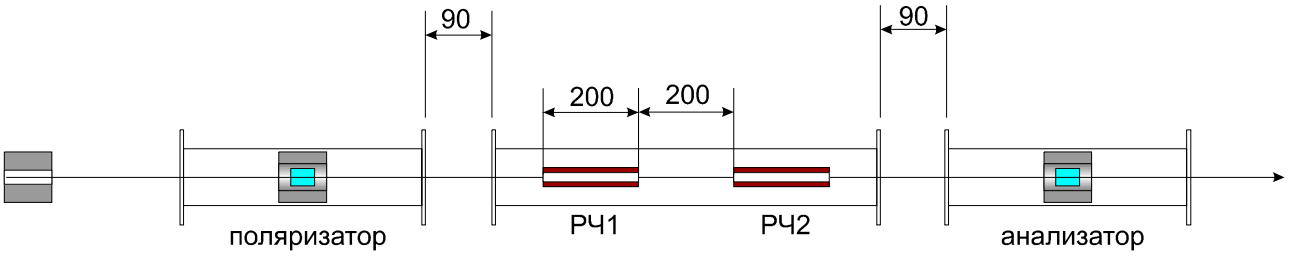


***Рис.1**. установка для исследования ядерного псевдомагнетизма. Размеры в мм*

Установка собрана на пучке Н-8 источника KENS и включает нейтронный поляризатор и анализатор нейтронной поляризации. Оба устройства выполнены на основе ячеек $^3$He с оптической накачкой. Между поляризатором и анализатором установлен соленоид, внутри которого расположены две скрещенные радиочастотные катушки, разделенные промежутком. После прохождения поляризатора, нейтронная поляризация $P_1$ направлена вдоль оси пучка. Радиочастотные катушки позволяют производить поворот вектора нейтронной поляризации в произвольном направлении и на произвольный угол.

Если ведущее поле в большом соленоиде равно $H_0$, а катушка создает *осциллирующее* поле $2H_1 \cos wt$, то эффективное поле во вращающейся системе координат, которое «видит» нейтрон есть:

$$H = H_0 - w/\gamma + H_1,$$

где $\gamma$ - гиромагнитное отношение для нейтрона. Далее, если подобрать частоту радиочастотного поля так, что она равна ларморовской частоте нейтрона в поле $H_0$, то

получим оптимальное условие $H = H_1$. Значит, чтобы при пролете через катушку за время $t_R$ повернуть вектор нейтронной поляризации, например на $\pi/2$, нужно выполнить условие: $\gamma H_1 t_R = \pi/2$.

Разумеется, $t_R$ зависит от энергии нейтрона, но амплитуду $H_1$ можно модулировать так, чтобы условие выполнялось для нейтронов в желаемом диапазоне энергий. После пролета через первую катушку, нейтрон проходит промежуток между катушками за время $t_P$, при этом вектор поляризации вращается с ларморовской частотой $w_0 = \gamma H_0$, а соответствующий угол поворота в плоскости перпендикулярной направлению движения: $\phi = w_0 t_P$. Теперь, если правильно синхронизовать работу обеих катушек, то можно вернуть вектор нейтронной поляризации к прежнему направлению вдоль оси пучка при пролете нейтронов через вторую катушку: $P_2 = P_1$. Если же поместить между катушками некий материал, который создает дополнительное поле вдоль оси пучка, то фаза, которую нейтрон приобретает при пролете между катушками, уже не будет равна $w_0 t_P$. Значит, после прохождения второй катушки, величина нейтронной поляризации будет отличаться от рассмотренного случая, т.е., $P_2 \neq P_1$. По величине и энергетической зависимости этого отклонения можно определить величину дополнительного поля создаваемого этим материалом.

Вторая реализация данной методики – использовать *вращающееся* поле вместо *осциллирующего*, т.е., вместо одной пары витков в каждой катушке использовать скрещенные пары, чтобы создать ортогональные поля $H_1 \cos wt$ и $H_1 \sin wt$. Все остальное рассмотрение остается без изменений. Использование *вращающегося* поля позволяет уменьшить амплитуду РЧ-поля в 2 раза, что снижает требования к мощности РЧ-усилителей.

Таким образом, методика измерения псевдомагнетизма представляет собой два последовательных измерения нейтронной поляризации, когда исследуемое вещество не поляризовано и поляризовано вдоль оси пучка. Были проведены исследования свойств созданной установки и последовательные измерения нейтронных времяпролетных спектров с выключенными и включенными РЧ-катушками и определены их отношения. На **рис.2** приведены некоторые примеры таких отношений. Красные линии – расчет (не подгонка).

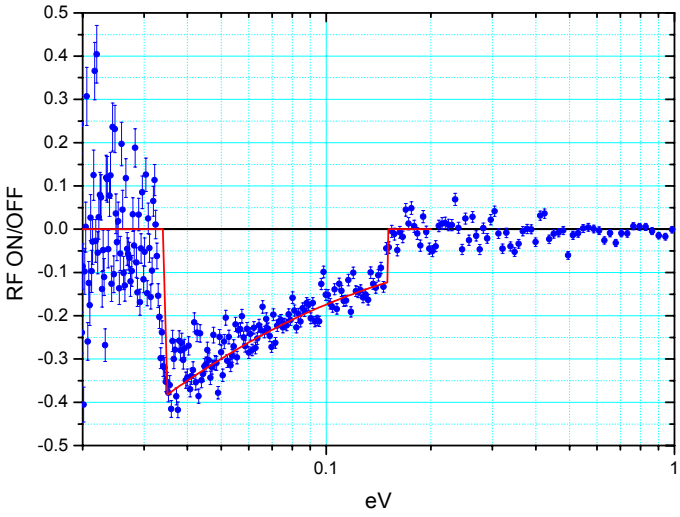


***Рис.2а.*** *Первая РЧ катушка в режиме спин флиппера (поворот нейтронной поляризации на $180^0$). Вторая катушка выключена. Вращающееся поле*

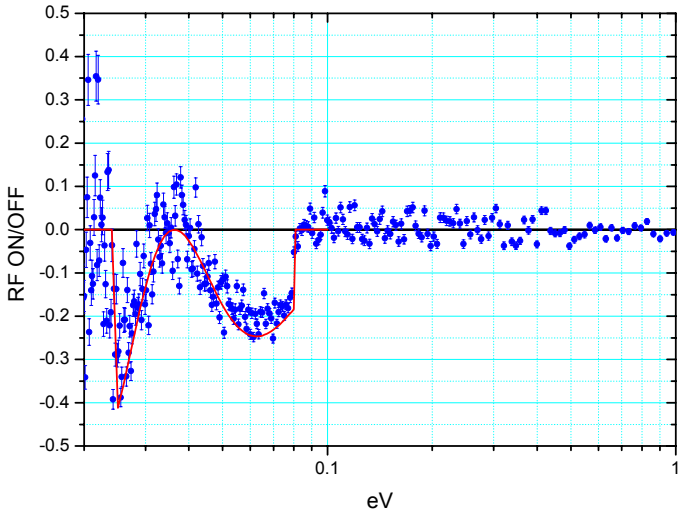


***Рис.2б***. *Обе катушки катушка в режиме поворота нейтронной поляризации на $90^0$. Фаза поля во второй катушке модулируется от 0 до $2\pi$ в диапазоне 0.025-0.08 эВ. Осциллирующее поле*

Обе катушки состоят из двух пар скрещенных колец по 10 витков каждая. Амплитуда радиочастотного поля ограничивается выходной мощностью РЧ-усилителя и не превышает 5 Гс. Величина ведущего поля большого соленоида 20 Гс, т.е, рабочая частота $w = w_0 \approx 60$ кГц.

Ячейки с $^3$He содержали 2.8 атм каждая, степень поляризации $^3$He была 54% для поляризатора и 24% для анализатора. Амплитуда $H_1$ модулировалась по закону $1/t_R$ с помощью программируемых синтезаторов (Arbitrary Waveform Generator). В дальнейшем, для имитации псевдомагнитного поля мы намерены поместить между катушками маленький соленоид и измерять отношения времяпролетных нейтронных спектров, когда этот соленоид выключен и включен. Кроме того, мы собираемся изготовить несколько меньшие РЧ-катушки и увеличить поле $H_1$, увеличив число витков до 15 в каждой скрещенной паре.

Методика также может быть использована при исследовании пара- и ферромагнитных веществ.

### *1.1.5. Исследования нарушения четности в малонуклонных системах*

**Поиски P-нечетного эффекта вылета тритонов в реакции $^6$Li(n,α)$^3$H**

В рамках экспериментов по поиску нейтральных токов в нуклон-нуклонных взаимодействиях и определению слабой π-мезонной константы связи на пучке холодных поляризованных нейтронов PF1B (ИЛЛ, Гренобль) проведен очередной 48 суточный сеанс измерений P-нечетной асимметрии ($\boldsymbol{\sigma}_n\mathbf{p}_t$) вылета тритонов в реакции $^6$Li(n,α)$^3$H ($\boldsymbol{\sigma}_n$ – спин нейтрона, $\mathbf{p}_t$ – импульс тритона). В качестве детектора тритонов использовалась 48-секционная ионизационная камера с 24 мишенями $^6$LiF, поглощавшими более 60% нейтронного потока (**рис.3**). Применялся интегральный (токовый) метод регистрации событий, техника компенсации флуктуаций мощности реактора и методика с периодическим переключением ведущего нейтронный спин магнитного поля на образцах для устранения возможных ложных эффектов. Результат с учетом поправок на поляризацию нейтронов и угла вылета тритонов $\alpha_t$ = -(9.3±2.5)·10$^{-8}$. Был проведен также ряд контрольных

экспериментов. По сумме результатов трех циклов наблюдается явный эффект в основных измерениях $\alpha_t = -(8.6\pm2.0)\cdot10^{-8}$.

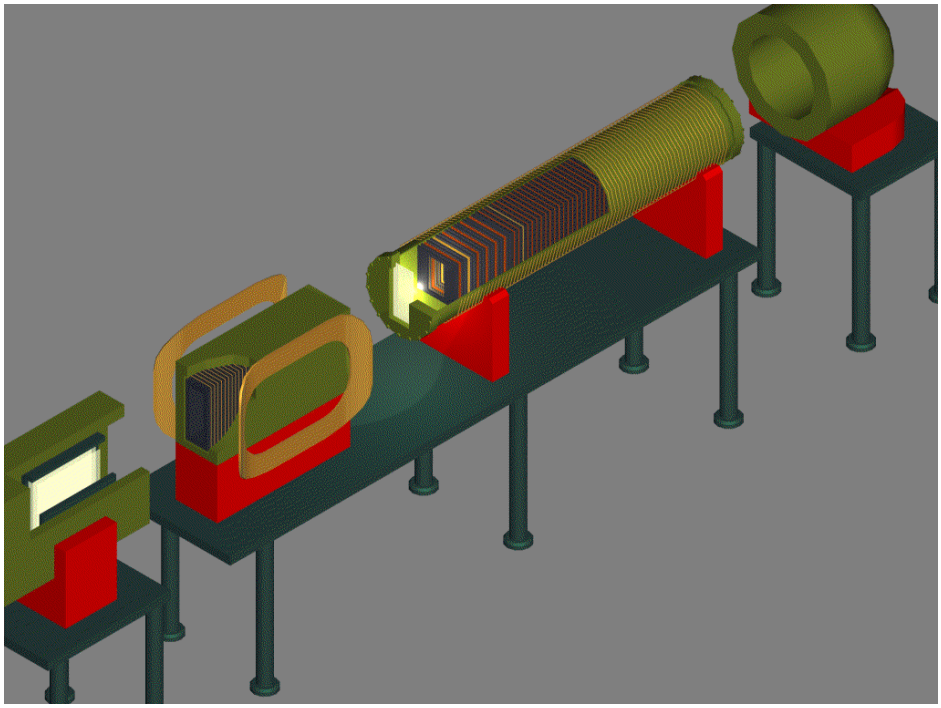

***Рис. 3.*** *Схема эксперимента: (слева-направо) поляризатор, РЧ-спин-флиппер с катушками ведущего поля, многосекционная ионизационная камера, бим-стоп*

**Подготовка измерения асимметрии γ-квантов в реакции np→dγ**

Коллаборацией NPDG с участием сотрудников ЛНФ проведены работы по проверке оборудования канала PF12 нейтронного источника LANSCE (Лос-Аламос) и аппаратуры для эксперимента по измерению P-нечетной асимметрии γ-квантов в реакции np→dγ с целью определения слабой π-мезонной константы связи.

### *1.2 Вынужденное и спонтанное деление*

#### *1.2.1 Измерение выхода запаздывающих нейтронов на реакторе ИБР-2*

На канале №11-Б реактора ИБР-2 завершена модернизация установки «Изомер» с целью развития работ по получению данных о выходах и постоянных распада групп запаздывающих нейтронов в делении минорных актинидов. В результате модернизации были улучшены параметрами установки и расширены её возможности. Для установки разработаны программы: управления перемещением Cd-фильтра; синхронизации процесса измерения данных с изменением условий регистрации; сортировки файлов данных на группы по условиям регистрации; вычисления времени экспозиции и пр.

Были проведены измерения на модернизированной установке и получены данные о выходе запаздывающих нейтронов при делении изотопа $^{237}$Np тепловыми нейтронами.

#### *1.2.2 Измерение множественности нейтронов в нейтронно-индуцированном делении $^{239}$Pu*

В 2005 году продолжались экспериментальные исследования индуцированного резонансными нейтронами деления ядер Плутония-239 и Урана-235. Результаты

исследований были доложены на международных конференциях, проведенных в России, Франции и США в 2005 году.

Эксперименты по измерению флуктуаций Полной Кинетической Энергии (ПКЭ) при вынужденном резонансными нейтронами делении урана-235 были выполнены в 1996-2000 на ИБР-30. Такие флуктуации были обнаружены в 1990 году в Бельгии на установке ГЕЛИНА и хорошо коррелировали с зависимостью флуктуаций множественности мгновенных нейтронов деления от энергии резонансных нейтронов, обнаруженных в начале 1970-х годов для ядер урана и плутония. Однако статистическая точность данных, полученных в Бельгии, была невысока из-за слабой интенсивности потока резонансных нейтронов, поэтому требовалось независимое подтверждение результатов с большей статистикой. В экспериментах, выполненных на ИБР-30, статистическая точность измерений была повышена боле, чем в 10 раз и полученные результаты очень хорошо совпали с результатами, полученными в Бельгии. Помимо этого была модифицирована процедура анализа экспериментальных данных с использованием более точных формул для фитирования данных, полученных в работах Брозы, Мюллера и Гроссмана. Результаты, полученные в Дубне, убедительно доказали наличие флуктуаций ПКЭ осколков деления в резонансной области энергий налетающих нейтронов, которые пока не удается полностью объяснить в рамках существующих теоретических моделей деления ядер при низких энергиях.

На установке GELINA (IRMM, Бельгия) проводятся совместные эксперименты по исследованию индуцированного резонансными нейтронами деления ядер $^{239}$Pu, флуктуаций множественности мгновенных нейтронов и полной кинетической энергии осколков деления. Эта работа выполняется с применением современных методов цифровой обработки сигналов, когда форма импульсов, как с детекторов нейтронов, так и с камеры деления в преобразуется цифровую последовательность, которая запоминается и анализируются в режиме off-line. Полученные предварительные результаты показывают, что применение цифровой обработки сигналов позволяет качественно изменить и саму процедуру измерений

### *1.2.3 Исследование массово-энергетических характеристик продуктов двойного и тройного деления*

На ускорителе К-130 в г.Ювяскюля (Финляндия) при участии сотрудников ЛНФ проведен многопараметрический эксперимент по измерению массово-энергетических распределений осколков деления $^{238}$U, индуцированного а-частицами. Установка позволяла регистрировать время пролета и энергию каждого осколка, что позволяло определить их массы независимым образом. Осколки деления регистрировались двумя мозаиками из кремниевых PiN-диодов, расположенными на расстоянии около 0,5 м от мишени. В качестве стартового детектора использовалась микроканальная пластинка, расположенная в непосредственной близости от мишени. Ведется обработка данных с целью поиска истинно тройного коллинеарного распада в делении. Началась подготовка к проведению аналогичного эксперимента по измерению нейтронно-индуцированного деления на пучке 6б реактора ИБР-2 с использованием детекторов «Мини-Фобос» совместно с ЛЯР.

Также в г.Ювяскюля (Финляндия) был проведен эксперимент по измерению полного энергетического спектра альфа-частиц в тройном спонтанном делении $^{252}$Cf. Как и в первом эксперименте, использовались мозаики из кремниевых PiN-диодов – в этом случае для регистрации легких заряженных частиц. Идентификация частиц проводилась методом TOF-E. В качестве стартового детектора также использовалась микроканальная пластинка, реагирующая на один из осколков деления, а для уменьшения фона был установлен дополнительный кремниевый детектор, регистрирующий второй осколок деления и включенный в схему совпадения со стартовым детектором. В качестве первого результата был получен полный энергетический спектр $\alpha$-частиц с нижней границей ~1 МэВ. Наблюдено отклонение формы спектра от Гауссовского распределения в

низкоэнергетической области. Предварительные оценки показывают, что такое отклонение не может быть полностью объяснено испусканием нейтронно-нестабильных ядер 5He, которые после распада идентифицируются как α-частицы.

### *1.2.4 Изучение вибрационных резонансов в делении*

В течение 2005 г. проводилась обработка данных экспериментов по программе коллаборации nTOF – изучение природы вибрационных резонансов в делении, индуцированном нейтронами и получение сечений деления для решения проблем ADS-систем и сжигания ядерных отходов.

### *1.3 Гамма-спектроскопия нейтронно-ядерных взаимодействий*

Из измеренных к настоящему времени в 51 ядре ($27<A<201$) интенсивностей двухквантовых каскадов между нейтронным резонансом и низколежащими уровнями составного ядра извлечены данные по плотностям уровней и силовым функциям первичных гамма-переходов. Это сделано для интервала энергии возбуждения ядра шириной от ~5 до ~9 МэВ. Такие данные впервые получены без привлечения любых ядерных моделей или непроверяемых гипотез. Найденные таким образом плотности уровней и радиационные силовые функции имеют значительно (практически - на порядок) меньшие систематические погрешности, чем любые имеющиеся аналогичные данные.

Лучшая точность позволила наблюдать сильное влияние структуры ядра на эти основные параметры его каскадного гамма-распада. Так, экспериментальные значения плотности уровней и в сферических, и в деформированных ядрах любой массы очень хорошо воспроизводятся суммой парциальных плотностей уровней, соответствующих разрыву до 5-ти куперовских пар нуклонов и возбуждению в ядре до 10-ти квазичастиц в сочетании с возбуждениями вибрационного типа. Доля последних в районе половины энергии связи нейтрона в 10-20 раз превышает долю чисто квазичастичных возбуждений.

Полученные результаты открывают новые возможности для экспериментального и теоретического изучения взаимодействия и взаимоперехода в ядре возбуждений фермионного и бозонного типов. Прежде всего - появилась реальная возможность практического определения корреляционных функций индивидуальных куперовских пар нуклонов при различных энергиях возбуждения ядра. Очень большие и принципиально неустраняемые систематические погрешности экспериментального определения плотности уровней исключают возможность получения достоверной информации об указанных параметрах ядра иными, разработанными к настоящему времени методиками.

### *1.4 Исследование реакций (n,p) и (n,α)*

**Угловые корреляции в (n,p) реакции**

Продолжались работы по исследованию угловых корреляций в реакции $^{14}N(n,p)^{14}C$. Проведена теоретическая оценка эффектов асимметрии в реакции $^{14}N(n,p)^{14}C$ в рамках модели смешивающих компаунд-состояний ядра (**рис. 4**). Проанализирован вклад резонансов в область энергии нейтронов до одного МэВ, а также влияние фаз на энергетический ход коэффициентов асимметрии (вперед-назад,, лево-правой и несохранение четности). Расчеты дают величины коэффициентов асимметрии вперед-назад и лево-правой порядка $10^{-1}$ и $10^{-2}$ , соответственно. Коэффициент корреляции, несохраняющей четность, получен на несколько порядков меньше имеющейся экспериментальной оценки.

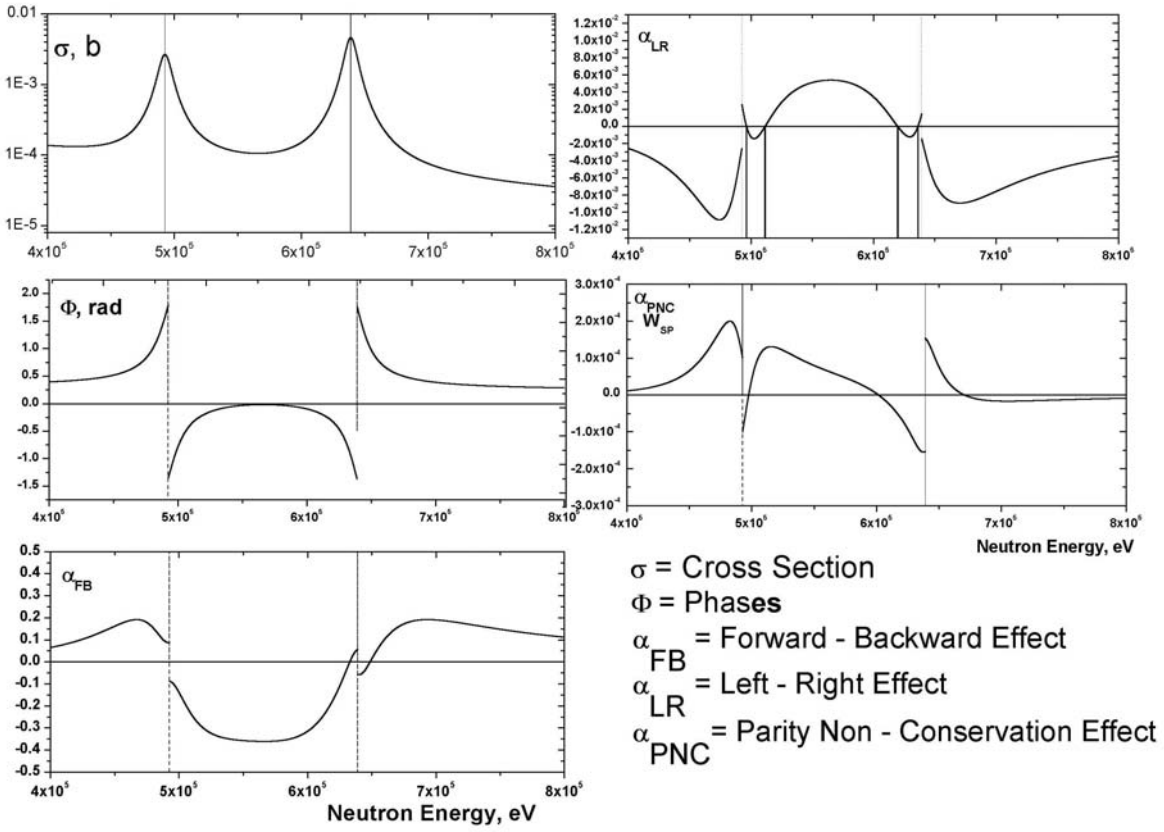


***Рис. 4***

Для дальнейшего экспериментального изучения Р-четных эффектов асимметрии на неполяризованных нейтронах проведен ряд работ по переоборудованию канала на ЭГ-5. В частности, смонтирован поворотный стол, позволяющий поворачивать детектор заряженных частиц как вокруг своей оси (необходимо для измерений собственно коэффициента вперед-назад), так и смещать детектор относительно нейтронной мишени, выводя его из прямого пучка нейтронов (для измерений фона).

На установке ЭГ-5 ЛНФ проведены исследования реакции $^{20}Ne(n,\alpha)^{17}O$. Нейтроны производились в реакции $D(d,n)^3He$ с использованием газовой дейтериевой мишени при энергии дейтронов $E_d \approx 2$ МэВ. Получаемый при этом диапазон энергий нейтронов $E_n$=3.7 – 4.1 МэВ охватывал группу нейтронных резонансов $^{20}Ne$. Регистрация и спектрометрия α-частиц осуществлялась с помощью двухсекционной ионизационной камеры с сеткой и электронной системой сбора многомерной информации. Объектом исследования служил газ Ne, наполняющий камеру. Обнаружены некоторые несоответствия между полученными данными и рекомендуемыми в нейтронных атласах положениями резонансов для этой реакции. Планируется продолжить дальнейшие исследования с использованием твердых дейтериевых мишеней в качестве источника нейтронов с целью уменьшения этого разброса.

Проводятся работы по конструированию новой газовой дейтериевой мишени, а также изготовлению литиевой мишени и приобретению тритиевой мишени. Эти мишени необходимы для получения на установке ЭГ-5 нейтронов в широком диапазоне энергий.

Совместно с сотрудниками Пекинского университета на ускорителе ЭГ-4.5 в Институте физики тяжелых ионов при Пекинском университете, Китай, проведены измерения сечения реакций $^{64}Zn(n,\alpha)^{61}Ni$ и $^{10}B(n,\alpha)^7Li$. Источником нейтронов являлась $D(d,n)^3He$ реакция на газовой дейтериевой мишени. В ходе измерений использовались энергии нейтронов $E_n$=4, 5, 6 МэВ. В качестве детектора α-частиц применялась

двухсекционная ионизационная камера с сеткой. Полученная многомерная информация находится в стадии обработки.

### *1.5 Фундаментальные свойства нейтрона*

#### *1.5.1. Исследование n-e рассеяния*

Разработанный в НЭОФЯ ЛНФ и описанный в трех публикациях 2003 – 2005 г.г. новый метод извлечения длины n,e-рассеяния $b_{ne}$ из данных по дифракции нейтронов на благородных газах был применен для обработки цифровых данных по дифракции нейтронов с длиной волны ~0,7Å. Эти данные, полученные в Гренобле и присланные в Дубну, содержали наборы структурных факторов $S(q)$ для газообразного изотопа $^{36}$Ar четырех разных плотностей в диапазоне переданного волнового вектора $q$ до ~10 Å$^{-1}$ и для семи разных состояний сжиженного Kr в диапазоне $q$ до ~16 Å$^{-1}$.

Экспериментальные значения $S(q)$, исправленные авторами на всевозможные искажающие эффекты, кроме n,e-рассеяния, описывались дифракционной затухающей синусоидой с добавлением к ней монотонного с $q$ вклада от n,e-взаимодействия.

В случае $^{36}$Ar фактически получен результат «нуль-эксперимента», поскольку у него вклад n,e-рассеяния составляет менее 0,2% от ядерного, тогда как естественный аргон имеет n,e-вклад ~1,9%. Два математически разных подхода к решению этой многопараметрической задачи дали такие результаты:

$$b_{ne} = -(1{,}33 \pm 0{,}28 \pm 0{,}57) \cdot 10^{-3} \text{ Фм},$$
$$b_{ne} = -(2{,}15 \pm 0{,}49) \cdot 10^{-3} \text{ Фм},$$

хотя и малой точности, но значащие.

Предварительный результат еще не законченного анализа данных по Kr таков:

$$b_{ne} = -(1{,}35 \pm 0{,}03) \cdot 10^{-3} \text{ Фм},$$

что уже выходит на уровень лучших по точности экспериментальных результатов.

С целью существенно улучшить точность извлекаемого значения $b_{ne}$ разрабатывался новый эксперимент для той же установки в Гренобле, где получались уже данные по $^{36}$Ar и Kr. Суть эксперимента заключается в проведении измерений с Ar, Kr и Xe поочередно с такими же измерениями с $^{36}$Ar в качестве «нормировочных».

Продолжалась работа по изготовлению установки для измерения $b_{ne}$ путем рассеяния медленных нейтронов газами Ar, Kr и Xe низкого давления (~1 атм.) с использованием метода времени пролета на нейтронных источниках в г.Троицке и на ИРЕН-1. Осталось изготовить только поворотно-юстировочное устройство.

#### *1.5.2 Эксперимент по прямому измерению сечения рассеяния нейтрона на нейтроне*

Продолжаются работы по подготовке эксперимента по прямому измерению сечения рассеяния нейтрона на нейтроне на реакторе ЯГУАР (РФЯЦ-ВНИИТФ, г.Снежинск). Для проверки правильности расчетов и выбора оптимального варианта защиты под реактором в 2004-ом году было выполнено тестовое измерение.

В 2005-ом году были проведены измерения на нейтронной установке Физико-Энергетического Института (Обнинск) для нейтронных детекторов, использованных в тестовых измерениях на ЯГУАРе. Проведенные калибровки позволили сравнить результаты

измерений фонов с расчётами. Измерения проводилось в трёх разных геометриях коллимационной системы. Наибольший интерес представляет измерение с геометрией №3. В этом случае фон быстрых нейтронов на дне шахты должен быть близок к фону в случае полномасштабной установки. На **рис. 5** приведены результаты расчётов и измерений для данного случая.

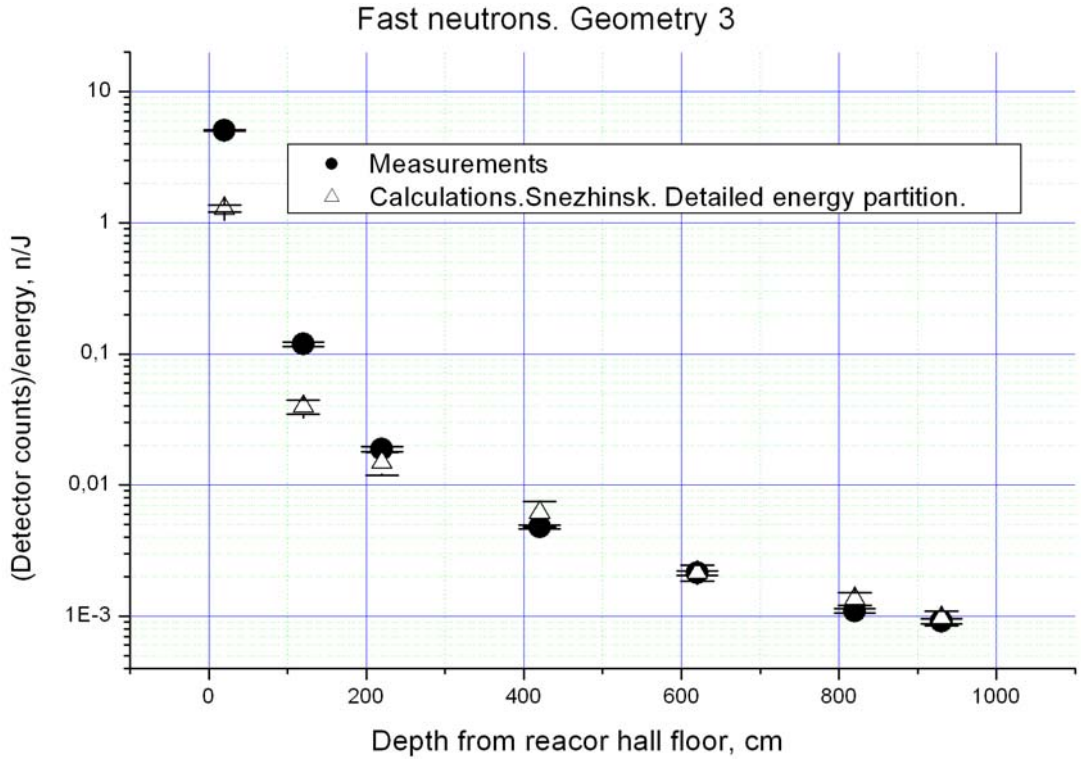


***Рис. 5***

Как видно из рис. 5 результаты расчётов группы из Снежинска на глубинах более 2 м полностью совпадают с результатами измерений (отклонение на малых глубинах связано с точностью описания геометрии защиты на уровне пола).

Таким образом, тестовые измерения показывают высокую степень достоверности проводимых расчётов. Расчёты фонов в полной геометрии эксперимента показали, что выбранная геометрия установки (**рис. 6**) позволит провести измерения сечения nn-рассеяния без доминирующей роли фона.

На здании реактора ЯГУАР (г.Снежинск) установлена задняя пролётная база экспериментальной установки (**рис. 7**).

Создан рабочий проект полной экспериментальной установки. В цехе опытного экспериментального производства ЛНФ ведутся работы по изготовлению нижней части установки. Проводится тестирование вакуумного оборудования

В 2006 году планируется закончить изготовление экспериментальной установки, провести её монтаж и наладку на реакторе ЯГУАР (г. Снежинск), осуществить калибровочные измерения - рассеяние нейтронов на инертных газах.

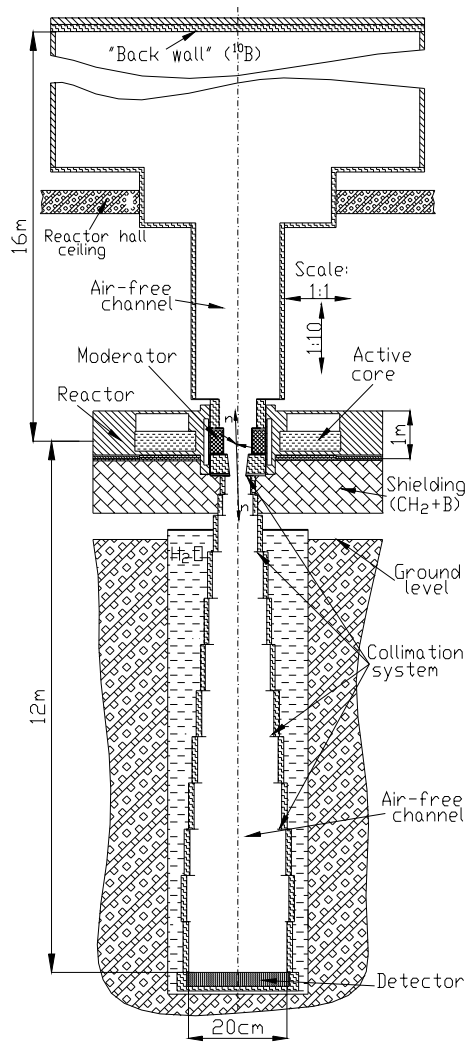


***Рис. 6***

***Рис. 7***

### *1.6 Физика ультрахолодных нейтронов, нейтронная оптика*

#### *1.6.1 Изучение взаимодействия холодных и очень холодными нейтронов с наноструктурами*

Данное исследование было инициировано работой, в которой высказывалась идея создания устройства для термолизации холодных нейтронов в область ультрахолодных. Для этой цели предлагалось использовать слабосвязанные наночастицы в сверхтекучем гелии. Первым шагом к экспериментальному изучению возможности реализации подобного источником должно было стать измерение сечения рассеяния нейтронов (наибольшую информацию содержит дважды дифференциальное сечение рассеяния) с наноструктурными объектами.

Для исследования взаимодействия нейтронов с наноструктурами и изучения возможности эффективного охлаждения очень холодных и холодных нейтронов в область ультрахолодных было разработано и изготовлено экспериментальное оборудование: гелиевый криостат (изготовлен в ИФТТ РАН, Черноголовка), селектор скоростей нейтронов

(для работы со скоростями 30÷180 м/с), 2π-детектор холодных нейтронов (изготовлены в ЛНФ ОИЯИ, Дубна).

На **рис. 8** представлен внешний вид 2π-детектора окружающего образец, а на **рис. 9** внешний вид гелиевого криостата.

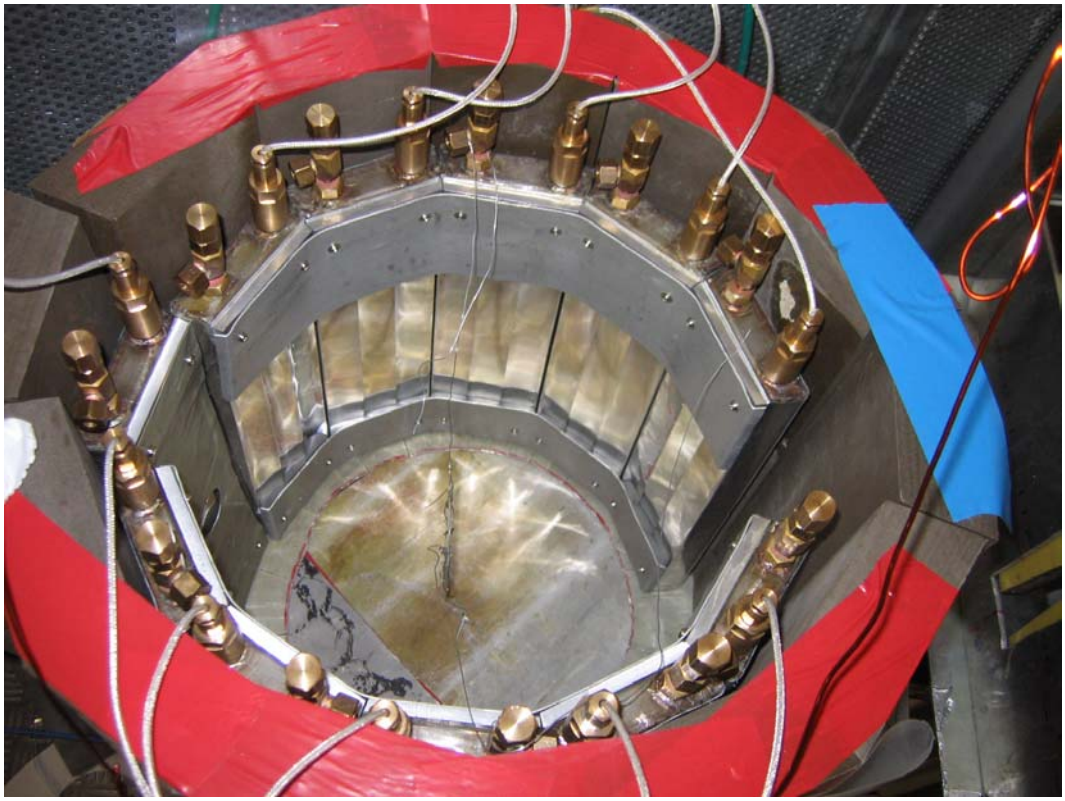

***Рис. 8***

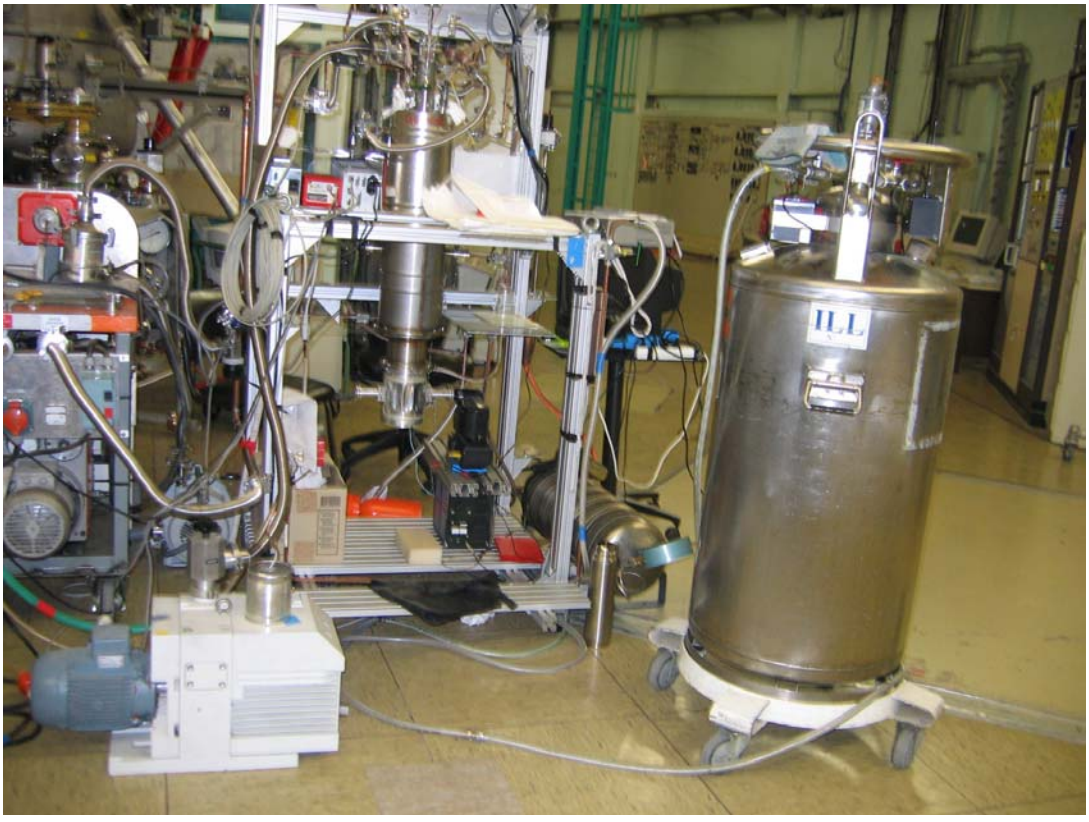


***Рис. 9***

Измерения проводились на пучках PF1b и PF2 высокопоточного реактора ИЛЛ (Гренобль). Измерялась вероятность рассеяния нейтронов со скоростями от 30 м/с до 1000 м/с в зависимости от угла рассеяния на структуре слабосвязанных наночастиц $D_2O$ и $D_2$, находящихся в сверхтекучем гелии («жели») и на образцах наноалмазных порошков. Измерения с образцами «жели» показывают, что вероятность рассеяния нейтронов на образцах достаточно велика и если процессы передачи энергии от нейтрона к образцу идут достаточно интенсивно, то «жель» можно использовать для охлаждения очень холодных и холодных нейтронов в область ультрахолодных. Полученного экспериментального материала достаточно для проверки правильности теории диффузии нейтронов в мелкодисперсной и нанодисперсной среде. Результаты также показывают, что нанодисперсные материалы, такие как наноалмазный порошок, могут использоваться как эффективные отражатели холодных и очень холодных нейтронов при создании источников таких нейтронах и при решении других экспериментальных задач.

На **рис. 10** представлены типичные экспериментальные зависимости счёта секций 2π-детектора при различных энергиях нейтронов и для различных образцов.

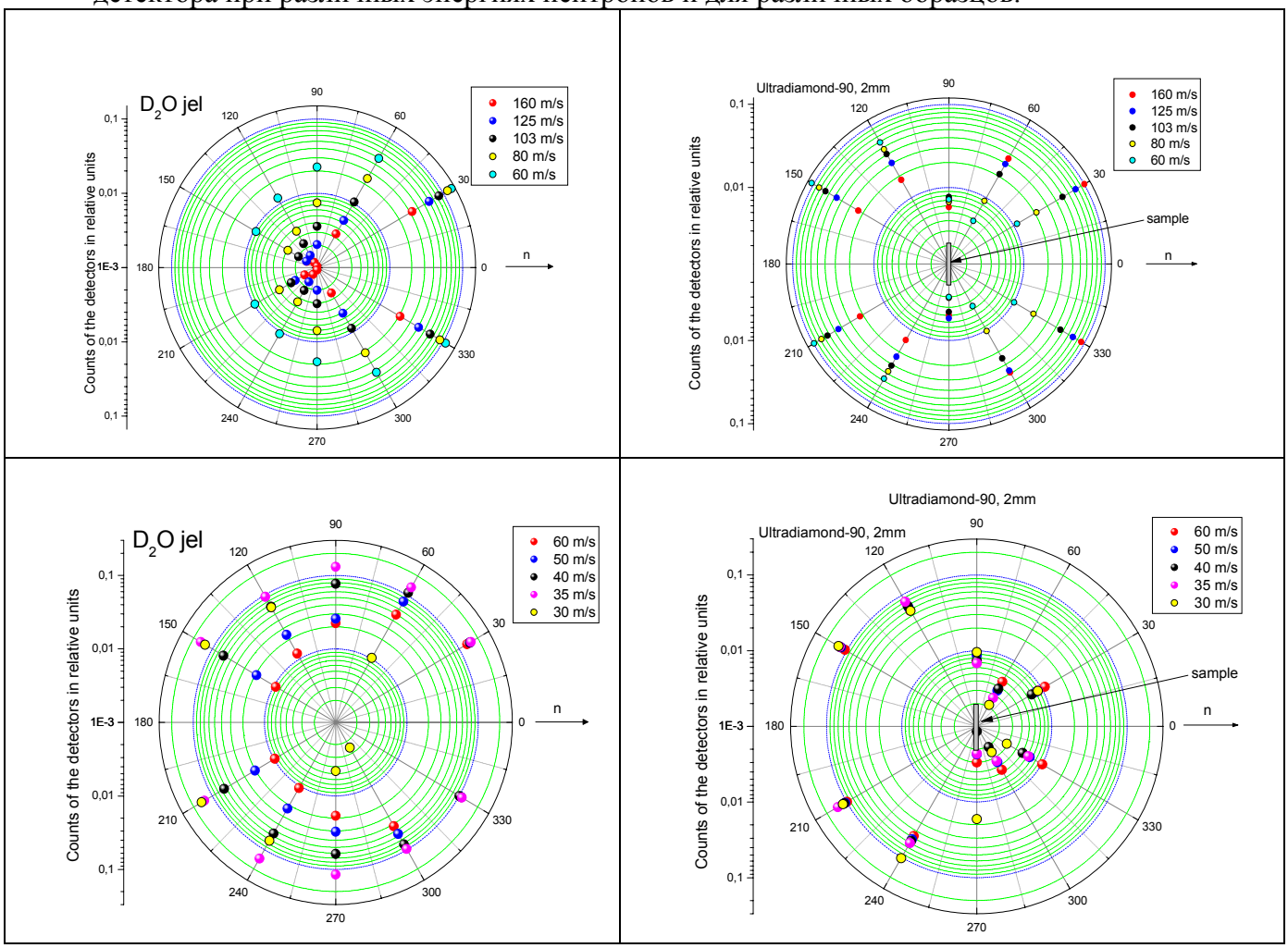


***Рис. 10***

### *1.6.2 Оптика ультрахолодных нейтронов*

Выполнен новый эксперимент по наблюдению изменения энергии нейтрона при прохождении через ускоренное вещество. Существование эффекта следует из справедливости принципа эквивалентности и детальных нейтронно-оптических расчетов. Обработка результатов еще не закончена, однако можно с уверенностью утверждать, что

указанный эффект впервые наблюден в опыте. Чтобы проиллюстрировать всю сложность эксперимента можно указать, что изменение энергии нейтрона, зарегистрированное в опыте составляло величину порядка $2\times10^{-10}$ эВ. При этом образец – кремниевая пластина, двигался со знакопеременным ускорением, достигавшем величины 7.5g. Соответствующее изменение энергии нейтрона регистрировалось гравитационным спектрометром УХН с интерференционными фильтрами в фазе с движением образца.

Поставлен новый эксперимент по проверке справедливости закона 1/v при взаимодействии УХН с образцом естественного гадолиния (сечение радиационного захвата порядка 25 Мбарн). В публикации 2003 года сообщалось, что в соответствии с полученными результатами закон 1/v выполняется в этом случае с точностью не хуже 6% при изменении скорости нейтрона в диапазоне 4-120м/сек. В новом эксперименте закон 1/v был проверен с точностью порядка 0.1% но для интервала изменения скоростей от 4 до 35м/сек.

### *1.6.3 Исследования малого нагрева и генерации УХН*

Измерены полные и дифференциальные сечения очень медленных нейтронов для жидких флюорополимеров при 80-300 К с целью изучения предельных возможностей в хранении УХН (эксп. ИЛЛ 3-14-185). Необходимы (и планируются) измерения при более низких температурах этих и других перспективных покрытий для хранения УХН.

Проведен эксперимент (ИЛЛ 3-14-192) по исследованию "малого нагрева" УХН при отражении от твердой поверхности. Обнаружен значительный эффект нагрева в мкэВ-область энергий. Готовится продолжение этих работ.

Проведен эксперимент (совместно с Институтом Пауля Шерера и ИЛЛ) по прямому измерению генерации УХН в газообразных, жидких и твердых дейтерии, кислороде и дейтерометане в диапазоне температур 8-100 К. Результаты обрабатываются и сравниваются с расчетами, точными и в некогерентном приближении. Планируются измерения плотности состояний на спектрометре неупругого рассеяния.

Проведены тестовые работы по запуску источника для генерации УХН в холодном твердо-дейтериевом замедлителе на импульсном реакторе "TRIGA"(Университет г. Майнц). Работы будут продолжены.

## 2. Теоретические исследования

Разработан метод аналитического описания отражения нейтронов от сред с размытыми границами раздела с целью изучения проникновения и затухания магнитного поля внутри высокотемпературных сверхпроводников. С помощью этого метода обработаны экспериментальные данные по измерению кривой отражения конкретной многослойной системы, и показано что по сравнению со стандартной численной подгонкой аналитическая подгонка оказывается в 7 раз быстрее.

Теоретически и экспериментально исследовано отражение поляризованных нейтронов от намагниченного зеркала с высокой коэрцитивной силой в слабом внешнем поле, направление которого варьируется по отношению к намагниченности зеркала. Показано, что граничные энергии зеркала определяются квантовыми правилами и не зависят от угла между внешним и внутренним полями. Рассчитаны граничные энергии для многослойных магнитных систем, в которых намагниченности соседних слоев направлены под заданным углом друг к другу, и найдена зависимость граничных энергий от этого угла.

Разработан новый метод для расчета альбедного отражения нейтронов от однородных и дисперсных сред, который имеет более широкую область применимости, чем стандартный

диффузионный метод. С помощью этого метода исследована эффективность ультрадисперсных отражателей в холодных замедлителях нейтронов.

В течение 2005 года продолжилось исследование радиационных поправок к бета-распаду нейтрона. В частности, было выяснено, что применение алгебры токов не может обеспечить корректное вычисление радиационных поправок, и их расчет должен проводиться согласно современной Стандартной Модели. В следующем году предлагается продолжить исследование электро-слабых процессов в рамках СМ, имея в виду последовательный учет структуры адрона.

## 3. Прикладные исследования

### *3.1 Разработка нейтронных детекторов для космических аппаратов*

В коллаборации с Институтом космических исследований РАН группой в составе сотрудников ЛНФ и ЛРБ была подготовлена методика калибровки детектора LEND (Lunar Exploration Detector), предназначенного для измерения потоков нейтронов от лунной поверхности с высоким пространственным разрешением на борту космического аппарата LRO (Lunar Reconnaissance Orbiter), запуск которого намечен на 2008 год. В ЛНФ изготовлены макеты полиэтиленовых коллиматоров, в ЛРБ проведены расчеты чувствительности лабораторного макета прибора. Проведены калибровки лабораторного макета прибора.

### *3.2 Исследование элементных составов различных веществ на ускорителе ЭГ-5*

Экспериментальные исследования на пучках заряженных частиц от электростатического генератора ЭГ-5 проводились в тесном сотрудничестве с представителями других лабораторий ОИЯИ, а также представителями различных институтов стран-участниц.

Так, совместно с сотрудниками Института Физики Университета имени Марии Кюри-Склодовской Д. Мончкой и М.Куликом выполнены исследования окисных слоёв кремния, имплантированных ионами германия.

Совместно с сотрудниками Электротехнического Института Словацкой Академии Наук в Братиславе Д. Махайдиком продолжались исследования методом RBS слоистых полупроводниковых структур $Si/HfO_2/Ru$, подвергавшихся отжигу при различных температурных условиях. Были выполнены исследования глубинных профилей элементов для 34 образцов, как в исходном состоянии, так и после отжига при температурах $800^0$ С, $900^0$ С и $1000^0$ С. В качестве примера на **рис.11** показаны экспериментальные (точки) и симулированные (линии) спектры для исходного и отожженного при температуре $1000^0$ С образцов. Толщина слоя рутения в исходном состоянии составляла около 11 нм, а толщина слоя окиси гафния – 3 нм, причём между ними находился слой смешанного состава толщиной около 6нм.

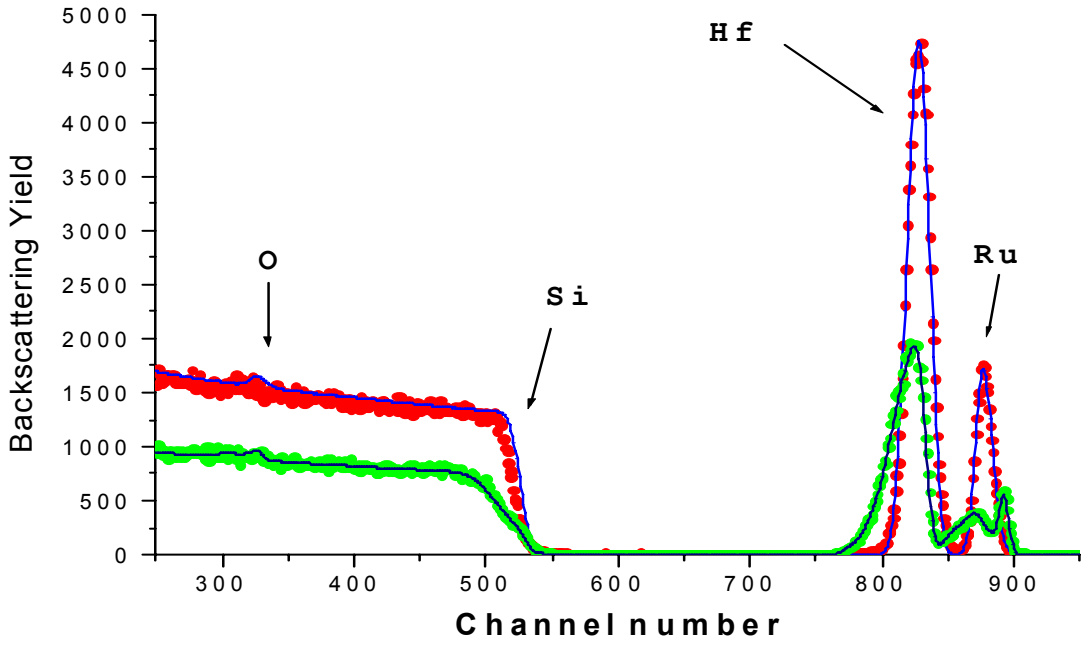


***Рис.11***. *Спектры резерфордовского обратного рассеяния для образца структуры Si|HfO2|Ru в исходном состоянии и после отжига при $1000^0$ С*

Совместно с Ё. Гураном из Электротехнического Института Словацкой Академии Наук в Братиславе проводились исследования карбид-кремниевых аморфных слоёв, допированных азотом, с использованием методики «протонов отдачи» в сочетании с методикой RBS. Были определены концентрации кремния, водорода, углерода и азота в слоях микронной толщины.

Исследования элементного состава аэрозолей в воздухе г. Улан-Батора были выполнены совместно с Ш. Гэрбишем ( Монголия ) и Ц. Амартайван также с помощью методик PIXE и RBS. В составе исследованных образцов обнаружены следующие микропримеси: F, Na, Mg, Al, S, Cl, K, Ca, Ti, Mn, Fe, Cu, Zn, As, Sr, Zr, Ba.

Проведен мониторинг элементного содержания человеческих зубов для контроля здоровья населения. Образцы зубов были проанализированы PIXE и RBS методами для 20 главных и trace элементов. Концентрация железа, цинка, хрома и меди в образцах превышают контрольные значения иногда в 10 раз. Стратегия мониторинга, используемая в настоящем исследовании, определяет факторы риска заболеваний, обусловленных некоторыми видами загрязнителей, особенно промышленным загрязнением. Определенные атмосферные загрязнители, вырабатываемые промышленностью, имеют высокий уровень удержания в человеческих зубах. Существенные корреляции между парами концентраций тяжелых металлов в зубах являются указателями источников загрязнения, характерных для местной промышленности и региональных автотранспортных сетей.

### *3.3 Разработка установки для обнаружения скрытых запрещённых веществ*

Проводились прикладные исследования, направленные на создание установки для обнаружения скрытых запрещённых веществ с использованием пучков быстрых меченых нейтронов. В качестве источника меченых нейтронов сейчас используется портативный нейтронный генератор со встроенным кремниевым 9-ти пиксельным альфа-детектором,

разработанный совместно с сотрудниками Всероссийского Научно-исследовательского Института Автоматики (Москва). Интенсивность нейтронного потока, создаваемого ИНГ-27, составляет $2x10^7$ сек$^{-1}$.

Энергетическое разрешение спектрометрических каналов регистрации характеристического ядерного γ-излучения на линии $E_\gamma$ = 4,43 МэВ, усредненное по всем 9 пучкам "меченых" нейтронов, возникающего при облучении исследуемого вещества потоком меченых нейтронов составляет 5,5 %.; На **рис.12** показан результат измерения временного разрешения всей системы ( скорость 14 МэВ-ного нейтрона составляет 5 см/нсек.)

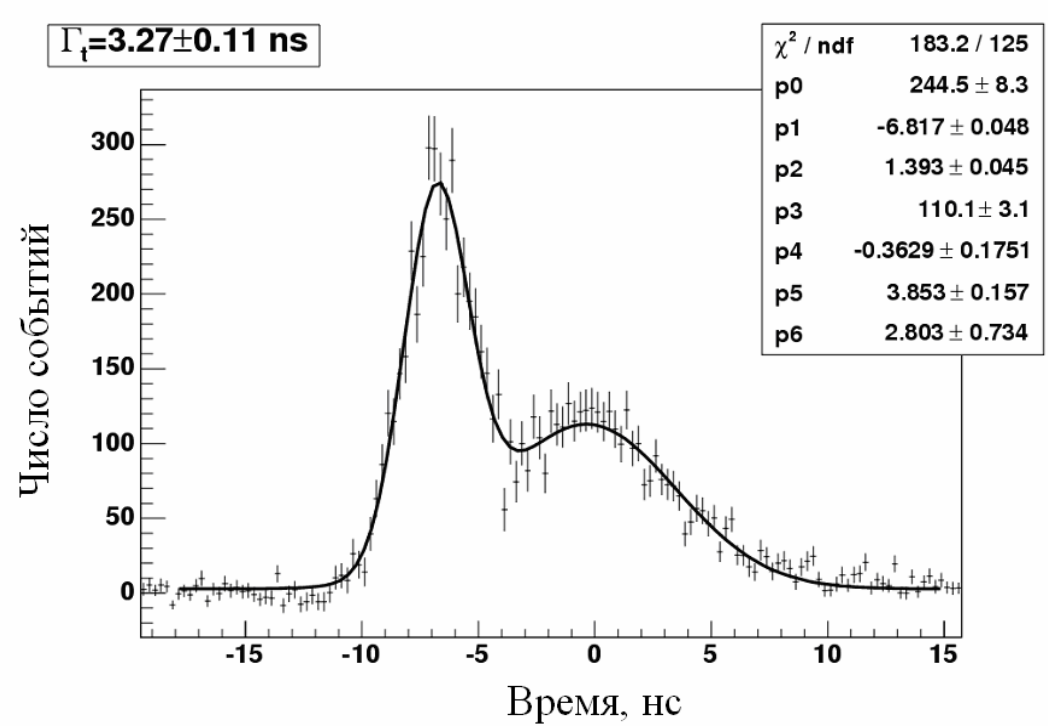


***Рис. 12**. Временной спектр α-γ совпадений полученный при облучении образца из $^{12}C$ размером 10×10×10 см$^3$ потоком нейтронов с энергией 14,1 МэВ.Сплошная линия – результат фитирования*

Выполнены эксперименты по идентификации меламина, экранированного различными веществами (бумага, древесина, кожа, сталь). Идентификация меламина осуществлялась с применением методики нейронных сетей.

## 4. Аналитические исследования на реакторе ИБР-2

### Методические работы

Совместно с сотрудниками Технического Университета в Праге (Чешская Республика) измерены спектры нейтронов в каналах облучения ПТУ РЕГАТА с помошью многоэлементных активационных детекторов.

### Экология

*Биомониторинг*

В 2005 году в связи с проведением очередного европейского одновременного сбора мхов-биомониторов (moss-survey) были продолжены работы по изучению атмосферных выпадений тяжелых металлов с применением техники биомониторирования, НАА и ГИС

технологий (проект РЕГАТА) на территории Центральной России (Тульская, Тверская, Ярославская и юго-восток Московской областей), Болгарии, Румынии, Словакии, Польши, Сербии и Македонии, а также Армении (Севан), Монголии и Вьетнама. Анализ образцов, собранных летом 2005 года на территории Белоруссии будет проведен в начале 2006 года. Завершен сравнительный анализ различных биомониторов (лишайников, коры деревьев) и почвы из района нефтеперерабатывающего завода в Констанце (Румыния). Определена зона воздействия этого завода на окружающую среду курортной зоны Черноморского побережья Румынии.

Все больший интерес в странах участницах и неучастницах ОИЯИ вызывают работы в новом для нас направлении активного биомониторинга с использованием чистых мхов, эскпонируемых в промышленных районах с высокой антропогенной нагрузкой. Подобные исследования проведены в районе городов Байа Марэ (Румыния), София (Болгария), Познань (Польша) и Афины (Греция).

*Оценка состояния экосистем*

Совместно с ИФИН (Бухарест) и Бухарестским Университетом проведены подготовительные работы к анализу образцов донных отложений, собранных в дельте Дуная. Анализ воздушных фильтров с территории Словакии одновременно с образцами хвои сосны и биологического материала животных (зубы косули) позволил лучше оценить степень воздействия ряда крупных промышленных объектов Словакии, в частности, завода по производству алюминия в Зиаре (Словакия) на экосистемы прилегающих территорий.

При участии Центра экологических исследований Польской Академии наук в рамках Гранта ПП Польши с использованием ядерно-физических аналитических методов проведена оценка вредного воздействия токсичных элементов на аквальную биоту и человека в районе Мазурских озер (Польша) и Рыбинского водохранилища (Центральная Россия)

*Продукты питания и здоровье человека*

Совместно с Геологическим институтом РАН в рамках Координационной программы МАГАТЭ и Технической кооперации с МАГАТЭ проведен сравнительный анализ элементного состава ряда продуктов питания, выращенных в условиях промышленного загрязнения. Результаты этих работ доложены на завершающем Рабочем совещании по Технической кооперации МАГАТЭ в ноябре 2005 года в Дубне.

В 2005 году выполнен анализ румынских экологических образцов (почва, вода и воздушные фильтры) и биосубстратов человека (волосы, ногти, зубы и др.) в рамках проекта «Мониторинг на рабочих местах и здоровье персонала, занятого в производстве фосфорных удобрений на ряде заводов России, Узбекистана, Польши и Румынии» (Европейская Программа 5, Коперникус). Результаты этих исследований позволили установить связь между уровнем содержания токсичных элементов в объектах окружающей среды и биосубстратах персонала, занятого в производстве фосфорных удобрений в Турну-Магуреле (Румыния).

Изучение содержания тяжелых металлов в пищевых ненасыщенных жирах, проведеное в рамках гранта ПП Румынии, позволило экспериментально установить корреляцию содержания металлов с окислительной способностью жиров.

**Биотехнологии**

Продолжены совместные работы с группой биофизиков Института физики АН Грузии по биотехнологии бактерий *Arthrobacter oxidans,* выделяемых из природных базальтов и используемых для изменения валентности хрома (перевод токсичного Cr-VI в нетоксичную форму Cr-III. Завершена обработка результатов НАА и ААС образцов биомассы сине-зеленой водоросли *Spirulina plat*ensis и выделенного из нее С-фикоцианина, при нагрузке питательной среды биогенными и токсичными элементами.

**Материаловедение**

*Археология*

Проведен элементный анализ 70 образцов керамик из курганов Смоленской области и Северного Кавказа в рамках сотрудничества с Государственным Эрмитажем. Определен элементный состав 65 образцов керамик и 25 образцов венецианских стекол для Исторического музея в Констанце (Румыния), в рамках сотрудничества с Университетом Овидия в Констанце.

*Новые материалы*

В рамках гранта ПП Белоруссии завершен анализ данных по изучению влияния нейтронов спектра деления на физические свойства мелкокристаллических алмазов, полученных в Институте физики твердого тела и полупроводников НАН Белоруссии (Минск).

# 2. NEUTRON SOURCES

## 2.1. THE IBR-2 PULSED REACTOR

In the year 2005 the IBR-2 reactor operated 2091 hours for physical experiments (see **Table 1**).

***Table 1***

The operation parameters of the IBR-2 reactor in 2005

| **Cycle №** | **1** | **2** | **3** | **4** | **5** | **6** | **7** | **8** | **TOTAL:** |
|---|---|---|---|---|---|---|---|---|---|
| **Time of cycle** | 17.01-28.01 | 14.02-26.02 | 14.03-25.03 | 11.04-22.04 | 16.05-28.05 | 17.10-28.10 | 14.11-25.11 | 05.12-16.12 | |
| 1. Operation for physical experiment, hr | 266 | 258 | 266 | 255 | 274 | 267 | 243 | 262 | **2091** |
| 2. Operation of MR-3, hr | 274 | 296 | 275 | 270 | 299 | 274 | 273 | 273 | **2234** |
| 3. Generated power, MW·hr | 401 | 393 | 401 | 387 | 414 | 402 | 369 | 396 | **3163** |
| 4. Number of emergency shutdowns (AES) | 0 | 3 | 0 | 2 | 1 | 1 | 2 | 1 | **10** |
| 5. Due to: | | | | | | | | | |
| 5.1. Voltage drops | | 2 | | 1 | 1 | 1 | 2 | 1 | **8** |
| 5.2. Instrumental malfunction or failure | | 1 | | 1 | | | | | **2** |
| 5.3. Electronic equipment failure | | | | | | | | | |
| 5.4. Personnel error | | | | | | | | | |

**Main results of the IBR-2 modernization in 2005:**

1) New fuel charge.
   - Works to create a working site for assembling fuel elements into a fuel rod array were completed. The working site was approved to be put into service by a commission of representatives of JINR, GSPI, VNIINM, NIKIET.
   - At present, the procedure of obtaining license for assembling fuel elements is under way.

2) Main equipment of the IBR-2M reactor.
   - In NIKIET the manufacturing of a new reactor jacket continued.
   - The manufacturing of an intra-jacket fuel-handling machine was completed.

3) In JINR EW the haulage equipment to place moderators for the IBR-2M reactor and shielding technological plugs were manufactured.
4) CSS of IBR-2M.
   - In NIKIET the development of the design documentation of the AES actuating mechanism was completed.
   - Prototypes of actuating mechanisms for an automatic controller and CR were manufactured in JINR EW.
   - In SNIIP-SYSTEMATOM the development of ACSS was completed, the manufacturing of a prototype is under way.
   - Works to create a system to control technological parameters were started (INEUM).
5) Moderator complex for IBR-2M.
   - Prototype works to transport balls made from $C_9H_{12}$ continued.
   - In NIKIET a preliminary design of the IBR-2M moderator complex was started.
   - In GSPI development of an engineering design of moderators was started.
   - In Geliimash the manufacturing of CHF-700/15 continued.

The financial provision of works on the IBR-2 modernization in 2005 is presented in **Table 2.**

***Table 2***

State of financing of the IBR-2 modernization in 2005 (k$) as of 30.12.2005

| | | 1995-2004 | 2005 |
|---|---|---|---|
| **JINR** | Plan | 2190 | 650 |
| | Fact | 1791 | 540 |
| | % | 81,7 | 83 |
| **Rosatom** | Plan | 1970 | 400 |
| | Fact | 1746 | 400 |
| | % | 88,6 | 100 |
| **Total:** | Plan | 4160 | 1050 |
| | Fact | 3537 | 940 |
| | % | 85 | 90 |

**Plans for 2006**

1. Assembling of fuel elements into a fuel rod array.
2. Completion of manufacturing of the reactor jacket.
3. Construction of an ACSS prototype.
4. Continuation of works on rolling shieldings and stationary reflectors of IBR-2M.
5. Completion of works to manufacture CHF-700/15 in «Geliimash».
6. Completion of development of a preliminary design of the moderator complex.
7. Development of an engineering design of the moderator complex.

.

**Moderator complex for the IBR-2M reactor**

**Neutron-physical calculations and optimization of material and geometry of cold moderators.** In the course of 2005 the work to optimize the position of cryogenic moderators at the IBR-2M reactor was carried out, and their combination with the configuration of moderators for thermal neutrons was also carried out. As a result, the problem to meet requirements of researchers on the extracted beams on neutron spectra was solved. For some channels the presence of more cold neutrons in the spectrum is required, for the second ones – of thermal ones and for the third ones – of mixed ones.

Thus, neutron spectra for channels 1, 2, 4-6, 8 and 9 will include more cold neutrons **(Fig.1).** Fig.1 and others illustrate the data of neutron flux density from one neutron generated in the reactor at the distance of 4.5 m from the moderator.

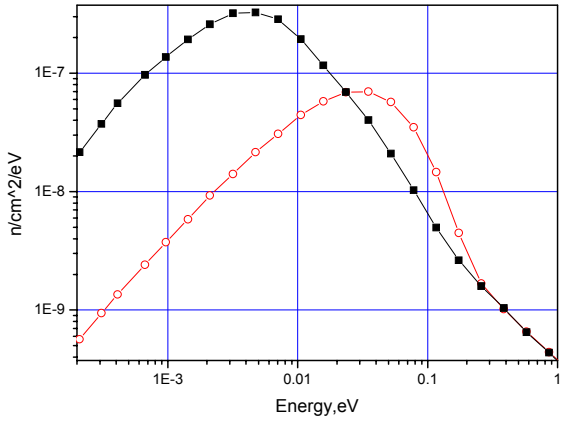


***Fig. 1.*** *Differential neutron spectra for research beam №5 normalized to one neutron of the source. Squares – the result of using mesitylene cryogenic moderator in the best configuration without beryllium; circles – the result of using room temperature water instead of cold moderator.*

Distribution of neutron flux density on the surface of cryogenic moderator of the direction of channels 4-6 is presented in **Fig. 2 (a, b).**

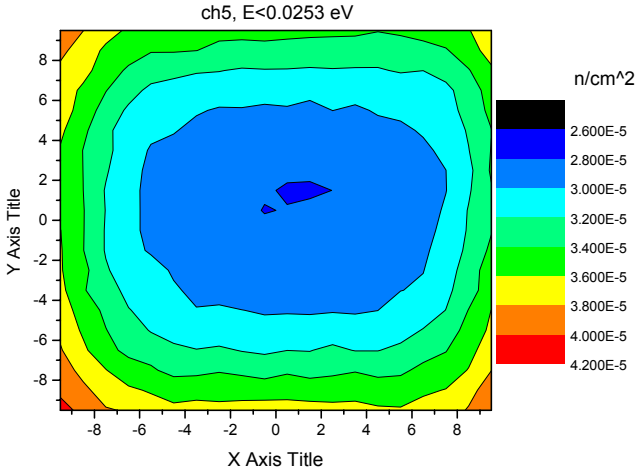


a)

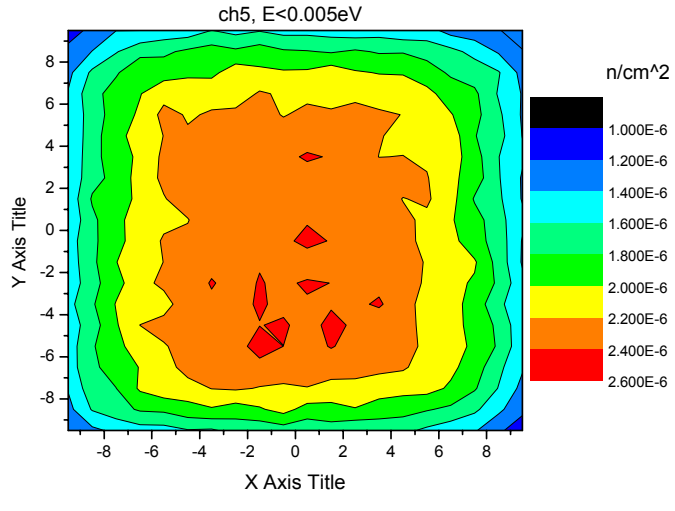


b)

***Fig. 2****. Results of calculations of distribution of integral densities of thermal a) and cold b) neutron flux normalized to one neutron of the source on the surface of cold moderator. The X axis represents width of the moderator, the Y axis – height of the moderator.*

Research channels 7 and 10 will have a mixed neutron spectrum **(Fig.3).**

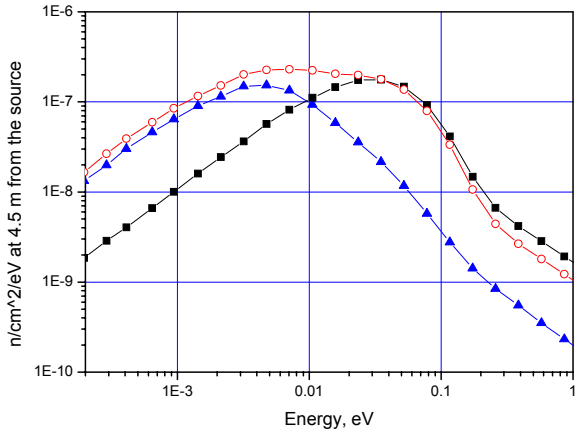


***Fig. 3.*** *Differential neutron spectra for channel 7 normalized to one neutron of the source. (Squares – pre-moderator only, circles – optimal configuration of moderators (cold one+comb-like thermal one), triangles – spectrum obtained only from the cold part taking into account a partial shading of the water moderator comb)*

For research channel №11 additional optimization of the thermal moderator was carried out. The thermal moderator will be arranged orthogonally to the given channel, that will increase the integral density of thermal neutron flux ~ by a factor of 3 **(Fig. 4).**

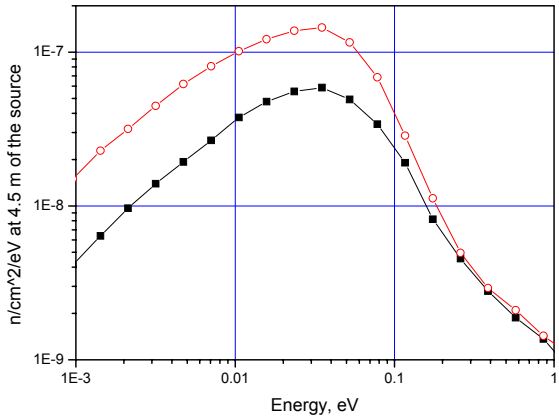


***Fig. 4.*** *Differential neutron spectra for channel 11. (Squares – pre-moderator only, circles – presence of the optimal moderator configuration)*

The method of calculating neutron spectrum was validated by comparison with the experimental data obtained on the JESSICA facility (Juelich, Germany).

New result, which has never been obtained before, is that a post-moderator in the form of a «frame» (water reflector around a plain moderator with the size of surface 18×18 cm) gains by a factor of 2 in the surface-average density of vector flux of the neutron escape, i.e. the same gain as the famous comb-like moderator gives (distribution of neutrons along the surface see in Fig. 2). Earlier it was considered that such configuration of moderator is effective only for a small surface on the order of 5×5 cm. Moreover, simultaneous use of the comb-like moderator and the «frame» increases the gain up to 2.4.

**Ball cold moderator.** In 2005 the design principle of a cold moderator was proposed and developed, based on the usage of balls of frozen mixture of mesitylene and *m*-xylene providing for the maximum possible cold neutron flux (at a level of the solid methane moderator being designed for the second target of the ISIS source) on IBR-2M at long-term continuous operation.

The ball cold moderator is able to operate at the temperature of 20 K-30 K without reloading of the working substance no less than three-five days in the fast neutron flux up to 2 $10^{13}$ n/cm$^2$/s. Solid balls of mixture of mesitylene and pseudocumene or *m*-xylene are periodically replaced in the moderator chamber by means of their defrosting and sink of the waste substance as a liquid. Such mixture in the frozen state has an amorphous structure, which is important in many respects – both for an increase of the cold neutron yield and for obtaining of regular homogenous balls. The moderator chamber has the form of a parallelepiped with the walls of the aluminum alloy; sizes of the chamber – 20 cm high, 4 cm thick and its width is from 15 to 20 cm (for different moderators). The chamber is surrounded by an aluminum casing to create vacuum heat insulation. The tube of cold helium supply and the tube of ball supply come from above to the chamber. Bottom of the chamber is made in the form of a net with the size of cells smaller than the size of balls (5 mm). The tube of cold helium removal and the tube of sink of waste liquid mesitylene go off from below the chamber.

At the beginning of work the cooled chamber is filled with balls, which are delivered by the cold helium flow with the temperature of 30-80 K (the most suitable temperature will be chosen after completing the investigations of ball transportation). The balls are cooled by this helium with the input temperature 20-22 K in the process of normal operation. After a lapse of time when the mesitylene burnout starts influencing the cold neutron yield (approximately 3-5 days; this time will be determined in the course of physical start-up of the moderator), the helium flow is interrupted, mesitylene is melted by nuclear heat and is poured out into a vessel for a subsequent utilization. The chamber and the whole cooling path are cleared from the mesitylene remainder by a flow of thermal helium and the operation cycle is repeated. A possible schematic diagram of cooling and circulation of balls is given in **Fig.5.**

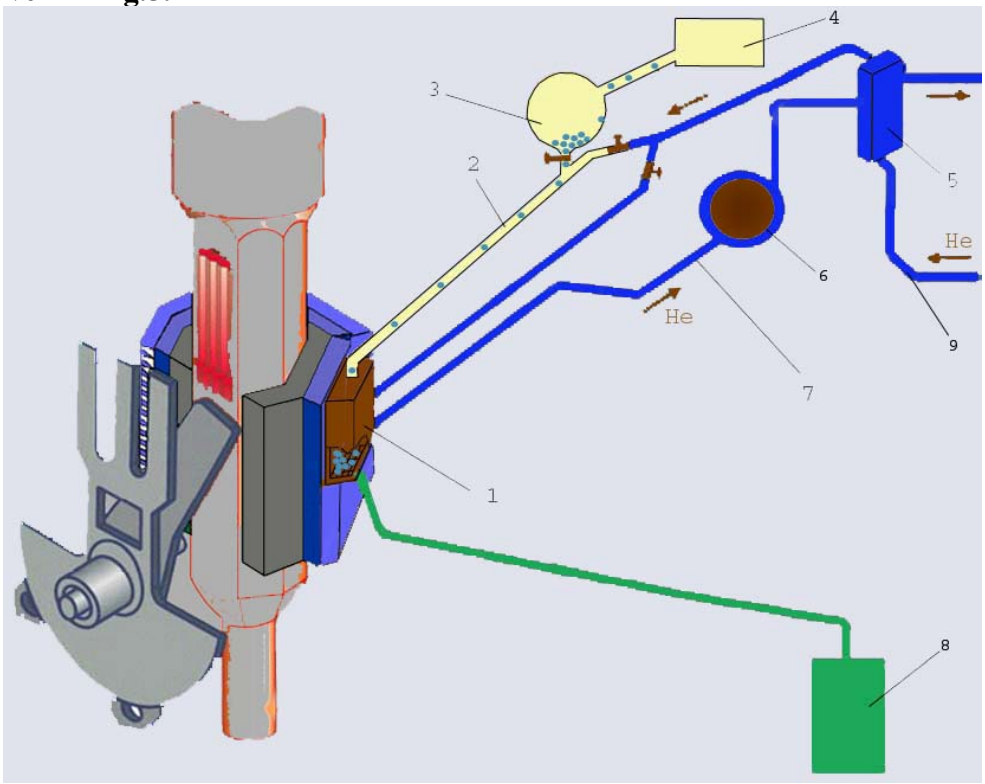


***Fig.5.*** *Diagram of ball supply and cooling of cold moderator. 1 – moderator chamber, 2 – channel of pneumatic loading of balls, 3 – lock of ball supply, 4 – device of ball generation, 5 – helium heat exchanger, 6 – helium coolant circulator, 7 – cold helium tubing of the secondary coolant circuit, 8 – collecting vessel for liquid mesitylene, 9 – cold helium tubing of the primary coolant circuit.*

Operating life of such ball moderator will be practically unlimited in contrast to the traditional block solid methane moderator; for example, at the ISIS source in the Rutherford Laboratory a methane moderator is replaced completely twice a year.

Data processing of irradiation experiments of solid mesitylene in a cylindrical steel casing using the COSMOS-M program package made it possible to determine the range of internal stresses in solid mesitylene. It was obtained that the internal pressure in mesitylene 70-75 bar corresponds to the observed pressure 10 bar on the cylindrical steel casing after irradiating by the dose of 10.8 MGy at the temperature of 130 K when the accumulated radiolytic hydrogen starts to yield. Hydrogen yields when ruptures of a material occur, i.e. stresses exceed the tensile strength of a material. Hence, the tensile strength of solid irradiated mesitylene at 130 K is 70-75 bar. Conversion for the irradiation conditions on the future reactor IBR-2M gives value of the internal pressure 62-67 bar/day at 33 K in mesitylene. The strength of molecular crystals is considerably higher at low temperatures. Therefore, there are reasons, according to the data on non-irradiated molecular crystals, to suppose that at 33 K the tensile strength of solid irradiated mesitylene will be no less than 270-300 bar. In that case it will be exceeded only after the irradiation for 4-5 days for the balls in the zone of the largest neutron flow and after 7-8 days – for the moderator-average flow.

Replacement of balls in the moderator chamber will have to be done no more than two times during a two-week operation cycle of the reactor. The reason for the ball replacement most likely will be the measure of degradation of cold neutron flux due to the mesitylene burnout.

Schematic diagram of helium cooling of the cold moderator is given in **Fig. 6.**

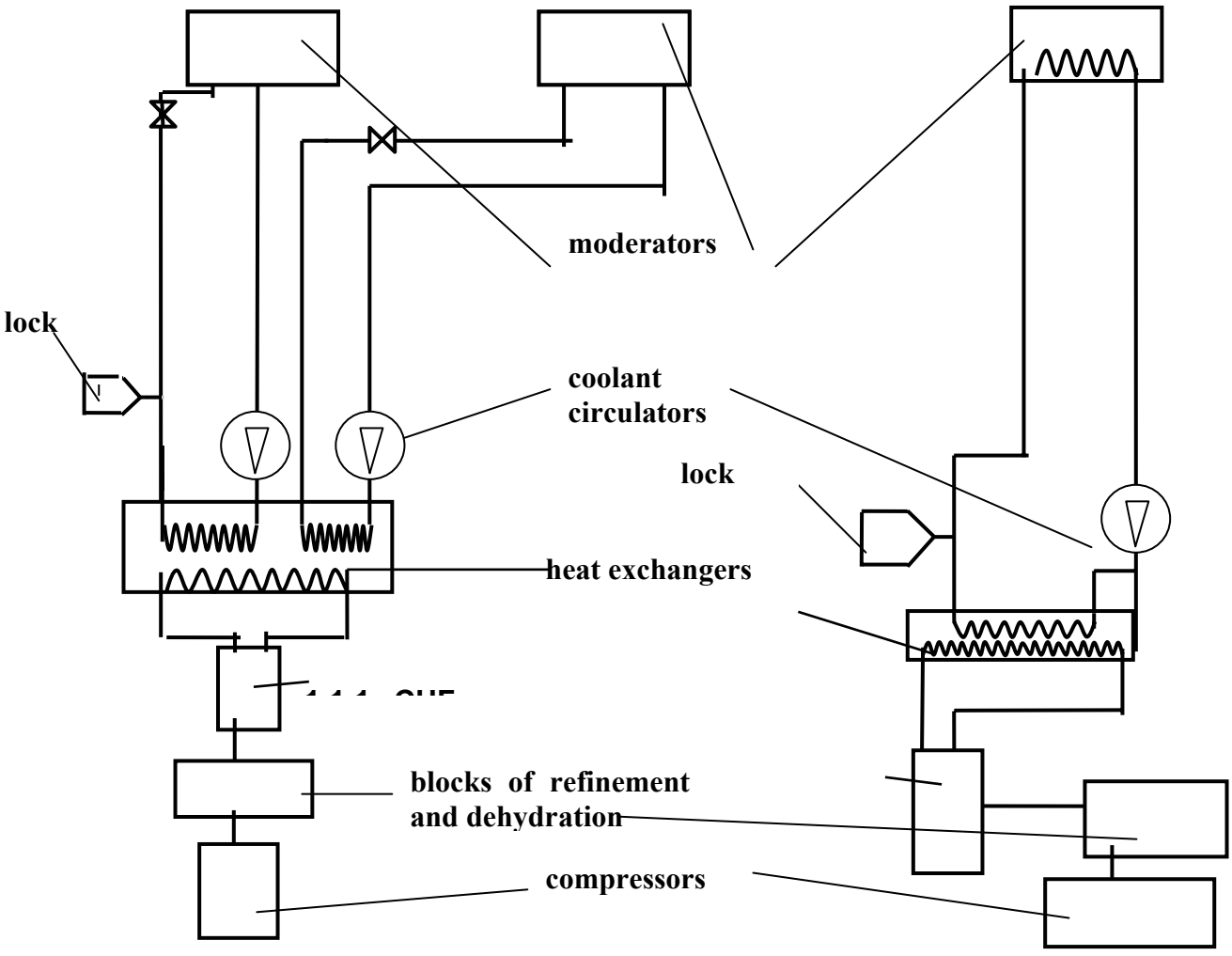


***Fig. 6**. Diagram of helium cooling of the cold moderator*

Cooling of the moderator is double-circuit. Helium circulates by means of a special coolant circulator BNHeP-25 of the firm Barber-Nicols with the productivity up to 100 $nm^3$/hr along the primary coolant circuit where the chamber is located. Each of the moderators has its own coolant circuit with a coolant circulator and a path of ball supply. The cooling helium facility is a source of the cold in the secondary coolant circuit. Since it is planned to install three cold moderators on the IBR-2M, there will be three primary coolant circuits and two secondary ones, respectively, with cooling helium facilities CHF-500 and CHF-700 with the cold productivity 500 and 700 Wt, respectively, at the temperature of 15 K. Each cooling helium facility gives the cold into primary coolant circuits through its own heat exchanger. Helium heating includes the following components:

- Nuclear heat in the moderator
- Heating in coolant circulators
- Heat penetration into tubes, heat exchangers and rectifiers.

Nuclear heat in mesitylene balls and in aluminum of the chamber is calculated using the MCNP-4 program and equals to 0.15 Wt/$cm^3$ in mesitylene and 0.05 Wt/g in aluminum. It will constitute 150-170 Wt for the dimensions of the moderator 15×20×4 cm.

Heating of helium in coolant circulators, in accordance with the equation of adiabatic process at the change of pressure for 10%, will be on the order of 1 degree, which is equivalent to the thermal power of about 60 Wt.

Heat penetration into tubes depends on their performance, let us assume quite a real value – 1.0 Wt/m. Summing up heat generation along the whole cooling path of moderator of the right and left direction (on the 2-nd and 8-th neutron beams), we will obtain 530-570 Wt, including the nuclear heat.

Summing up heat generation along the whole cooling path of moderator of the central direction (on the 4-th – 6-th neutron beams), we will obtain about 300 Wt. Thus, for both loops heat generation is smaller than the designed cold productivity of cooling helium facilities. For the direction of the 4-6 beams installation of a post-moderator made of cold beryllium is possible; in this case heat power increases for ~ 100 Wt and will be ~ 400 Wt. The minimal calculated temperature of mesitylene on the ball surface (on the helium inlet to the chamber) equals to $T_{не}$ (0)+5.5 K; the maximal temperature of mesitylene (on the outlet of the chamber) - $T_{не}$ (0)+10.5 K. Based on the condition not to exceed the critical temperature of hydrogen 33 K, we obtain the upper limit of helium temperature on the inlet of the moderator chamber 22 K.

**Ball transportation and test-bench for development of the transportation.** As was mentioned above, the supply of mesitylene balls will be performed pneumatically – by a cold helium flow. Characteristics of the supply path are determined by the following conditions:

- The ball speed should not exceed the top speed, at which they may break down at a blow with the wall of a transport tube or chamber (assessed value – 4 m/s, determined by throwing cold balls from certain height on the metallic surface).
- Time of the chamber filling should not exceed 0.5 – 1 hour;
- Stopping up of balls in the transport tube should be eliminated.

The last condition is fulfilled if the tube diameter exceeds 2.2 of the ball diameter. This is due to geometrical reasons: any spatial placement of balls in this case will be unstable. The tube diameter will be 16 mm at the ball diameter 7 mm (maximum allowable diameter due to heat extraction reasons).

At the maximal length of the path 25 meters, ball diameter 7 mm, volume of the moderator chamber 1.2 litre and the total number of balls $N$ = 3000 let us take on the average value of ball speed to be equal to 2 m/s. Then at the time of filling 1 h the number of balls located simultaneously in the tube should be no less than 10, and at the time of filling 0.5 h – 20. These figures seem reasonable – at the distance between balls 1–2 meters the mode of gas flow is not disturbed, since this distance is on the order of 100 diameters of the tube, which is quite enough to restore stable mode. All the balls will behave as if there is one ball in the path. This makes it possible to simplify the experiments of ball transportation on the test-bench. The experiments have shown that simultaneous motion of 10 balls does not change distinctly their speed.

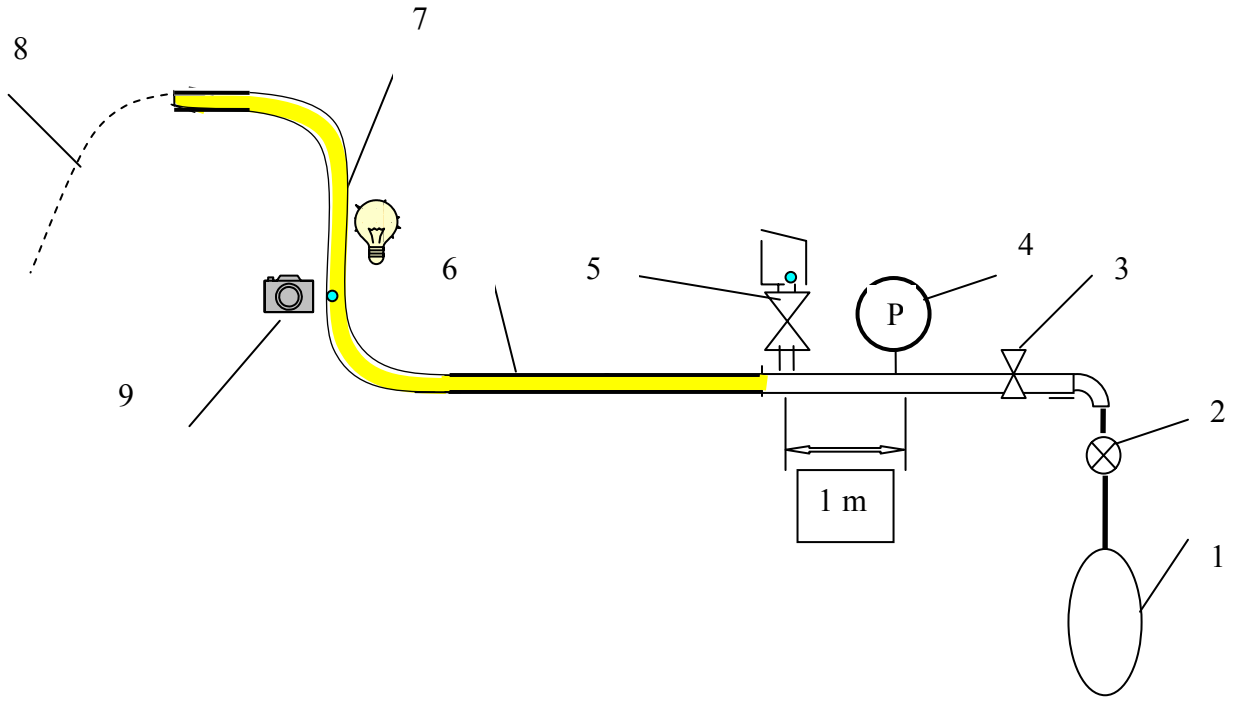


***Fig.*** *7. Diagram of the test-bench for experiments of ball transportation. Notation: 1 – compressed-gas cylinder, 2 – reducer, 3 – throttle flap, 4 – flowmeter, 5 – lock of ball loading, 6 – straight transport tube about 5 m of length, 7 – curved part of tube (up to 1 m of height), 8 – track of a ball after escape from the tube, 9 – digital camera in the video mode and illuminating.*

**Comparison of the calculated coefficient of resistance and the experimental one.** The comparison was carried out on the basis of the experiments to retain balls in an inclined tube ($45^0$) by a nitrogen flow of room temperature. Input data: tube diameter – 14 mm, diameters of balls and their densities: 5 mm – 2.3 gr/cm$^3$, 6 mm – 1.7 gr/cm$^3$, 8 mm – 1 gr/cm$^3$. The calculation of resistance coefficients was performed for the laminar regime of ball streamline. It was obtained that the experiments are in good line with the theory. However, this does not cause optimism because of the following reasons:

- The error of experimental values of the coefficient of resistance is ± 20 %;
- The comparison is performed for the ball speed equaling to zero; it is not clear whether the theory works at the non-zero ball speed or it is necessary to use a more general approach.

In consequence of what has been said, it is proposed to carry out experiments to measure speed and acceleration of a ball in the process of moving along the tube. And it is necessary to investigate straight parts, as well as curves and inclines. On the basis of these data it will be possible to draw an unambiguous conclusion concerning which equation should be applied to calculate the ball motion. It is sufficient to measure the «acceleration-speed» function for straight tube in a wide range of ball speed and this will be sufficient for the subsequent calculation of ball motion in any tube configuration (at the same diameters of a tube and a ball and the same gas flow as in experiment). The ball speed is measured simultaneously at several points using digital cameras in the video mode, **Fig.8.**

Schematic layout of ball generator is given in **Fig. 9.**

**Obtaining of balls, diagram of generator.** The technique of obtaining solid balls of mesitylene is based on freezing of liquid mesitylene drops in nitrogen. The fundamental parameters to obtain a homogenous solid ball are a short time of being of a ball in nitrogen and also an addition of certain amount of *m*-xylene into the liquid solution. The latter gives an amorphous structure, more strong in regard to cracking. The principle of mass generation of mesitylene balls has been worked out.

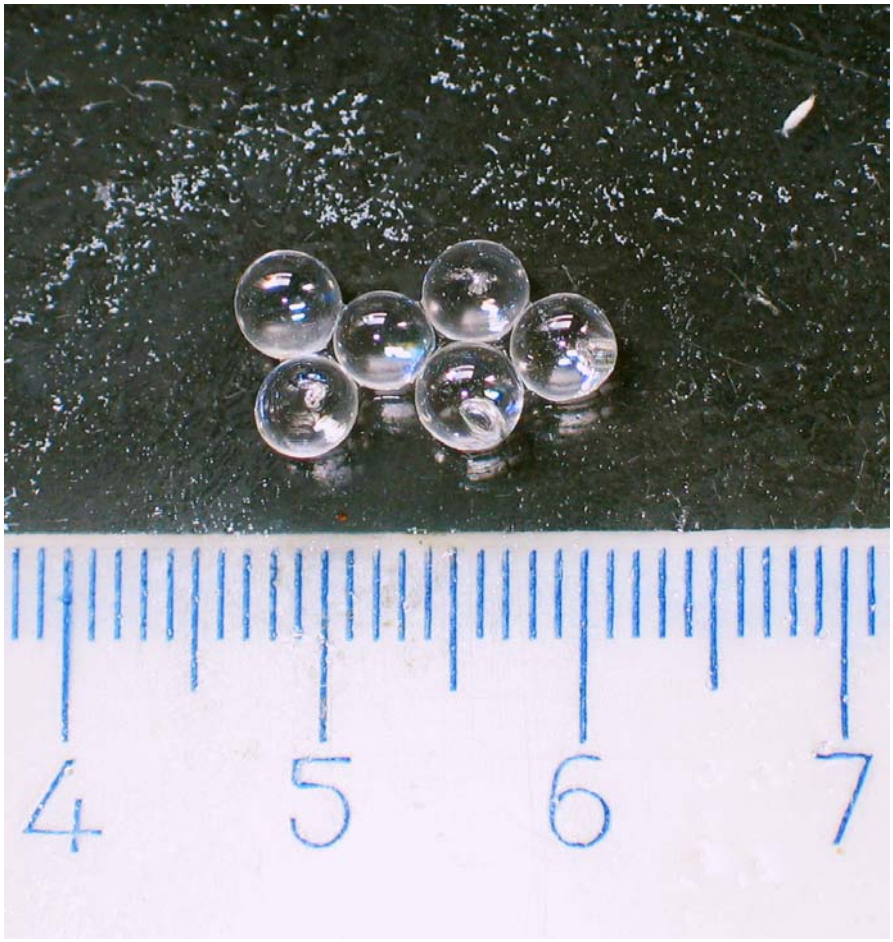


***Fig. 8.*** *Balls of solid mesitylene; large points of ruler – in centimeters.*

**Conclusion**

Main results of works on the project of the moderator complex for IBR-2M in 2005 and conclusions:

1. The proposed principle of operation of mesitylene moderators (usage of solid balls of mixture of mesitylene and *m*-xylene, their transportation by cold helium, periodic melting of balls and their replacement without a break in the reactor operation) is quite realizable and can provide for a practically unlimited resource of moderator operation.
2. Density of the cold neutron flux on the moderator surface of mesitylene balls with the temperature 20 K will reach 3 $10^{13}$ n/cm$^2$/s/srad/ Å at 4 Å, which is a record value for the European sources.
3. It is possible to provide for helium temperature 20-22 K to cool three mesitylene moderators with the help of two cooling facilities – CHF-500 and CHF-700.
4. Requirements specification (together with NIKIET and GSPI) has been worked out for implementation of the preliminary design of the moderator complex for the IBR-2 reactor.

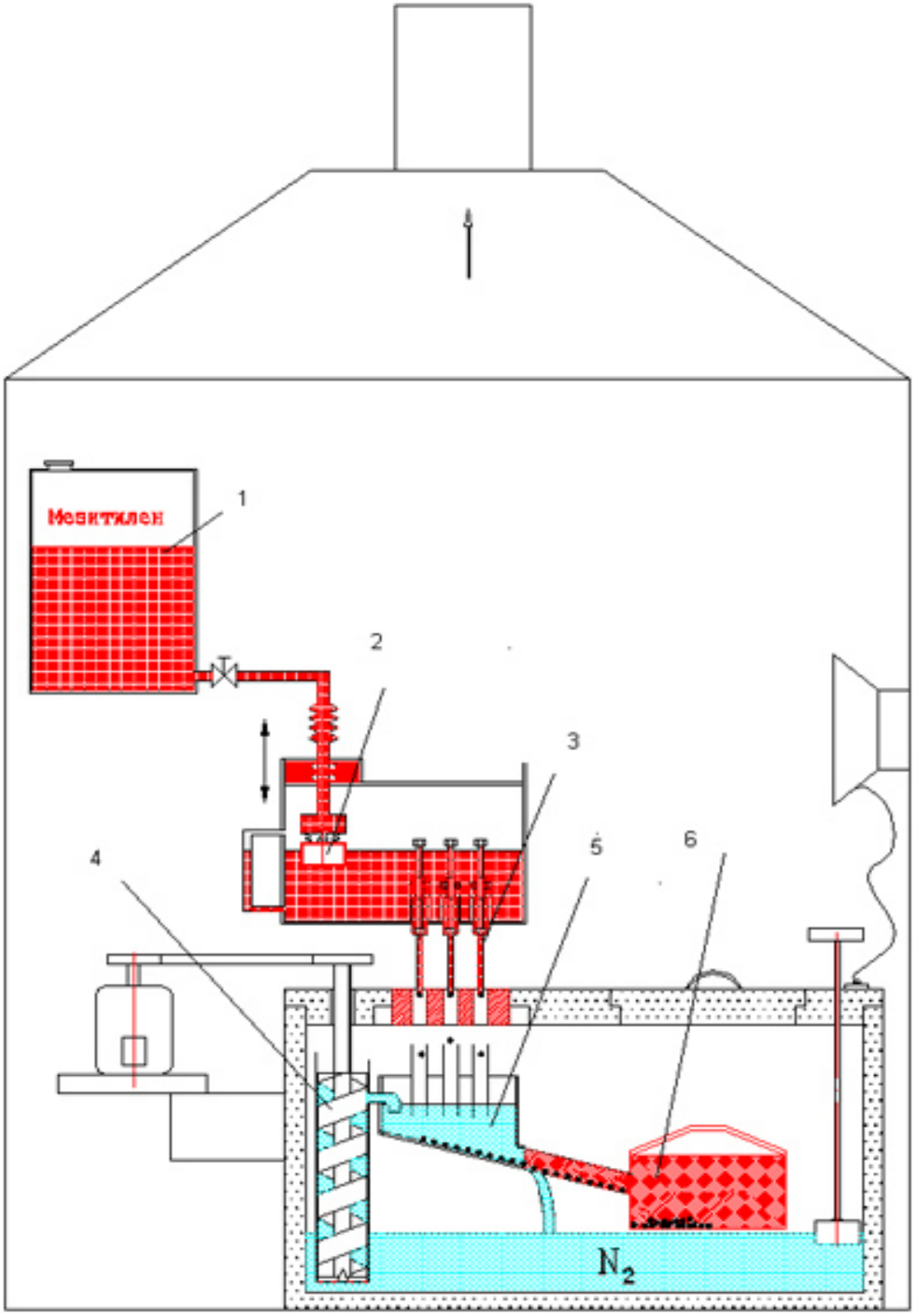


***Fig. 9.*** *Schematic diagram of generator of large amount of balls. 1 – vessel with liquid solution of mesitylene and m-xylene; 2 – regulator of level of liquid; 3 – droppers; 4 – pump for liquid nitrogen circulation; 5 – vessel with inclined bottom and outlets for nitrogen sink; 6 – tank-collector of balls.*

## 2.2. The IREN Project

The main efforts and funds have been focused on the completion of preparation and carrying out of works to dismantle the IBR-30 reactor.

In order to secure the positive ecological assessment of the IBR-30 decommissioning project, a system of key wells to control the condition of groundwater has been designed and created in the DLNP area. The final training of the staff to perform specific technological operations of dismantling the reactor equipment and defueling has been conducted. Due to the painstaking work of the FLNP administration and the laboratory technical subdivisions in the middle of October it became possible to start the reactor decommissioning. A major part of the reactor activated equipment was disassembled and transported to bldg. 117/b for temporary storage. By the middle of November the drilling-out of uranium inserts from the moveable parts of the IBR-30 core was completed. The removed fuel was evacuated for storage in DRFM JINR. By the end of the year it is planned to complete the defueling of the main reactor core and to transport the spent fuel for storage in DRFM JINR. The completion of disassembling of the rest of the IBR-30 reactor equipment is scheduled for the first half of 2006.

Some progress has been made in the construction of the LUE-200 linac. After the purchase of a missing part of a special copper tube, the works to wind the coils of a solenoid for a magnetic focusing system (suspended in September, 2004) were resumed. By the beginning of the 4-th quarter these works were completed. The conducted magnetic measurements have shown that the parameters of the manufactured coils conform to the design values. Until the end of the year the test assembling of the magnetic focusing system will be completed on the LPP test bench. After that, the system will be transported to bldg. 43 of FLNP for assembling and adjustment at a regular place.

The assembling of the modulator M350 has been completed in the accelerating hall of bldg. 43. At present, the testing of the modulator systems and the preparation for its startup are in the completion stage. The vacuum tests of the magnetic spectrometer equipment have been successfully carried out. Works on its test assembling on a test bench are started.

Computational investigations to model the electron beam dynamics in the accelerating tract of the LUE-200 have been conducted with the purpose of optimization of the focusing system and minimization of particle losses, the criteria of allowing for errors of magnetic fields in the accelerator tract have been determined.

A large volume of work on detail designing of the water-cooling system of the linac LUE-200 has been performed by the specialists of JINR and GSPI. Its completion is scheduled for the end of the year.

The work on a working draft of a power supply system for the accelerator has been started.

The development of the project of reconstruction of the LUE-200 control room and rooms in bldg. 43 intended to house the power-supply and water-cooling systems has been completed. The works to repair and reequip the above-mentioned rooms have been started.

In the third – fourth quarters the invoices under the contracts with BINP, Novosibirsk, have been paid at last. This gives us hope that the equipment necessary for the completion of the assembling and complex adjustment of the LUE-200 equipment will be delivered in 2006.

Unfortunately, we failed to perform works on the LUE-200 linac planned for 2005 in full measure, because of delay or lack of planned financing. Nevertheless, the necessary reserve to carry out the tasks specified in the JINR Topical Plan for 2006 has been created with an ultimate aim to start up the first stage of the IREN facility with a non-multiplying neutron-producing target and a test bench for applied investigations by the end of 2007.

# 2. НЕЙТРОННЫЕ ИСТОЧНИКИ

## 2.1. ИМПУЛЬСНЫЙ РЕАКТОР ИБР-2

В 2005 г. ИБР-2 отработал на физический эксперимент 2091 час (см. **таблицу 1**).

***Таблица 1***

Эксплуатационные показатели работы реактора ИБР-2 в 2005 г.

| **№ цикла** | **1** | **2** | **3** | **4** | **5** | **6** | **7** | **8** | **ВСЕГО:** |
|---|---|---|---|---|---|---|---|---|---|
| **Время цикла** | 17.01-28.01 | 14.02-26.02 | 14.03-25.03 | 11.04-22.04 | 16.05-28.05 | 17.10-28.10 | 14.11-25.11 | 05.12-16.12 | |
| 1. Наработка на физический эксперимент, час | 266 | 258 | 266 | 255 | 274 | 267 | 243 | 262 | **2091** |
| 2. Наработка ПО-3, час | 274 | 296 | 275 | 270 | 299 | 274 | 273 | 273 | **2234** |
| 3. Энергонаработка, МВт·час | 401 | 393 | 401 | 387 | 414 | 402 | 369 | 396 | **3163** |
| 4. Количество срабатываний аварийной защиты (АЗ) | 0 | 3 | 0 | 2 | 1 | 1 | 2 | 1 | **10** |
| 5. Причины срабатываний АЗ: | | | | | | | | | |
| 5.1. Посадки напряжения | | 2 | | 1 | 1 | 1 | 2 | 1 | **8** |
| 5.2. Неисправности и отказы оборудования | | 1 | | 1 | | | | | **2** |
| 5.3. Сбои в электронной аппаратуре | | | | | | | | | |
| 5.4. Ошибки персонала | | | | | | | | | |

**Основные результаты по модернизации ИБР-2 в 2005 г.:**

1) Новая топливная загрузка.
   - Завершены работы по созданию участка сборки ТВЭЛ в ТВС. Участок принят в эксплуатацию комиссией из представителей ОИЯИ, ГСПИ, ВНИИНМ, НИКИЭТ.
   - В настоящее время идет процедура по получению лицензии на сборку ТВЭЛ.

2) Основное оборудование реактора ИБР-2М.
   - В НИКИЭТ продолжалось изготовление нового корпуса реактора.
   - Завершено изготовление внутрикорпусного перегрузочного устройства.

3) В ОП ОИЯИ изготовлены откатные устройства для размещения замедлителей реактора ИБР-2М и защитные технологические пробки.
4) СУЗ ИБР-2М.
   - В НИКИЭТ завершена разработка конструкторской документации исполнительного механизма аварийной защиты.
   - Изготовлены опытные образцы исполнительных механизмов АР и КО.
   - В СНИИП-СИСТЕМАТОМ завершена разработка АСУЗ, ведется изготовление опытного образца.
   - Начаты работы по созданию системы контроля технологических параметров (ИНЭУМ).
5) Комплекс замедлителей ИБР-2М.
   - Продолжались макетные работы по транспортировке шариков из $C_9H_{12}$.
   - В НИКИЭТ начат технический проект комплекса замедлителей ИБР-2М.
   - В ГСПИ начата разработка технологической части проекта замедлителей.
   - В Гелиймаше продолжалось изготовление КГУ-700/15.

Финансовое обеспечение работ по модернизации ИБР-2 в 2005 г. видно из **таблицы 2.**

***Таблица 2***

Состояние с финансированием модернизации ИБР-2 в 2005 г. (k$) на 30.12.2005 г.

| | | **1995-2004** | **2005** |
|---|---|---|---|
| **ОИЯИ** | План | 2190 | 650 |
| | Факт | 1791 | 540 |
| | % | 81,7 | 83 |
| **Росатом** | План | 1970 | 400 |
| | Факт | 1746 | 400 |
| | % | 88,6 | 100 |
| **Всего:** | План | 4160 | 1050 |
| | Факт | 3537 | 940 |
| | % | 85 | 90 |

**Планы на 2006 г.**

1. Сборка ТВЭЛ в ТВС.
2. Завершение изготовления корпуса реактора.
3. Создание опытного образца АСУЗ.
4. Продолжение работ по откатным защитам и стационарным отражателям ИБР-2М.
5. Завершение работ в «Гелиймаше» по изготовлению КГУ-700/15.
6. Выпуск технического проекта комплекса замедлителей.
7. Разработка технологической части проекта комплекса замедлителей.

**Комплекс замедлителей для реактора ИБР-2 М**

**Нейтронно-физические расчеты и оптимизация материала и геометрии холодных замедлителей.** В течение 2005 года была проведена работа по оптимизации размещения криогенных замедлителей на реакторе ИБР-2М, а также сочетание их с конфигурацией замедлителей для тепловых нейтронов. В результате решен вопрос в удовлетворении требований исследователей на выведенных пучках по спектрам нейтронов. Для некоторых каналов присутствие в спектре нейтронов больше холодных, для других тепловых и для третьих смешанных.

Таким образом, спектры нейтронов для каналов 1, 2, 4-6, 8 и 9 будут иметь в своем составе больше холодных нейтронов (**Рис.1**). На этом и других рисунках приведены данные для плотности потока нейтронов от одного нейтрона, рожденного в реакторе, на расстоянии 4.5 метра от замедлителя).

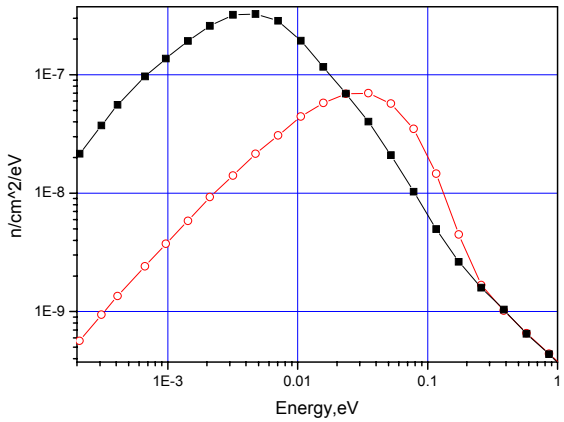


***Рис. 1.*** *Дифференциальные спектры нейтронов для исследовательского пучка №5, нормированные на один нейтрон источника. Квадраты – результат использования мезитиленового криогенного замедлителя в наилучшей конфигурации без бериллия; окружности – результат использования воды комнатной температуры на месте холодного замедлителя.*

Распределение плотности потока нейтронов на поверхности криогенного замедлителя направления каналов 4-6 представлено на **рисунке 2 (а, б).**

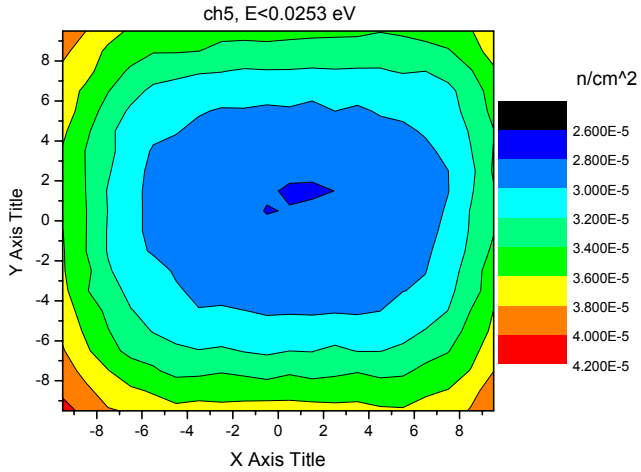


а)

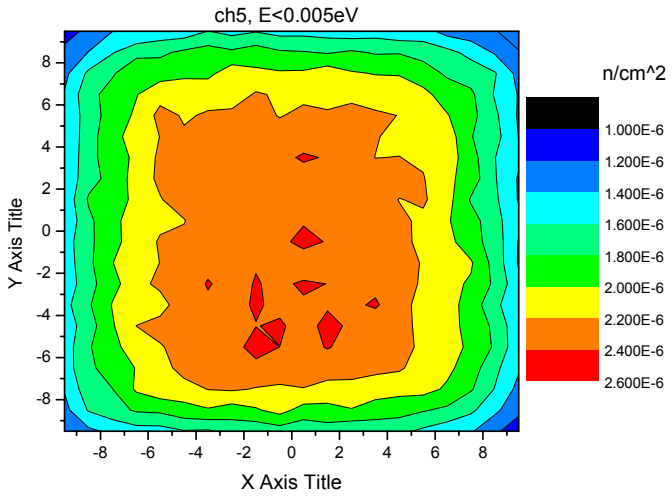


б)

***Рис. 2.*** *Результаты расчетов распределения интегральных плотностей потока тепловых а) и холодных б) нейтронов, нормированных на один нейтрон источника, на поверхности холодного замедлителя. По X – откладывается ширина замедлителя, по Y – высота.*

Исследовательские каналы 7 и 10 будут иметь смешанный спектр нейтронов **(Рис.3).**

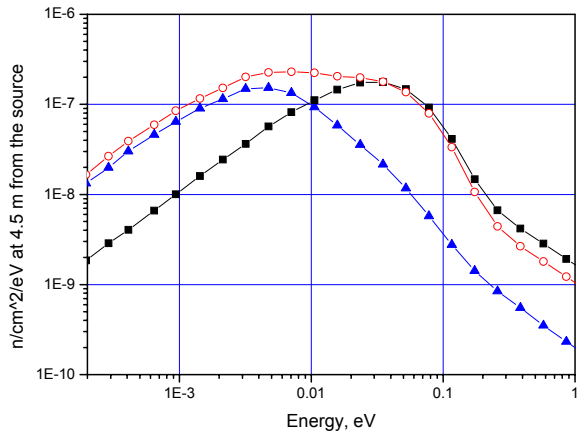


***Рис. 3.*** *Дифференциальные спектры нейтронов для 7 канала, нормированные на один нейтрон источника. (квадраты – только предзамедлитель, окружности - оптимальная конфигурация замедлителей (холодный+гребенчатый тепловой), треугольники – спектр полученный только с холодной части с учетом частичного затенения гребнями водяного замедлителя)*

Для исследовательского канала №11 проведена дополнительная оптимизация теплового замедлителя, который будет расположен ортогонально данному каналу, что увеличивает интегральную плотность потока тепловых нейтронов ~ в 3 раза **(Рис. 4).**

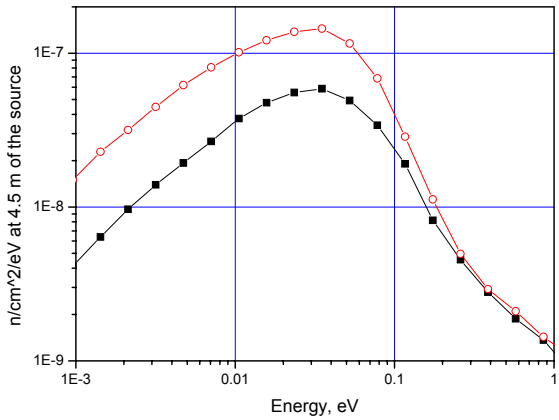


***Рис. 4.*** *Дифференциальные спектры нейтронов для 11 канала. (квадраты – только предзамедлитель, окружности - наличие оптимальной конфигурации замедлителей)*

Методика расчета спектра нейтронов обоснована сравнением с экспериментальными данными полученными на установке JESSICA (Юлих, Германия).

Новым, ранее никем не полученным результатом является то, что постзамедлитель в виде «рамки» (водяной отражатель вокруг плоского замедлителя с размером поверхности 18×18 см) дает выигрыш в средней по поверхности плотности векторного потока утечки нейтронов в 2 раза, т.е. столько же, сколько известный гребенчатый замедлитель (распределение нейтронов по поверхности см. на рис. 2). Ранее считалось, что такая конфигурация замедлителя эффективна лишь для малой поверхности порядка 5×5 см. К тому же, одновременное использование гребенчатого замедлителя и «рамки» увеличивает выигрыш до 2.4.

**Шариковый холодный замедлитель.** В 2005 году был предложен и разработан принцип конструкции холодного замедлителя, основанный на использовании шариков из замороженной смеси мезитилена и m-ксилола, обеспечивающий предельно-возможный поток холодных нейтронов (на уровне проектируемого твердометанового замедлителя второй мишени источника ISIS) на реакторе ИБР-2М при длительной непрерывной работе.

Шариковый холодный замедлитель способен работать при температуре 20К-30К без перезагрузки рабочего вещества не менее трех-пяти дней в потоке быстрых нейтрронов до 2 $10^{13}$ н/см$^2$/с. Твердые шарики из смеси мезитилена с псевдокумолом или *m*-ксилолом периодически сменяются в камере замедлителя путем их размораживания и слива отработанного вещества в виде жидкости. Такая смесь в замороженном состоянии имеет аморфную структуру, что важно во многих отношениях – как для увеличения выхода холодных нейтронов, так и для получения правильных однородных шариков. Камера замедлителя имеет форму параллелепипеда со стенками из алюминиевого сплава АМг; размеры камеры– 20 см высота, 4 см толщина и ширина от 15 до 20 см (для разных замедлителей). Камера окружена также алюминиевой оболочкой для создания вакуумной теплоизоляции. К камере сверху подходит труба подвода холодного гелия и трубка подачи шариков. Дно камеры выполнено в виде сетки с размером ячеек, меньше, чем размер шариков (5 мм). Снизу от камеры отходит труба отвода холодного гелия и труба для слива жидкого отработанного мезитилена.

В начале работы охлажденная камера заполняется шариками, которые доставляются потоком холодного гелия с температурой 30-80К (наиболее адекватная температура будет выбрана по окончанию исследований по транспорту шариков). Этим же гелием с входной температурой 20-22 К шарики охлаждаются в процессе нормальной работы. По истечению времени, когда выгорание мезитилена уже начнет сказываться на выходе холодных нейтронов (примерно 3-5 дней; это время будет определено во время физического пуска

замедлителя ), поток гелия прерывают, мезитилен расплавляется ядерным теплом и в жидком виде сливается в емкость для последующей утилизации. Камера и весь тракт охлаждения очищаются от остатков мезитилена потоком теплого гелия, и цикл работы повторяется. Принципиальная возможная схема охлаждения и циркуляции шариков дана на **рисунке 5**

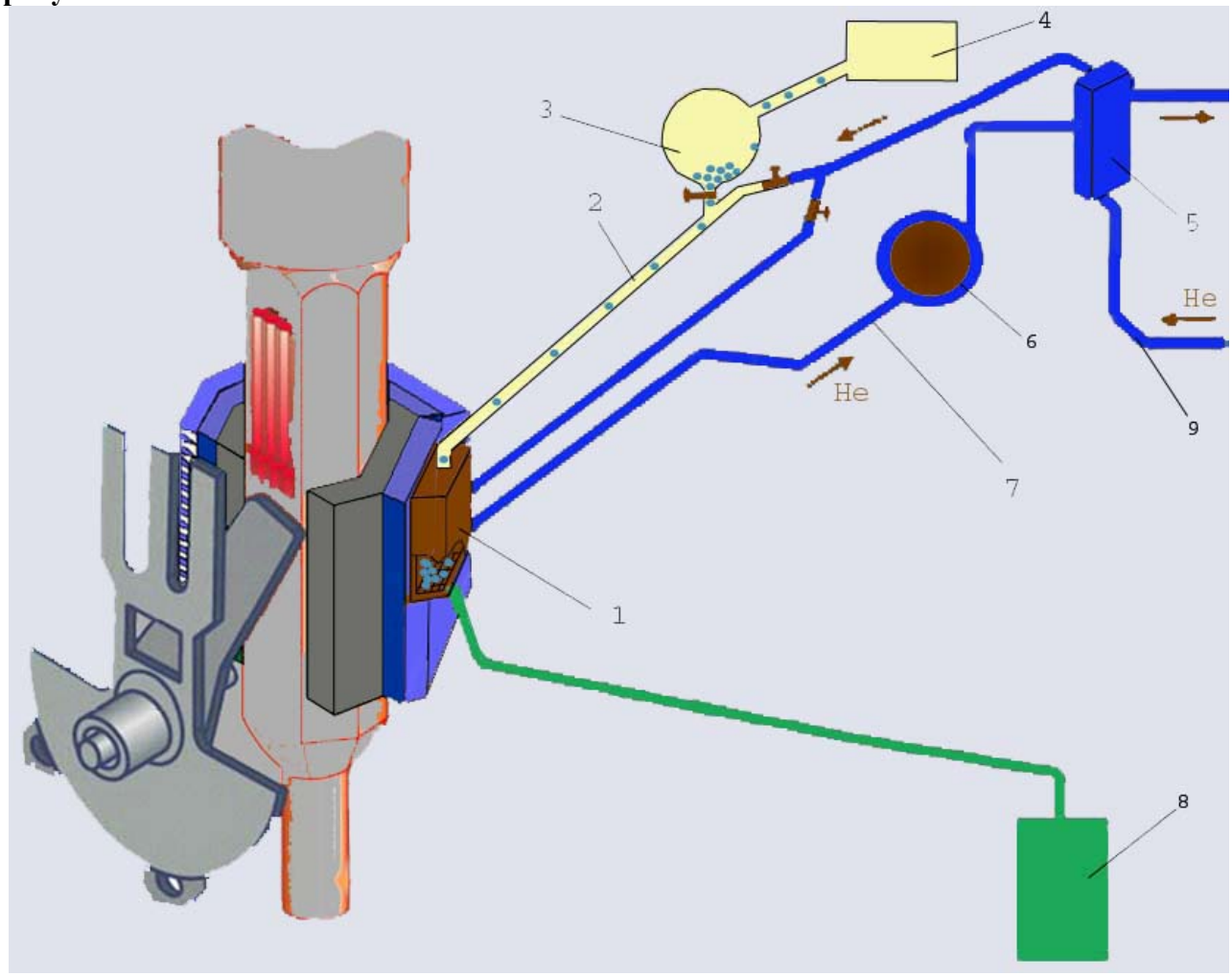


***Рис.5***. *Схема подачи шариков и охлаждения холодного замедлителя. 1 – камера замедлителя, 2 – канал пневматической загрузки шариков, 3 – шлюз подачи шариков, 4 – устройство генерации шариков, 5 – гелиевый теплообменник, 6 – гелиевая газодувка, 7 – трубопровод холодного гелия второго контура, 8 – сливная емкость для жидкого мезитилена, 9 - трубопровод холодного гелия первого контура.*

Ресурс работы такого шарикового замедлителя будет практически не ограничен, в отличие от традиционного блочного твердометанового замедлителя; например, на источнике ISIS в Резерфордовской Лаборатории метановый замедлитель полностью заменяется дважды в год.

Обработка данных облучательных экспериментов твердого мезитилена в цилиндрической стальной оболочке с привлечением пакета программ COSMOS-M позволила установить диапазон внутренних напряжений в твердом мезитилене. Было получено, что наблюдаемому давлению на стальную цилиндрическую оболочку в 10 бар после облучения дозой 10.8 МГр при температуре 130 К, когда начинает выходить накопленный радиолитический водород, соответствует внутреннее давление в мезитилене 70-75 бар. Водород выходит тогда, когда появляются разрывы материала, т.е. напряжения превышают предел прочности материала. Значит, предел прочности твердого облученного мезитилена при 130 К – 70-75 бар. Пересчет на условия облучения на будущем реакторе ИБР-2М дает

значение внутреннего давления в мезитилене 62-67 бар/сутки при 33 К. Прочность молекулярных кристаллов значительно выше при низких температурах. Поэтому есть основания полагать, опираясь на данные по необлученным молекулярным кристаллам , что при 33 К предел прочности твердого облученного мезитилена будет не менее 270-300 бар. В таком случае, он будет превышен только после облучения в течение 4-5 суток для шариков в зоне наибольшего потока нейтронов, и после 7-8 суток - для среднего по замедлителю потока.

Смену шариков в камере замедлителя нужно будет производить не чаще 2-х раз в двухнедельном цикле работы реактора; основанием к замене шариков, скорее всего, будет служить мера деградации потока холодных нейтронов вследствие выгорания мезитилена.

Принципиальная схема гелиевого охлаждения холодного замедлителя дана на рисунке 6.

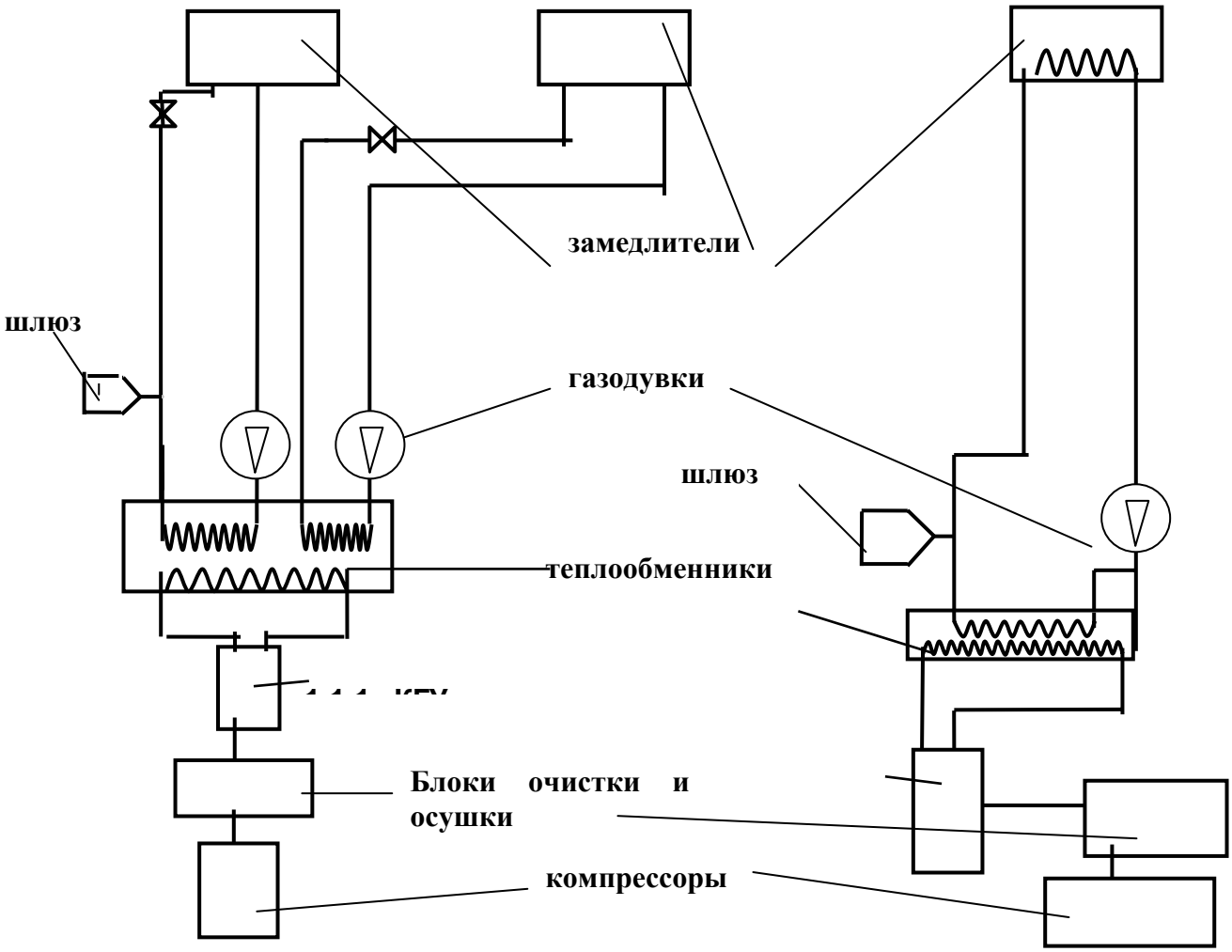


***Рис. 6.*** *Схема гелиевого охлаждения холодного замедлителя.*

Охлаждение замедлителя – двухконтурное. По первичному контуру, в котором находится камера, гелий циркулирует специальной газодувкой BNHeP-25 фирмы Barber-Nicols производительностью до 100 нм$^3$/час. Для каждого из замедлителей – свой контур с газодувкой и трактом подачи шариков. Во вторичном контуре источником холода является холодильная гелиевая установка. Так как на реакторе ИБР-2М предусматривается установить три холодных замедлителя, будет соответственно три первичных контура и два вторичных с холодильными гелиевыми установками ХГУ-500 и КГУ-700 хладопроизводительностью соответственно 500 и 700 Вт при температуре 15 К. Каждая холодильная гелиевая установка

отдает холод в первичные контуры через свой теплообменник. Нагрев гелия складывается из следующих составляющих:

- Ядерное тепло в замедлителе
- Нагрев в газодувках
- Приток тепла в трубах, теплообменниках и вентилях.

Ядерное тепло в шариках мезитилена и в алюминии камеры рассчитано по программе MCNP-4 и равно 0.15 Вт/см$^3$ в мезитилене и 0.05 Вт/г в алюминии. Для размеров замедлителя 15 на 20 на 4 см это составит 150 - 170 Вт.

Нагрев гелия в газодувках, согласно уравнению адиабатического процесса при изменении давления на 10%, составит порядка 1 градуса, что эквивалентно тепловой мощности около 60 Вт .

Приток тепла в трубах зависит от их исполнения; примем вполне реальное значение – 1.0 Вт/м. Суммируя тепловыделение по всему тракту охлаждения замедлителей правого и левого направлений (на 2-ой и 8-ой нейтронные пучки) , получим 530-570 Вт, включая ядерное тепло.

Суммируя тепловыделение по всему тракту охлаждения замедлителя центрального направления (на 4-ой - 6-ой нейтронные пучки) , получим около 300 Вт. Таким образом, для обеих петель тепловыделение меньше проектной хладопроизводительности холодильных гелиевых установок. Для направления 4-6 пучки возможна установка пост-замедлителя из холодного бериллия; в этом случае тепловая мощность возрастает на ~ 100 Вт и составит ~ 400 Вт. Расчетная минимальная температура мезитилена на поверхности шарика (на входе гелия в камеру) равна $T_{не}(0)$+5.5 К; максимальная температура мезитилена (на выходе из камеры) - $T_{не}$ (0)+10.5 К. Исходя из условия не превышения критической температуры водорода 33 К, получаем верхний предел температуры гелия на входе в камеру замедлителя 22 К.

**Транспорт шариков и стенд для отработки транспорта.** Как сказано выше**,** подача шариков мезитилена в камеру замедлителя будет осуществляться пневматически – потоком холодного гелия. Характеристики тракта подачи определяются следующими условиями:

- Скорость шариков не должна превышать предельной скорости, при которой они могут разрушиться при ударе о стенку транспортной трубы или камеры (оценочное значение – 4 м/с, определенное по бросанию с определенной высоты холодных шариков на металлическую поверхность).
- Время заполнения камеры не должно превышать 0.5 – 1 часа;
- Должна быть исключена закупорка шариков в транспортной трубе.

Последнее условие выполняется, если диаметр трубы превышает 2.2 диаметра шарика. Это следует из геометрических соображений: любое пространственное размещение шариков в этом случае будет неустойчиво. При диаметре шариков 7 мм (максимально допустимый диаметр по соображениям теплосъема) диаметр трубы составит 16 мм.

При максимальной длине тракта 25 метров, диаметре шариков 7 мм, объеме камеры замедлителя 1.2 литра и полном числе шариков N = 3000 примем среднее значение скорости шариков равным 2 м/с. Тогда при времени заполнения 1 час число шариков, одновременно находящихся в трубе, должно быть не менее 10, а при времени заполнения 0.5 часа – 20. Эти цифры выглядят разумно – при расстоянии между шариками 1–2 метра не нарушается режим течения газа, так как это расстояние порядка 100 диаметров трубы, что вполне достаточно для восстановления стабильного режима. Все шарики будут вести себя так, как если бы в тракте был один шарик. Это позволяет упростить эксперименты по транспорту шариков на стенде. Опыты показали, что одновременное движение 10 шариков не изменяет заметно их скорости.

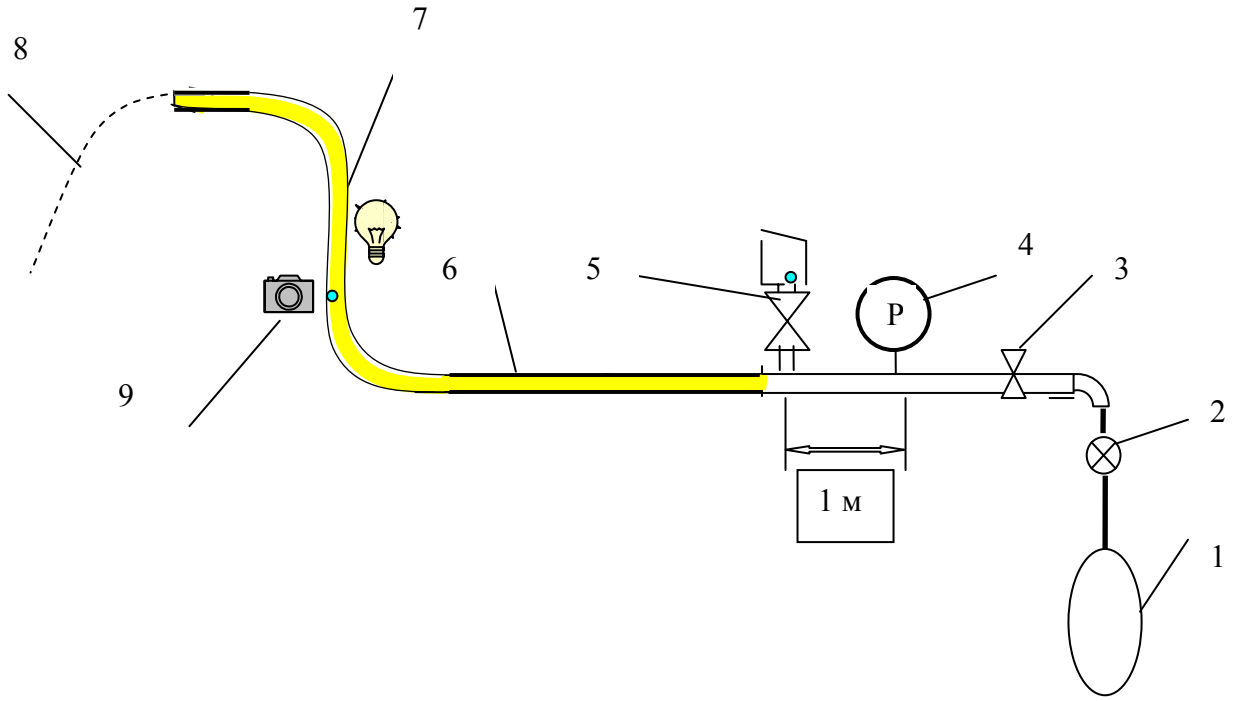


***Рис. 7.*** *Схема стенда для опытов по транспорту шариков. Обозначения: 1 – баллон со сжатым газом, 2 – редуктор, 3 – дроссельный вентиль, 4 – расходомер, 5 – шлюз загрузки шариков, 6- прямая транспортная труба длиной около 5 м, 7 – изогнутая часть трубы ( до 1 м высотой), 8 – траектория шарика после вылета из трубы, 9 – цифровая фотокамера в режиме видео и подсветка.*

**Сравнение расчетного и экспериментального коэффициентов сопротивления.** Сравнение было сделано на основе экспериментов по удержанию шариков в наклонной трубе ($45^0$) потоком азота комнатной температуры. Исходные данные: Диаметр трубы – 14 мм, диаметры шариков и их плотности: 5 мм – 2.3 г/см$^3$ , 6 мм – 1.7 г/см$^3$ , 8 мм – 1 г/см$^3$ . Расчет коэффициентов сопротивления делался для ламинарного режима обтекания шарика. Получено хорошее согласие экспериментов с теорией. Однако это не вызывает оптимизма по следующим причинам:

- Погрешность экспериментальных значений коэффициента сопротивления составляет ± 20 %;
- Сравнение сделано для скорости шарика равной нулю; не ясно, работает ли теория при ненулевой скорости шариков или надо использовать более общий подход.

Вследствие сказанного, предполагается сделать эксперименты по измерению скорости и ускорения шарика в процессе движения по трубе. Причем исследовать надо как прямые участки, так и изгибы и наклоны. Из этих данных можно будет сделать однозначное заключение о том, какое уравнение надо применять для расчета движения шарика. Достаточно измерить функцию «ускорение-скорость» для прямой трубы в широком диапазоне скорости шарика, и этого будет достаточно для последующего расчета движения шарика в любой конфигурации трубы (при тех же диаметрах трубы и шарика и того же расхода газа, что и в эксперименте). Скорость шариков измеряется сразу в нескольких точках с помощью цифровых фотокамер в режиме видео **(рис. 8).**

Принципиальное устройство генератора шариков дано на **рис. 9**.

**Получение шариков, схема генератора.** Метод получения твердых шариков мезитилена основан на замораживании капель жидкого мезитилена в азоте. Принципиальными параметрами для получения однородного твердого шарика является короткое время нахождения шарика в азоте, а также добавление некоторого количества m-ксилола в жидкий раствор. Последнее дает аморфную структуру, более прочную в

отношении растрескивания. Был разработан принцип генерации массового количества шариков мезитилена.

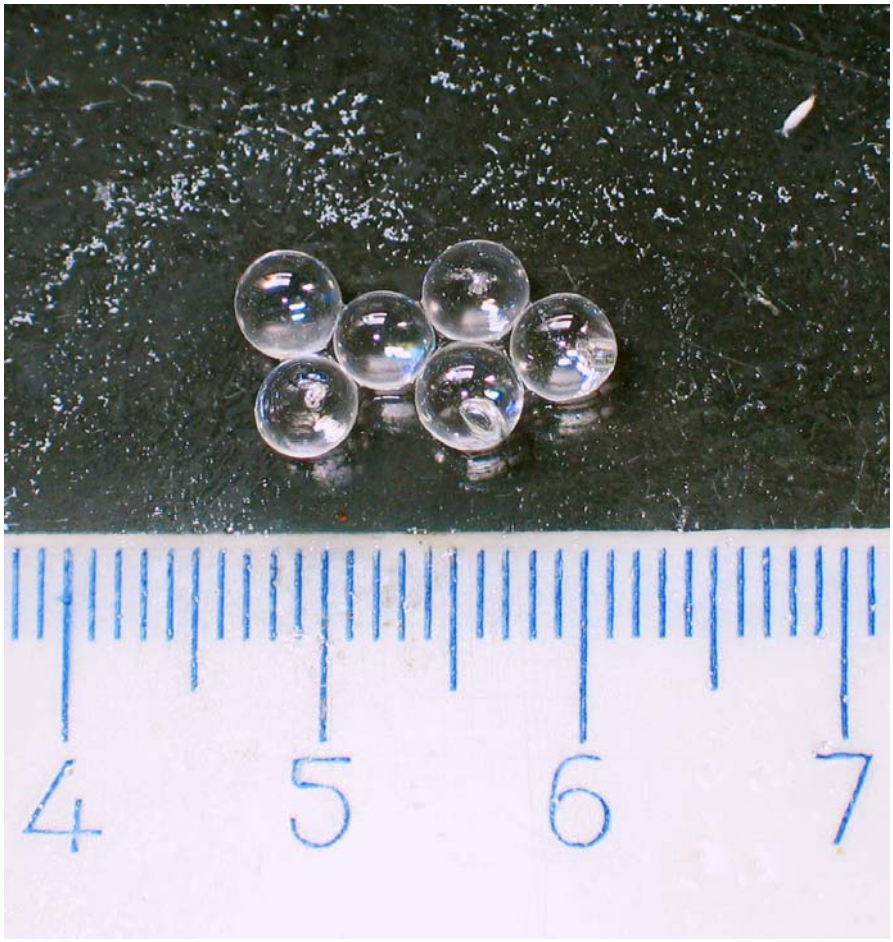


***Рис. 8.*** *Шарики твердого мезитилена; крупные деления линейки – в сантиметрах.*

**Заключение**

Главные результаты работ по проекту комплекса замедлителей для ИБР-2М в 2005 году и выводы:

1. Предложенный принцип работы мезитиленовых замедлителей (использование твердых шариков из смеси мезитилена и *м*-ксилола, их транспортировка холодным гелием, периодическое расплавление шариков и их замена без перерыва в работе реактора) вполне реализуем и может обеспечить практически неограниченный ресурс работы замедлителей.
2. Плотность потока холодных нейтронов на поверхности замедлителя из шариков мезитилена с температурой 20 К будет достигать 3 $10^{13}$ н/см$^2$ /с/ср/ангстрем при 4 ангстремах, что является рекордным значением для европейских источников.
3. Можно обеспечить температуру гелия 20-22К для охлаждения трех мезитиленовых замедлителей при наличии двух холодильных машин – ХГУ-500 и КГУ-700.
4. Составлено техническое задание (совместно с НИКИЭТ и ГСПИ) на выполнение технического проекта комплекса замедлителей для реактора ИБР-2.

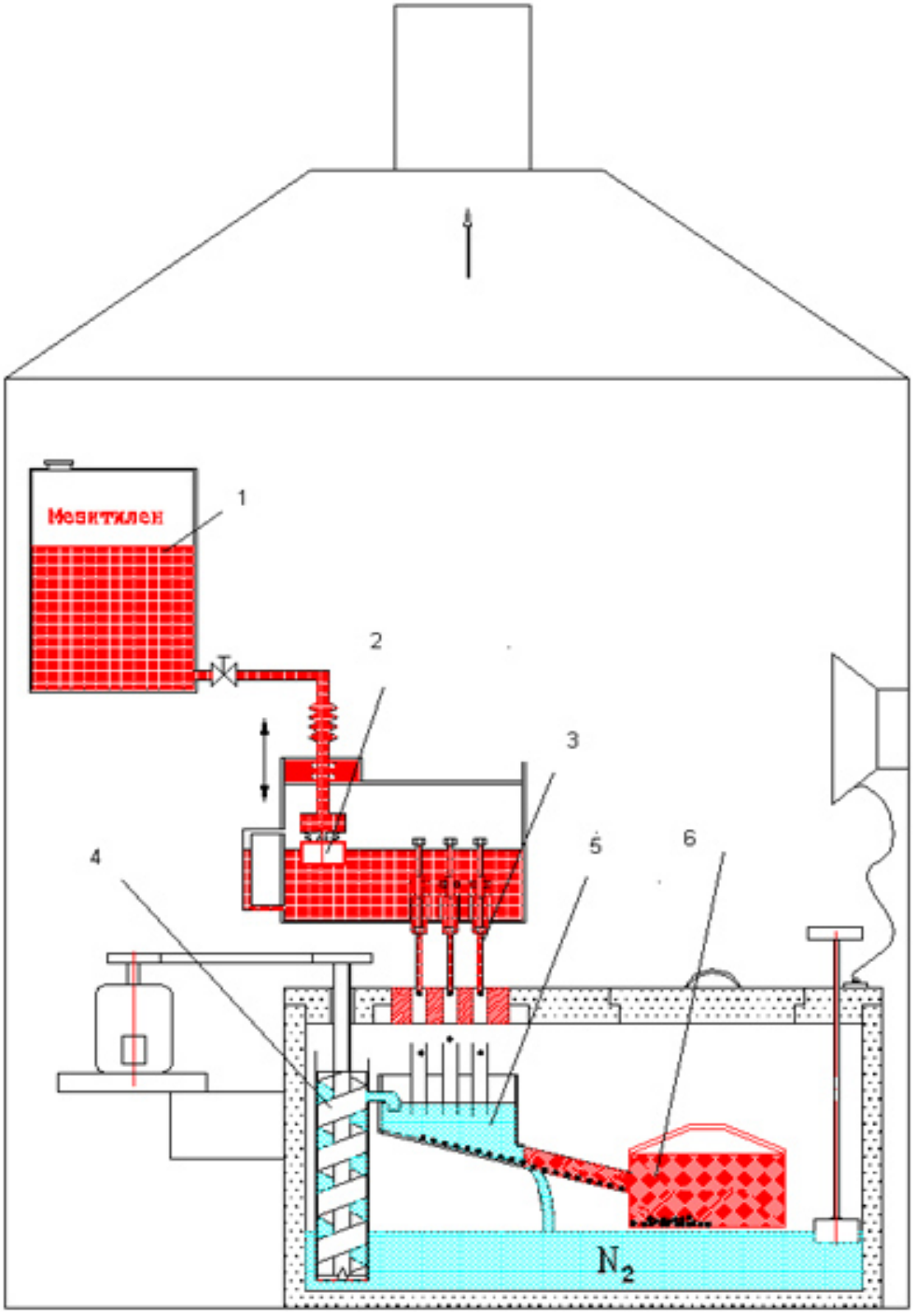


***Рис. 9.*** *Принципальная схема генератора массового количества шариков. 1 – сосуд с жидким раствором мезитилена и м-ксилола; 2 – регулятор уровня жидкости; 3 – капельницы; 4 – насос для циркуляции жидкого азота; 5 – сосуд с наклонным дном и отверстия для слива азота; 6 - емкость-коллектор шариков.*

## 2.2. Проект ИРЕН

Основные усилия и средства были сосредоточены на завершении подготовки и проведении работ по демонтажу реактора ИБР-30.

Для получения положительной экологической экспертизы проекта вывода из эксплуатации ИБР-30 была спроектирована и создана сеть опорных скважин для контроля состояния подземных вод на площадке ЛЯП. Были проведены завершающие тренировки персонала по выполнению отдельных технологических операций демонтажа оборудования реактора и разгрузки активной зоны. Благодаря настойчивой работе руководства ЛНФ и ее технических подразделений в середине октября удалось начать демонтаж реактора. Значительная часть активированного оборудования реактора была демонтирована и перевезена на временное хранение в зд. 117/6. К середине ноября была закончена высверловка урановых вкладышей из подвижных частей активной зоны ИБР-30. Освобожденное топливо было эвакуировано на хранение в ОРДВ ОИЯИ. К концу года планируется завершить разгрузку основной активной зоны реактора и перевезти отработанное топливо на хранение в ОРДВ. Окончание демонтажа остального оборудования реактора ИБР-30 запланировано на первую половину 2006 года.

Определенный прогресс был достигнут и в создании линака ЛУЭ-200. После приобретения недостающей части специальной медной трубки были продолжены остановленные в сентябре 2004 года работы по намотке катушек соленоида магнитной фокусирующей системы. К началу 4-го квартала эти работы были завершены. Проведенные магнитные измерения показали соответствие параметров изготовленных катушек проектным значениям. До конца года будет завершена контрольная сборка магнитной фокусирующей системы на стенде ЛФЧ, после чего система будет перевезена в зд. 43 ЛНФ для сборки и наладки на штатном месте.

Завершены работы по монтажу модулятора М350 в ускорительном зале зд.43. В настоящее время завершается тестирование систем модулятора и подготовка к его пуску. Успешно завершились вакуумные испытания оборудования магнитного спектрометра. Начинаются работы по его контрольной сборке на стенде.

Были проведены численные исследования по моделированию динамики пучка электронов в ускорительном тракте ЛУЭ-200 с целью оптимизации системы фокусировки и минимизации потерь частиц, определены критерии учета погрешностей магнитных полей в тракте ускорителя.

Большая работа была проведена специалистами ОИЯИ и ГСПИ по рабочему проектированию системы водоохлаждения ускорителя ЛУЭ-200. Планируется ее завершение к концу года.

Начата работа по созданию рабочего проекта системы электроснабжения ускорителя.

Завершен проект реконструкции помещения пультовой ЛУЭ-200 и комнат для размещения систем электропитания и водоохлаждения в зд. 43. Начаты работы по ремонту и переоборудованию указанных помещений.

В третьем – четвертом кварталах были, наконец, оплачены счета по договорам с ИЯФ, Новосибирск, что позволяет надеяться на поставку в 2006 году оборудования, необходимого для завершения монтажа и комплексной наладки оборудования ЛУЭ-200.

К сожалению, не удалось в полном объеме выполнить работы ускорителя ЛУЭ-200, намеченные на 2005 год, в основном, из-за задержки или отсутствия запланированного финансирования. Тем не менее, создан необходимый задел для выполнения задач, предложенных в ПТП 2006 года, с конечной целью пуска к концу 2007 года первой очереди установки ИРЕН с неразмножающей нейтронно-производящей мишенью и стендом для прикладных исследований.

## 3. DEVELOPMENT AND CREATION OF ELEMENTS OF NEUTRON SPECTROMETERS FOR CONDENSED MATTER INVESTIGATIONS

In 2005 work in the framework of the theme was focused on the following main activities:

- creation of neutron detectors;
- development of sample environment systems;
- development of data acquisition systems and computing infrastructure.

### 3.1. Creation of neutron detectors

In 2005 pilot models of 1D detector and 2D monitor were constructed and tested on a test bench with a source and at the IBR-2 beams. Both detectors are based on multiwire proportional chambers with delay line data readout. This allowed us to unify to a maximum extent the readout electronics (preamplifiers, discriminators, etc.) and data acquisition electronics (data conversion and filtering, histogramming, etc.) as well as basic program modules and interfaces. Data accumulation and visualization are carried out on personal computers.

The methodical studies conducted earlier and the prototyping of individual units made it possible to plan with a high degree of reliability the following characteristics of the 2D monitor and 1D detector (Table 1):

Table 1

| | 2D monitor | 1D detector |
|---|---|---|
| Gas mixture | 50 mbar $He^3$+950 mbar $CF_4$ | 2000mbar $He^3$+1000mbar $CF_4$ |
| Efficiency | 0.1% | 40% |
| Sensitive area | 100×100 $mm^2$ | 200×80 $mm^2$ |
| Coordinate resolution | 4×4 $mm^2$ | 2 mm |
| Count rate | up to $10^5$ events/s | up to$10^5$ events/s |
| Differential nonlinearity | <5% | <5% |
| Readout | Delay line | Delay line |

The trials of the monitor and 1D detector performed during two spring and three autumn cycles at IBR-2 have verified the specified characteristics.

#### 3.1.1. 2D monitor

The 2D monitor is a multiwire proportional chamber. The overall dimensions of the chamber are 320×320×23 mm, the thickness of the entrance and exit windows is 1 mm **(Fig.1).** This thickness value has been chosen on the one hand to minimize the influence on an incident neutron flux, and on the other hand to make it possible to endure mechanical loads under changes of atmospheric pressure. High voltage of positive polarity is fed via an MHV connector. Five BNC connectors serve for signal output. The detector has 2 gas connectors of the "Swagelock" type and this permits the use of the detector in a flow operating mode.

In the chamber volume two cathode and one anode electrodes are positioned. Each of the electrodes is a textolite frame with a cut-out window with wound fine wires of gold plated tungsten. The thickness of anode wires is 10 μm and of cathode wires – 50 μm. The anode wire spacing is 2 mm. The anode wires are connected by a common bus. The cathode wire spacing is 1 mm and the cathode wires are connected together in pairs and brought out to the delay line, each element of which delays signals by 2.9 ns. The cathode spacing is 12 mm, the anode is positioned in the middle.

***Fig.1.*** *2D monitor case.*

To detect neutrons, the chamber volume is filled with a mixture of neutron converter gas $He^3$ and quenching gas $CF_4$. (For high fluxes $N_2$ can be used as a neutron converter). The quenching gas is necessary to reduce the path length of charged particles formed as a result of interaction of neutrons with the converter, as well as to suppress secondary effects. The total pressure of the gas mixture is 1000 mbar, the partial pressure of $He^3$ is from 1 to 50 mbar depending on a maximum load. **Figure 2** illustrates the result of uniform exposure of the monitor during the test trials using a neutron source.

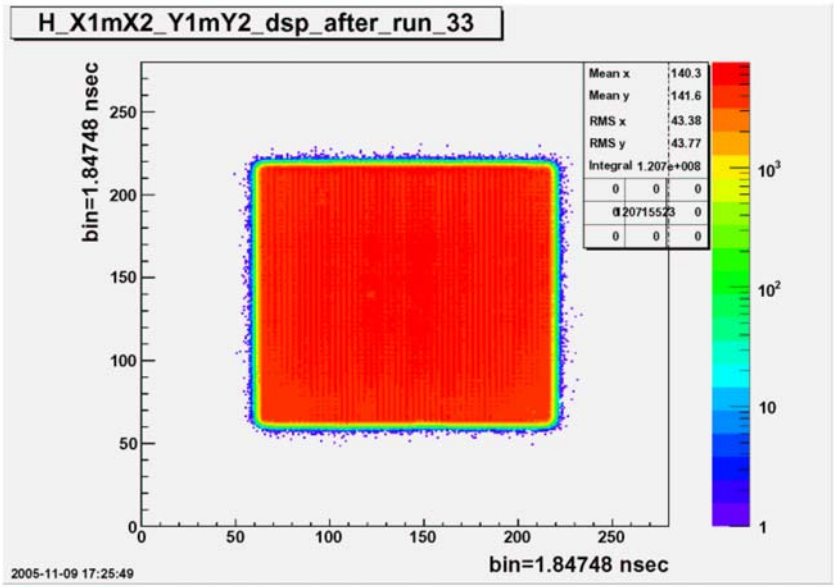


***Fig.2.*** *Uniform exposure of the 2D monitor.*

The coordinate resolution was measured in the following way. The detector with a cadmium mask was placed in a neutron beam. The mask is a cadmium plate 1 mm thick with the cut slits 0.5 mm wide. The slit spacing is 10 mm. The obtained spectra were summed over the Y-axis (with the resulting integrated spectrum over the X-axis). The peaks were approximated by the Gauss distribution, full width at half maximum was determined. The coordinate resolution measured by this method proved to be no worse than the planned 4 mm (3.7 mm at the centre, 3.9 at the edges). Also, during the measurements the profiles of beams 6b and 10 were obtained. These spectra are presented in **Figs. 3** and **4**.

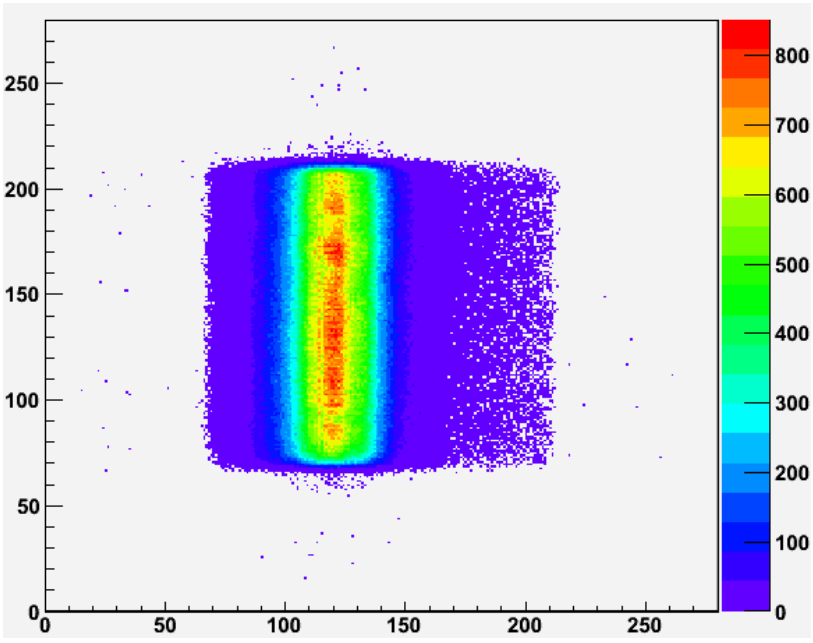


***Fig. 3.*** *Measurement of beam profile (beam 6b) of the IBR-2 reactor. Gas mixture — 50 mbar $He^3$ + 950 mbar $CF_4$. Measurement time — 5 min. Voltage across the anode — +3300V.*

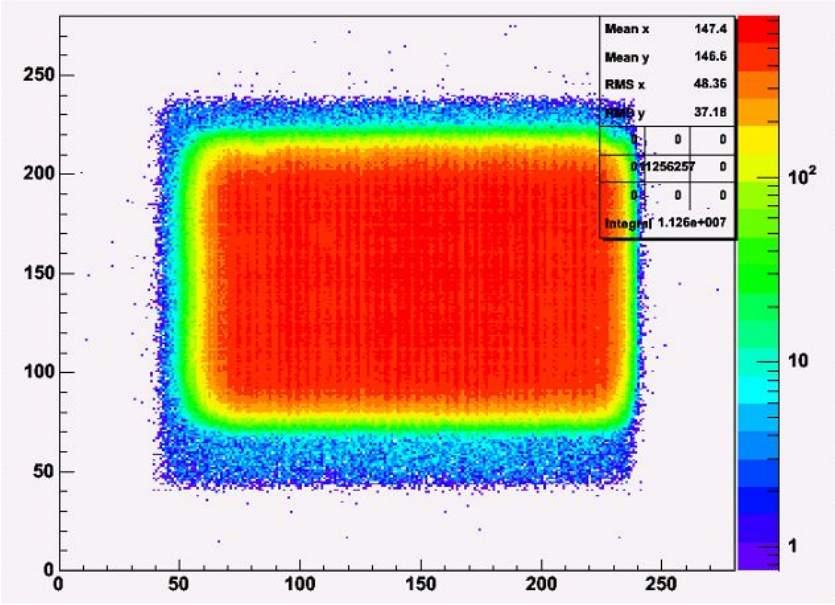


***Fig. 4.*** *Measurement of beam profile (beam 10) of the IBR-2 reactor. Gas mixture — 50 mbar $He^3$ + 950 mbar $CF_4$. Measurement time — 15 min. Voltage across the anode — +3300V.*

The specified gas mixture composition is intended for work in medium-intensity beams ($10^4$-$10^6$ neutron×s/cm$^2$). To work with high fluxes ($10^6$-$10^8$ neutron×s/cm$^2$) the possibility to use $N_2$ as a converter gas is to be studied.

For visual evaluation of the detector performance a cadmium mask with letters "ЛНФ" and its image obtained with the help of the detector are given in **Fig.5.**

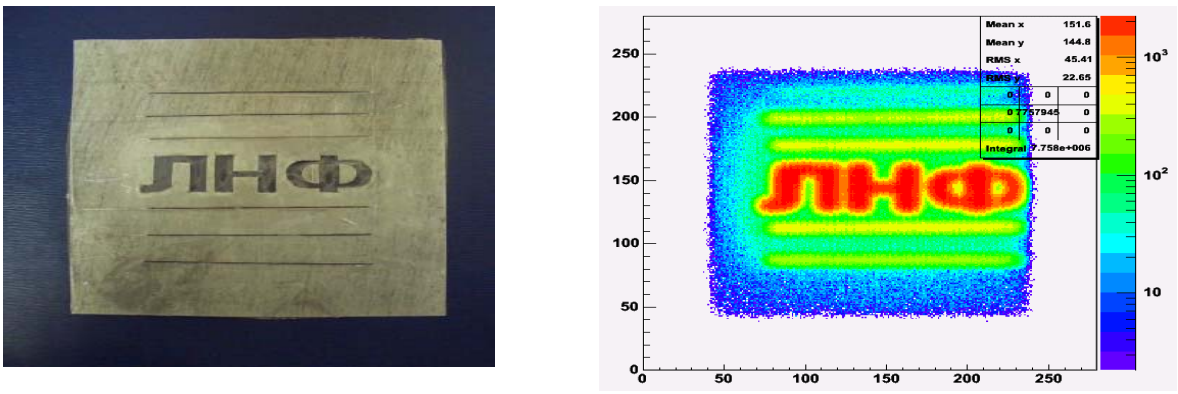


***Fig. 5.*** *Exposure measurement using a cadmium mask "ЛНФ". 50 mbar $He^3$ + 950 mbar $CF_4$. Measurement time — 15 min. Voltage across the anode — +3300V.*

### 3.1.2. One-dimensional PSD

**Figure 6** presents a photo of the 1D detector case made by the same technology on the basis of a multiwire proportional chamber. In the chamber volume there are cathode, anode and drift electrodes. The thickness of anode wires is 10 μm and of cathode wires – 50 μm. The anode wire spacing is 2 mm and the cathode spacing is 1 mm.

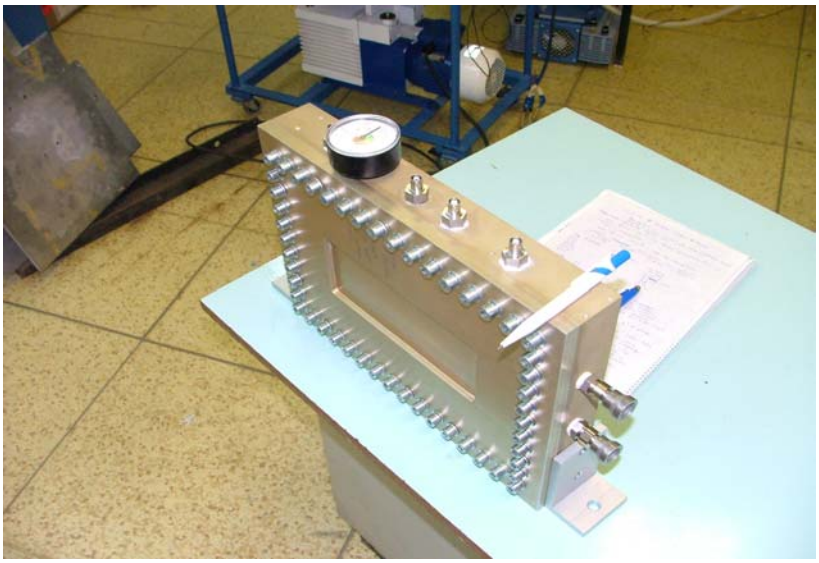

***Fig.6.*** *1D detector case.*

**Figure 7** illustrates the result of uniform exposure/illumination of 1D detector filled with a test mixture during measurements with a neutron source. The obtained differential nonlinearity is no more 8%.

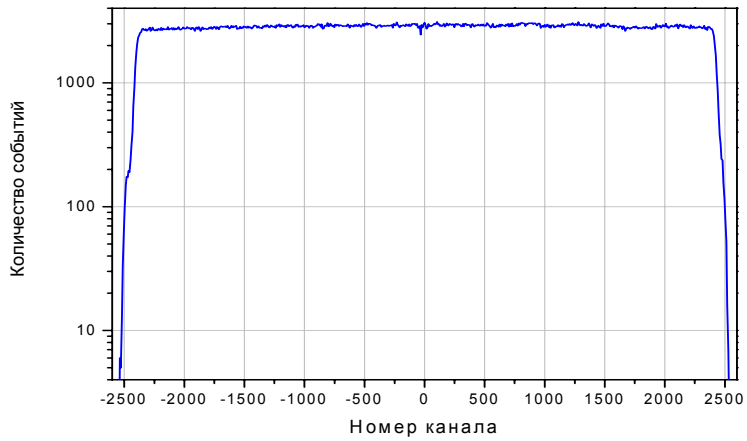


***Fig.7.*** *Uniform exposure of 1D detector (+U=+3600 V, –U=–2000 V).*

During the 6th cycle of the IBR-2 reactor (October 17-28, 2005) test and routine diffraction measurements were carried out at the TEST spectrometer (beam 6b) and the HRFD diffractometer (beam 5). A block scheme of the measuring channel is given in **Fig.8.**

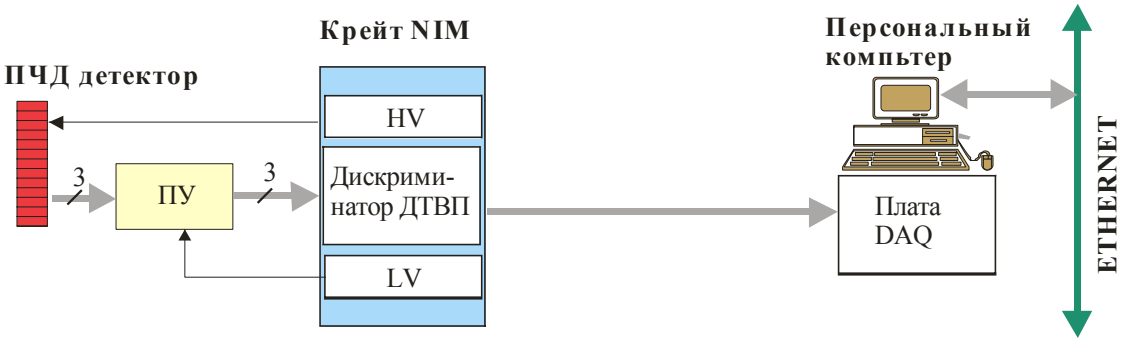


***Fig.8.*** *Block scheme of the measuring channel*

The detector characteristics were measured on beam 6b of the IBR-2 reactor. The 1D detector was filled with a gas mixture composed of neutron converter gas $^3$He and quenching gas $CF_4$ (partial pressure of $^3$He – 2.5 bar and of $CF_4$ – 1.5 bar) and placed in a scattered beam at a distance of 80 cm from the scatterer. The whole detector except for an entrance window was covered with cadmium, and the window was screened by a mask with 9 vertical slits 0.55mm wide (slit spacing – 20 mm).

A typical coordinate spectrum of the detector is presented in **Fig. 9**. For the anode and drift voltage parameters specified in the figure the coordinate resolution in the center of the detector was 2.0 mm and along the edges – 2.4 mm (measurement time – 15 hr).

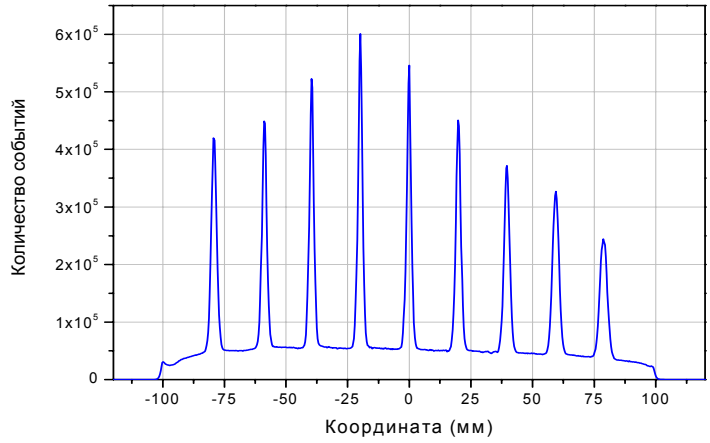


***Fig.9.*** *Coordinate spectrum of PSD with a slit mask. +Hv=3500 V –Hv=–1500 V*

The coordinate resolution dependence on anode and drift voltages was studied as well (**Fig.10**).

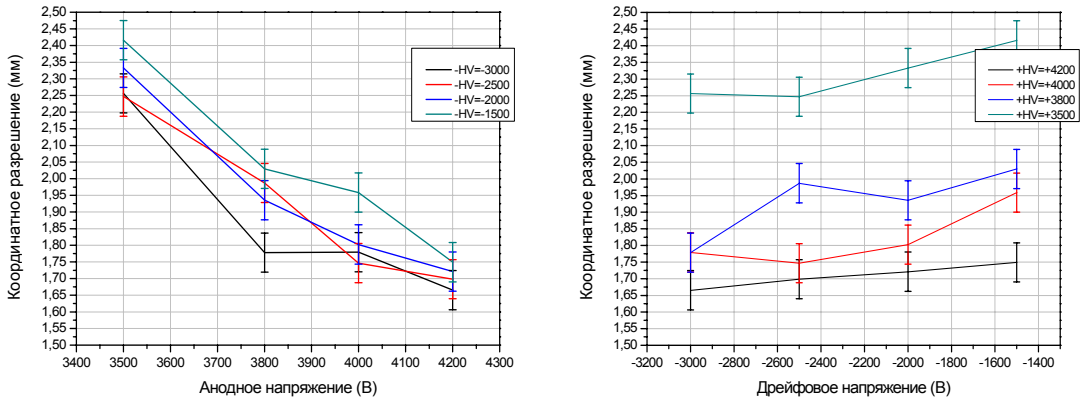


***Fig.10.*** *Coordinate resolution dependence on anode voltage (left) and on drift voltage (right) for the third slit at the left. Measurement time – 2 min.*

Thus, an increase in anode and drift voltages improves the detector coordinate resolution. +Hv=4200V –Hv=–3000V were chosen as working values. The coordinate resolution at the center of the detector was 1.6 mm and at edges – 1.9 mm. With further increasing voltages, the detector may fail to operate in a proportional mode.

At HRFD using the 1D detector the diffraction spectra of $(La_{0.1}Pr_{0.9})_{0.7}Ca_{0.3}MnO_3$ (manganite with CMR effect in which an AFM phase occurs at low temperatures) were obtained at $T$=10 K and 290 K. Spectrum accumulation time was about 2 hr. The measured distributions are presented in **Fig.11**.

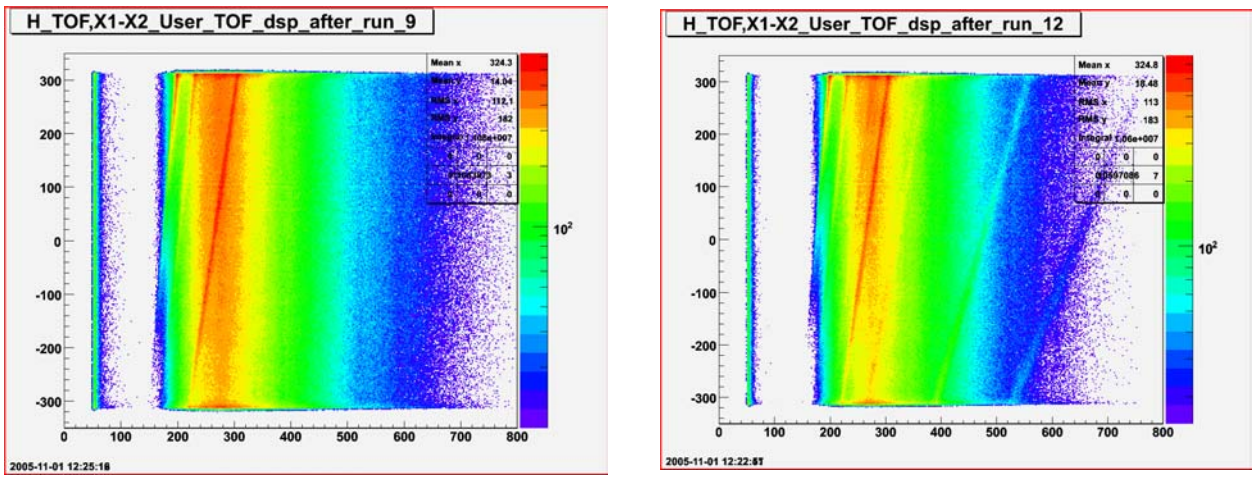


***Fig.11.*** *Diffraction spectra of LPCM-90 obtained at room temperature (at the left) and at low temperatures (at the right). The horizontal axis is the time channel number (channel width is 64 μs) and the vertical axis is the detector position channel number (channel width is 0.32 mm). +Hv=4000 V –Hv=-2000 V. The detector is positioned at 2θ=30° with $L_2$=103 cm, correspondingly diffraction spectra are obtained in the $d_{hkl}$ range from 3.4 to 12 Å. In the figure they are slant lines in accordance with the Wulf-Bragg law, a vertical line in the vicinity of the 55$^{th}$ channel is a fast neutron pulse. At T=290 K only nuclear peaks are visible in the spectrum, at T=10 K there appear diffraction peaks ($d_{hkl}$ ≈ 8 and 11 Å) connected with magnetic ordering.*

The total time of measurements with the 1D detector on beam 5 was about 180 hr. During the experiments the electronics and software operated trouble free in all measuring modes.

### 3.2. ZnS/$^6$LiF-based scintillation detectors for the FSD diffractometer

Sixteen additional modules of the ASTRA detector along with the mechanical positioning system have been tested and installed at the diffractometer **(Fig. 12)**.

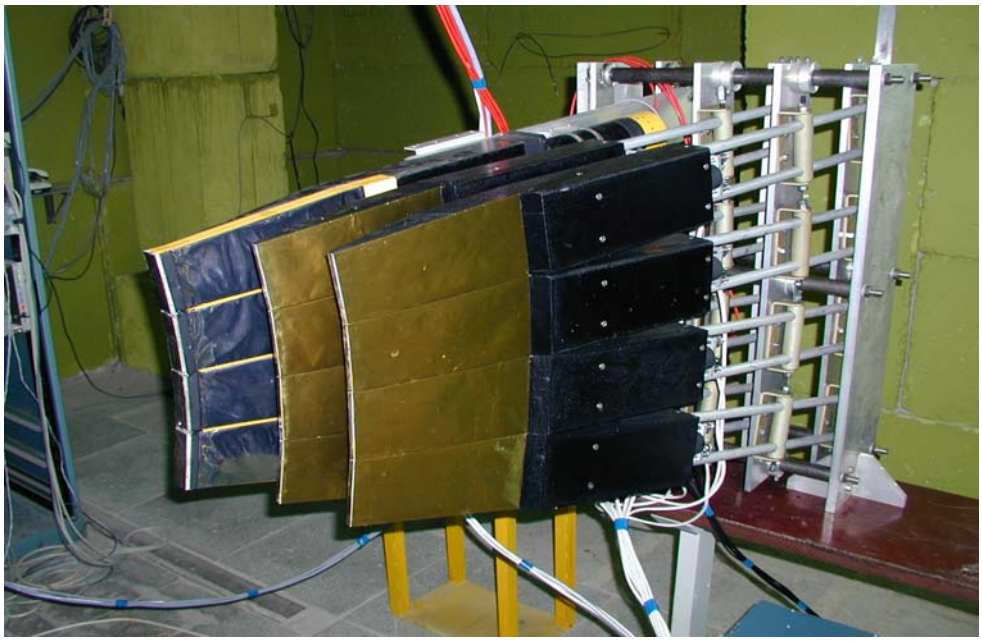

***Fig.12.*** *Sections N 7,6,5 of the FSD detector located at the left of a sample*

Counting characteristics of the scintillation counters of the 6-th section are presented in **Fig. 13.** The detector control system on the basis of programmable microprocessor has been developed and installed at the diffractometer. The system makes it possible to control a built-in high-voltage source, to adjust the detector in an automated mode and to control the event selection logic. All

electronic modules of the system are interconnected into a shared network and connected to a computer via CAN interface. A program to control, adjust and measure characteristics of individual modules has been designed and debugged. The detector system has been put into trial operation.

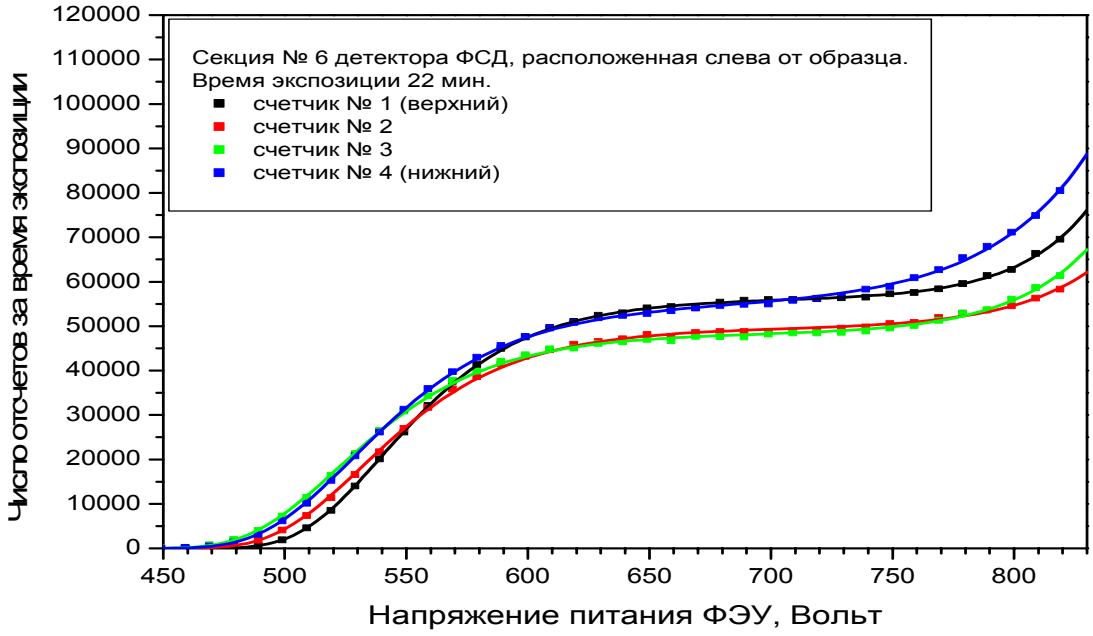


***Fig.13.*** *Counting characteristics of scintillation thermal neutron counters of the 6th section of FSD detector*

### 3.3. Development of control systems of actuating mechanisms and sample environment systems

In 2005 work to automatize actuating mechanisms for the IBR-2 spectrometers continued. At the YuMO spectrometer a device for moving PSD along the neutronguide and a device for vertical and horizontal positioning of PSD have been put into service (**Fig.14**).

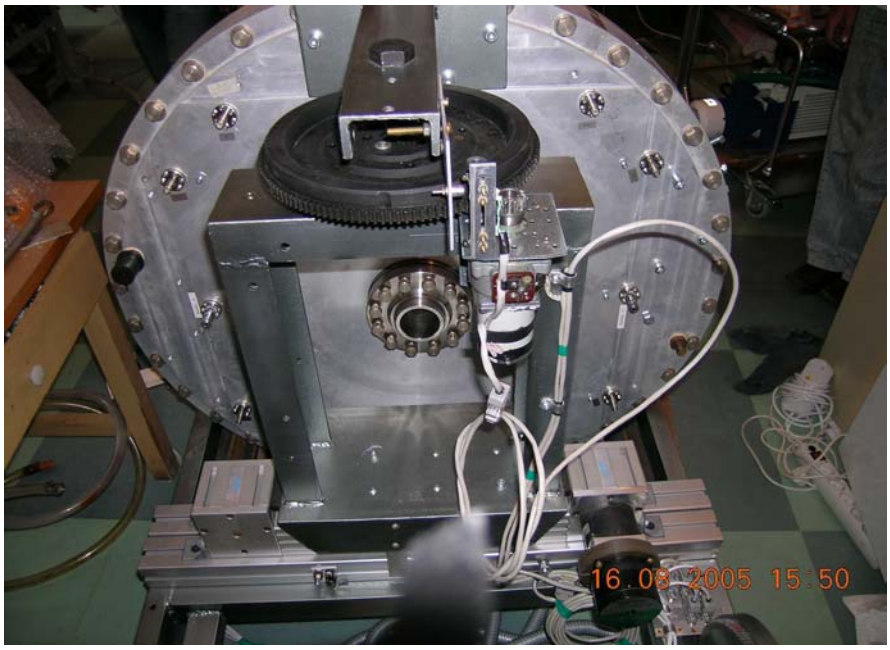


***Fig.14.*** *A system for moving and positioning of PSD.*

At the REMUR spectrometer a device for moving a diaphragm, a control device for two goniometer axes and for moving a pivoting platform on the basis of high-current motors DBM120 have been installed.

During the last few years the electronics controlling the speed of rotation and the synchronization of chopper rotation phase with a reactor start has been almost completely renewed, namely, almost all choppers are controlled using microcontroller-based electronics. At the same time the situation with the service reliability of power electric drives of disk background choppers operating at beams N4, 5, 7, 8 (2 pieces) and N10 of the IBR-2 reactor deteriorated drastically. These drives (EKT2D-63/380 40 kW) were installed in 1982 and require much labour inputs and routine attention to provide for the necessary level of performance reliability. The number of failures in the operation of choppers because of electric drive malfunctions increases gradually. In this connection in 2005 a new power electric drive EKT4 was purchased and put into trial operation at beam 10 of IBR-2 **(Fig. 15)**. It provides the accuracy of chopper phase stabilization of 185-200 μs.


***Fig.15.*** *Power electric drives EKT2 (left) and EKT4 (right).*

For beams 6a and 6b test-bench trials of drum choppers to suppress background (manufactured by the JINR Experimental Workshops) and of chopper control systems (**Fig.16**) have been carried out. The accuracy of phase stabilization is 25-50 μs.

***Fig.16.*** *Beam chopper of channel 6b on the basis of direct current electric drive (left) and control system (right).*

For the NERA-PR spectrometer a cryostat with a refrigerator on pulsed tubes PT405 (Cryomech, USA) with a working temperature range of 250-3 K has been developed and tested. At present, a temperature of 2.8 K has been obtained (**Fig.17**).

***Fig.17****. Refrigerator-cryostat RC2.5-300.*

### 3.4. Development of data acquisition systems and computing infrastructure

In 2005 works within the framework of this project were carried out in accordance with the long-term plan of development of DAQ systems of the IBR-2 spectrometer complex and computing infrastructure.

Among the most important results in the current year are the purchase of a new central server *Sun Fire X4200*, bulk storage device *Storage Array* (6.4 Tbyte) and acquisition of two high-speed network switches *Cisco 3750* (1 Gbit).

As is known, at present the central file-server *Enterprise 3000* of the firm *SUN Microsystem* (two processors *ULTRA SPARC* 250 MHz, RAM – 250 Mbyte, HDD – 200 Gbyte) is the only powerful computer and provider of shared disk space in the FLNP LAN. The server has been in service for 8 years, which resulted in the following problems:

- at present, the support of processors of the given type is not provided any longer, and consequently, the operating system *Solaris 2.6* cannot be updated with fresher versions (*Solaris 2.10* and higher);
- because of small capacity of the shared disk memory, the users have to store a part of experimental data on their personal computers, which frequently results in data loss and complicates the processing procedure;
- extension of the shared disk space is a problem, since disk manufacturers have changed over to faster interfaces;
- in case of failure of one of the disks, problems arise with providing safety and reliability of information storage.

In addition, the cost of providing service and upgrading of the SUN equipment currently in use on the basis of *RISK* architecture (*Enterprise 3000*, *Sun Workstations*) is unacceptable for us. At the same time, a sharp increase in computing power of computer systems based on *X86* architecture and evolution of *AMD-64* platform are observed. These factors have predetermined the replacement of basic servers of the FLNP computing cluster by modern powerful systems on the basis of Intel Pentium IV Xeon and AMD Opteron 64.

In 2005 e-mail processing, spam and virus filtering were performed by a dedicated server on the basis of *Intel Pentium* platform under the operating system *Solaris 9*. Web service is also being transferred to an analogous server. In the near future the installation of a new central server *Sun Fire X4200* (AMD-64) with OS *Solaris 10* is planned, thus making it possible to use maximally the advantages of 64-bit architecture and multi-core processors. The installation of the server and Mass storage will allow us to solve the above-mentioned problems. The available server *Enterprise 3000*

will be used for work with applications written for the old operating system till it exhausts its resource completely.

Along with the installation of servers, it is planned to create a new architecture of FLNP LAN and to change over to *Gigabit Ethernet* for main backbones (**Figs.18, 19**).

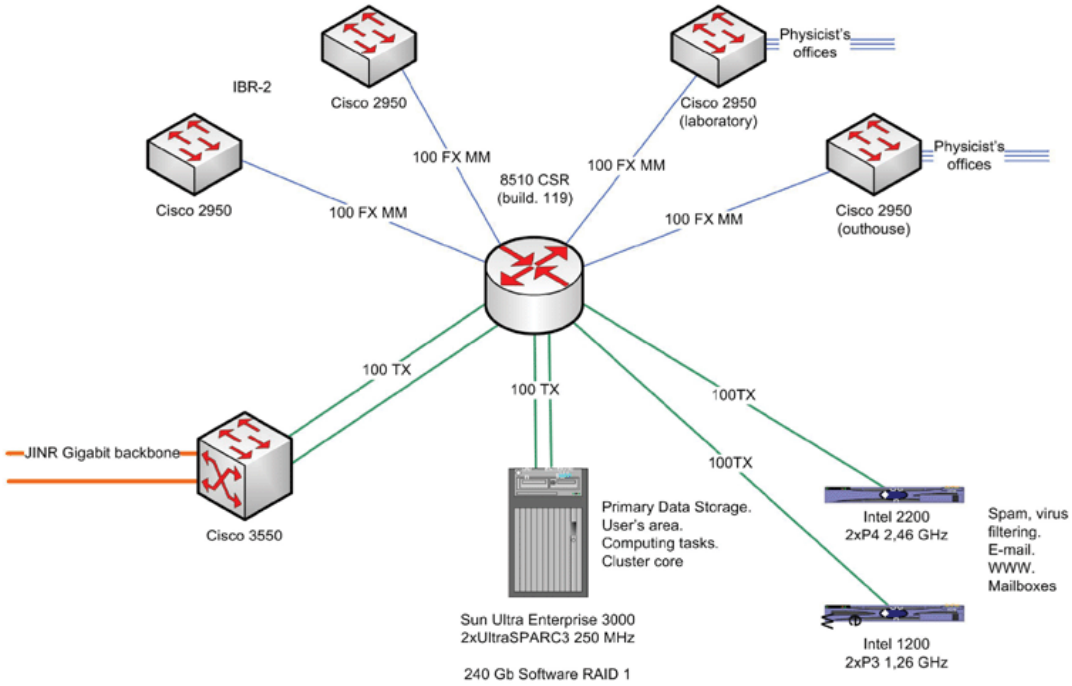


***Fig.18.*** *Current configuration of FLNP LAN (central core).*

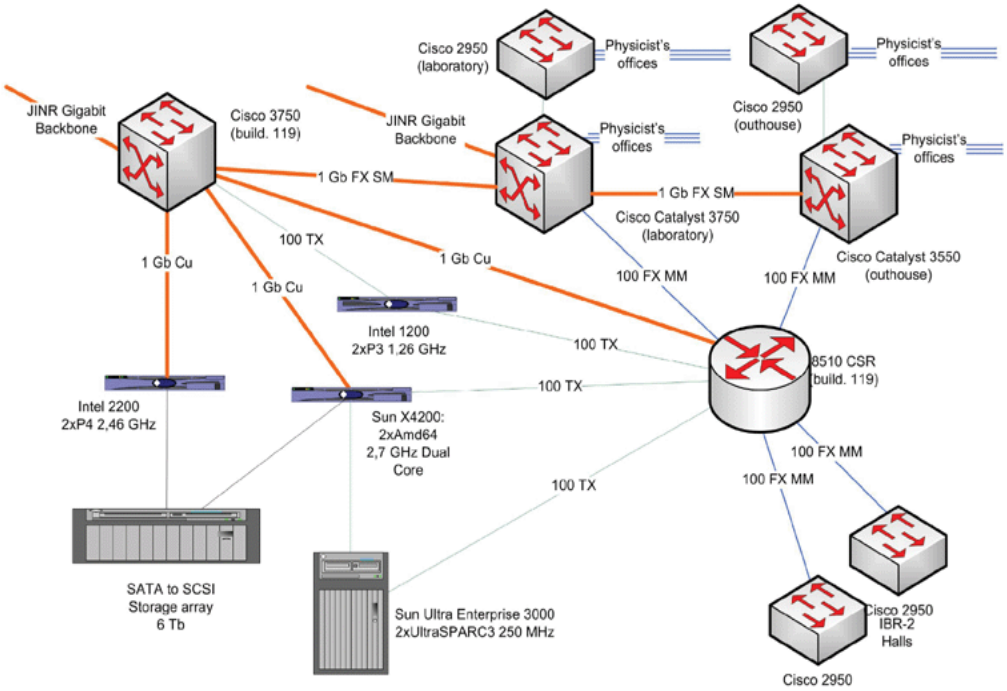


***Fig.19.*** *New architecture of FLNP LAN*

At present, the central switch of FLNP LAN *Cisco 8510CSR* is connected to the JINR network via two links with total throughput of 200 Mbit/sec. Under conditions of ever increasing traffic and load on the routing equipment, this connection cannot provide stable service for users any more. Besides, *CSR8510* does not make it possible to effectively control data transfer at virus and DDOS attacks. A change-over of the available switches of the network core to routing switches Cisco 3750, the installation of interface with 1Mbit/sec to *CSR8510* and the application of high-speed communication in the main FLNP LAN links will make it possible to solve the specified problems, to enhance the reliability of network operation and to provide connection with the JINR network and other networks at Gigabit rates.

In 2005, an *Intel Pentium* dual-processor server for data acquisition systems based on application of VME-PCI adapters was installed as well. Practically all network equipment was unified, including the segment of bldg.117 (EPSILON spectrometer). At two spectrometers uninterruptible power supplies were installed. The program package *Sonix+* was put into operation at the REMUR spectrometer. In the framework of Sonix+ complex:

- a new version of modules responsible for script interpretation was developed;
- a new spectrum visualization program *Spectra Viewer* for data from 1D and 2D detectors in Sonix+ format was designed;
- work to improve the package components, script libraries, etc. was carried out.

Along with the above-mentioned installation of DAQ and control electronics for scintillation detectors at the FSD spectrometer, work to develop and test the DAQ board software for MWPC detectors has been carried. In particular, two versions of FPGA programs for operation of the board with one-dimensional detectors and with a built-in monitor counter have been designed and tested. The development of new DAQ electronics with USB interface for multi-counter systems is in progress.

Electronic and software support was constantly provided during the IBR-2 reactor cycles.

# 3. РАЗРАБОТКА И СОЗДАНИЕ ЭЛЕМЕНТОВ НЕЙТРОННЫХ СПЕКТРОМЕТРОВ ДЛЯ ИССЛЕДОВАНИЯ КОНДЕНСИРОВАННЫХ СРЕД

Работы по теме велись в следующих основных направлениях:

— создание нейтронных детекторов;
— развитие систем окружения образца;
— развитие систем сбора данных и вычислительной инфраструктуры.

**1. Создание нейтронных детекторов**

В 2005г. изготовлены опытные образцы 1D детектора и 2D монитора и проведены их испытание на стенде с источником и на пучках ИБР-2. Оба детектора выполнены на основе многопроволочных пропорциональных камер со съемом информации с линии задержки. Это позволило в максимальной степени унифицировать электронику считывания (предусилители, дискриминаторы и др.) и накопления данных (преобразование и фильтрация данных, гистограммирование и др.), а также основные программные модули и интерфейсы. Накопление и визуализация данных осуществляется на персональном компьютере.

Проведенные ранее методические исследования и макетирование отдельных узлов позволили с высокой степенью достоверности планировать следующие технические характеристики 2D монитора и 1D детектора (**Табл. 1**):

***Таблица 1***

| | **2D монитор** | **1D детектор** |
|---|---|---|
| Газовая смесь | 50 мбар $He^3$+950мбар $CF_4$ | 2000 мбар $He^3$+1000мбар$CF_4$ |
| Эффективность | 0.1% | 40% |
| Чувствительная область | 100x100 $мм^2$ | 200x80 $мм^2$ |
| Коорд. разрешение | 4x4 $мм^2$ | 2 мм |
| Скорость счета | до $10^5$ соб./сек. | до$10^5$ соб./сек. |
| Диффер.неоднородность | <5% | <5% |
| Съем сигнала | Линии задержки | Линия задержки |

Испытания монитора и 1D детектора, проведенные в течение двух весенних и трех осенних циклов на ИБР-2,подтвердили указанные характеристики.

**1.1. 2D монитор**

2D монитор представляет собой многопроволочную пропорциональную камеру. Внешние габариты камеры составляют 320x320x23 мм, толщина входного и выходного окон 1 мм (**Рис.1**). Эта цифра была выбрана для того, чтобы, с одной стороны, как можно меньше влиять на падающий нейтронный поток, и, с другой стороны, чтобы детектор был способен выдерживать механические нагрузки, возникающие при изменении атмосферного давления. Высокое напряжение положительной полярности подается через разъем MHV, для вывода сигналов служат 5 разъемов BNC. Детектор имеет 2 газовых разъема типа «Swagelock», что позволяет использовать его в проточном режиме работы.

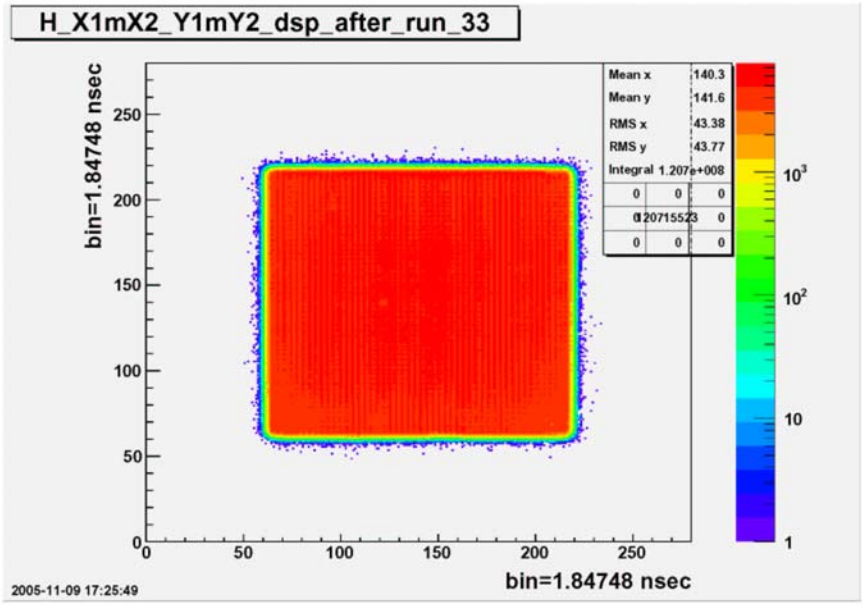


***Рис.1.*** *Корпус 2D монитора.*

***Рис.2*** *Равномерная засветка 2D монитора.*

В объеме камеры расположены два катодных и один анодный электроды. Каждый из электродов представляет собой текстолитовую рамку с выфрезерованным окном, в котором натянуты тонкие проволоки из позолоченного вольфрама. Толщина анодных проволочек 10 микрон, катодных – 50 микрон. Анодные проволочки намотаны с шагом 2 мм и соединены общей шиной, катодные проволочки намотаны с шагом в 1мм, объединены по две и выведены на линию задержки, одно звено которой задерживает на 2,9 нс. Расстояние между катодами составляет 12 мм, анод расположен посередине.Для регистрации нейтронов внутренний объем камеры заполнен смесью, состоящей из газа-конвертера нейтронов He3 и гасящего газа CF4. Гасящий газ необходим для уменьшения длины пробега заряженных частиц, образующихся в результате взаимодействия нейтронов с конвертером, а также для подавления вторичных эффектов. Полное давление газовой смеси 1000 миллибар, парциальное давление He3 составляет от 1 до 50 миллибар, в зависимости от максимальной загрузки. На рис.2 показан результат равномерной засветки монитора в ходе тестовых испытаний с помощью источника нейтронов.

Оценка координатного разрешения на пучках была проведена следующим способом. Детектор с кадмиевой маской помещался в поток нейтронов. Маска представляет собой кадмиевую пластину толщиной 1 мм с прорезанными в ней щелями шириной 0,5 мм. Расстояние между щелями – 10 мм. Полученные спектры суммировались вдоль оси Y (получался интегральный спектр по оси X). Пики аппроксимировались распределением Гаусса, определялась его ширина на полувысоте. Координатное разрешение, измеренное этим методом, оказалось не хуже, чем запланированные 4мм (3,7 мм в центре, 3,9 мм по краям). Так же в ходе измерений были получены профили пучков N6б и N10 реактора ИБР-2. Эти спектры представлены на **рис.3,4**. Указанный выше состав газовой смеси предназначен для работы в пучках со средней интенсивностью $10^4$-$10^6$ нейтрон*сек./см$^2$. Для работ в пучках высокой

интенсивности ($10^6$-$10^8$ нейтрон*сек./см$^2$) планируется исследовать возможность использования азота $N_2$ в качестве газа-конвертера.

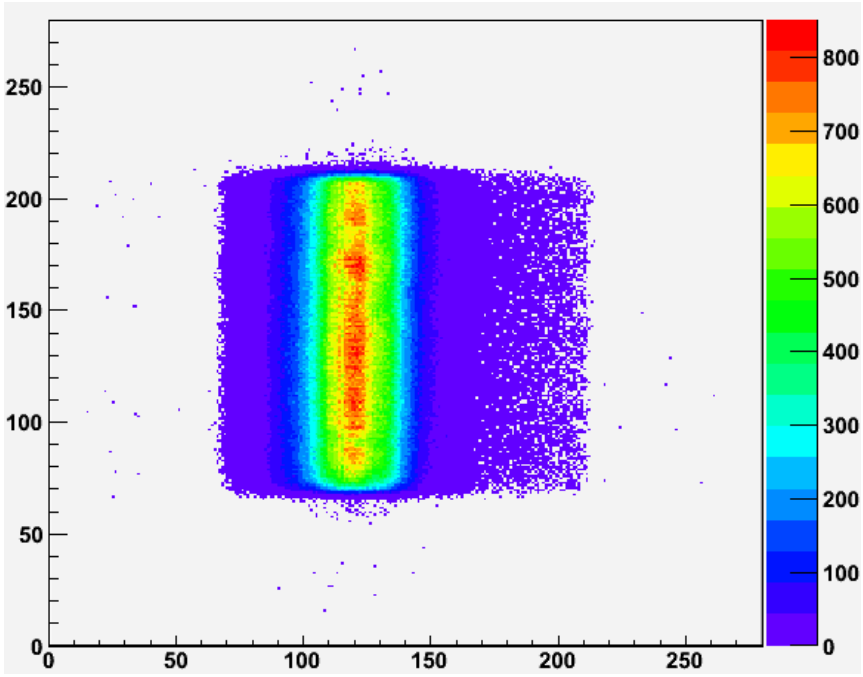


***Рис.3.*** *Измерение профиля пучка N6б реактора ИБР-2. Газовая смесь 50мбар $He^3$ + 950мбар $CF_4$. Время измерения 5 минут. Напряжение на аноде +3300В.*

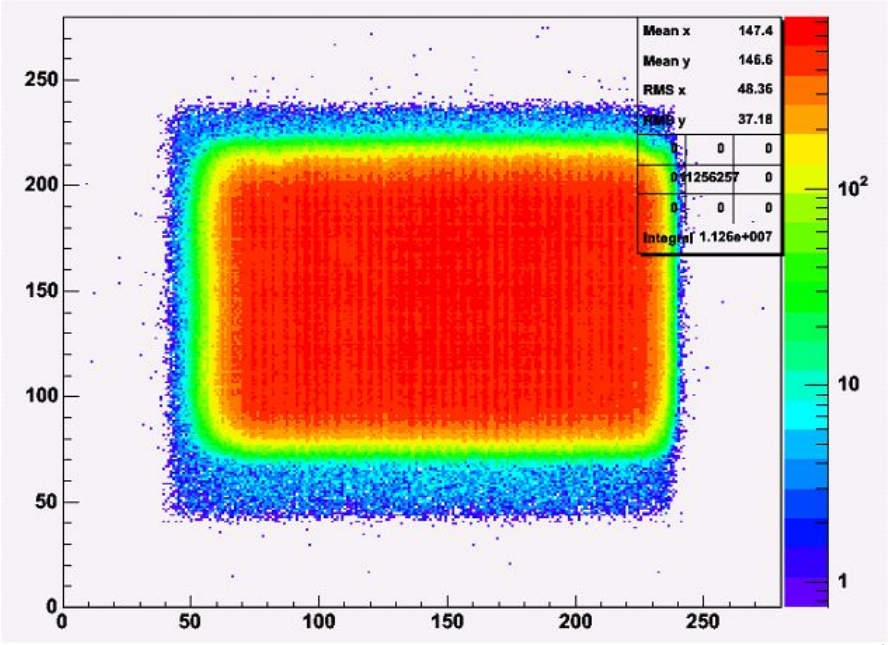


***Рис.4.*** *Измерение профиля пучка N10 реактора ИБР-2. Газовая смесь 50мбар $He^3$ + 950мбар $CF_4$. Время измерения 15 минут. Напряжение на аноде +3300В.*


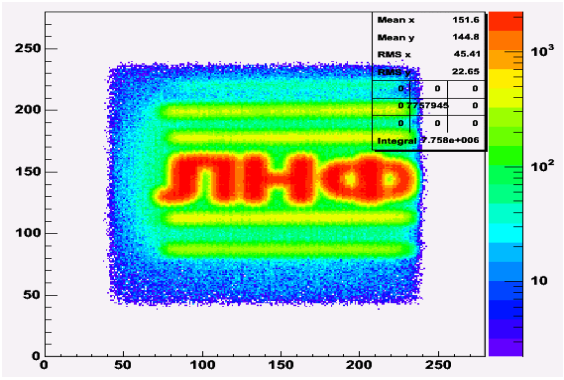


***Рис.5.*** *Измерение засветки с кадмиевой маской «ЛНФ» на 10 пучке ИБР-2. Газовая смесь 50мбар $He^3$ + 950мбар $CF_4$. Время измерения 15 минут. Напряжение на аноде +3300В.*

### 1.2 Однокоординатный ПЧД

На **рис.6** показана фотография корпуса 1D детектора, выполненного по той же технологии на основе многопроволочной пропорциональной камеры. В объеме камеры расположены катодный, анодный и дрейфовый электроды. Толщина анодных проволочек 10 микрон, катодных – 50 микрон. Анодные проволочки намотаны с шагом 2 мм и катодные - 1 мм.

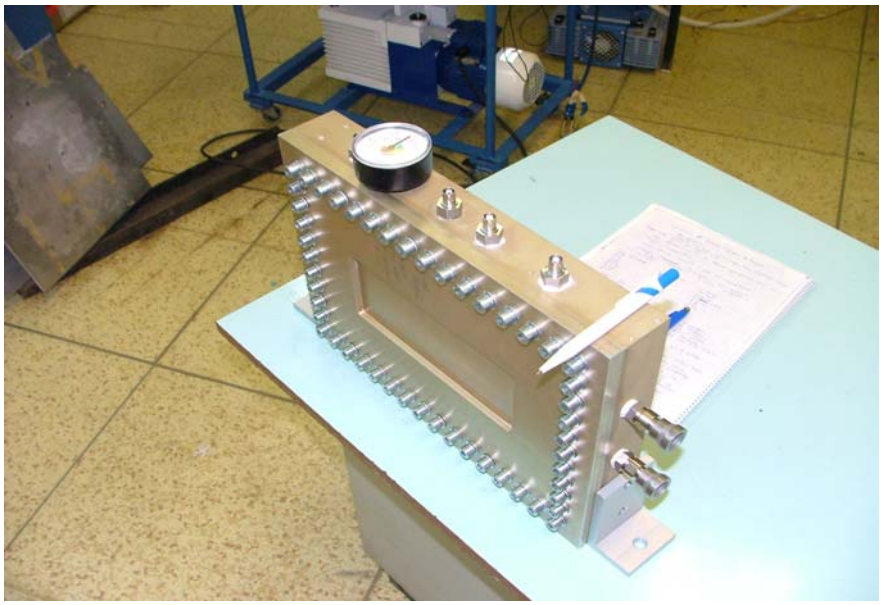

***Рис.6.*** *Корпус 1D детектора.*

На **рис.7** показан результат равномерной засветки 1D детектора с тестовой смесью в ходе испытаний с помощью источника нейтронов. Полученная дифференциальная неоднородность не более 8%.

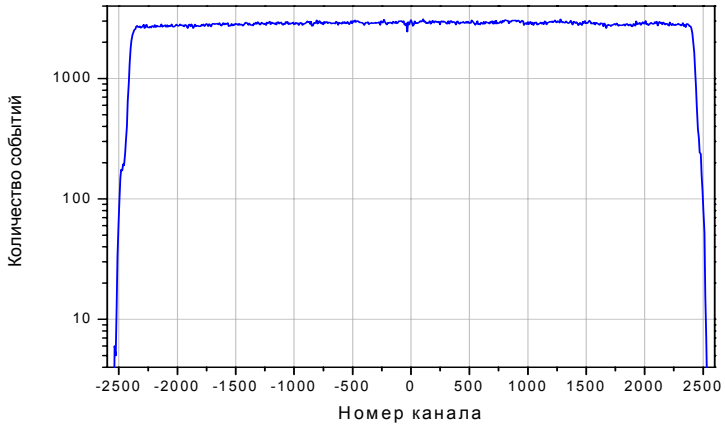


***Рис.7.*** *Равномерная засветка 1D детектора (+U=+3600 В, -U=-2000В).*

В 6 цикле реактора ИБР-2 с 17 по 28 октября 2005 года на спектрометрах ТЕСТ (6б канал реактора) и ФДВР (5 канал) были проведены тестовые и рабочие измерения дифракционных спектров.Блок-схема измерительного тракта показана на **рис.8**.

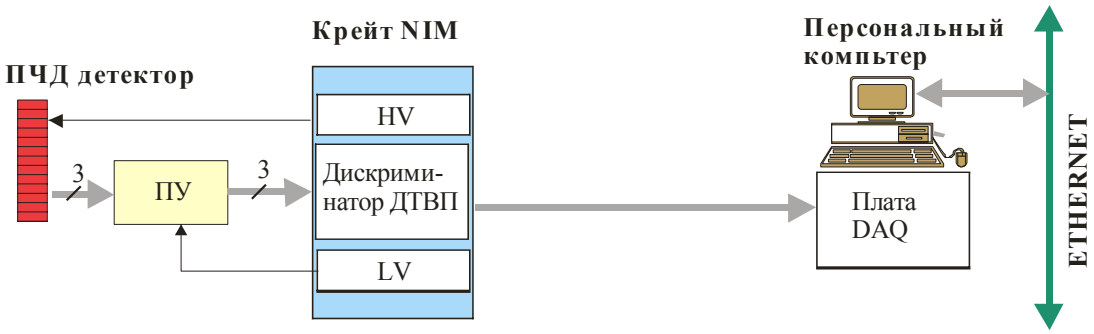


***Рис.8.*** *Блок-схема измерительного тракта.*

Характеристики детектора измерялись на 6б канале реактора ИБР-2. 1D детектор был заполнен газовой смесью, состоящей из газа-конвертера нейтронов $^3$He и гасящего газа $CF_4$ (парциальное давление $^3$He - 2,5 бар и $CF_4$ – 1,5 бар), и установлен в рассеянный пучок на расстоянии 80 см от рассеивателя. Весь детектор, кроме входного окна был закрыт кадмием, а на окно была установлена маска с 9 вертикальными щелями. Ширина щели составляла 0,55 мм, расстояние между щелями - 20 мм.

Типичный координатный спектр детектора представлен на **рис.9**. При указанных на рисунке параметрах анодного и дрейфового напряжений координатное разрешение в центре детектора составило 2,0 мм, а на краях детектора 2,4 мм (время набора 15 часов).

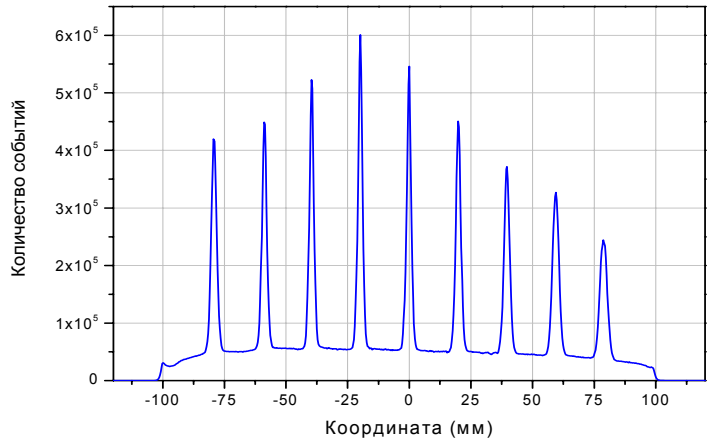


***Рис.9.*** *Координатный спектр ПЧД со щелевой маской. +Hv=3500 В –Hv=-1500 В.*

Были сняты зависимости координатного разрешения детектора от анодного и дрейфового напряжений (**рис.10**).

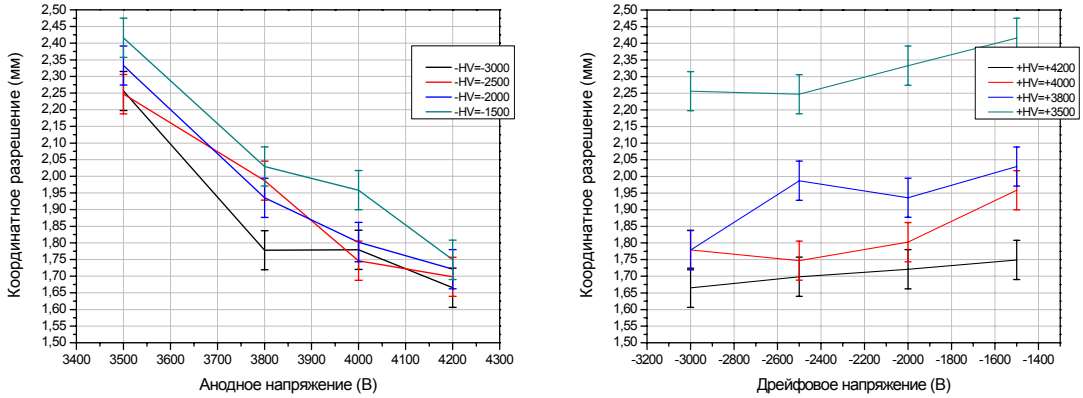


***Рис.10.*** *Зависимость координатного разрешения от анодного напряжения (слева) и дрейфового напряжения (справа) для третьей слева щели на маске. Время набора 2 мин.*

Таким образом, увеличение анодного и дрейфового напряжений улучшает координатное разрешение детектора. В качестве рабочих значений были выбраны +Hv=4200 В –Hv=-3000 В. При этом координатное разрешение в центре детектора составило 1,6 мм, а на краях детектора - 1,9 мм. При дальнейшем увеличении напряжений детектор может выйти из пропорционального режима.

Одним из экспериментов на 5 канале ИБР-2 было измерение дифракционных спектров $(La_{0.1}Pr_{0.9})_{0.7}Ca_{0.3}MnO_3$ (манганит с CMR эффектом, в котором при низкой температуре возникает АФМ фаза) при $T$=10 K и 290 K. Время накопления спектров составляло около 2 часов. На **рис. 11** показаны измеренные распределения.

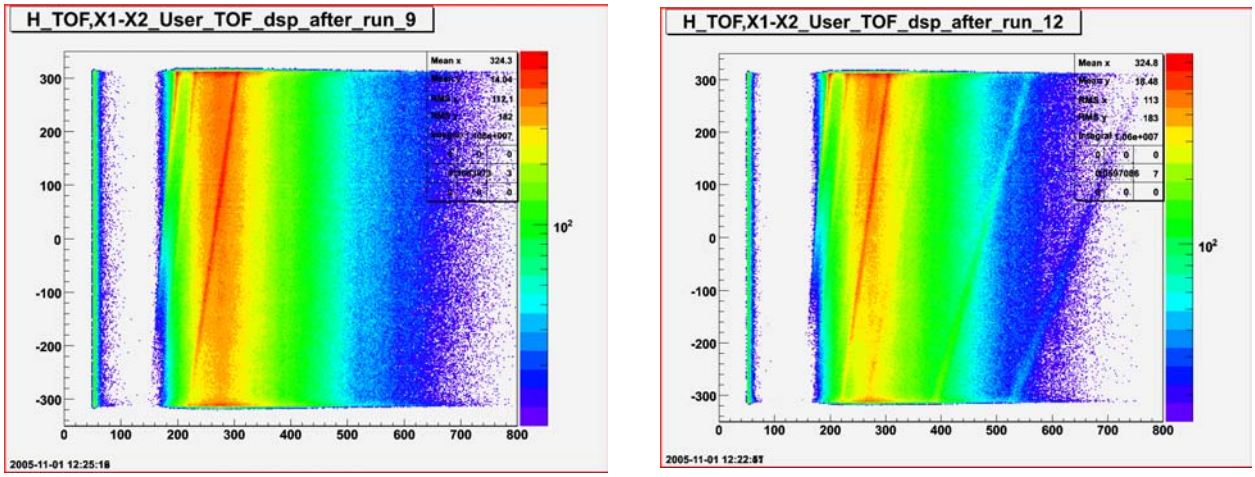


***Рис.11.*** *Дифракционные спектры от LPCM-90, измеренные при комнатной (слева) и низкой (справа) температурах. По горизонтальной оси – номер временного канала (ширина канала 64 мкс), по вертикальной оси – номер позиционного канала детектора (ширина канала 0,32 мм). +Hv=4000 В –Hv=-2000 В. Детектор размещен при 2θ=30° с* $L_2$*=103 см, соответственно дифракционные спектры регистрируются в диапазоне* $d_{hkl}$ *от 3.4 до 12 Å, на рисунке они представляют наклонные полосы в соответствии с законом Вульфа-Брегга, вертикальная полоса в районе 55 канала – импульс быстрых нейтронов. При T=290 K в спектре видны только ядерные пики, при T=10 K в спектре появляются дифракционные пики (при* $d_{hkl} \approx 8$ *и 11 Å), связанные с магнитным упорядочением.*

Общее время измерения образцов на 5 канале составило около 180 часов. При этом электроника и программное обеспечение работали стабильно во всех режимах измерений.

## 2. Сцинтилляционные детекторы на основе ZnS/$^6$LiF для дифрактометра ФСД

Шестнадцать дополнительных модулей детектора АСТРА испытаны и установлены на дифрактометре совместно с механической системой юстировки (**рис.12**).Счетные характеристики сцинтилляционных счетчиков 6-й секции показаны на **рис.13**. Разработана и установлена на дифрактометре система управления детектора на базе программируемого микропроцессора. Система позволяет управлять встроенным источником высокого напряжения, в автоматизированном режиме настраивать детектор и управлять логикой отбора событий. Все электронные модули системы объединены в общую сеть и соединены с компьютером на основе CAN интерфейса.Разработана и отлажена программа для управления, настройки и измерения характеристик отдельных модулей. Детекторная система сдана в опытную эксплуатацию.

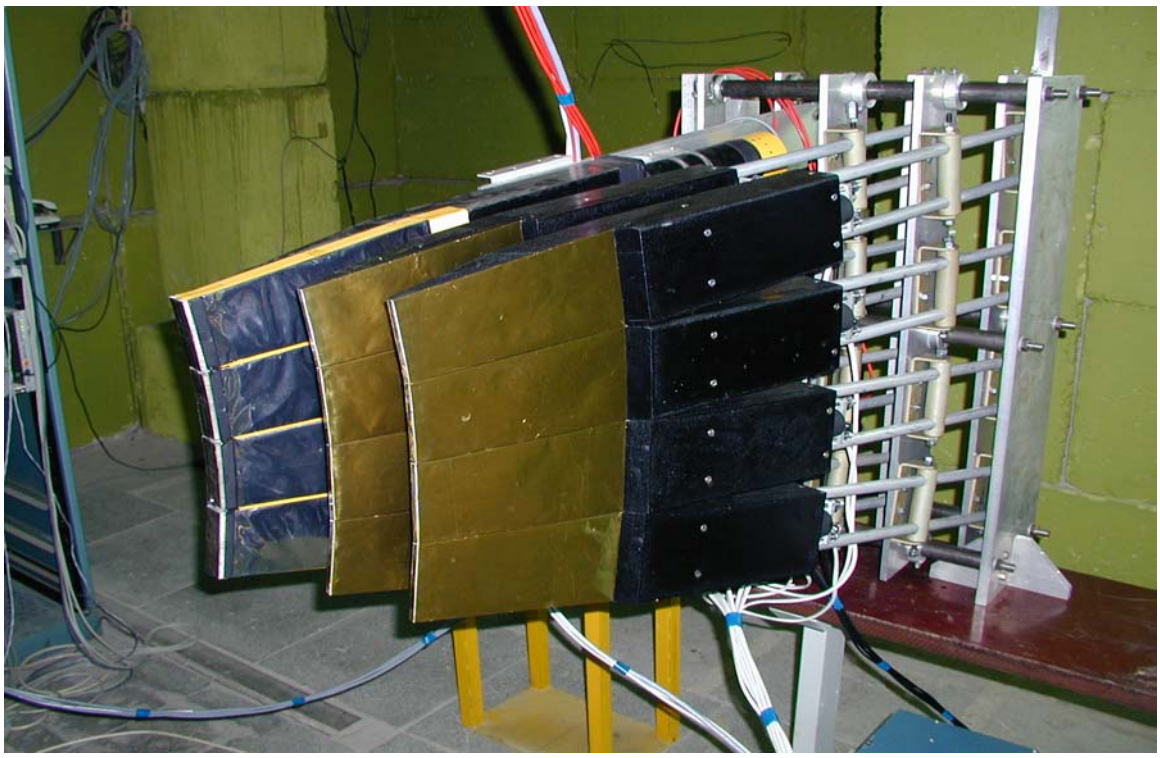

***Рис.12.*** *Секции № 7, 6, 5 детектора ФСД расположенные слева от образца.*

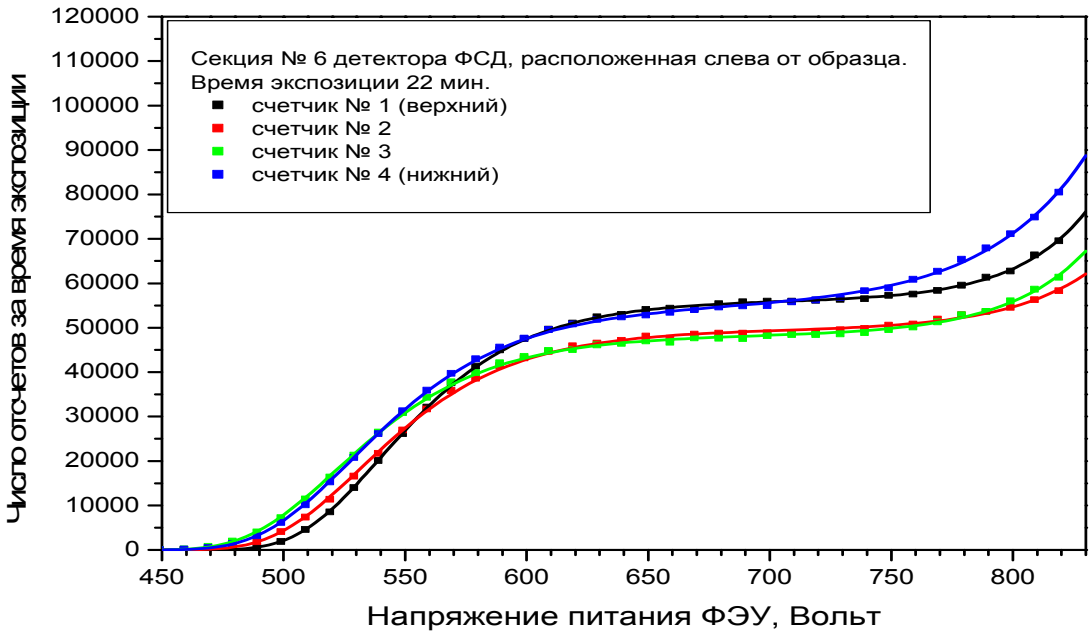


***Рис.13.*** *Счетные характеристики сцинтилляционных счетчиков тепловых нейтронов входящие в состав секции № 6 детектора ФСД.*

**3. Развитие систем управления исполнительными механизмами и систем окружения образца**

В 2005 году была продолжена автоматизация исполнительных устройств для спектрометров ИБР-2.На спектрометре ЮМО введено устройство перемещения ПЧД детектора вдоль нейтроновода и устройство вертикальной и горизонтальной юстировки ПЧД детектора (**рис.14**).

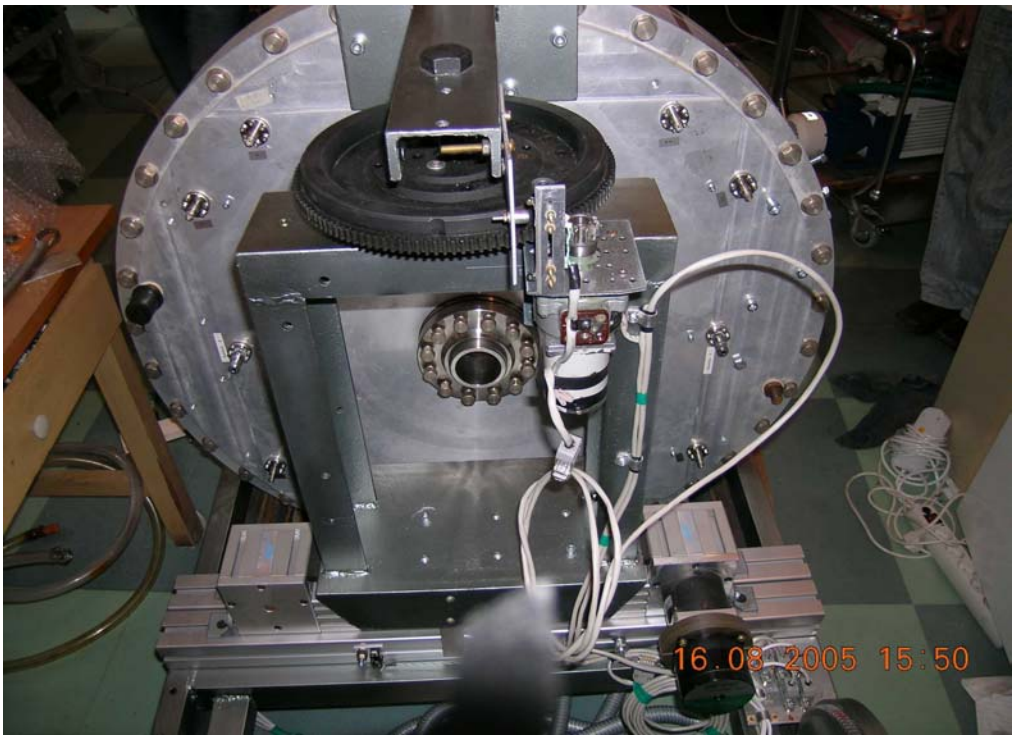


***Рис.14.*** *Система перемещения и юстировки ПЧД детектора ЮМО.*

На спектрометре РЕМУР установлены устройство перемещения диафрагмы, устройство управления 2-мя осями гониометра и перемещением поворотной платформы на основе сильноточных двигателей ДБМ 120.

В последние несколько лет была почти полностью обновлена электроника управления скоростью и синхронизации фазы вращения прерывателей со стартом реактора, а именно, почти все прерыватели переведены на управление с помощью микроконтроллеров. В то же время резко обострилась ситуация с надежностью работы силовых электроприводов дисковых фоновых прерывателей, работающих на каналах 4, 5, 7, 8 (2 шт.) и 10 реактора ИБР-2.Эти приводы (ЭКТ2Д-63/380 на 40 кВт) установлены в 1982 году и требуют больших трудозатрат по профилактике, обслуживанию и обеспечению необходимой надежности работы. Количество отказов в работе прерывателей из-за нарушения работы электропривода постепенно растет. В связи с этим в 2005году был приобретен и введен в опытную эксплуатацию на 10 канале ИБР-2 новый силовой электропривод ЭКТ4 (**рис.15**). Точность стабилизации фазы прерывателя составила 125-200 мкс.


***Рис.15.*** *Силовые электроприводы ЭКТ2 (слева) и ЭКТ4 (справа).*

Для каналов 6а и 6б проведены стендовые испытания барабанных прерывателей для подавления фона производства ОП ОИЯИ и систем управления прерывателями (**рис.16**).Точность стабилизации фазы составила 25-50 мкс.

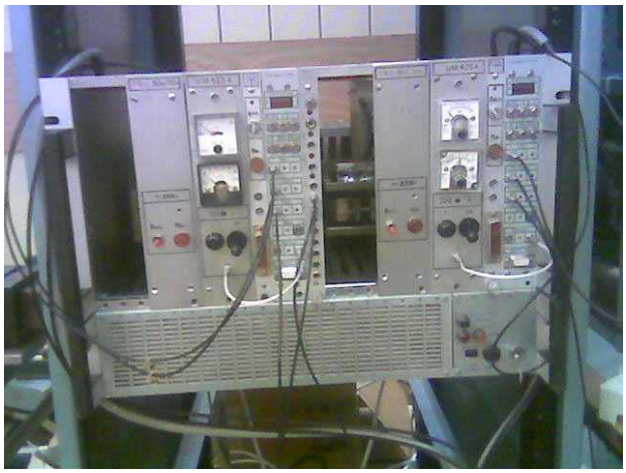

***Рис.16.*** *Прерыватель канала 6б на базе электропривода постоянного тока (слева) и система управления (справа).*

Для спектрометра HEPA-ПР разработан и испытан криостат (**рис.17**) с рефрижератором на импульсных трубках PT405 (Cryomech, USA) для работы в диапазоне температур 250–3 К. В настоящее время получена температура 2.8 К.

***Рис.17.*** *Рефрижератор-криостат RC2.5-300.*

## 4. Развитие систем сбора данных и вычислительной инфраструктуры

В 2005 г. работы по данному направлению выполнялись в соответствии с принятым ранее долгосрочным планом развития компьютерной инфраструктуры ЛНФ и систем сбора данных с комплекса спектрометров ИБР-2.

К числу наиболее важных результатов в текущем году следует отнести приобретение нового центрального сервера Sun Fire X4200,устройства массовой памяти Storage Array (6,4 TByte), и двух высокоскоростных сетевых коммутаторов Cisco 3750 (1 Gbit).

Как известно, в настоящее время единственным мощным вычислителем и поставщиком общего дискового пространства в LAN ЛНФ является центральный файл-сервер Enterprise 3000 фирмы SUN Microsystem (два процессора ULTRA SPARC 250 MHz, RAM – 256 MByte, HDD – 200 GByte). Сервер находится в эксплуатации 8 лет, что привело к возникновению следующих проблем:

- на данный момент поддержка процессоров данного типа прекращена, соответственно, обновление операционной системы Solaris 2.6 на более свежие версии Solaris 2.10 и выше невозможно;
- ввиду небольшого объёма общей дисковой памяти, пользователи вынуждены держать часть экспериментальной информации на своих персональных компьютерах, что часто приводит к потере данных и усложняет процедуру их обработки;
- расширение общего дискового пространства затруднено ввиду перехода производителей дисков на более быстрые интерфейсы;
- возникают трудности с обеспечением надёжности и безопасности хранения информации при выходе из строя одного из дисков.

Кроме того, используемое в настоящее время оборудование SUN на основе RISK архитектуры (Enterprise 3000, Sun Workstations) имеет неприемлемую для нас стоимость обслуживания и развития. В то же время происходит резкий рост производительности вычислительных систем, построенных на основе архитектуры X86, и развитие платформы AMD-64. Эти факторы и предопределили замену основных серверов вычислительного кластера ЛНФ современными мощными системами на основе Intel Pentium IV Xeon и AMD Opteron 64.

В 2005 г. обработка электронной почты, фильтрация спама и вирусов была вынесена на выделеный сервер на платформе Intel Pentium под управлением OS Solaris 9. Web сервис также переводится на аналогичный сервер.В ближайшее время планируется установка нового центрального сервера Sun Fire X4200 (AMD–64) с OS Solaris 10, что позволит максимально использовать преимущества 64-разрядной архитектуры и многоядерных процессоров. Установка сервера и Mass storage позволит решить названные выше проблемы. Существующий сервер Enterprise 3000 будет использоваться до полного износа для работы с приложениями, написанными под старую операционную систему.

Наряду с установкой серверов, планируется создание новой архитектуры LAN ЛНФ и переход на использование Gigabit Ethernet на основных магистралях сети (**рис.18,19**). В настоящее время центральный коммутатор сети ЛНФ Cisco 8510CSR соединён с сетью Института двумя линками с общей пропускной способностью 200 Mbit/sec. Такое подключение уже не может обеспечить устойчивое обслуживание пользователей в условиях постоянного увеличения объёма трафика и нагрузки на маршрутизирующее оборудование. Кроме того, CSR 8510 не позволяет эффективно управлять передачей данных при вирусных и DDOS-атаках на сеть. Перевод ядра сети на маршрутизирующие коммутаторы Cisco 3750, установка интерфейса 1Mbit/sec в CSR8510 и использование высокоскоростных соединений на основных линках LAN ЛНФ поможет решить указанные проблемы, повысить надёжность работы сети и обеспечить связь с сетью ОИЯИ и другими сетями на гигабитных скоростях.

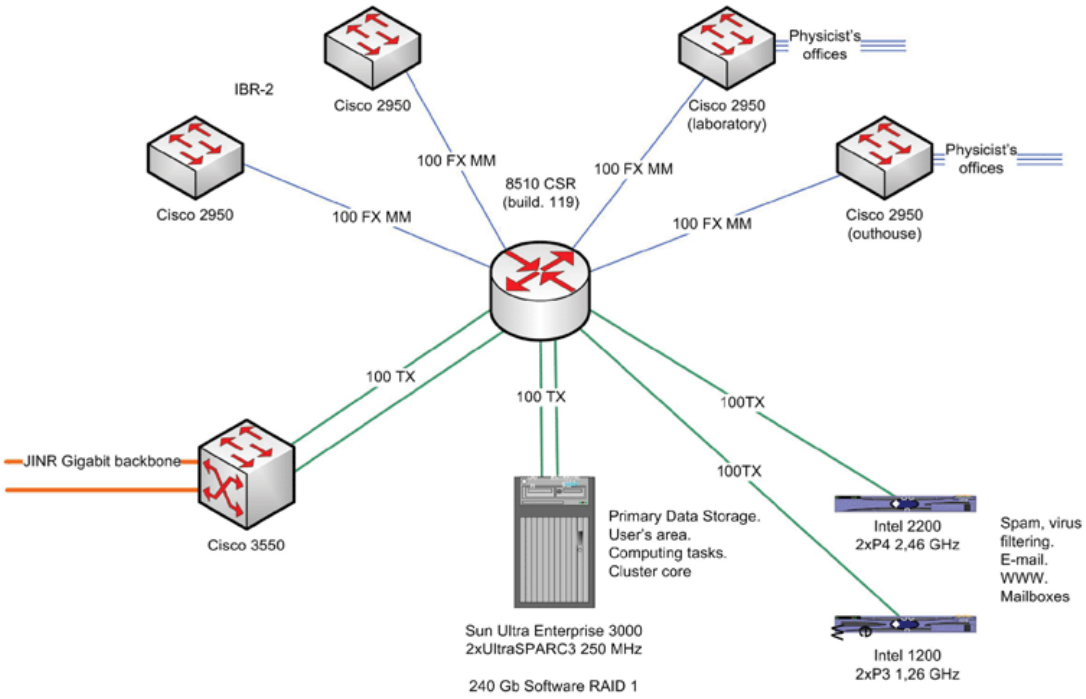


***Рис.18.*** *Текущая конфигурация LAN ЛНФ (центральное ядро).*

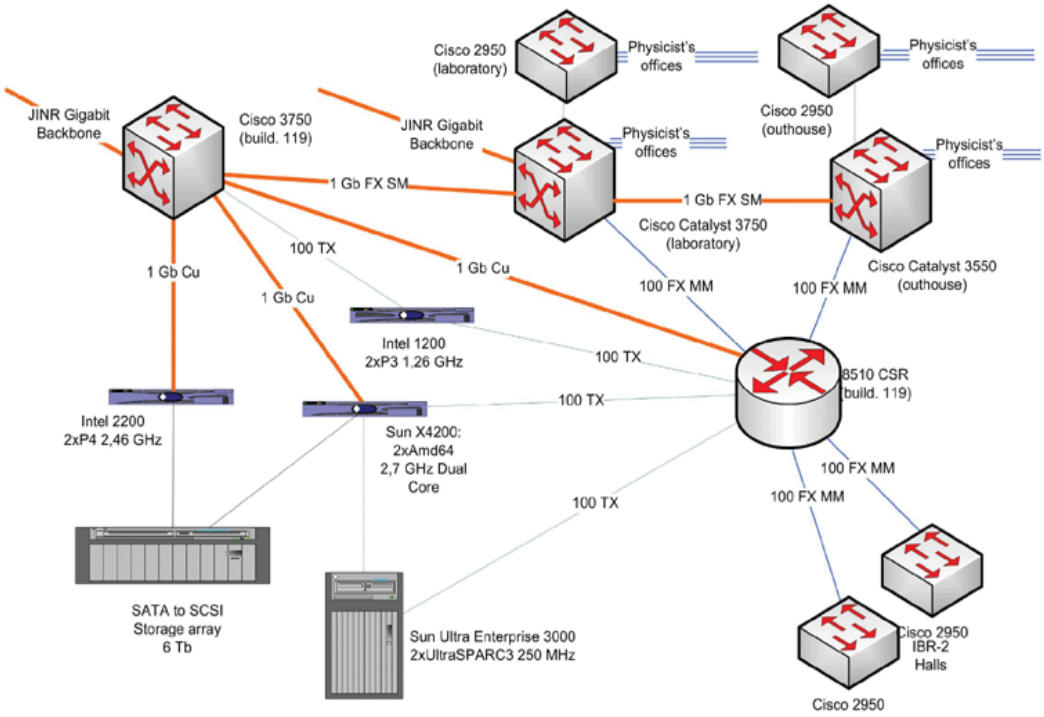


***Рис.19.*** *Новая архитектура LAN ЛНФ.*

В 2005 г. установлен также двухпроцессорный сервер Intel Pentium для систем сбора данных, базирующихся на применении VMI-PCI адаптеров. Унифицировано практически всё сетевое оборудование, включая сегмент здания 117 (спектрометр EPSILON). На двух спектрометрах установлены источники бесперебойного питания. Программный комплекс Sonix+ введён в эксплуатацию на спектрометре РЕМУР. В рамках комплекса Sonix+:

- разработана новая версия модулей, отвечающих за интерпретацию скрипта;
- разработана новая программа визуализации спектров Spectra Viewer для данных с 1D и 2D детекторов в формате Sonix+;
- проводилось совершенствование компонентов комплекса, библиотек скриптов и т.д.

Наряду с упомянутой выше электроникой регистрации данных и управления для сцинтилляционных детекторов,выполнены работы по развитию и тестированию программного обеспечения платы сбора данных для MWPC детекторов.В частности,разработаны и испытаны две версии FPGA программ для работы платы с однокоординатными детекторами и со встроенным мониторным счетчиком.Ведется разработка новой электроники сбора данных с USB интерфейсом для многосчетчиковых систем.

Во время циклов ИБР-2 постоянно осуществлялась электронная и программная поддержки экспериментов.

# 4. EXPERIMENTAL REPORTS

## 4.1. CONDENSED MATTER PHYSICS

### Diffraction

Structural Origin of the Giant Oxygen Isotope Effect in $Re_{0.5}Sr_{0.5}MnO_3$ Perovskites
*A.M.Balagurov, I.A.Bobrikov, V.Yu.Pomjakushin, D.V.Sheptyakov, N.A.Babushkina, O.Yu.Gorbenko, A.R.Kaul*

Determination of Magnetic Moments and Hyperfine Magnetic Fields in $ScFe_2$ Laves Phase Compound
*M.Wiertel, Z.Surowiec, A.I.Beskrovny, J.Sarzynski, M.Budzynski*

High-Pressure Effects on the Crystal and Magnetic Structure of the Frustrated Antiferromagnet $YMnO_3$
*D.P.Kozlenko, S.E.Kichanov, S.Lee, J.-G.Park, V.P.Glazkov, B.N.Savenko*

Neutron Diffraction Studies of a $Bi_{2.53}Li_{0.29}Nb_2O_9$ at the High Temperature
*S.G.Vasilovskij, A.I.Beskrovny, V.G.Simkin, M.Sarrion, L.Mestres, M.Herraiz*

Anisotropy of Elastic Properties of Amphibolites and Gneisses from the Kola Superdeep Well at High Pressures (up to 600 MPa) and High Temperatures (up to 600$^o$C)
*T.I.Ivankina, H.M.Kern, A.N.Nikitin*

Determination of Renal Stones Type by X-Ray and Neutron Diffraction
*M.Baeva, A.I.Beskrovny, I.G.Shelkova*

Verification experiments on FSD diffractometer
*A.M.Balagurov, G.D.Bokuchava, A.V.Tamonov, V.V.Sumin, I.V.Papushkin, S.G.Sheverev*

### Inelastic Neutron Scattering

Internal Dynamics of Norethisterone by IINS, NMR and QC Methods
*K.Holderna-Natkaniec, I.Natkaniec, K.Jurga, D.Nowak, A.Szyczewski*

Comparative INS Studies of Methane, Methanol, Mesitylene and Water as Neutron Moderator Materials at Low Temperatures
*I.Natkaniec, E.Shabalin, S.Kulikov, K.Holderna-Natkaniec*

Low Frequency Internal Modes of 2,3,5,6,-Tetramethylbenzene, 2,3,5,6-Tetramethylpyrazine and Tetramethyl-1,4-Benzoquinone, INS, Raman IR and Theoretical DFT Studies
*A.Pawlukojc, I.Natkaniec, G.Bator, L.Sobczyk, E.Grech, J.Nowicka-Scheibe*

Inelastic Neutron Scattering on AgCuSe
*D.Trots, A.Skomorokhov, V.Semenov, N.Bickulova, Yu.Stepanov, H.Fuess*

### Small-Angle Neutron Scattering

SANS Contrast Variation in Organic Magnetic Fluid of New Type
*Mikhail V.Avdeev, Artem V.Feoktystov, Maria Balasoiu, Doina Bica, Ladislau Vekas*

Study of the Structural Modification Induced on the Coal Tar Pitch by Addition of Single, Multiwalled Carbon Nanotubes and Nanocarbon Fibers
*I.Ion, A.-M.Bondar, Y.Kovalev, C.Banciu, A.Bara, Pasuk, A.Kuklin*

The Study of Magnetic Elastomers by Small Angle Neutron Scattering and Scanning Electron Microscopy
*C.M.Muresan, E.M.Anitas, I.Bica, A.I.Kuklin, M.Balasoiu, O.Orelovitch, Y.Kovalev*

Structural Reorganization of Mitochondrial Membrane under Low-Amplitude Swelling Studied by Small Angle Neutron Scattering
*T.N.Murugova, V.I.Gordeliy, A.Kh.Islamov, A.I.Kuklin, I.M.Solodovnikova, L.S.Yaguzhinsky*

## 4.2. NEUTRON NUCLEAR PHYSICS

### Gamma-Spectroscopy of Neutron-Nuclear Interaction

About Nucleus "Superfluid-Normal" State Transition Dynamics
*A.M.Sukhovoj, V.A.Khitrov*

General Trend in the Changing of Nuclear Excited States Structure
*V.A.Khitrov, A.M.Sukhovoj*

### Fundamental Properties of Neutrons

On the Possibility to Estimate the n,e-Scattering Length from Structure Factors for Liquid Krypton
*L.V.Mitsyna, V.G.Nikolenko, S.S.Parzhitski, A.B.Popov, G.S.Samosvat*

### Applied Research

Interaction of Microalgae *Spirulina Platensis* with Metals Studied by NAA and AAS
*M.V.Frontasyeva, S.S.Pavlov, N.G.Aksenova, E.I.Kirkesali, L.M.Mosulishvili, A.I.Khizanishvili, A.N.Rcheulishvili*

NAA and AAS for Air Pollution Study in Macedonia
*L.Barandovski, M.V.Frontasyeva, S.S.Pavlov, T.Stafilov, V.Urumov*

# Structural origin of the giant oxygen isotope effect in $Re_{0.5}Sr_{0.5}MnO_3$ perovskites

Anatoly M. Balagurov,[a] Ivan A. Bobrikov,[a] Vladimir Yu. Pomjakushin,[a,b]
Denis V. Sheptyakov,[b] Nataliya A. Babushkina,[c] Oleg Yu. Gorbenko,[d] Andrej R. Kaul[d]

[a]*Frank Laboratory of Neutron Physics, Joint Institute for Nuclear Research, 141980 Dubna, Moscow region, Russia*
[b]*Laboratory for Neutron Scattering, ETH Zürich & Paul Scherrer Institut, 5232 Villigen PSI, Switzerland*
[c]*RSC "Kurchatov Institute", Kurchatov sq.1, 123182 Moscow, Russia*
[d]*Department of Chemistry, Moscow State University, 119899 Moscow, Russia*

The "giant" oxygen isotope effect in complex manganese oxides – transition from metallic to insulating ground state upon $^{16}O \rightarrow {}^{18}O$ substitution – continues to be one of the most intriguing phenomena in physics of these compounds. Here we report on the preliminary results of diffraction experiments with $(Nd_{1-y}Tb_y)_{1-x}Sr_xMnO_3$ (NTSM hereafter) samples for $y$ = 0.228 (S1 sample, $\langle r_A \rangle$ = 1.229 Å) and $y$ = 0.456 (S2 sample, $\langle r_A \rangle$ = 1.221 Å. The second is the analogue (the same $\langle r_A \rangle$) of $Sm_{0.5}Sr_{0.5}MnO_3$ (SSM hereafter) compound, in which the giant isotope effect has been recently discovered [1]. We show that at low temperature in both compositions, two phases with the same crystal symmetry but with different type of magnetic ordering coexist. These results allow us to reconsider the diffraction data for SSM and to find the structural origin for the giant isotope effect in this compound.

Neutron diffraction patterns were collected at HRFD (pulsed reactor IBR-2, Dubna), HRPT and DMC (both at SINQ source, PSI) instruments. The first two are high resolution diffractometers with $\Delta d/d \approx 0.001$, which promotes analysis of coexisting phases and peak broadening effects. DMC was used for the measurements of magnetic intensities. Additionally, S1 sample was measured at SLS synchrotron light source (PSI) at several important temperatures.

At room temperature, the crystal structure of NTSM and SSM can be well described in conventional *Pnma* space group (P1 phase). At low temperature diffraction patterns contain additional peaks from another *Pnma* phase (P2), one of the features of which is much shorter *b*-axis length than in the P1 phase. The appearance (at cooling) of the P2 phase takes a very broad temperature range: in S1 sample the first indication appears at about 250 K, while the well-defined narrow diffraction peaks are seen at temperatures below 170 K.

In Fig. 1 the temperature dependences of the lattice parameters, Mn-O bond lengths, and Mn-O-Mn angles for both phases in the S1 sample are shown. For the P1 phase these parameters are safely refined for all temperatures, while for the P2 phase it could only be done for $T$ < 170 K. In the P1 phase, all Mn-O distances are close to each other; on the contrary, in the P2 phase, the $MnO_6$ octahedra are strongly distorted ($\sigma_{JT} \approx 0.03$ Å) with Mn-O1 (out-of-plane) bond shorter than the two others. The sample volume occupied by the P2 phase does not change significantly with temperature and amounts to about 40%. Diffraction peaks belonging to the P2 phase are broad up to 150 K (~1.7 times broader than those of the P1 phase) and get even broader at higher temperatures. At the moment it is not clear, what exactly is the reason for this broadening – internal microstresses ($\Delta a/a \approx 0.0035$), short coherent lengths ($L \approx 100 - 700$ Å) or continuous distribution of the lattice parameters across the sample. The same behavior was found for the S2 sample with $y$ = 0.456. The essential difference is that the second structural phase appears at lower temperature ($T$ < 150 K) and occupies a smaller part of sample volume (< 25%).

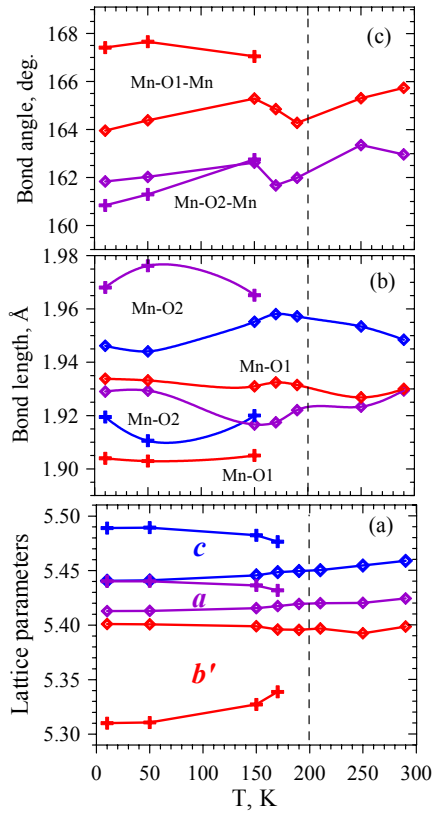


Fig. 1. Temperature dependences of the unit cell parameters ($b' = b/\sqrt{2}$) (a), the Mn-O bond lengths (b), and the Mn-O-Mn valence angles (c) in the P1 (diamonds) and P2 (crosses) phases of the S1 sample. The symbol sizes are larger (a) or comparable (b, c) with the experimental errors. The vertical dashed line indicates the onset temperature of the long range FM and AFM order. The definite refinement of the structural parameters P2 phase is only possible below 170 K.

At low temperature neutron diffraction data show appearance of the FM order in the P1 phase and $AFM_A$ (ferromagnetic planes coupled antiferromagnetically along $b$) order in the P2 phase in both S1 ($T_C \approx T_N \approx 200$ K) and S2 ($T_C \approx T_N \approx 100$ K) samples. At $T < 50$ K in the P1 phase (Nd,Tb) magnetic moments are also ordered in the same direction (along the $c$-axis) as Mn moments. The temperature dependences for these magnetic components are presented in Fig. 2. One may see that the FM and $AFM_A$ structures appear simultaneously and their temperature behavior is similar. It means that the volume fractions of the phases are about constant down to helium temperature. At $T = 10$ K, the values of magnetic moments in both phases are close to the nominal value of 3.5 $\mu_B$ for compositions with $Mn^{3+}/Mn^{4+} = 1/1$, which means that the long range magnetic ordering occupies practically the whole sample volume.

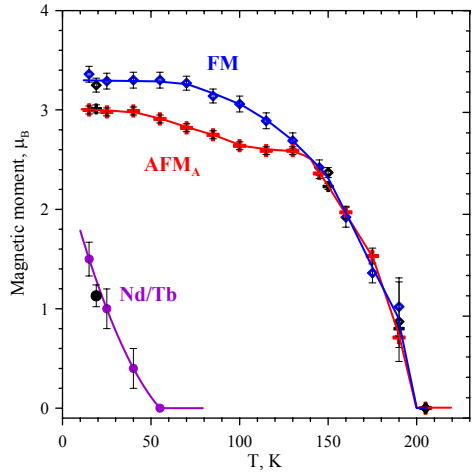


Fig. 3. Temperature dependences of the Mn ordered magnetic moment magnitude in the FM phase (diamonds), $AFM_A$ phase (crosses) and (Nd/Tb) moment in FM phase (circles) for S1 sample with $y = 0.228$. The moment values are normalized on the phase fraction in the sample.

The new data obtained with NTSM allowed us to reconsider the refinement of SSM diffraction patterns introducing the two crystal phases. Indeed we have found that in both SSM samples with $^{16}O$ and $^{18}O$ isotopes, two crystal phases coexist, their parameters are very close to that of the NTSM-S2 sample. In the SSM compound with $^{16}O$, which is metallic, the P1 phase with regular $MnO_6$ octahedra and $M_{FM} = 3.5 \pm 0.2\ \mu_B$ occupies around 65% of sample volume. In the insulating $^{18}O$ compound the relative volume of the P1 phase is only about 18% and the long range FM order is absent. As in the NTSM, the P2 phase of this compound has the $AFM_A$ magnetic ordering type below $T_N \approx 100$ K with $M_{AFM} = 2.59 \pm 0.02\ \mu_B$.

The new data on the P1 and P2 phases in SSM samples confirm the percolative nature of the metal-insulator transition in the Sm-compounds upon $^{16}O$ for $^{18}O$ substitution due to a sharp (from 65% to 18%) decrease of the ferromagnetic metallic fraction. Instead of the coexisting FM and AFM clusters, only the AFM long range order survives upon the isotope substitution. The same phenomenon has been earlier found for the $(La_{0.25}Pr_{0.75})_{0.7}Ca_{0.3}MnO_3$ [2] compound, where the AFM-I phase is of the CE-type. The last means that the $^{16}O \rightarrow {}^{18}O$ driven metal-insulator transition in manganites does not depend on the specific nature of the AFM structure and related orbital order.

This work was supported by the Russian Foundation for Basic Research (projects 02-03-33258, 03-02-16954). Neutron diffraction experiments were performed on HRFD (IBR-2, Dubna, Russia), HRPT and DMC (Swiss spallation neutron source SINQ, Paul Scherrer Institute, Switzerland) instruments.

**References**

N.A. Babushkina et al., Phys. Rev. B **67**, 100410(R) 2003.
A.M. Balagurov et al., Phys. Rev. B **60** (1999) 383.

# DETERMINATION OF MAGNETIC MOMENTS AND HYPERFINE MAGNETIC FIELDS IN $ScFe_2$ LAVES PHASE COMPOUND.

M. Wiertel [a)], Z. Surowiec[a)], A. I. Beskrovnyy[b)], J. Sarzyński [a)] and M. Budzyński [a)]

[a)] *Institute of Physics, UMCS, pl. M. Curie-Skłodowskiej 1, 20-031 Lublin, Poland*
[b)] *Frank Laboratory of Neutron Physics, JINR 141980 Dubna, Moscow Reg., Russia*

From a few years we have investigated quasibinary alloys $A(Fe_{1-x}M_x)_2$ or $(A_{1-x}A'_x)Fe_2$-type. They are treated by us as a kind of a model phase in which magnetic, electrical and mechanical properties are modified by means a gradual Fe/M substitution. Recently we have begun a study of $Sc(Fe_{1-x}M_x)_2$ series with M= Al, Cu or Si. The initial alloy for them is $ScFe_2$ Laves phase. It is known that this phase may crystallize in one of the structure: the cubic C15 (cF24), hexagonal C14 (hP12) or C36 (hP24) [1]. It depends strongly on details of the sample preparation. At high temperatures ($1453 < T < 1838$ K) this alloy should crystallize in the last from above mentioned types of structures [2]. We produced $ScFe_2$ in polycrystalline form by arc melting exactly stoichiometric amounts of Sc and Fe of 4N purity, in an inertial argon atmosphere. In order to achieve sufficient homogeneity the sample was remelted a few times. XRD, magnetization, Mössbauer spectroscopy and ND measurements were performed. Powder x-ray and neutron diffraction revealed that our $ScFe_2$ sample has C36 (hP24, space group *$P6_3/mmc$*) crystal structure in which Fe atoms occupy three crystallographically nonequivalent positions: *6g, 6h* and *4f* (Wyckoff notation). They form the sublattice of regular tetrahedra linked alternately by their apexes or by their bases. Only a few weak peaks of foreign phases were detected in this sample. They are identified on the basis of ND spectra as $Sc_2O_3$, $Fe_2O_3$, $Fe_3O_4$ and pure $\alpha$-Fe and taken into consideration in the final fitting. The content of these admixtures not exceeds 4 -6 at. %.

From the temperature dependence of magnetization for the $ScFe_2$ sample shown in Fig. 1 the Curie temperature was determined. It is equal approximately 642 K and is by 100 K higher than $T_C$ for C14 version of this compound. It is interesting that these structures are almost identical. The latter has only the parameter *c* two times smaller than the former. The observed increasing of magnetization of the sample with temperature below $T_C$ and it appearance again above $T_C$ is probably related to the increasing of the oxides and pure iron contents in the sample during of the sample heating.

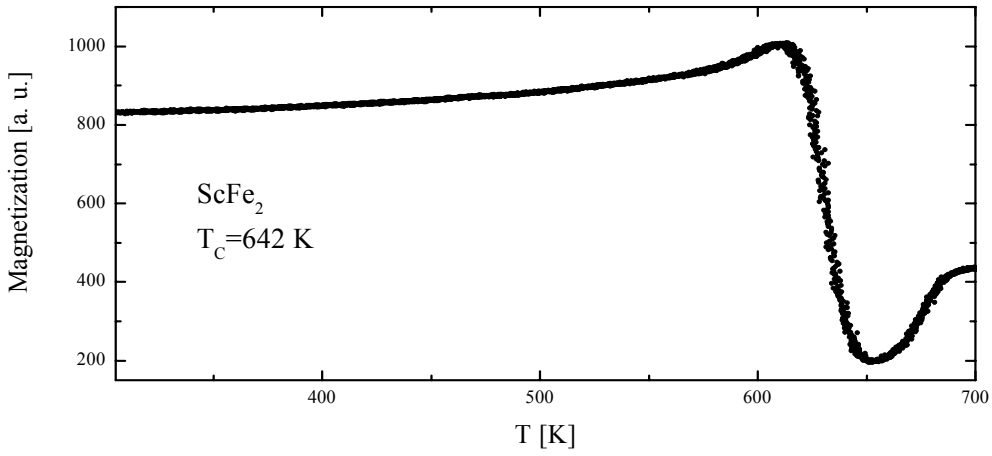


Fig. 1. *The AC magnetization of $ScFe_2$ measured at v=229 Hz in a field of 10 Oe. The heating rate- 100K/min.*

The $ScFe_2$ was reported to be ferromagnetic [3] but the electronic structure calculations [4] for these compounds gave the Fe magnetic moments values of about 1.5 $\mu_B$ and an antiparallel moments of about -0.5 $\mu_B$ induced at Sc sites as a result of the hybridization of the *3d* Fe and *3d* Sc bands. The [001] direction is the magnetic moments ordering axis in $ScFe_2$.

The neutron diffraction (ND) experiments were performed with the DN2 time-of-flight powder diffractometer at the fast pulsed reactor, IBR-2 in the Frank Laboratory of Neutron Physics, Joint Institute for Nuclear Research. The diffraction patterns were refined by the FULLPROF Rietveld refinement program. A convolution pseudo-Voigt with double exponential function was chosen to generate the line shape of the diffraction peaks. In the final run such parameters as background coefficients, unit-cell parameters, pseudo-Voigt parameters, positional coordinates, isotropic thermal factors were refined from the ND data. In the obtained $ScFe_2$ neutron diffraction patterns three pairs of peaks with the strong dependence of their intensity on temperature were founded (see Fig. 2). The pairs of the (102) and (112) peaks at $d \approx 3.80$ Å, of the (111) and (101) peaks at $d \approx 4.16$ Å and of the $(1\bar{1}0)$ and (100) peaks at $d \approx 4.29$ Å come from practically pure magnetic scattering. Nuclear scattering contributions to these peaks from different atoms at different crystallographic sites cancel each other out to a large extent. This fact allows us to determine the magnitude of the Fe and Sc ordered magnetic moments.

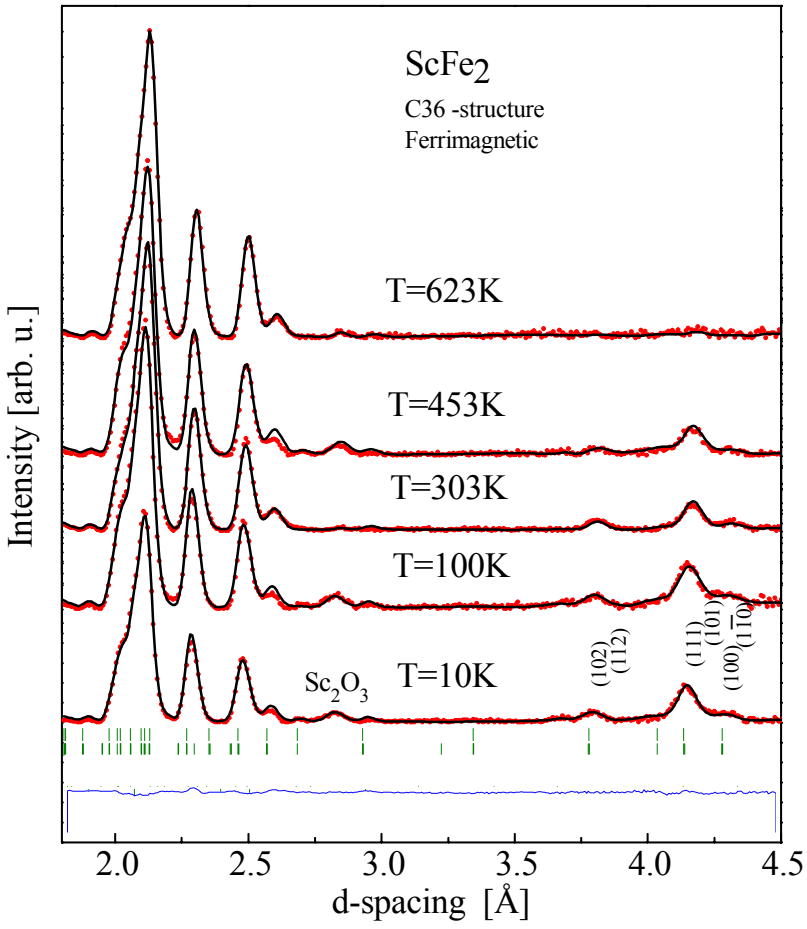


Fig. 2. *The change of the neutron diffraction peaks (102), (112), (111), (101),* $(1\bar{1}0)$ and (100) *with temperature for polycrystalline* $ScFe_2$ *sample. The most strong peak (222) for the* $Sc_2O_3$ *(Ia* $\bar{3}$ *space group) admixture of about 4 at. % is marked on the lowest pattern. The points represent experimental data, the full lines show calculated pattern. The short vertical marks below the diffraction pattern at 10 K indicate the calculated nuclear Bragg position (upper row) and the magnetic ones (lower row) and the lower curve the difference between observations and calculations for 10 K.*

The initial model of magnetic structure had been accepted on the basis of the data from NMR measurements [1], theoretical calculations [4] and from the results of the $^{57}$Fe Mössbauer spectroscopy measurements performed by us.

The selected Mössbauer spectra are shown in Fig.3. At temperature below $T_C$ the experimental pattern was good fitted with three subspectra (sextets) for $^{57}$Fe atoms located at respective crystallographic positions. At high temperature spectra apart from one paramagnetic doublet the sextet of weak intensity for pure Fe is visible. It indicates firstly, that quadrupole splitting parameter value equals of about 0.21(1) mm/s is the same for all three Fe positions, and secondly that at temperature above about 650 K pure Fe, magnetite and hematite precipitation occurs in accordance with AC-magnetization and neutron diffraction measurement results.

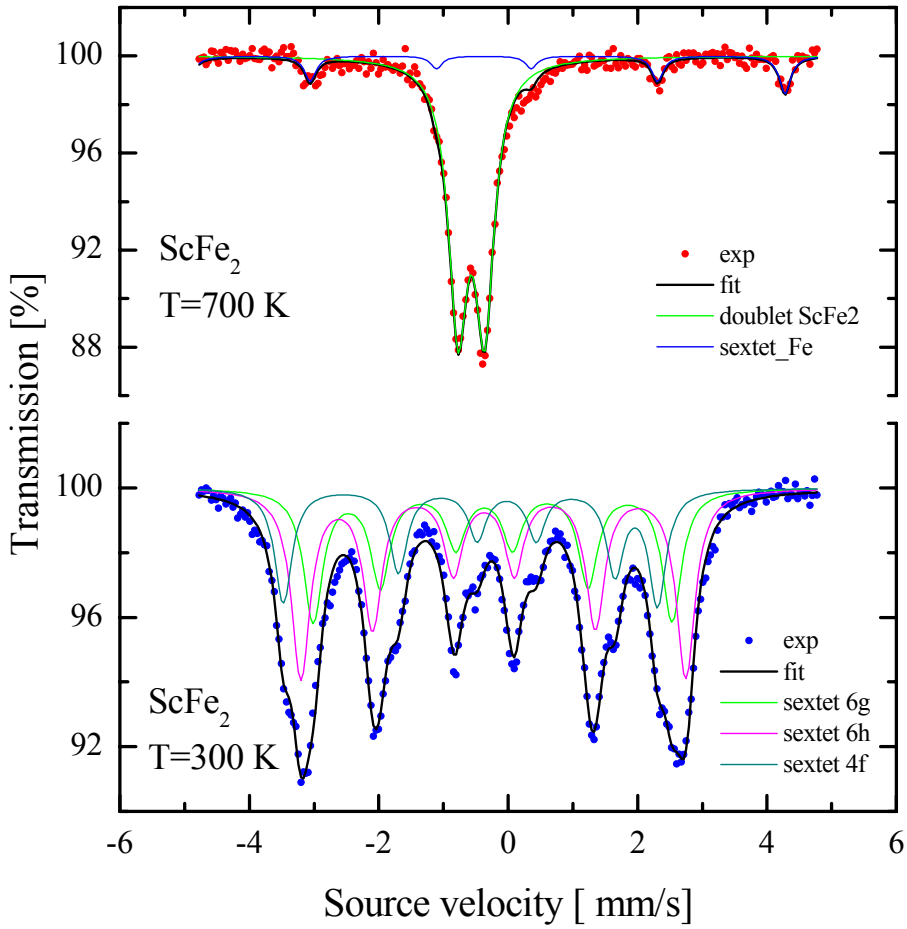


Fig. 3. *The Mössbauer spectra measured for $ScFe_2$ compound at 300 and 700 K respectively. The black full lines represent the calculated pattern, the points the observed one and the others colour full lines show fits for spectra components at respective Fe positions in the crystal lattice.*

The Table 1 collected the main results of our investigations of $ScFe_2$ compound. Careful analyses of the neutron diffraction patterns confirm the occurrence of magnetic moments at Sc positions antiparallel to Fe magnetic moments. In the temperature range from 10 K to 650 K we estimated the values of Sc moment at 4e and 4f sites in crystal lattice. They are similar at these two types of positions and change from about $-0.7\mu_B$ at the lowest temperature to zero for temperature above $T_C$. Such estimation for Sc moments is in a good accordance with results of the theoretical calculations carried out by authors of paper [4] mentioned above. On the other hand the magnetic moments values determined in our measurements are about 30 % bigger than that estimated in NMR measurements [5] for $ScFe_2$ with C36 structure. However in our investigation the magnetic

moments of Fe atoms and the hyperfine magnetic fields at their nuclei were determined independently, while in the paper [5] other procedure was used.

*Table 1. Magnetic moments of Fe atoms, the hyperfine magnetic fields at $^{57}Fe$ nuclei and the lattice parameters a and c in the intermetallic $ScFe_2$ compound at different temperatures.*

| T [K] | $\mu_{Fe}$ [$\mu_B$] (*6h*) | $\mu_{Fe}$ [$\mu_B$] (*4f*) | $\mu_{Fe}$[$\mu_B$] (*6g*) | $B_{hf}$ [T] Fe(*6h*) | $B_{hf}$ [T] Fe(*4f*) | $B_{hf}$ [T] Fe(*6g*) | Lattice parameters *a* and *c*[Å] |
|---|---|---|---|---|---|---|---|
| 10 | 1.983(25) | 1.831(25) | 1.715(30) | | | | 4.945(8) 16.167(12) |
| 100 | 1.943(28) | 1.791(30) | 1.652(28) | | | | 4.953(9) 16.189(10) |
| 200 | 1.896(13) | 1.749(13) | 1.524(13) | | | | 4.960(10) 16.224(14) |
| 303 | 1.771(9) | 1.521(9) | 1.311(9) | 19.5(2) | 18.3(2) | 16.8(3) | 4.969(9) 16.246(10) |
| 453 | 1.450(38) | 1.320(37) | 1.100(34) | 16.0(3) | 15.5(1) | 14.7(2) | 4.971(9) 16.247(13) |
| 623 | 0.571(29) | 0.521 (26) | 0.311(32) | 9.5(1) | 8.9(2) | 8.1(1) | 4.990(8) 16.306(10) |
| 650 | 0.000(30) | 0.000(29) | 0.000(30) | 0 | 0 | 0 | 4.997(8) 16.400(11) |

First the hyperfine magnetic fields were measured by means of NMR. Then accepting for $ScFe_2$ a value of hyperfine coupling constant for the Laves compounds based on Fe with Y and Zr, the values of magnetic moments were estimated. On the basis of data given in the table we can determine the hyperfine coupling constant between Fe magnetic moments and hyperfine magnetic fields at $^{57}Fe$ nuclei. For example this constant at room temperature is equal about 12 T/$\mu_B$. It is considerably lower than the value accepted in [5] which is equal about 14 T/$\mu_B$. This is a reason of some discrepancy between our results and the results of NMR measurements.


[1] V. Pokatilov, V. Golikova, A. Tsvyashchenko, L. Fomichova, Hyperfine Interactions 59 (1990) 529.
[2] O.I. Bodak, B. Y. Kotur, I.S. Gavrilenko V. Y. Markiv, V. G. Ivanchenko, Dopov Akad. Nauk Ukrain. RSR, Ser. A N 4 (1978) 365.
[3] K. Ikeda, T. Nakamichi, T. Yamada, M. Yamamoto, J. Phys. Soc. Jap. **36**, 611 (1974)
[4] S. Asano, S. Ishida, J. Phys. F: Met. Phys. **18**, 501 (1988)
[5] В.С. Покатилов, В.В. Садчиков, О-В. Утенкова, Доклады Академии наук СССР 281, №3 (1985)

**High-Pressure Effects on the Crystal and Magnetic Structure of the Frustrated Antiferromagnet $YMnO_3$.**

D.P. Kozlenko[1], S.E. Kichanov[1], S. Lee[2], J.-G. Park[2,3], V.P. Glazkov[4] and B.N. Savenko[1]

[1] *Frank Laboratory of Neutron Physics, JINR, 141980 Dubna, Russia*
[2] *Department of Physics and Institute of Basic Science, Sung Kyun Kwan University, Suwon 440-746, Korea*
[3] *Center for Strongly Correlated Materials Research, Seoul National University, Seoul 151-742, Korea*
[4] *Russian Research Center "Kurchatov Institute", 123182, Moscow, Russia*

The hexagonal manganites belong to unusual type of magnetoelectric materials showing coexistence of ferroelectric behavior and magnetic ordering and the ferroelectric transition temperature $T_C$ ~ 600 - 900 K is found to be much higher in comparison with antiferromagnetic (AFM) ordering temperature of $T_N$ ~ 70 – 130 K [1]. Magnetic properties of $RMnO_3$ manganites depend substantially on the ionic radius of R cation *r*. A rich variety of magnetic properties of hexagonal manganites reflects the modification of the balance between different in-plane and inter-plane magnetic interactions due to changes of the geometry of Mn-O-Mn network upon variation of the *r* value [2]. Apart from the variation of ionic radius of R cation, interatomic distances and angles in the structure can be modified directly by application of high external pressure. In order to study the interplay between modifications of the crystal structure and relevant changes of the magnetic structure of the hexagonal manganites, we have performed neutron diffraction experiments at high external pressures up to 5 GPa with $YMnO_3$ compound, which possesses no magnetic moment at the R sublattice and does not exhibit spin-reorientation transitions at ambient pressure.

At ambient pressure, below $T_N$ = 70 K in $YMnO_3$ a triangular AFM state of $\Gamma_1$ [3] irreducible representation occurs and it coexists with a minority spin-liquid state. At high pressure, a spin-reorientation phase transition was observed and the triangular antiferromagnetic structure evolves from $\Gamma_1$ to $\Gamma_1$+$\Gamma_2$ representations [4]. The value of Mn magnetic moment at $T$ = 10 K decreases from 3.27(8) $\mu_B$ to 1.52(9) $\mu_B$ and the enhancement of diffuse scattering above $T_N$ occurs with the pressure increase from 0 to 5 GPa. Both observations indicate the increase of the spin-liquid state volume fraction and suppression of the ordered AFM phase.

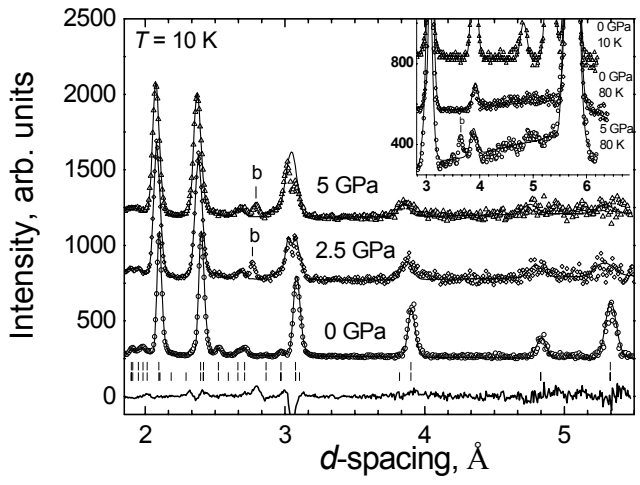


**Fig.1**. *Neutron diffraction patterns of $YMnO_3$ measured at P = 0, 2.5 and 5 GPa,T = 10 and 80 K at scattering angles 2θ = 90˚ and 45.5˚ (inset) and processed by the Rietveld method. Experimental points (symbols), calculated profiles (lines) and difference curve (for P = 5.0 GPa, bottom) are shown. Ticks below the data points represent the calculated positions of nuclear (upper row) and magnetic (lower row) diffraction peaks of $YMnO_3$.*

The distortion of triangular atomic arrangement of Mn and O ions mediating the difference in the strength of nonequivalent in-plane superexchange interactions is reduced at high pressure. As a result, the enhancement of geometrical frustration effects occurs, which subsequently leads to the decrease of the ordered Mn magnetic moment value and the increase of diffuse scattering above $T_N$. Such observations indicate the suppression of the ordered AFM phase and the increase of the volume fraction of the spin-liquid state at high pressure.


[1] T.Katsufuji, M.Masaki, A.Machida and et.al., Phys. Rev. B **66**, 134434 (2002).
[2] J.E.Greedan, M.Bieringer, J.F.Britten and et.al., J. Solid State Chem. **116**, 118 (1995).
[3] A.Munoz, J.A.Alonso, M.J.Martinez-Lope and et.al. Phys. Rev. B **62**, 9498 (2000).
[4] D.P. Kozlenko, S.E. Kichanov, S.Lee and et.al. JETP Lett., **82**, 193 (2005).

**Neutron diffraction studies of a $Bi_{2.53}Li_{0.29}Nb_2O_9$ at the high temperature.**

S.G. Vasilovskij[1], A.I. Beskrovny[1], V.G. Simkin[1],
M. Sarrion[2], L. Mestres[2], M. Herraiz[2]

[1] Frank Laboratory of Neutron Physics, JINR, 141980 Dubna, Russia
[2]Departament of inorganic chemistry, University of Barselona, 08028, Barselona, Spain

Arivillius phases (compounds with chemical formula $(A_2O_2)^{2+}(A'_{n-1}B_nO_{3n+1})^{2-}$, $n$=1, 2, 3, 5 and 8) are known as ferroelectric materials, structurally related to perovskites. Structures of this type show hide variability of physical properties when substituting of cations of metal. This opens greater possibilities at syntheses of new material. Except the ferroelectric properties, the Aurivillius phases are studied as potential ionic conductors that can be used, e.g., in the manufacture of lithium accumulators.

Crystal structure of the new Aurivillius phase $Bi_{2.53}Li_{0.29}Nb_2O_9$ was investigated at room and low temperature (10 K) earlier [1, 2]. The crystal structure described by a space group $Cmc2_1$, with lattice parameters of an orthorhombic unit cell as ***a***=24.840(5), ***b***=5.449(6), ***c***=5.450(9) Å. The phase transition in this temperature range was not observed.

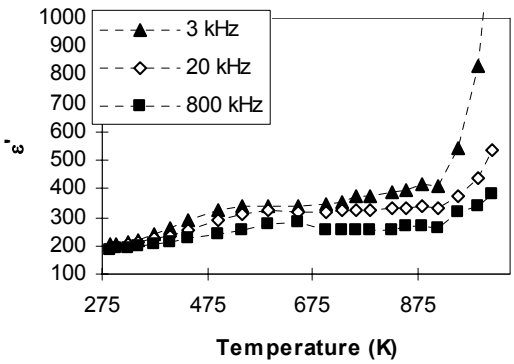


**Fig. 1.** Dielectric constant ε´of $Bi_{2.53}Li_{0.29}Nb_2O_9$ vs. temperature for different frequencies.

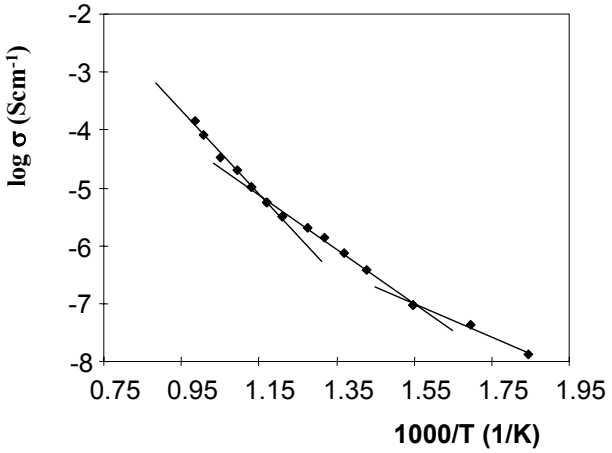


**Fig. 2.** Arrhenius plots conductivity for $Bi_{2.53}Li_{0.29}Nb_2O_9$.

Variation of the dielectric constant (ε') as the function of the temperature for different frequencies during the heating run was carried out (Figure 1). There are two anomalies in the behaviour of this constant; the first one of approximately 573 K and the second one at 873 K. the maximum corresponding to the first one shifts to lower temperatures with decreasing frequency. This kind of behaviour of the dielectric constant is typical of materials with a diffuse phase transition, and is also found for different ferroelectric material. For temperatures above 873 K a further increase of the dielectric constant was observed as the increasing electric conductivity leads to a dielectric breakdown.

Measurement of conductivity also has been executed (Figure 2). The plot is not linear and a slope changes around the same temperatures where the dielectric permittivity plots show anomalies. That may be attributed to a structural phase transition. In other side, at initial state the Aurrivillius phases describe is I4/mmm space group.

The measuring executed at high temperatures (up to 850 K) on a diffractometer with the medium resolution DN-2, have shown, nonlinear dependence of change of parameters of a unit cell with growth of temperature.

Because of this peculiarity, the crystal structure investigation of $Bi_{2.53}Li_{0.29}Nb_2O_9$ at high temperatures was perform at the high resolution Fourier diffractometer.

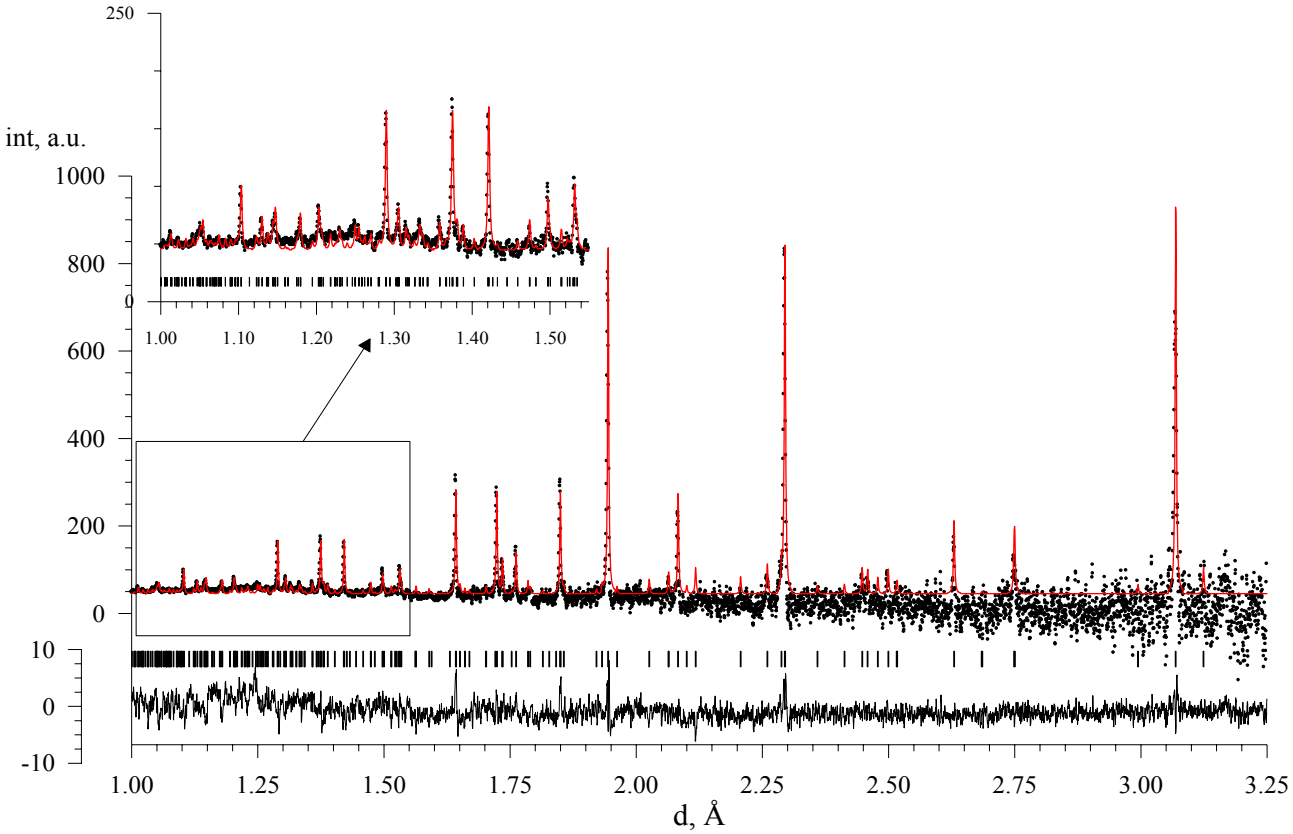


**Fig. 3.** Neutron diffraction spectrum of $Bi_{2.53}Li_{0.29}Nb_2O_9$ measured on a high-resolution Fourier diffractometer (dots) at T=1000 K. The solid line shows the same spectrum processed by the Rietveld method. Vertical lines indicate the calculated positions of the diffraction spectra. Below, the difference (experiment minus calculation) curve normalized to the mean square deviation at the point is shown.

The structural phase transitions are not observed up to 1000 K. The crystal structure is orthorhombic with space group $Cmc2_1$, lattice parameters of a unit cell as ***a***=24.9942(2), ***b***=5.4974(1), ***c***=5.5003(1) Å. Rietveld refinement was performed (Figure 3).

References

1. M.L.Martinez Sarrion, L.Mestres, M.Herraiz, A.V.Belushkin, A.M.Balagurov, A.I.Beskrovnyi, S.G.Vasilovskiy, L.S.Smirnov «X-ray and neutron diffraction studies of a new Aurivillius phase of $Bi_{2.53}Li_{0.29}Nb_2O_9$», Frank Laboratory of the Neutron Physics, Joint Institute for Nuclear Researches, Dubna, Annual report 2000, p 84-86.
2. A.I.Beskrovnyi, S.G.Vasilovskiy, A.V.Belushkin, L.S.Smirnov, A.M.Balagurov, M.L. Martinez Sarrion, L.Mestres, M.Herraiz «Structural study of new compound $Bi_{2.53}Li_{0.29}Nb_2O_9$ by the powder diffraction method, Crystallography Reports, Vol. 48, No. 3, 2003, pp. 396-400.

# ANISOTROPY OF ELASTIC PROPERTIES OF AMPHIBOLITES AND GNEISSES FROM THE KOLA SUPERDEEP WELL AT HIGH PRESSURES (UP TO 600 MPA) AND HIGH TEMPERATURES (UP TO 600 °C)

*T. I. Ivankina [1], H.M. Kern [2], A. N. Nikitin [1]*

*[1] Joint Institute for Nuclear Research, Frank Laboratory of Neutron Physics, 141980, Dubna, Moscow Region, Russia*
*[2] Institut für Geowissenschaften, Universität Kiel, 24098 Kiel, Germany*

## Introduction

Elastic anisotropy is an important property of most rocks constituting the Earth crust and upper mantle. Anisotropy in the geological materials has various sources. Most important is lattice (crystallographic) preferred orientation (LPO) due to the anisotropic properties of the rock-forming minerals and the texture of the polycrystalline aggregates. In addition, oriented microcracks, grain shape preferred orientation (SPO), and (at in situ conditions) presence of partial melt may also be of importance.

This paper reports results of experimental and theoretical investigations on two gneiss (K8802, K9002) and two amphibolite (K8752, K11345) cores samples recovered from the Archean basement of the Kola superdeep borehole SG-3 near Zapolyarny (Russia). The sample numbers indicate the depths of sample recovery in meters. We used two different methods to determine the seismic anisotropy and to discriminate between the contribution of oriented cracks and the lattice preferred orientation (LPO) of the minerals to bulk anisotropy. First, we measured P- and S-wave velocities in three orthogonal directions as a function of pressure and temperature, and second, we calculated 3D-velocities from measured LPO (texture) and the known single-crystal properties. The LPO of the rock-forming minerals was measured by TOF neutron diffraction. A main focus of the investigation is to elucidate the relationship between the crystallographic fabric and the elastic properties (velocity anisotropy, shear wave splitting and shear wave polarisation) and to discuss the role of propagation and polarization directions in anisotropic (foliated) rocks.

## Seismic laboratory measurements

The seismic measurements were done in a multianvil pressure apparatus using the ultrasonic pulse transmission technique with transducers (lead zirconium titanate) operating at 2 MHz (Kern, 1982). A state of near-hydrostatic stress is achieved by pressing six pyramidal pistons in the three orthogonal directions onto the cube-shape specimens (43 mm edge length). One end of each piston next to the specimen is surrounded by a furnace, and heat is transmitted from the pistons to the specimen. Thus a very homogeneous temperature distribution is obtained within the large-volume specimens. A schematic diagram of the transducer/buffer/sample assembly for the measurements of velocities at pressure and temperature is shown in Figure 1 (refer to Kern et al. (1997)).

The special arrangement of the apparatus allows simultaneous measurements of compressional (P) and orthogonally polarised shear wave velocities (S1, S2) in three perpendicular directions of the sample cubes. Due to the oblique orientation of the foliation plane to the core axis and the limited core diameter (60 mm), it was not possible to prepare cubes with the standard 43 mm edge length, using foliation (XY plane) and lineation (X) as the reference frame. In this investigation we therefore used the sample reference frame A, B, C which is basically related to the borehole axis: [C] is parallel to the borehole, and [B] and [A] normal to it, with a rough relationship of [A] to lineation.

Measurements were done over a range of pressures up to 600 MPa at room temperature and from room temperature up to 600 °C at 600 MPa confining pressure. Each set of experimentally

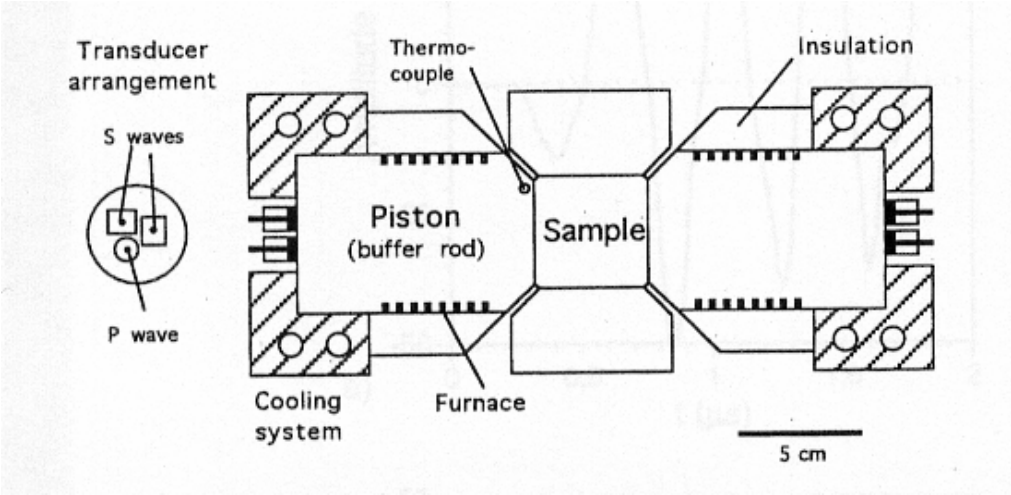


*Fig.1*. Schematic of the transducer/piston(buffer)/sample assembly for velocity measurements at pressure and temperature.

determined data comprises three P-wave velocities, six S-wave velocities, and the pressure (and temperature) dependent linear (and volumetric) strain. As an example, Figure 2 shows the directional dependence of P- and S-wave velocities as a function of pressure for the amphibolite sample K8752. In all samples, the velocity vs. pressure relations for P- and S-waves show typical slopes: a steep, non-linear velocity increase up to about 200 MPa, giving way for linear behaviour at higher pressures. A strong correlation between the slopes of the velocity versus pressure curves and volumetric strain curves (not shown here) indicates that the non-linear increase in velocity is mainly due to closing of microcracks. The "crack-closing pressure" is indicated by the transition from non-linear to linear behaviour. At 600 MPa where most of the cracks are closed, Vp is highest parallel to A, intermediate parallel to C, and lowest parallel to B (Fig. 2a). Interestingly, there is no difference in velocities for the two S-waves propagating parallel to A (Fig. 2b). By contrast, marked differences in shear wave velocities are observed for S-waves propagating parallel to B (Fig.2c) and C (Fig. 2d), with highest values for the C direction.

Raising the temperature has an opposite effect on wave velocities, because differential thermal expansion of the minerals causes grain boundaries to widen and new cracks to open. It is important to note that microfracturing, induced by the rapid thermal change of volume of the mineral phases will be increasingly suppressed as pressure is raised until at some value of several hundred MPa it does not take place (Kern, 1982). Thus, a confining pressure of 600 MPa is high enough to prevent thermal cracking, so that the temperature dependence of wave velocities (not shown here) is also almost linear up to about 600°C. The linear parts of the velocity vs. pressure and the velocity vs. temperature curves represent the intrinsic rock properties (matrix properties). These are controlled by the volume percentage of major minerals, their single crystal elastic properties, and their lattice preferred orientations (LPO).

The P- and S-wave velocities measured in the A ,B, C directions of the sample cubes do not necessarily represent the maximum and minimum velocities. Consequently, the corresponding calculated coefficients of velocity anisotropy A* = [(Vmax – Vmin)/Vmean)] x100 (%) are not in any case the extreme values of velocity anisotropies. Anisotropy is almost highest at low pressures resulting from a constructive interference of the effects caused by effective oriented microcracks and by lattice preferred orientation of the major minerals (LPO). Increasing pressure reduces the effect of cracks in a non-linear slope approaching nearly constant values at high pressures. The residual, nearly pressure-independent part of seismic anisotropy is mainly due the LPO of major minerals. The experimentally determined coefficients A* of P-velocity anisotropies (600 MPa) of the amphibolite samples are 8.27 % (K8752) and 0.86% (K11345), those of the gneiss samples 2.71 % (K8802) and 2.74 % (K9002).

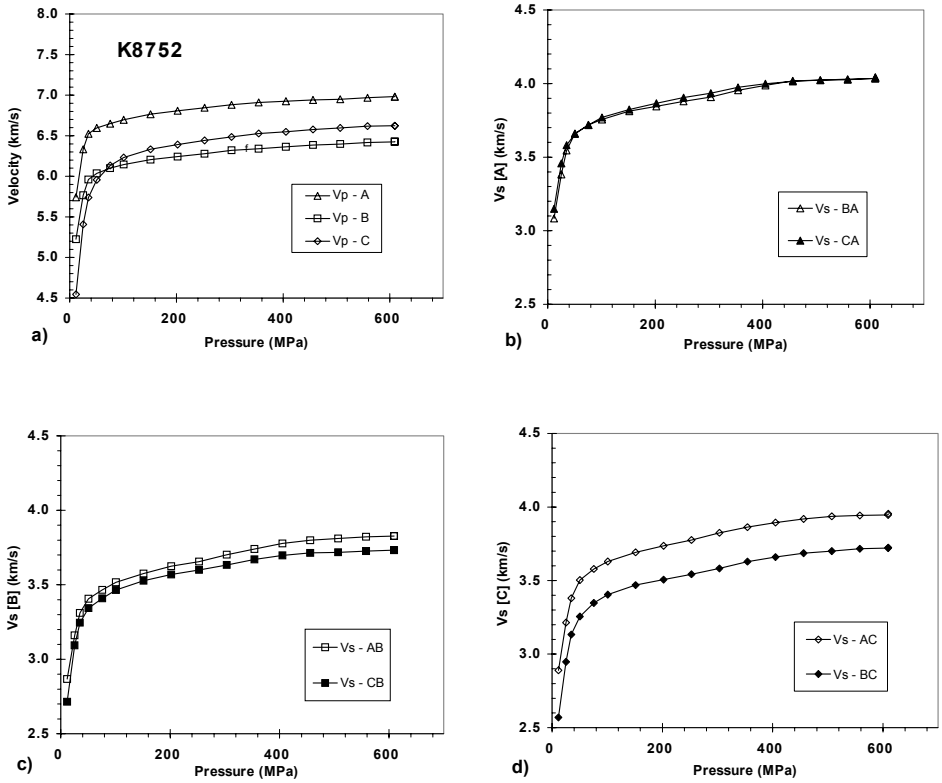


*Fig.2*. Directional dependence of P- and S-wave velocities (S1, S2) in amphibolite K8752 as a function of pressure. a) P-wave velocities; b) S-wave velocities in [A]; c) S-wave velocities in [B]; d) S-wave velocities in [C].

**Neutron diffraction and quantitative texture analysis**

We applied neutron diffraction for the determination of textures of the major rock-forming minerals. The measurements were carried out by means of the texture diffractometer SKAT of the pulsed reactor IBR-2 at Dubna (Russia), using the time-of flight (TOF) method (for details see Ullemeyer et al., 1988).

The TOF measurements were carried out on the same sample cubes (43 mm edge length) that were used for the laboratory seismic measurements. Because the samples are composed of low-symmetry minerals (triclinic plagioclase, monoclinic hornblende and mica, trigonal quartz) the texture determination of such polyphase rocks is not trivial due to the complex diffraction patterns exhibiting many overlapping peaks (Nikitin and Ivankina, 2004). Nevertheless, due to the high resolution of the SKAT diffractometer a sufficient number of pole figures of the main rock-forming minerals could be extracted from the diffraction spectra. From the experimental pole figures we derived the orientation distribution functions (ODFs), and recalculated the pole figures for the predominant mineral phases. Pole figures are presented as normalised density distributions and plotted as equal area projections on the BC plane of the sample reference system.

As an example, Figure 3 presents the ODF-derived pole figures of hornblende and plagioclase of the amphibolite samples K8752. The crystallographic preferred orientation of hornblende is most pronounced in sample K8752, compared to the plagioclase. The hornblende pole figures of sample K8752 are characterized by unimodal concentrations of the (001)-, (010)- and (100)-normals. The coexisting plagioclase minerals show maximum concentrations of the (001)- and (100)-normals on great circles, and the poles of the (010) planes occupy broad maxima.

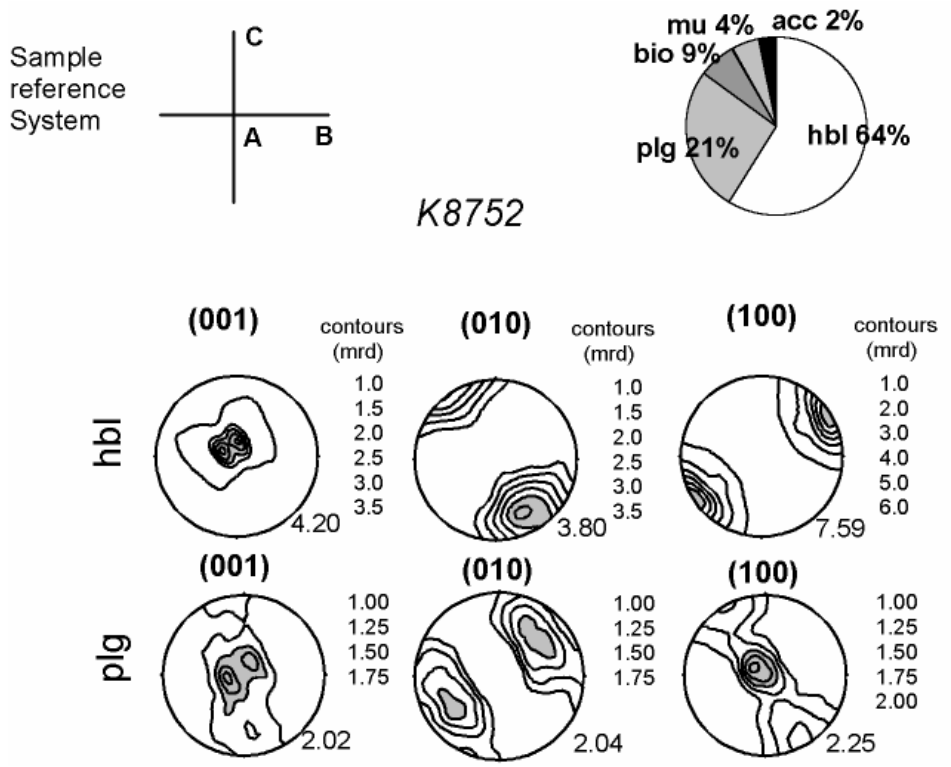


*Fig.3.* Principal pole figures of hornblende and plagioclase for the amphibolite sample K8752, recalculated from TOF neutron diffraction measurements. Equal area projection. The modal composition of the rock is displayed by the pie diagram.

**Numerical calculations of elastic rock properties**

The numerical calculations of Vp and Vs distributions of the polycrystals were carried out by means of the computer program BEATREX (Wenk et al., 1998), and the averaged bulk sample velocity distributions were determined by summarizing the velocity distribution of the aggregates according to the volume fractions of the constituent minerals.

In order to compare directly fabric anisotropy (pole figures) with velocity anisotropy, we present P- and S- wave velocities and shear wave splitting in the form of contour sterograms. The calculated three-dimensional variations of Vp and Vs1-Vs2 of the mineral aggregates (100 vol.-%) (a) and the corresponding data of bulk Vp and shear wave splitting (b) of the amphibolite sample K8752 are shown in Figure 4a. In Fig. 4b (right) we have rotated the diagrams along with the sample reference frame A, B, C to bring them in accordance with the standard setting X,Y,Z used in structural geology. The diagrams indicate that large variations in P- and S-wave velocities can occur as functions of the relative angle of the incoming propagating wave with respect to the orientation of the material anisotropy.

In the amphibolite sample K8752 (Fig.4) P-wave velocities are highest subparallel to lineation within the foliation and lowest normal to foliation. On the Vs1-Vs2 diagram an overall rhombic symmetry is apparent. The foliated amphibolite exhibits market shear wave splitting within the foliation plane with the fast split shear wave parallel to foliation. Normal to foliation (parallel to Z), a second shear wave will practically not be generated.

The marked Vp-anisotropy (6.81 %) calculated for the amphibolite sample K8752 is mostly caused by the strong LPO of the anisotropic hornblende minerals (Fig. 4) and their high volume percentage. Interestingly, the Vp velocity distribution calculated from the LPO of the constituent

plagioclase minerals give hints for a dissolution of the bulk Vp-anisotropy because it superimposes the hornblende pattern in a deconstructive way.

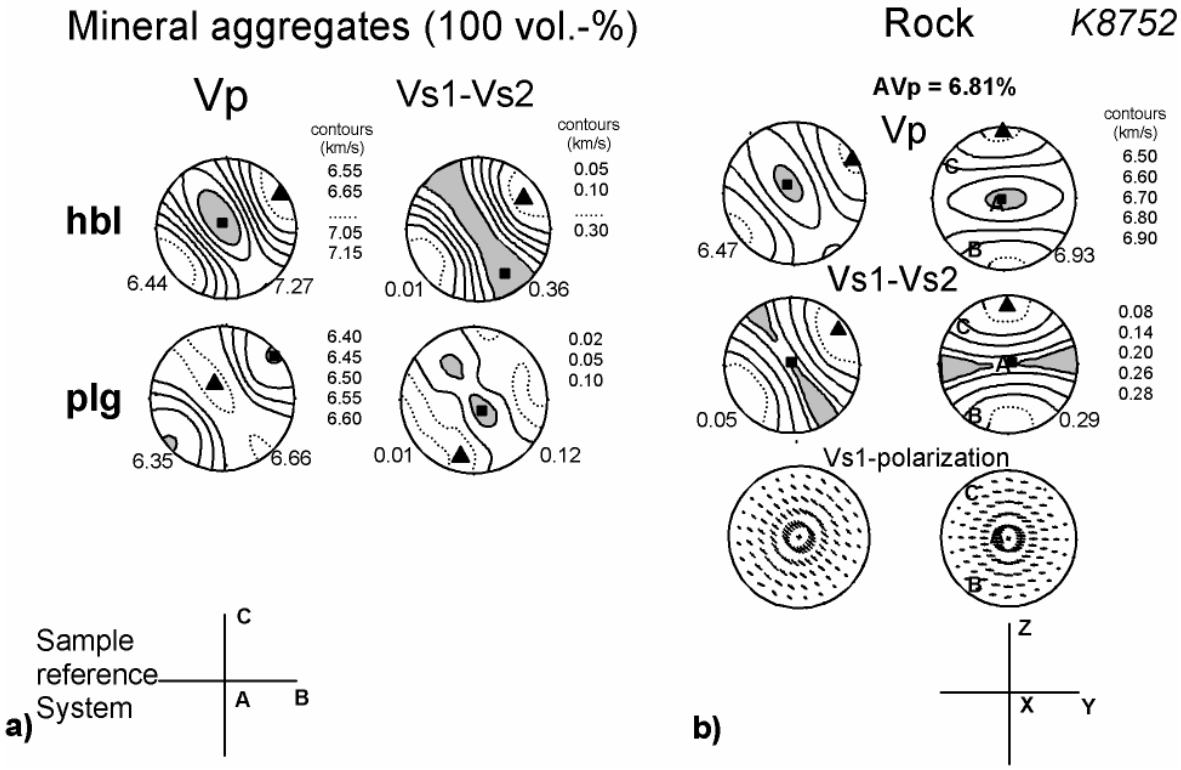


*Fig 4.* **Amphibolite K8752.** Calculated velocity surfaces of Vp and Vs1-Vs2 for the mineral aggregates (a) (100 vol.-%) and of the whole-rock (b), together with the orientation of the polarization plane of the fast split shear wave. The corresponding reference systems are indicated in the lower line. In the rotated stereograms (Fig. 4b, right) the XY-plane indicates foliation and X lineation.

**Comparison of measured with calculated velocity data**

As an example and for a more detailed comparison of experimental with calculated data we will discuss the anisotropic response to foliation tilt for elastic wave propagation on amphibolite sample K8752, exhibiting the largest P-wave anisotropy (measured as well as calculated). The discussion is based on the LPO-related velocity profiles calculated for the XY-, ZY-sections (Fig.5a) and for the BA-, CB- sections (Fig.5b), respectively.

From the sections referring to the structural frame X, Y, Z (along the symmetry planes of the velocity surfaces) presented in Fig. 5a it is clear that the maximum difference in shear wave velocities (shear wave splitting) occurs for shear waves propagating parallel to foliation (perpendicular to the foliation normal) with particle motion for the fast shear waves parallel to foliation (XY-plane) and for the slow shear waves (XZ-plane) normal to foliation. For the two shear waves propagating normal to foliation (parallel to Z) the difference in velocities is very low. The propagation of the elastic waves generated and recorded in the A, B, C directions by the sending and receiving transducers (Fig.5a) were generally not parallel to the inherent rock symmetry planes.

In Figure 5b we compare the LPO-based calculated velocity profiles for the **AB**- and **AC**-sections with the P- and S- wave velocities measured in the three directions **A**, **B**, **C**. It is evident that the variation of measured P- and S- wave velocities as well as the relative variation in differences of shear wave velocities with propagation direction is similar to that calculated for the three propagation directions, although the absolute values are different. Vp is highest in **A**,

intermediate in **C** and lowest in **B** as is seen on the profiles for the calculated velocities. Also the differences in measured shear wave velocities are qualitatively consistent with those calculated for direction **B** and direction **C.**

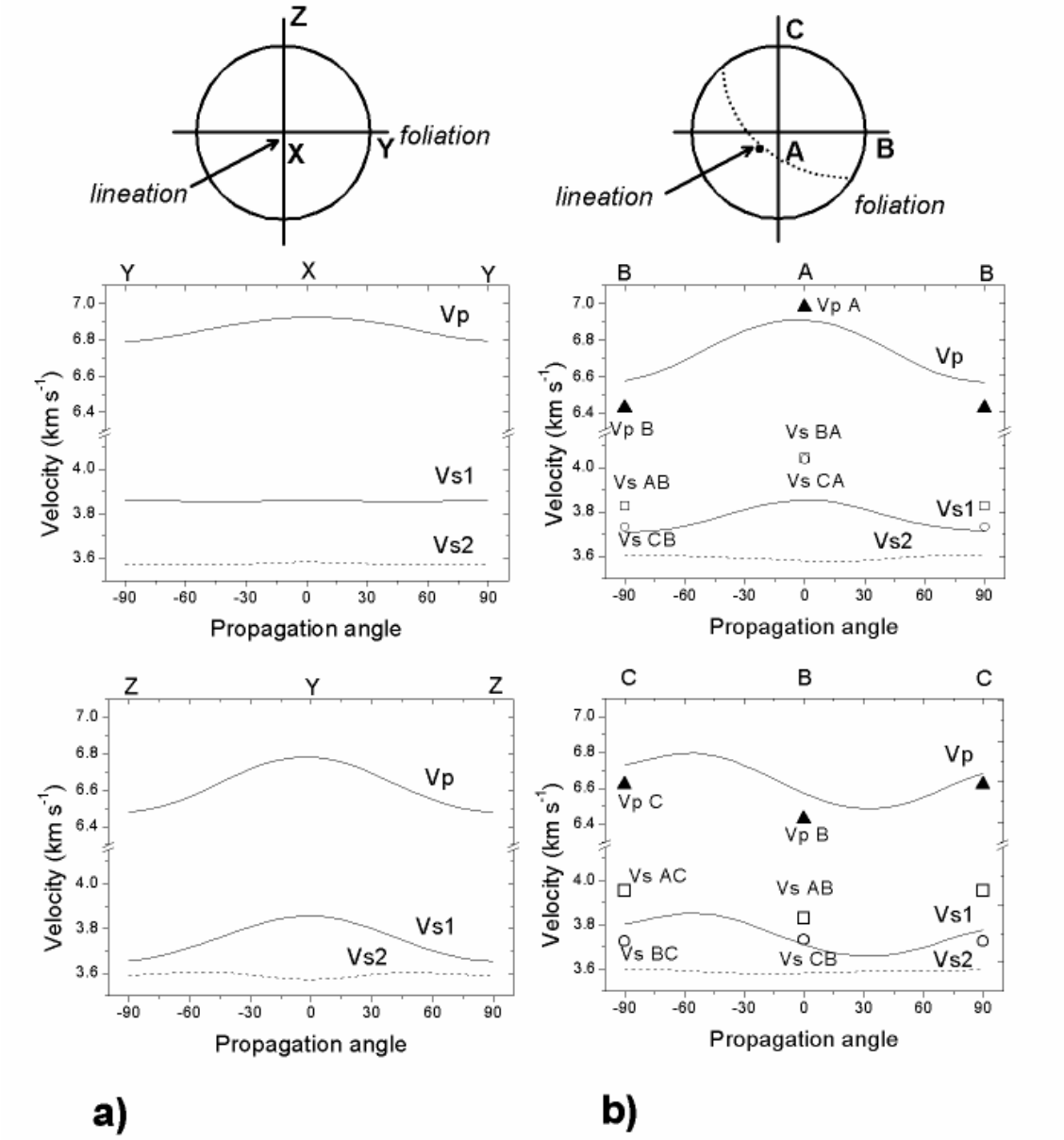


*Fig.5.* Amphibolite sample 8752. Velocity profiles for Vp and Vs1-Vs2 along YX and ZY (a) and BA and CB (b) of the calculated velocity surfaces presented in Fig. 4b. The schematics (top) indicate the reference system X,Y,Z and the reference system A,B,C in its relation to foliation and lineation. a) Propagation angle from X and Y; b) Propagation angle from A and B. Velocities recorded by the receiving transducers are indicated in Fig. 5b: Vp by triangles; Vs1 and Vs2 by open squares and open circles.

Highest shear wave velocities were measured for the shear wave with particle motion parallel to lineation, and slowest for shear waves with particle motion normal to lineation. There are however, marked differences between measured and calculated shear wave velocities for direction **A**. The two receiving transducers recorded the same high velocities for Vs-*CA* and Vs-*BA***,** that is, there is no difference observed between both S-velocities, although the difference in the LPO-based calculated

shear velocities (shear wave splitting) is at maximum in direction **A**. This can be explained by the fact that in the experiment the particle motion of the two shear waves propagating parallel to **A** (sub-parallel to lineation) is at about 45° to foliation for both S-waves. Consequently, there is no difference in shear wave velocities recorded by the two receiving transducers. These findings convincingly demonstrate the role of particle motion for S-wave propagating through anisotropic rocks, in addition to the propagation direction.

## Conclusions

We have measured compressional (Vp) and shear wave velocities (Vs1, Vs2) on two amphibolite and two gneiss samples from the Kola superdeep borehole in three orthogonal directions which were in general not parallel to inherent rock symmetry axes or planes. The experimental data are compared with 3D-velocities calculations based on lattice preferred orientation (LPO) of the main rock-forming minerals obtained by TOF (Time Of Flight) neutron diffraction analysis allowing the investigation of bulk volumes up to several cubic centimetres due to the high penetration depth of neutrons. The pole figures exhibit moderate to strong crystallographic preferred orientation of the constituent minerals. The crystallographic fabric is most pronounced in the amphibolites.

The LPO-based numerical velocity calculations give important information on the different contribution of the various rock-forming minerals (hornblende, plagioclase) to bulk elastic anisotropy and on the relationship between the crystallographic fabric (LPO) and the seismic properties of the rocks such as velocity anisotropy, shear wave splitting and shear wave polarization. The directions of intrinsic maximum and minimum Vp and Vs as well as the elastic birefringence (shear wave splitting) are controlled by the LPO of the rock-forming minerals and closely related to the structural frame of the rocks (foliation, lineation).

Comparison with the measured velocities obtained for the three propagation directions that were not in accordance with the structural frame of the rocks demonstrate the important role of particle motion for S-wave, in addition to propagation direction. The study shows that shear wave splitting in the foliated rocks is not properly measured with propagation and polarization directions of the sending and receiving transducers that are not parallel and normal to foliation and lineation, respectively.

## References


Kern H. P and S wave velocities in crustal and mantle rocks under the simultaneous action of high confining pressure and high temperature and the effect of the rock microstrucrure. In: High Pressure Researches in Geoscience, ed. W.Schreyer. Schweizerbart'sche, Stuttgart, 1982, 15-45.

Kern H., Liu B., Popp T., Relationship between anisotropy and P- and S- wave velocities and anisotropy of attenuation in serpentinite and amphibolite. J. Geophys. Res. 102, 1997, 3051-3065.

Nikitin, A.N. and Ivankina, T.I. Neutron Scattering in Geosciences. Paricles&Nuclei. Scientific review journal, 2004, vol.35, part 2, 348-407.

Ullemeyer K., Spalthoff P., Heinitz J., Isakov N.N., Nikitin A.N., Weber K. The SKAT texture diffractometer at the pulsed reactor IBR-2 at Dubna: experimental layout and first measurements. Nucl. Instrum. Methods Phys. Res., 1998, A 412/1, 80-88.

Wenk H.R., Matthies S., Donovan J., Chateigner D. BEARTEX: a windows-based program system for quantitative texture analysis.. J. Appl. Crystallogr., 1998. 31, 262-269.

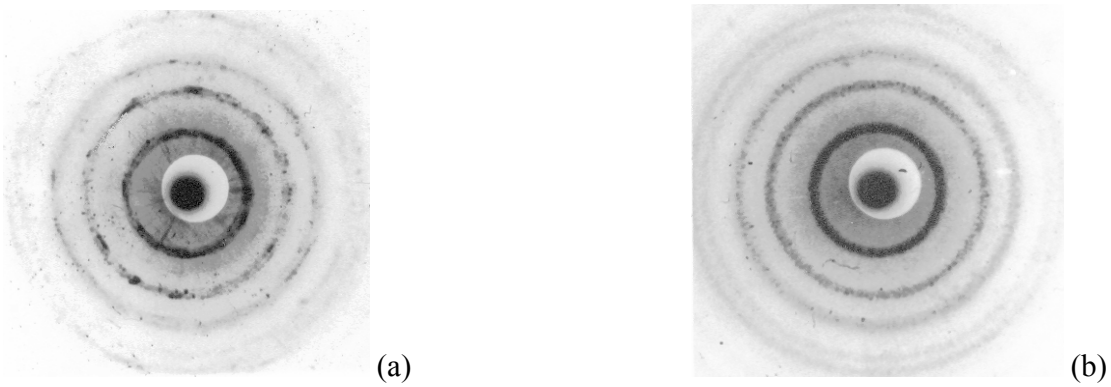

(a) (b)

*Fig. 1. Röntgenograms with X-ray diffraction reflections of calcium oxalate monohydrate: (a) renal stone, (b) standard sample.*

From the XRD investigated 61 renal stones we observed the next cases of discrepancy with their diagnostic given by chemical analysis : eight renal stones marked in the hospitals as urate stones, obviously do not coincide with the urate standard (Fig. 2); they have röntgenograms and interplanar spasings entirely coinciding with Ca-oxalate monohydrate standard (Fig. 1 b). Furthermore, five of the stones, marked in the hospitals as oxalates, gave an unambiguously picture and interplanar spacings which are typical solely for the cystine standard $\mathbf{C_6H_{12}N_2O_4S_2}$. Six stones, marked in the hospitals as calcium oxalate monohydrate, show röntgenograms equal with calcium oxalate dihydrate standard.

In general, our results revealed that in nearly 30 % the chemical analysis made in the hospitals gives wrong diagnosis of the stone type.

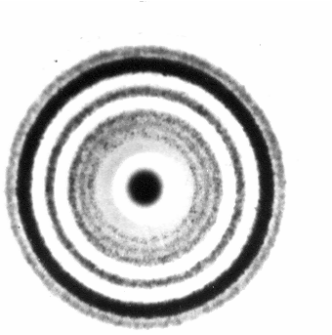

Fig. 2. *Röntgenograms with reflections of X-ray diffraction urate standard* $\mathrm{C_5H_4N_4O_3}$.

Additional advantage of the proposed by us method concerns the minimal weight of the investigated renal stone. For chemical analysis the stone must be with weight higher than 50 mg [1], while for X-ray diffraction analysis the stone can be under 50 mg, including stones as small as 2 mg weight [2]. In this aspect, for the stones spontaneously thrown out (usually being very small) the method proposed by us appears as only one possible for determination of stone type crystalising in the kidneys of such patients.

Having in view so high percentage of renal stone disease, the present investigation is very actual one. With the aim to prevent a recurrence of the stone formation, the exact

determination of composition and structure of the stone is very important. And the presented method of XRD gives the necessary accuracy, relatively to the chemical analysis:

Besides, chemical analysis is impossible for stones under 50 mg, which are the stones thrown out by the natural way. For such patients XRD of stone identification appears as single one to help the stone formers against the risk of recurrence of the disease.

**Neutron Diffraction**

It is well known that the XRD can not reveal the presence of the phase in amounts lower than 3 – 4 volume %. In this aspect the neutron experiments give additional information about the available phases in content lower than 4 volume %. By this reason, urate and oxalate (mineralogical name whewwelite) were investigated by neutron diffraction with the aim to verify whether given stone could be of mixtured type (for example, oxalate+urate, oxalate+ cystine and so on).

The neutron diffraction spectra were obtained by neutron time-of-flight (TOF) method on the DN-2 Neutron Diffractometer at the Fast Pulse Reactor IBR-2. Neutron spectra of urate and oxalate are shown in Figure 3 and Figure 4, respectively.

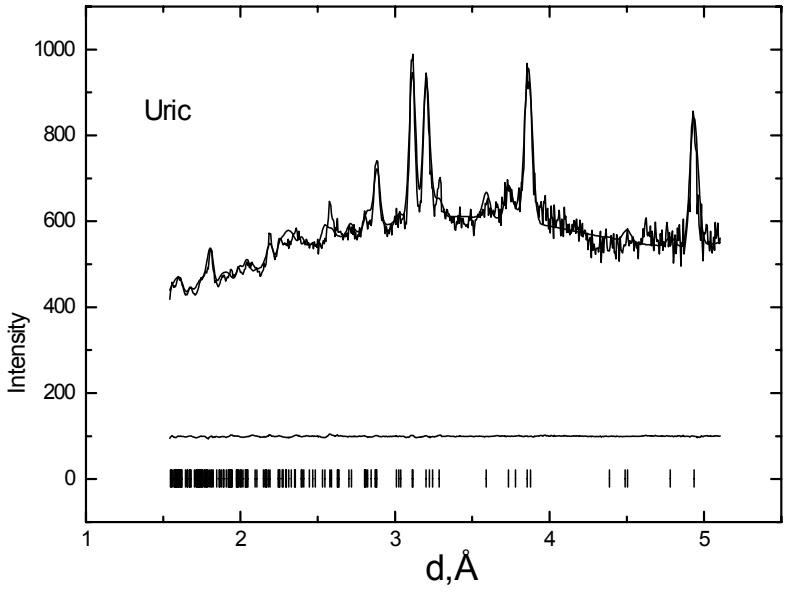


*Fig. 3. Neutron spectrum of urate renal stone.*

# DETERMINATION OF RENAL STONES TYPE BY X - RAY AND NEUTRON DIFFRACTION

M. Baeva*, A.I. Beskrovnyy*, I.G. Shelkova**

*Institute of Solid State Physics BAS, Sofia, Bulgaria
**JINR, Dubna, Russia

By X-ray and neutron diffraction methods the type of stones formed in human kidneys are investigated. X-ray structural investigations were realized in Solid State Physics Institute BAS, Sofia, and neutron experiments were carried out at the spectrometer DN-2 at IBR-2 pulsed reactor, JINR Dubna.

## Introduction

The renal stone disease (urolithiase) is an illness with a social significance. It hits hard predominantly the people in the active life of work (30-60 years). By the World Health Organisation data this disease hits 4 % of population.

The physicians have a classification of the renal stones (made by quite approximate chemical tests), which puts the stones into four basic groups: urates, oxalates, phosphates, and cystines. In these groups different chemical compounds exist, which crystallize in strictly different crystalline structures. Their mineralogical relation simply can be determined by X-ray analysis. It is a method, which appears entirely objective concerning the type of the urolithiase. This fact was the reason to develop XRD methods for stone type determination in laboratory "X-ray diffraction" at Institute of Solid State Physics – BAS. The samples submitted to us by the hospitals in Bulgaria have been taken by an open surgery or by shock waves lythotripsy.

After such hard interventions, with the aim to prevent the illness recurrence (which usually arises in 80 % after 3 –5 years) the patient is forced to carry out a prolonged prophilaxis. The latter obligatory must be considered with stone type. It means that the diets and drugs recommended for the patients suffering from a given type stone, appear harmful to the patient with the other type stone formation.

## X-Ray Diffraction

X-ray diffraction method was used for determination of the renal stone type. Röntgenograms were obtained with $CuK_\alpha$ radiation ($\lambda$ = 1.54 Å) by flat-plate Debye camera. The identification of the stones was made by a juxtaposition of the stone röntgenogram with röntgenograms of pure chemical compounds - standards. As standards we used pure chemical compositions (polycrystalline powders with particles size of 10 mkm). The röntgenograms of 4 standard substances and 61 renal stones were made. The interplanar spacings $\mathbf{d_n}$ values were calculated according to Brag equation. The standards were polycrystals with equal particles size of about 10 mkm and due to this, the intensity along the every Debye ring is equable. The inequality of the intensity along the Debye rings (see Fig. 1a) is due to the particles with a size above 10 mkm available in renal stones.

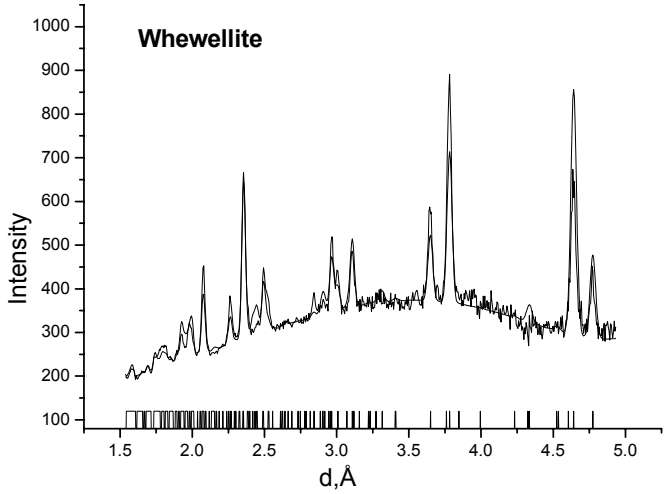


*Fig. 4. Neutron spectrum of oxalate renal stone.*

The neutron spectra approve the data obtained by XRD. They showed that both the oxalate and urate concrements usually consist of one type stone, i.e. they crystallize in pure one form.

For to be able such conclusion to be made as some rule in the medical practice, a greater amount of stones must be measured by neutron diffraction.

**References**

[1] E.J. Westbury, British J. of Urology, **46** (1976) p. 215

[2] M. Baeva, M. Ivanova, Patent No. 99992/11.09.1995, "X-ray structural method for identification of renal stone type", Patent registered by the Bulgarian Patent Institution.

**Acknowledgement**

The authors are grateful to the Bulgarian Agency of Nuclear Regulation for the financial support; Contract "Determination of concrements type at renal stone disease by X-ray and neutron diffraction methods".

# Verification experiments on FSD diffractometer

A.M.Balagurov, G.D.Bokuchava, A.V.Tamonov, V.V.Sumin, I.V.Papushkin, S.G.Sheverev

*Frank Laboratory of Neutron Physics, JINR, 141980 Dubna, Russia*

Due to expanding the detector base by two detectors "ASTRA" and carrying out repair works on the "TIRA-TEST" facility, it appeared to be necessary to verify the FSD stress-diffractometer. This work included three stages:

Determining of the resolution function of the spectrometer with new detectors.

Testing of the loading machine "TIRA-TEST" to determine Young modulus of the standard sample at the uniaxial loading.

Checking of the stress-scanner operation to determine the spatial distribution of deformations on the samples subjected to a four-point bend.

## 1. Determination of Fourier diffractometer resolution function.

Measurement of the FSD resolution function was carried out in January, 2005. Measurements were carried out on the standard polycrystalline sample NAC ($Na_2Al_2Ca_3F_{14}$) NIST standard, which does not contain residual stresses at the speed of the Fourier chopper rotation equaling 6000 resolutions per minute.

On the basis of the obtained data, the FSD diffractometer resolution function was determined and is given below:

$$R = \Delta d/d = [(\Delta t_0/t)^2 + (\Delta\theta/tg\theta)^2 + (\tau_0/N)^2 + (\Delta L/L)^2]^{1/2} \quad (1)$$

where $\Delta t_0$ - width of a neutron pulse, $t = 252.778L\lambda$ - total time of flight (in μs), $L$ – flight path from the source to the detector (in m), $\lambda$ - length of a neutron wave (in Å), $\theta$ - Braegg angle, $\tau_0$ - channel width of the TOF analyzer, N - number of channel of the TOF analyzer (accounting for the delay). The first item represents uncertainty of the flight time, the second one includes all geometrical uncertainties, connected with the process of scattering onto the different angles, the third one is connected with the final width of the time channel, and the fourth one is the uncertainty of the flight path.

Thus, the following values of the resolution function were obtained (Table 1).

*Table 1.*

*Values of the resolution function (RF) for FSD different detectors.*

| | Time part of RF at *d=2* Å | Geometrical part of RF | **Total value of RF at *d=2* Å** |
|---|---|---|---|
| **Back Scattering detector** | $1{,}461\times10^{-3}$ | $1{,}701\times10^{-3}$ | $\mathbf{2{,}243\times10^{-3}}$ |
| **ASTRA detector** | $1{,}506\times10^{-3}$ | $3{,}251\times10^{-3}$ | $\mathbf{3{,}582\times10^{-3}}$ |

Practically, the accuracy of determination of residual deformation of crystalline lattice is approximately by one order higher than the accuracy of determination of the diffractometer resolution function. Really, the results of processing by Ritweld method (Ritweld full profiled analysis) of the measured diffraction spectra show that the accuracy of determination of the crystalline lattice parameter $\alpha$ reaches $3{,}5\times10^{-5}$ (for the case of measuring the iron powder α-Fe

the value of $a=2,86653\pm0,00010Å$ is obtained, which corresponds to the accuracy of determination of the residual deformation of crystalline lattice $\varepsilon$ = (a/a = 0,00010 / 2,86653 = 3,5(10-5), which determines an error of measurement of residual deformations of a crystalline lattice in the direction of neutron scattering vector.

2. Determination of moduli of elasticity at the uniaxial tension.

Determination of moduluss of elasticity at the uniaxial tension of standard samples of duralumin D-16 was carried out on the "TIRA-TEST" facility.

Samples are stretched in the loading machine “TIRA-TEST 2560” and the applied force is measured by the dynamometer “DMS Kraftaufnehmer” - the device of the first class accuracy DIN 51 221 Teil 1 (type STC-2t with the certificate of calibration № 32021/445. Calibration is carried out by the technique of State Standard 8.287-78.). During the experiment deformation of a sample is simultaneously measured by two methods. On the one hand, total deformation of samples is measured by means of the nonexpendable extensometer "MiniMFA", which is included in the “TIRA-TEST 2560” loading machine set, attached to a measured sample. And on the other hand, deformation of samples in the elastic area is determined by change of the crystalline lattice parameter of material $(\varepsilon=\Delta a/a)$ at the change of external loading ($\sigma=F/S$, where $F$ - *indications* of the dynamometer of the loading machine, and $S$ - the area of cross-section of a sample).

The data of four such measurements are presented in Fig. 1.

Fig. 1 illustrates the dependence of deformation of a crystalline lattice of samples on the imposed load for all four samples. According to the theory of elasticity, the dependence of total deformation $\varepsilon$ on the imposed load $\sigma$ in the region of elastic deformations (for D16 up to 300MPa) should be a linear dependence. As is seen from Fig. 1 experimentally obtained dependences of deformation of the crystalline lattice on the imposed load are well described by linear functions in the region of elastic deformations. The deviation of total deformation from the linearity in the region >0,005 testifies the beginning of transition of the deformation from elastic into plastic region.

Here, determining an angle of straight lines inclination, it is possible to find the value of Young modulus for the investigated material. Thus, the experiments resulted in the following values of Young modulus for alloy D16 (Table 2):

*Table 2.*

*Experimentally obtained values of Young modulus for alloy D16.*

| | | | | |
|---|---|---|---|---|
| $E_i$, GPa | 67,212 | 69,948 | 68,788 | 68,511 |
| $\sigma_i^2$ | 1.968 | 1.778 | 0.03 | 0.011 |

Calculation of the average experimentally obtained value of Young modulus gives value with confidential borders of a casual error at the confidential probability P=0.95, $\langle E \rangle_{av}$ = 68,62 ± 0,82 GPa, thus the error does not exceed 3,5 %. The obtained experimental value of Young modulus is very well in line with the tabulated one $E_{tabular\ D16}$ = 70 GPa.

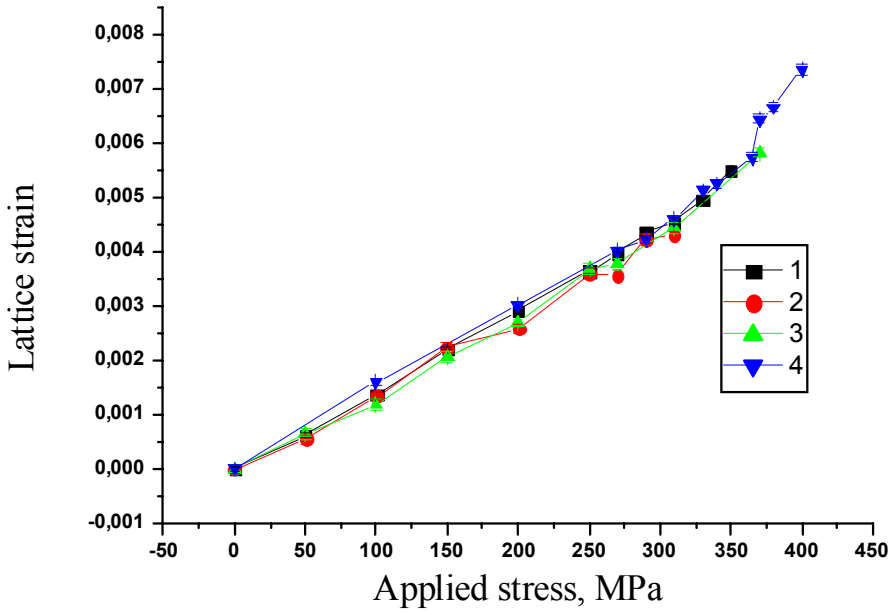


*Fig. 1. Dependences of the D16 deformation of crystalline lattice on the imposed load during experiments on uniaxial tension. Transition into the region of plasticity is shown on sample №4.*

Determination of the spatial distribution of the crystalline lattice deformations.

In order to display the opportunity of determination of the spatial distribution of deformations, the experiment on a four-point bend plate is carried out by means of the neutron method on the FSD diffractometer. According to the theory of elasticity, the dependence of the found deformation $\varepsilon$ on the coordinate $z$ of the measured points, lying along the load line, should represent a linear dependence, at the same time the curved side is in the state of pure tension (without shift), and the concave one is in the state of pure compression.

The value of the measured deformation $\varepsilon$ is determined by the following expression:

$$\varepsilon = - 24 f I/k^3(3a/k - 4a^3/k^3) \quad (2),$$

where $f$ is the value of plate deflection, measured by the deflection indicator (Fig. 10),
k – distance between lower bearing points
b – plate width
a – distance between lower and upper bearing points from one side of the device axis
h – plate height
$I = bxh^3/12$ – moment of inertia of the cross-section.

The distribution of the deformation depending on z coordinate along the vertical axis is determined by the following expression:

$$\varepsilon = P \times a \times z / I \times E \quad (3)$$

At the same time, the dependence of the deformation ε on z coordinate (distance to the plate center), experimentally obtained on FSD, is presented on Fig.2. From this figure, it is well seen that the experimentally obtained values of the deformation at different distances from the plate center are well described by the linear function, which corresponds to the theoretical one.

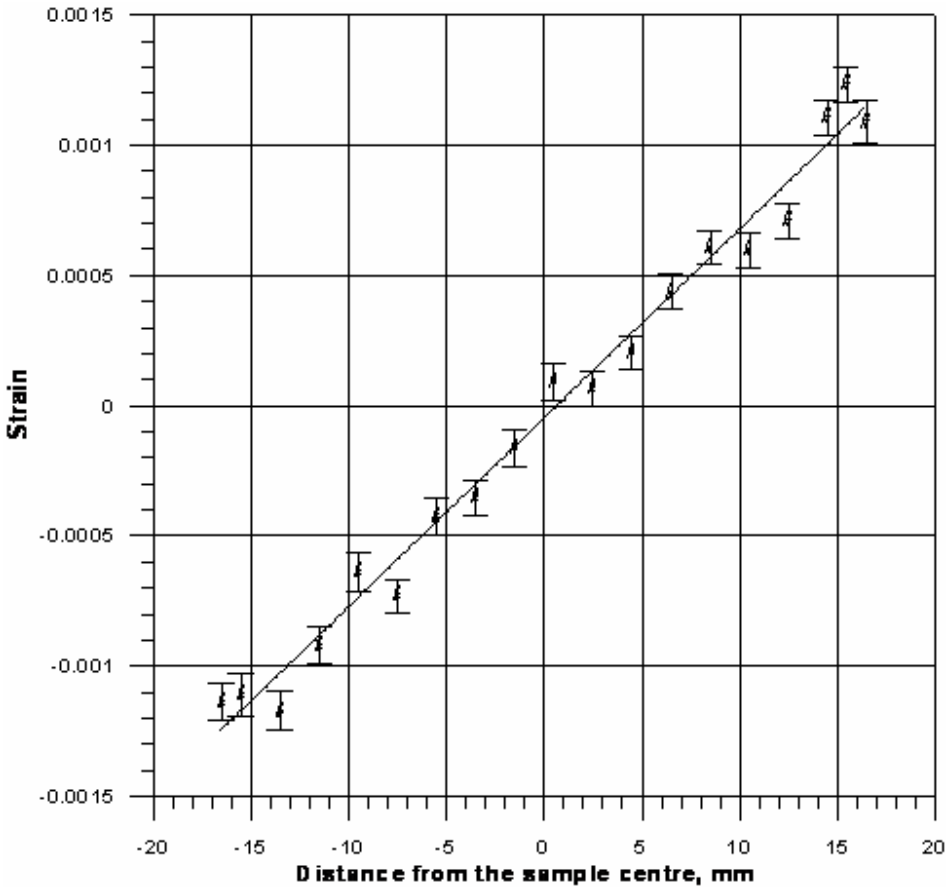


Fig.2 Dependence of the plate deformation on z coordinate of the measured point. Point of origin is located in the plate center.

# Internal dynamics of norethisterone by IINS, NMR and QC methods

K. Holderna-Natkaniec[1], I. Natkaniec[2,3], K. Jurga[1], D. Nowak[1], A. Szyczewski[1]

[1] *Departament of Physics Adam Mickiewicz University, 61-614 Poznan, Poland*
[2] *Frank Laboratory of neutron Physics, Joint Institute for Nuclear Research, 141980 Dubna. Russia*
[3] *H. Niewodniczanski Institute of Nuclear Physics, Polish Academy of Sciences, 31-342 Krakow, Poland*

**Abstract.** The low-temperature inelastic incoherent neutron scattering (IINS) spectrum of norethisterone was compared with that calculated by the density functional theory (DFT) method. The quantum chemical calculations permitted proposing the assignment of the vibrational modes. In particular, the dynamics of the methyl group substituted at C(13) of the steroid skeleton was analysed on the basis of the neutron scattering spectra and temperature dependence of the spin-lattice relaxation time ($^1$H NMR).

## Introduction

Norethisterone (19-nor 17-ethynyltestosterone**)** of the chemical formula $C_{20}H_{26}O_2$ is built of a four-ring steroid carbon skeleton: three cyclohexane rings are denoted henceforth as A, B and C, and a single cyclopentane ring denoted as D. In norethisterone one methyl group is attached to the carbon atom labelled (C13) (Fig. 1). In the molecules studied carbon atom C(17) is attached not only to the hydroxyl group, but also to the ethynyl group lying nearly perpendicular to the steroid skeleton [1]. Substitution of the steroid ring with a methyl group at C(13) and with a hydroxyl OH and ethynyl groups C≡CH at C(18) in norethisterone leads to much stronger progestenic or female hormone properties than those of progesterone.

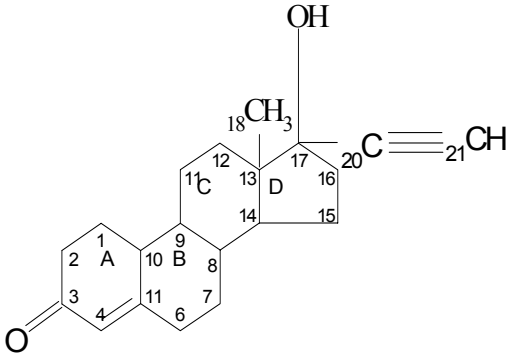


**Fig. 1.** Structure of norethisterone molecule with used atoms notation**.**

The study was undertaken to establish the dynamics of protons, especially those in methyl groups by the IINS, $^1$H NMR and quantum chemistry calculations. Molecular dynamics of the methyl groups is affected by inter- and intra-molecular interactions. If the methyl group spins are strongly coupled with the crystal lattice, then the phonon energy absorbed by the methyl group from the crystal lattice permits overtaking the barrier hindering the rotation and it is further passed to the lattice. The $^1$H NMR method permits investigation of the internal dynamics of molecular groups whose characteristic time of reorientation is of an order of $10^{-6}$ s. The process can be described by two parameters: the height of the barrier for reorientation with respect to the triple symmetry axis of C-C bond, $E_a$, and the correlation time $\tau_c$ [2,3]. The IINS method gives insight into internal dynamics of molecule taking into regard the intensity of subsequent bands of normal modes [4]. Calculation of the vibrational spectra by quantum chemistry methods permits determination of the frequency and intensity of the normal modes. This in turn allows also an interpretation of particular bands in terms of molecular dynamics.

## Experimental

The neutron scattering studies were performed on the inverted geometry NERA-PR spectrometer by the time-of-flight method [5]. This spectrometer was operating on the pulsed reactor IBR-2 in Dubna. The quantum chemical calculations were performed by the density functional theory (DFT), B3LYP method [6]. The spin-lattice relaxation times were determined by the saturation method on the $^{1}H$ NMR pulse spectrometer, made in our lab, operating at the frequency of 30 MHz in the temperature range from 100 K to 400 K.

## Results

The inelastic incoherent neutron scattering spectra were recorded at two temperatures, 290K and 20K. The experimental spectra collected from 16 detectors, arranged at different angles of scattering from the range $20^{o}$ - $160^{o}$, were summed up. Next, the cryostat and cassette background was subtracted from this total spectrum and it was normalised taking into account the amount of incident neutrons. The IINS spectra were converted into the generalized phonon density of state spectra $G_{exp}(\nu)$ in one-phonon scattering approximation. The low-temperature $G_{exp}(\nu)$ spectrum is compared in Fig. 1, with that calculated for the isolated molecule by the DFT method. On heating of norethisterone to room temperature the with of subsequent normal modes increases and the $G_{exp}(\nu)$ at 290K becomes much less structural.

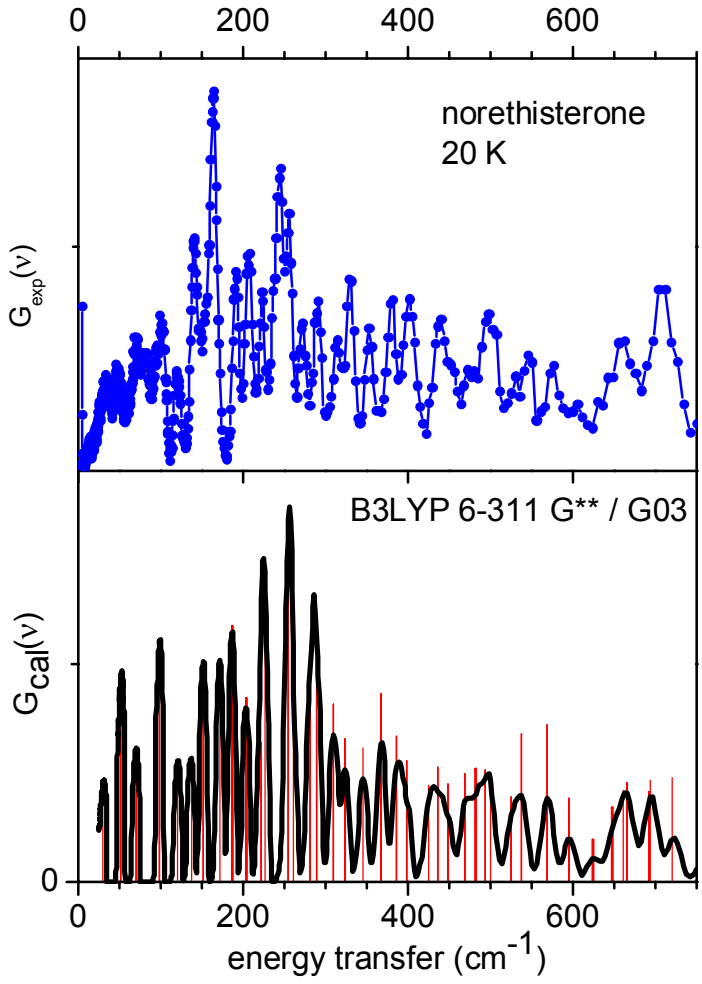


**Fig. 3.** Comparison of the phonon density of state spectra $G_{exp}(\nu)$ of norethisterone obtained after transformation in one phonon scattering approximation of the IINS spectra at 20 K, with the $G_{cal}(\nu)$ spectra calculated by B3LYP method with 6-311G** basis set by Gaussian 03 programme. The sticks showing the frequency and intensity of each normal mode [7] are convoluted with the resolution function of the NERA-PR spectrometer [8].

The deformational in-plane vibration δ[C-C(3)-O] in the spectrum of norethisterone occurs at 440.2 $cm^{-1}$, while in the spectrum of ethisterone at 502 $cm^{-1}$ [10]. In the spectrum of norethisterone the δ[C-C(17)-O(23)] mode is observed at 577 $cm^{-1}$, while in the spectrum of ethisterone - at 327, 339 and 413 $cm^{-1}$. The reason for the occurrence of the bands assigned to δ[C-C-O] at different frequencies in the spectra of these two compounds, seems to be the presence of intermolecular hydrogen bonds: OH...O made by the carbonyl group C(3)O(3) and hydroxyl group C(17)-O(23)H of neighbouring molecules, and CH...O formed between carbonyl group C(3)=O(3) and the ethynyl group -C(20)≡C(21)H.. The character of the bond CH...O in these two compounds is different. In ethisterone it is a direct bond between the hydrogen of ethynyl group and oxygen O(3) of carbonyl group (2.318 Å), whereas in norethisterone it is a cooperative bond C(21)H...O(23)...O(3) (2.942 and 2.899 Å). The singularities appearing in the lattice modes of the $G_{exp}(\nu)$ spectra of ethisterone [10] and norethisterone can be related to these intermolecular interactions as suggested by the calculations performed for the dimer clusters [11].

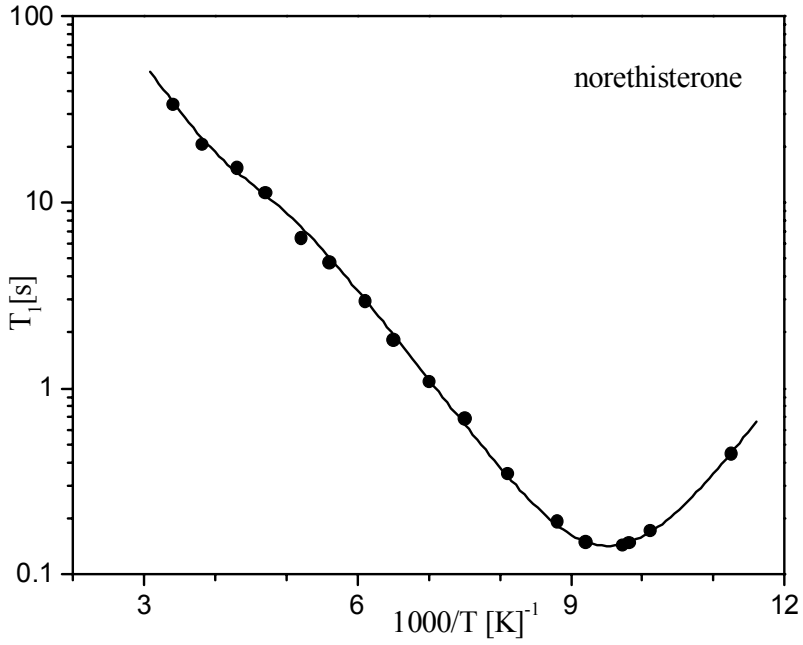


**Fig. 2**. Temperature dependence of spin-lattice relaxation time - $T_1$ of norethisterone at 30.MHz.

The temperature dependence of the spin-lattice relaxation time shows a characteristic minimum that can be interpreted in terms of the Bloembergen, Purcell and Pound theory of dipole-dipole interactions [12]. The line presented in Fig. 2 was obtained by the fit of the following equation to the experimental values:

$$\frac{1}{T_1} = C\left[\frac{\tau_c}{1+\omega_0^2\tau_c^2} + \frac{4\tau_c}{1+4\omega_0^2\tau_c^2}\right]. \qquad /1/$$

The interpretation was made assuming a single process of relaxation characterised by the relaxation constant C, and the correlation time described by the Arrhenius equation:

$$\tau_c = \tau_0\, exp\left(\frac{E_a}{RT}\right). \qquad /2/$$

The activation parameters determined as $\tau_o=1*10^{-13}$ s, $E_a$= 9.0 kJ/mol. The relaxation constant C was calculated for the methyl group reorientations assuming the proton-proton distance of 1.79 Å, and permitted estimation of the relaxation time at the minimum as 0.15 s. This value is very close to that measured at 105 K at 30 MHz being of 0.14 s. Therefore, it can be concluded that the methyl group reorientation about the triple symmetry axis of the bond C(13)-C(18) is the effective mechanism of relaxation.

**Table 1**. Frequencies of the out-of-plane torsional modes of the methyl groups in ethisterone and norethisterone and the heights of barriers of the methyl group reorientations with respect to the triple axis of the bond C-C.

| Assignment of internal modes | frequency of bands in $G_{exp}(\nu)$ spectrum of ethisterone [10] [$cm^{-1}$] | Activation energy [10] [kJ/mol] | frequency of bands in $G_{exp}(\nu)$ spectra of norethisterone [$cm^{-1}$] | Activation energy [kJ/mol] |
|---|---|---|---|---|
| $\chi$[CC(18)$H_3$] | 74, 83, 187 | 6.7[a]<br>**<6.7[b]** | 189 | **9.0±0.9 [b]** |
| $\chi$[CC(19)$H_3$] | *248*<br>*278*<br>*289*<br>*294* | 7.0 [a]<br>**10.8±0.8 [b]** | | |

[a]*-calculated value of activation energy*
[b]*-activation energy for methyl group reorientation determined from spin-lattice relaxation time measurements.*

The analysis of the bond lengths and torsional angles C(18)-C(13)-C(17)-C(20), C(18)-C(13)-C(17)-O(23) and C(18)-C(13)-C(12)-C(11) in the two molecules studied has shown that they take similar values of -169.89°, -44.86°, -67.62° in ethisterone and -167.14°,-42.41°, -69.20° in norethisterone [ 1, 12, 16 ] therefore, the dynamics of the methyl group C(18)$H_3$ in the two compounds is similar. However, it seems that the dynamics of the methyl group C(18)$H_3$ seems to be affected by the intermolecular hydrogen bond O...HO.

**Acknowledgements**

Financial support within the grant of the Polish Plenipotentiary at JINR is gratefully acknowledged by the authors (KHN, IN, DN).

The calculations have been performed at the PCSC in Poznan.

**References**

[ 1] J.P. Marnon, J. Lepicard , J. Delettre , C.R. Acad. Sci. Paris C 282 (1976) p. 387.
[ 2] A. Abraham, *The Principle of Magnetism*, Oxford University Press, Oxford, 1961
[ 3] C.P. Slichter, *Principles of Magnetic Resonance*, Springer-Verlag Berlin Heidelberg New York, 1978
[ 4] S.W. Lovesey, *Theory of Neutron Scattering from Condensed Matter*, Clarendon Press, Oxford, 1984.
[ 5] I. Natkaniec, S.I. Bragin, J. Brankowski, J. Mayer, *Proceedings of the ICANS XII Meeting*, Abington, 1993, vol. I, 1994, RAL Report, 94-025, I, p.89, and www.jinr.ru
[ 6] M.J. Frish, G.W. Trucks, H.B. Schlegel, G.E. Scuseria, M.A. Robb, J.R. Cheeseman, et all., *GAUSSIAN 03*, Gaussian Inc., Pittsburgh PA, 2003.
[ 7] A.J.J. Ramirez-Cuesta, Comp. Phys. Commun., **157**, (2004) 226
[ 8] V. Yu. Kazimirov, I. Natkaniec, Comm. JINR, P14-2003-48, Dubna 2003
[ 9] L. Laaksonen, gOpenMol 2.32, Center for Scientific Computing, Espoo, Finland, 2002.
[10] K. Holderna-Natkaniec, K. Jurga, I. Natkaniec, D. Nowak, A. Szyczewski, Chem.Phys. 317 (2005) p.178.
[12] N. Blombergen, E.M. Purcell, R.V. Pond, Phys. Rev., **73**, (1948) p.679

# Comparative INS studies of methane, methanol, mesitylene and water as neutron moderator materials at low temperatures

I. Natkaniec[1,2], E. Shabalin[1], S. Kulikov[1], K. Holderna-Natkaniec[3]

[1] Frank Laboratory of Neutron Physics, Joint Institute for Nuclear Research, 141980 Dubna, Russia
[2] H. Niewodniczanski Institute of Nuclear Physics, Polish Academy of Science, 31-342 Cracow, Poland
[3] Faculty of Physics, A. Mickiewicz University, 61-614 Poznan, Poland

## Introduction

The hydrogen density and the vibrational density of states - G(ν) of moderator materials play an important role in neutron slowing down phenomena. The solid methane is one of the best materials from this point of view and is used as the moderator medium of the cold neutron sources operating at the recent medium power pulsed neutron sources [1, 2]. However, exploitation test of solid methane moderator on the IBR-2 pulsed reactor, at the 2 MW average power, show many inconvenient technical problems caused by irradiation effects [3, 4].

Radiation resistance of moderator materials at low temperature is the first priority task for design of advanced cold neutron source. For investigation of irradiation effects on potential substances for cold moderator materials, the URAM-2 cryogenic irradiation facility [5], was designed and constructed on the IBR-2 pulsed reactor of the JINR at Dubna. The comparative studies on structure and dynamics of materials-candidates for cold moderator are performed on the NERA inverted geometry spectrometer [6].

Solid methane at ambient pressure stay in the FCC orientationally disorder phase I, down to 20.4 K. In this phase all $CH_4$ molecules can easily rotate around center of mass and the low energy rotational excitations of crystal lattice play most important role in deep neutron slowing down process. In phase II, below 20 K, the $CH_4$ molecules occupy different type of sublattices: 25% are orientationally disordered and perform almost free rotation in week crystalline potential of cubic symmetry, while 75% are orientationally ordered by strong potential of tetrahedral symmetry [7].

Methanol is a relatively simple substance, which molecules form one-dimensional chains of hydrogen bonds. It is known to exist in at least three solid modifications: the ordered α-phase stable below 160 K, the disordered β-phase stable till the melting at 175 K, and an amorphous or glassy phase, which transforms to the α-phase at about 130 K [8,9]. An amorphous or glassy phase, which can be obtained by vapor depositions at low temperatures or by fast cooling of liquid, shows translational and orientational disorder, while the β-phase shows only orientational disorder of methyl groups.

Mesitylene or 1,3,5-trimethylbenzene is a well known organic solvent characterized by the relatively low freezing (228K) and high boiling (437K) temperatures. Because of high content of hydrogen and the assumed weakly hindered rotation of methyl groups in the solid phase this compound has been recommended as cold neutron moderator [10] and used for construction of the TCNS cold neutron source at the TRIGA Mark II pulsed reactor of the NETL in Austin [11]. However, the structure and dynamics of solid mesitylene has not been well investigated. Liquid mesitylene freezes in a disordered phase II, which at 90K transforms to the low symmetry ordered phase III [12]. Annealing of phase II at about 200K, it transforms to the cubic symmetry phase I, which is stable from the melting point at 228K down to liquid helium temperatures [13].

Liquid water is most popular moderator of the thermal neutrons sources. The p,T phase diagram, as well as the structure and dynamics of solid phases of water are well investigated, see for instance ref. [14]. At ambient pressure water freeze in hexagonal framework of hydrogen bonded $H_2O$ molecules, know as the ice Ih, which is stable down to liquid helium temperatures.

## The vibrational spectra of neutron moderator materials

The experimental INS spectra of investigated materials transformed to the amplitude weighed density of states G(ν) are compare in Figure 1.

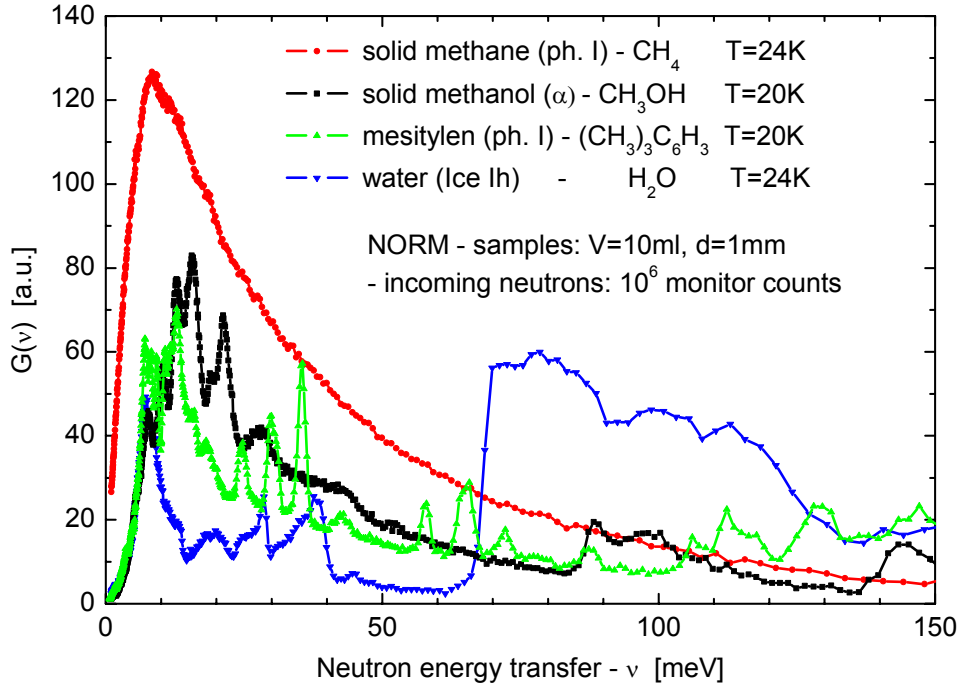


*Figure 1: Comparison of the G(ν) spectra of solid methane, methanol, mesitylene and water calculated in one-phonon scattering approximation from the INS spectra measured at 20K or 24K.*

One can see that G(ν) spectra of orientationally disorder phase I of methane differ significantly from the solid phases of α-methanol, phase I of mesitylene and water ice Ih. The characteristic feature ordered crystalline phases is a parabolic dependence of $G(\nu) \approx \nu^2$ for acoustic phonon branches, in consistence with the Debye theory of crystal thermo-dynamics. The G(ν) of investigated materials, except the phase I of methane, show such behavior below 6 meV. The optical phonons and internal vibrations of molecules forms individual bands at higher energies in the G(ν) spectra of crystalline materials.

Dynamics of disordered materials can be much better approximate by dumping oscillators, which frequency distribution are given by the G(ν) spectra. The characteristic feature of amorphous or glassy materials, as well as orientationally disordered crystalline phases (protonic glasses), is lack of phonon singularities in the frequency range of lattice dynamics, and non Debaye behaviour of G(ν) at low frequencies. These features one can see on the G(ν) spectra of orientationaly disordered phase I of solid methane in Figure 1, and in Figure 2 for glassy solid formed by freezing 1:1 volume solution of liquid methanol and water.

Comparing the results of INS spectroscopy, lattice dynamics and quantum chemistry calculations of vibrational spectra of different methyl derivatives of benzene [15-17], one can see that rotational dynamics of methyl groups depend on molecule conformation and crystal structure. Among these compounds, mesitylene molecule contains the highest number of methyl groups with low internal rotational barrier around the aromatic ring. The most promising material as a moderator for cold neutron sources seems to be the disordered phase II of solid mesitylene. However, orientationally disorder phase II of mesitylene is not stable and transfer to phases I or III.

It was shown that solutions of mesitylene with toluene, *m*-xylene or 1,2,4-trimethylbenzene (pseudocumene) freezes in a glassy solids, which are stable in all temperature range below the melting point [17,18]. The amplitude weighted density of vibrational states G(ν) of a glassy solids: the 3:2 volume solution of liquid mesitylene and pseudocumene, the 1:1 volume solution of liquid methanol and water, are compared to the G(ν) of the orientationally disordered phase I of solid methane in Figure 3.

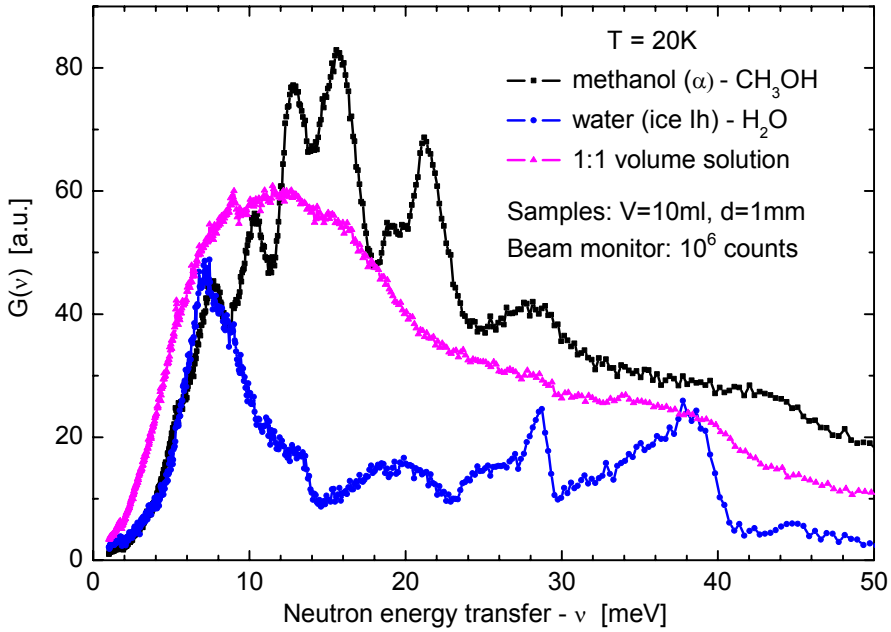


*Figure 2: Comparison of the low energy part of the G(ν) spectra of solid water and methanol with the 1:1 water-methanol solution.*

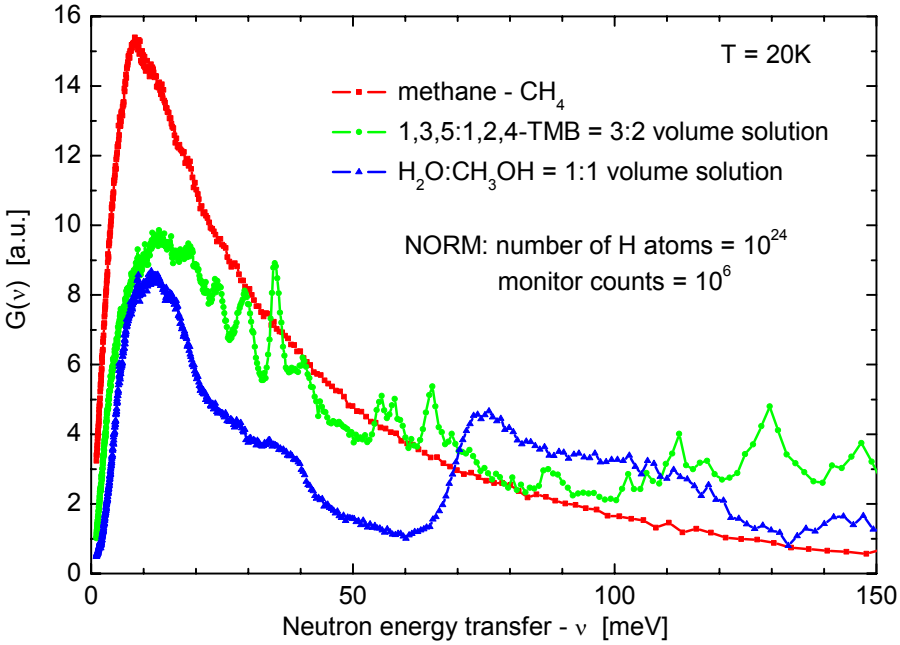


*Figure 3: Comparison of the G(ν) spectra of solid methane with a glassy states of the 3:2 volume solution of liquid mesitylene (1,3,5-TMB) and pseudocumene (1,2,4-TMB), and 1:1 water-methanol solution. The G(ν) spectra were normalized to the same number of hydrogen atoms and the same number of incoming neutrons. The volume and thickness of investigated samples were identical.*

The G(ν) spectra of a glassy materials of trimethylbenzenes or methanol-water solutions, below 50 meV, are much more similar to the G(ν) spectrum of orientationally disorder phase I of methane, than corresponding spectra of crystalline substances compared in Figure 1. However, maximum value of the G(ν) spectra at about 10 meV, normalized to the same density of hydrogen atoms, for methane is about twice more higher than for other materials. Probably it is caused by large amplitudes of the rotational oscillations of methane molecules in comparison to vibrational amplitudes of hydrogen atoms in other materials.

## Conclusions

Additional density of state over parabolic dependence in crystalline solids was observed in the disordered solid phase of toluene and mesitylene. It is shown that solutions of mesitylene with toluene, *m*-xylene and pseudocumene form glassy solids, which are stable in the whole temperature range below the melting point. The vibrational spectra of glassy states of mesitylene in solution with toluene, *m*-xylene or pseudocumene indicate relatively low barriers for methyl librations and, typical for disordered solids, additional density of states at low frequencies, which makes these materials preferable as potential moderators for cold neutron sources.

Spontaneous release of stored energy was detected in solid methane, water ice, hydrates of methane and in frozen mixtures of water ice with atomic hydrogen scavengers. Negligible amount of energy is accumulated in aromatic hydrocarbons, so as, they display no spontaneous self heating under irradiation [19,20].

Based on the **NERA** and **URAM-2** experiments we could make suggestion to use glassy states of mesitylene solutions with similar derivatives of methyl-benzene compounds as neutron moderating media at low temperatures.

## References


[1] S. Ikeda, N. Watanabe, S. Satoh et al. In: Proc. ICANS-IX, PSI Willigen, 1986, vol. II, p. 118-127.
[2] J. Carpenter, In: Proc. of Intern. Workshop on Cold Neutron Sources. LANCE, Los Alamos, 1990, LA-12146C, p. 131-153.
[3] E.P. Shabalin, JINR Comm., E17-95-141 (Part I) and E17-95-142 (Part II), Dubna 1995.
[4] A.A. Belyakov, V.V. Melikhov, Yu.N. Popelyoshev, E.P. Shabalin, Journal of Neutron Research, Vol. 3, 1996, p.209-221.
[5] E.P. Shabalin, V.V. Golikov, S.A. Kulikov et. al., JINR Comm., E13-2002-143, Dubna 2002.
[6] I. Natkaniec, S.I. Bragin, J. Brankowski, J. Mayer. In: Proc. ICANS-XII, Abingdon 1993, RAL Report 94-025, (1994), Vol. I., p. 89-96.
[7] B. Asmussen, M. Prager, W. Press, H. Blank, C.J. Carlile, J. Chem. Phys., **97**(2) (1992) 1332-1342.
[8] H.G. Carlson, E.F. Westrum Jr., J. Chem. Phys., **54** (1971) 1464-1469.
[9] B.H. Torrie, O.S. Binbrek, M. Strauss, I.P. Swainson, J. of Solid State Chemistry, **166** (2002) 415-420.
[10] M. Utsuro, M. Sugimoto, J. Nuc. Sci. Technol., **14**(5) (1977) 390-392.
[11] K. Unlu, C. Rios-Martinez, B.W. Wehring, *J. Radioanal. Nucl. Chem.*, **193** (1995) 145-154.
[12] M. Yamazaki, M. Tanaka, T. Inoue, at al., *Bull. Chem. Soc, JPN.,* **73** (2000) 837-842.
[13] I. Natkaniec, K. Holderna-Natkaniec. In: Proc. of 6th Meeting of the Collaboration on Advanced Cold Moderators, Juelich, 11–13 September 2002, Ed. H. Conrad, Matter and Materials. Vol. 20, p.103-111, Forschungszentrum Julich, 2004.
[14] *Physics and Chemistry of Ice*, N.Maeno and T.Hondoh Eds, Hokkaido University Press, Sapporo 1992.
[15] J. Kalus, M. Monkenbusch, I. Natkaniec, M. Prager, J Wolfrum, F. Worlen, *Mol. Cryst. Liq. Cryst*., **268** (1995) 1-20.
[16] I. Natkaniec, K. Holderna-Natkaniec, J. Kalus, V.D. Khavryutchenko. In: Neutrons and Numerical Methods, Grenoble 1998, Ed. M.R. Johnson, G.J. Kerlay, H.G. Buttner, AIP Conference Proceedings 479, p. 191-194.
[17] I. Natkaniec, K. Holderna-Natkaniec, J. Kalus, I. Majerz. In: Proc. ICANS-XVI, Ed. By G. Mank and H. Conrad, ISSN 1433-559X, Forchungszentrum Julich 2003, Vol. I. pp 903-910.
[18] I. Natkaniec, K. Holderna-Natkaniec, J. Kalus, *Physica B,* **350** (2004) 651-653.
[19] E. Shabalin, E. Kulagin, S. Kulikov, V. Melikhov, *Radiation Physics and Chem.*, **67** (2003) 315-319.
[20] E. Kulagin, S. Kulikov, V. Melikhov, E. Shabalin. *Nuclear Instr. and Methods in Physics Research B*, Vol **215**(1-2) (2004) 181-186.

# Low frequency internal modes of 2,3,5,6-tetramethylbenzene, 2,3,5,6-tetramethylpyrazine and tetramethyl-1,4-benzoquinone, INS, Raman IR and theoretical DFT studies.

A. Pawlukojć[a,d], I. Natkaniec[a,e], G. Bator[b], L. Sobczyk[e], E. Grech[c], J. Nowicka-Scheibe[c]

[a] *Frank Laboratory of Neutron Physics, Joint Institute for Nuclear Research, 141980 Dubna, Russia,*
[b] *Faculty of Chemistry, University of Wroclaw, Joliot-Curie 14, 50-383 Wroclaw, Poland,*
[c] *Institute of Chemistry and Environmental Protection, Technical University, Piastow al. 12, 71-065 Szczecin, Poland,*
[d] *Institute of Nuclear Chemistry and Technology, Dorodna 16, 03-195 Warszawa, Poland*
[e] *H. Niewodniczanski Institute of Nuclear Physics, Radzikowskiego 152, 31-342 Krakow, Poland*

## Abstract

The results of inelastic neutron scattering (INS), Raman and infrared (IR) studies on 2,3,5,6-tetramethylbenzene (durene), tetramethylpyrazine (TMP) and tetramethyl-1,4-benzoquinone (TMBQ) in the solid state are reported. The observed frequencies are analyzed on the basis of DFT calculations. The low frequency region, below 400 $cm^{-1}$, related to the torsional and bending out-of-plane vibrations of methyl groups, is of particular interest. The detailed analysis is possible due to the simulation of the INS spectra by using the auntie-CLIMAX program. It is shown that the observed low frequency INS bands are dramatically shifted, compared to the calculated ones, towards higher frequencies. Although one cannot exclude deficiencies of theoretical methods as applied to low frequency modes, it seems more probable the interpretation based on an existence of non-conventional C-H···π, C-H···N, C-H···O hydrogen bonds formed by the methyl groups in crystalline phases.

## Introduction

In this report we have chosen for comparison three dynamically similar molecules (of same $D_{2h}$ symmetry) containing four $CH_3$ groups in the phenyl ring (Fig.1). The molecules are characterized by different either intra or intermolecular interactions in the crystalline lattice. The packing of the molecules is very well known for 2,3,5,6-tetramethylbenzene (durene) [1], tetramethylpyrazine (TMP) [2,3] and tetramethyl-1,4-benzoquinone (TMBQ) [4].

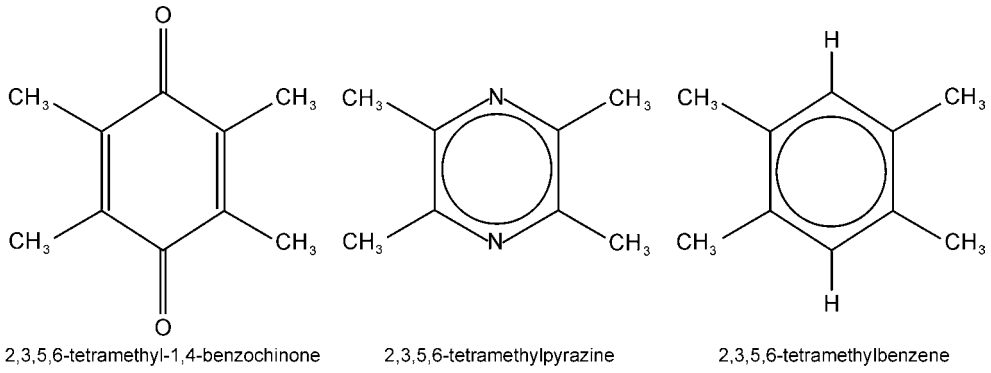


Fig. 1. Schematic view of investigated molecules.

In analysis of the solid state of durene, one can distinguish the interaction between methyl groups and π-electrons of the phenyl rings (non-conventional C-H···π hydrogen bonds), while in the cases of TMP and TMBQ, there are interactions via C-H···N and C-H···O hydrogen bonds. We will try to show the effect of the unconventional hydrogen bonds on the frequencies of the $CH_3$ torsional and C-

$CH_3$ wagging modes. The values of the frequencies for the crystalline state will be compared with those modeled by using the DFT calculations. For more complete recognition, we decided to compare the INS results with those based on Raman and Infrared (IR) spectra.

**Experimental and calculation**

Neutron scattering data were collected at the pulsed IBR-2 reactor in Dubna using the inverted time-of-flight spectrometer NERA-PR [5] at 20 K. For energies between 5 and 100 meV the relative INS resolution was estimated to be ca. 3%. The IR spectra were recorded at room temperature in the KBr discs or in Nujol as well as in Fluoroluble (low frequencies) suspensions using either KBr or CsI windows on a FT-IR Bruker IFS 113v spectrometer with a resolution of 2 $cm^{-1}$. The Raman spectra of powder samples were recorded on a Nicollet Magna 860 FT Raman Spectrometer. Nd:YAG laser was the exciting source, with a power of ca. 200 mW. The back scattering geometry was applied. The resolution was 2 $cm^{-1}$. The structure optimization and frequencies as well as IR intensities and Raman activities of the molecules were calculated by using the GAUSSIAN 98 program [6] on the B3LYP level with 6-31G(d,p) basis set. The corresponding modes were defined by means of internal coordinates according to Pulay et al. [7]. Mass weighted normal vibrational coordinates were used to calculate the INS spectral profiles by the auntie-CLIMAX program [8].

The comparisons of experimental INS spectra with those simulated by auntie-CLIMAX program together with Raman and IR spectra are presented in Figs. 2-4. Calculated and experimental INS, IR and Raman frequencies for three investigated compounds are compared in Tables 1-3.

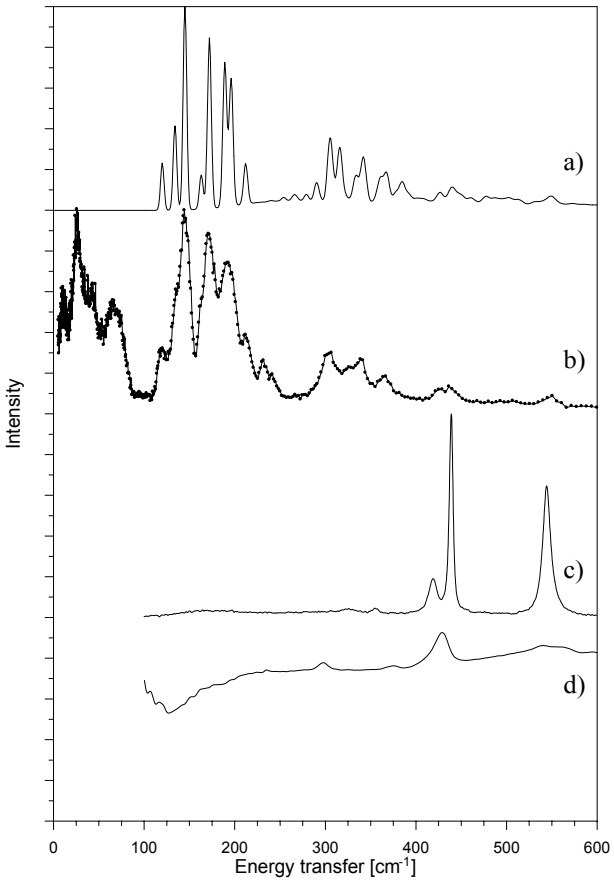


Fig.2. Calculated a) and experimental b) INS spectra of TMBQ in the frequency range below 600 $cm^{-1}$ compared with Raman c) and IR d) spectra.

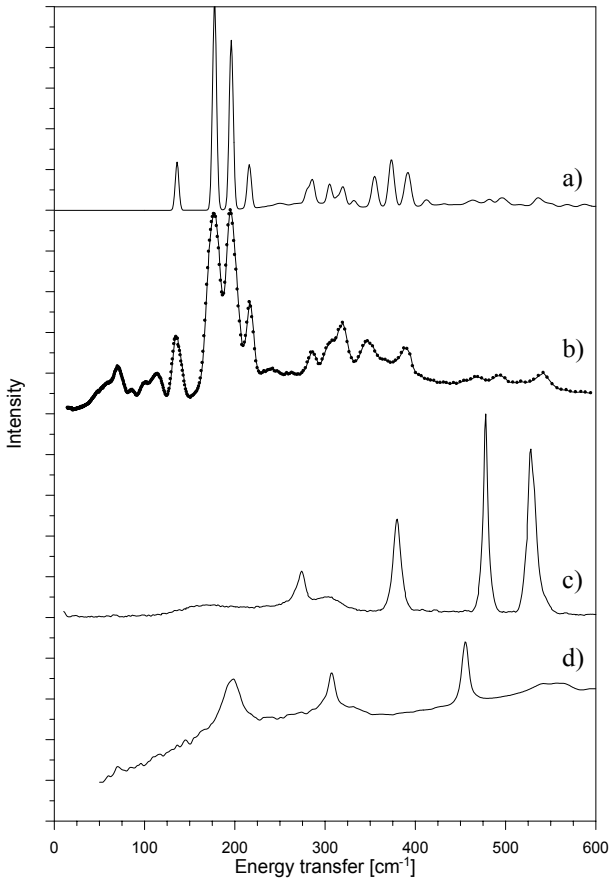


Fig.3. Calculated a) and experimental b) INS spectra of TMP in the frequency range below 600 $cm^{-1}$ compared with Raman c) and IR d) spectra.

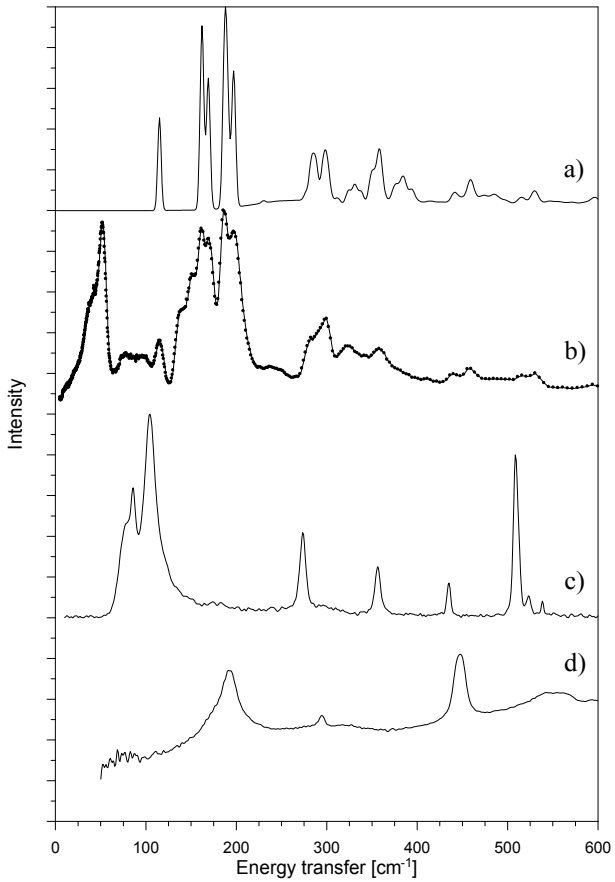


Fig.4. Calculated a) and experimental b) INS spectra of durene in the frequency range below 600 $cm^{-1}$ compared with Raman c) and IR d) spectra.

Table 1. Calculated and experimental frequencies for TMBQ.

| Approximate assignments | Calculated B3LYP/6-31G** | Experiment INS | IR | Raman |
|---|---|---|---|---|
| ring torsion | 65 | 120 | --- | |
| $CH_{3\ tors.}$ | 75 | 145 | n.a. | n.a. |
| $CH_{3\ tors.}$ | 85 | 172 | | --- |
| ring torsion | 108 | 134 | n.a. | n.a. |
| $CH_{3\ tors.}$ | 109 | 189 | | --- |
| ring torsion | 114 | 196 | | --- |
| $CH_{3\ tors.}$ | 117 | 163 | --- | |
| $C\text{-}CH_{3\ wagg.}$ | 205 | 212 | --- | |
| $C\text{-}CH_{3\ bend.}$ | 303 | 304 | 298 | |
| $C\text{-}CH_{3\ bend.}$ | 304 | 306 | | --- |
| $C\text{-}CH_{3\ bend.}$ | 314 | 315 | --- | |
| $C\text{-}CH_{3\ wagg.}$ | 322 | 342 | | --- |
| $C\text{-}CH_{3\ bend.}$ | 366 | 367 | | 355 |
| ring def. | 420 | 427 | | 419 |
| $C\text{-}CH_{3\ wagg.}$ | 435 | 439 | | --- |
| $C{=}O_{\ bend.}$ | 440 | 441 | 429 | |
| ring def. | 444 | 444 | | 439 |
| $C\text{-}CH_{3\ str.}$ | 546 | 545 | | 544 |
| $C\text{-}CH_{3\ wagg.}$ | 552 | 550 | n.a. | n.a. |

## Discussion

The analysis of modes related to the torsional vibrations of the CH3 groups in durene, TMP and TMBQ possessing the same symmetry, allows us to distinguish, among seven low frequency modes, four ones, into which neat CH3 torsional vibrations contribute. These modes are practically not visible in IR and Raman spectra due to either selection rules or extreme low intensities. In contrast to IR and Raman spectra these modes are characterized by high intensities in the spectra of inelastic neutron scattering.

Table 2. Calculated and experimental frequencies for TMP.

| Approximate assignments | Calculated B3LYP/6-31G** | Experiment INS | IR | Raman |
|---|---|---|---|---|
| ring torsion | 86 | 130 | n.a | n.a |
| $CH_{3\ tors.}$ | 115 | 171 | | --- |
| $CH_{3\ tors.}$ | 117 | 171 | n.a | n.a |
| $CH_{3\ tors.}$ | 134 | 190 | --- | |
| $CH_{3\ tors.}$ | 150 | 190 | | --- |
| ring torsion | 188 | 211 | 198 | |
| ring torsion | 263 | 280 | | --- |
| $C\text{-}CH_{3\ bend.}$ | 271 | 300 | | 273 |
| $C\text{-}CH_{3\ bend.}$ | 290 | 313 | 307 | |
| $C\text{-}CH_{3\ bend.}$ | 290 | 313 | 307 | |
| $C\text{-}CH_{3\ wagg.}$ | 366 | 382 | | 379 |
| $C\text{-}CH_{3\ wagg.}$ | 456 | 463 | 455 | |
| ring def. | 465 | 491 | | 478 |
| $C\text{-}CH_{3\ bend.}$ | 510 | 536 | | 528 |
| ring def. | 515 | 543 | 556 | |
| $C\text{-}CH_{3\ wagg.}$ | 592 | 616 | n.a. | n.a. |

Table 3. Calculated and experimental frequencies for durene.

| Approximate assignments | Calculated B3LYP/6-31G** | Experiment INS | IR | Raman |
|---|---|---|---|---|
| Ring torsion | 114 | 115 | n.a. | n.a. |
| $CH_{3\ tors.}$ | 136 | 187 | | --- |
| $CH_{3\ tors.}$ | 138 | 197 | --- | |
| $CH_{3\ tors.}$ | 140 | 162 | --- | |
| $CH_{3\ tors.}$ | 162 | 169 | | --- |
| Ring torsion | 188 | 190 | 191 | |
| Ring torsion | 267 | 283 | | 273 |
| $C\text{-}CH_{3\ bend.}$ | 288 | 288 | | --- |
| $C\text{-}CH_{3\ bend.}$ | 296 | 296 | 294 | |
| $C\text{-}CH_{3\ bend.}$ | 307 | 300 | --- | |
| $C\text{-}CH_{3\ wagg.}$ | 349 | 359 | | 356 |
| Ring def. | 438 | 441 | | 434 |
| $C\text{-}CH_{3\ wagg.}$ | 463 | 459 | 447 | |
| Ring def. | 514 | 515 | | 509 |
| $C\text{-}CH_{3\ bend.}$ | 529 | 530 | | --- |
| $C\text{-}CH_{3\ wagg.}$ | 595 | 597 | n.a. | n.a. |

The experimental INS spectra are very well reproduced by using the auntie-CLIMAX program based on calculated

frequencies by means of the GAUSSIAN 98 program.
The experimental frequencies appeared, as a rule, higher than calculated ones, that can be interpreted either in the terms of the limitations of the standard DFT calculations or by assuming interactions of the CH3 groups in the crystalline lattice. These interactions can be treated in terms of the unconventional hydrogen bonds of the C-H...p, C-H...N and C-H...O type. The influence of the unconventional hydrogen bonds on the torsional CH3 vibrations would be analogous to the conventional hydrogen bonds, which lead to blue-shifting of the d and g vibrations. The analysis of the packing show that the strongest interaction takes place in TMBQ and weakest ones in durene that could be expected from the comparison of experimental and calculated frequencies for the compounds studied.

**References**

[1] M.A. Neumann, M.R. Johnson, P.G. Radaelli, H.P. Trommsdorff, S.F. Parker, J. Chem. Phys. 110 (1999) 516,
[2] A.W.M. Braam, A. Eshuis, A. Vos, Acta Crystallogr., B37 (1981) 730,
[3] V.R. Thalladi, A. Gehrke, R. Boese, New J. Chem., 24 (2000) 463,
[4] D. Rabinovich, G.M.J. Schmidt, E. Ubell, J. Chem. Soc. B (1967) 131,
[5]. I. Natkaniec, S.I. Bragin, J. Brankowski, J. Mayer, Procedings of the ICANS-Xiii, vol.1, Abington, RAL Report 94-025, (1993) .89,
[6]. M.J. Frisch et al., GAUSSIAN 98, Rev. A9 Program, Gaussian Inc, Pittsburgh, PA, 1998,
[7]. P. Pulay, G. Forgasi, F. Pang, J.S. Boggs, J. Am. Chem. Soc. 101, (1979) 2550,
[8]. A.J. Ramirez-Cuesta, Comp. Phys. Commun. 157 (2004) 226,

**Acknowledgments**

A partial financial support by the Ministry of Science and Informatics (Grant 4 T09A 05125) and the Plenipotentiary Representative of Polish Republic in JINR is acknowledged.

# Inelastic neutron scattering on AgCuSe

D. Trots[1], A. Skomorokhov[2], V. Semenov[2], N. Bickulova[3], Yu. Stepanov[3] and H. Fuess[1]

[1]*Institute for Materials Science, Darmstadt University of Technology, Darmstadt, Germany*
[2]*Institute for Physics and Power Engineering, Obninsk, Russia*
[3]*Sterlitamak State Pedagogical Academia, Sterlitamak, Russia*

For a long time silver and copper chalcogenides attracted the attention of scientists due to their exceptional physical properties. Recently, the high value of ionic conductivity in AgCuSe has renovated the practical interest to this ternary superionic compound [1].

In the present communication we report results on neutron scattering experiments on AgCuSe carried out with DIN-2PI spectrometer. The neutron scattering spectra of non-superionic β- and superionic α-AgCuSe were collected at 285 and 505 K. To reduce the absorption and extend the kinematical range the high value of the incident neutron energy of 18.496 meV was chosen. A polycrystalline sample was placed in a slab sample holder and mounted in a sample chamber at the angle $60^o$ between incident beam and normal to the slab (reflection geometry). The sample chamber was evacuated up to $10^{-2}$ mbar. Neutron scattering data were collected simultaneously at 12 scattering angles in the kinematical range from 1.94 $Å^{-1}$ to 5.50 $Å^{-1}$. The energy resolution of the spectrometer was about 5-8% and the range of energy transfer varied from about –13 meV to 160 meV (negative values correspond to neutron energy loss). Empty cans and vanadium normalization runs were also made. The standard corrections for background from the empty container (taking into account self-shielding of sample geometry), energy efficiency and relative efficiency of each detector were made for time-of-flight data. Absorption cross section of the sample at the chosen incident energy was nevertheless sufficiently high, that in conjunction with the slab-sample geometry permit us to neglect multiple scattering effects. Finally, the dynamic structure factor $S(Q,\varepsilon)$ was derived from the time-of-flight data.

$S(Q,\varepsilon)$ in β-AgCuSe could be described as consisting of two components. The first one is a narrow elastic component at zero energy transfer, and the second one is a broad inelastic component centred around elastic one (fig. 1). The absence of pronounced traces of low-energy excitations in $S(Q,\varepsilon)$ spectra of β-AgCuSe should be noted. Such excitations in non-superionic phases were clearly observed by neutron spectroscopy in AgI [2, 3], $Cu_2Se$ [4]. The existence of such LE-excitations in Cu- and Ag-based superionics only just below the superionic phase transition has been reported in [5]. Accordingly [6] the low-energy mode is assigned to an optical phonon at the lowest frequency, originating from a transverse-zone-edge acoustic phonon. It should be noted that for a number of ternary Ag-based superionics with two kind of mobile ions and silver as the heavier mobile ion (for instance, $KAg_4I_5$, $RbAg_4I_5$ and $NH_4Ag_4I_5$), the proportionality of the observed energy modes (about 2 meV) to the square root of the mass of silver is evident [6]. Therefore, we can suppose the existence of low-energy optic modes at an energy transfer of about 2 meV in β-AgCuSe. However, the low-energy modes in our experiment have not been observed in β-AgCuSe probably due to poor resolution.

The spectra of α-AgCuSe could be qualitatively compared with spectra of superionic silver iodide [2, 7]: an increase of the low energy scattering is observed in the superionic phase in these spectra. We suggest that an increase of the low energy intensity in $S(Q,\varepsilon)$ spectra is connected with an increase of the quasielastic scattering. The quasielastic scattering

in our case is a result from diffusive motion of copper and silver ions. Analysis of quasielastic scattering was hampered by the overlap of the quasi- and inelastic contributions.

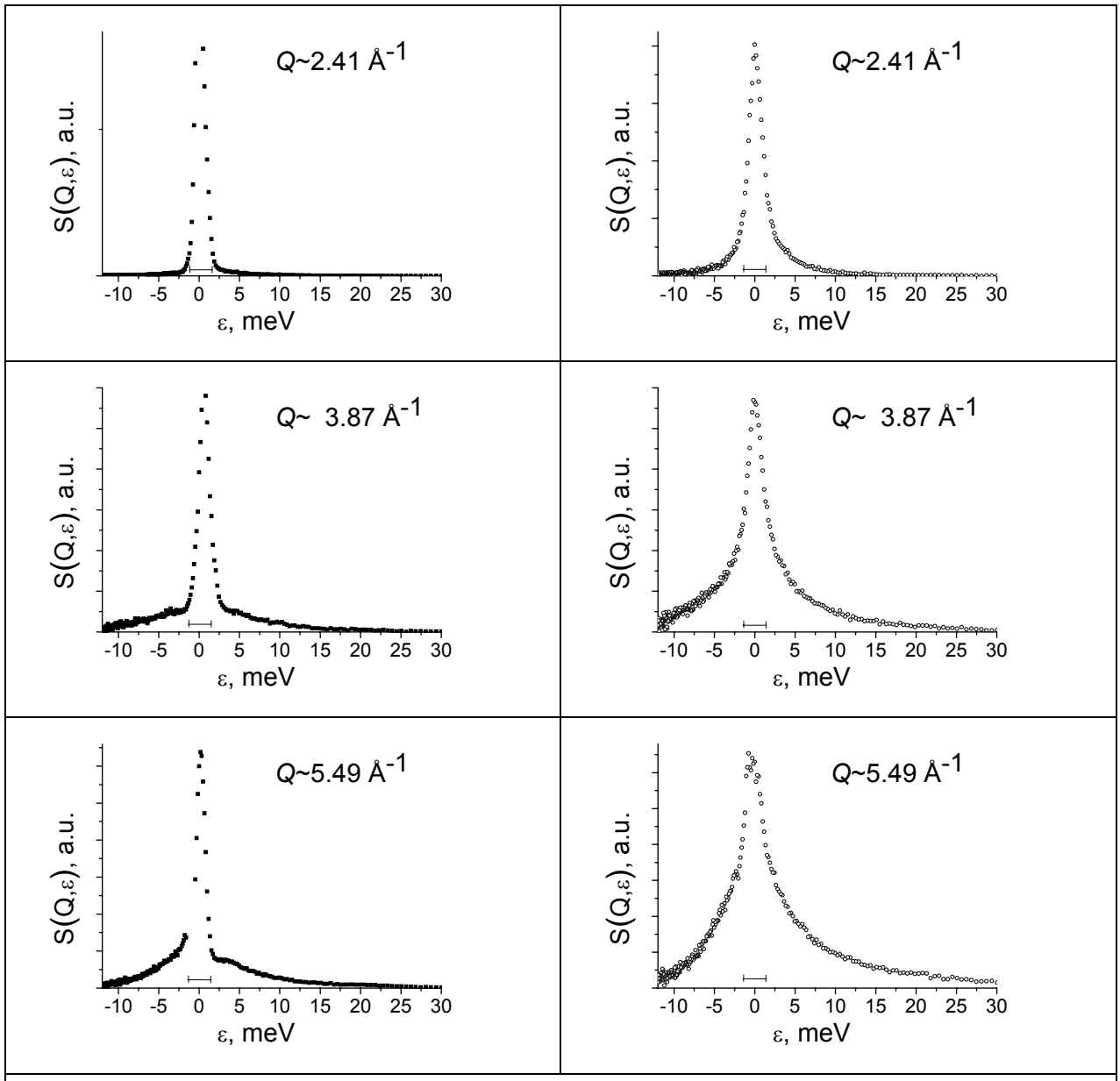


Fig.1. The $S(Q,\varepsilon)$ spectra for selected $Q$-values in β-AgCuSe at 285 K (left column) and α-AgCuSe at 505 K (right column). Energy resolution is marked on the figure by pointer.

**Literature**


[1] S. Miyatani, Journal of the Physical Society of Japan 34 (1973) 423-432.
[2] K. Funke, J. Kalus, R.E. Lechner, Solid State Communications 14 (1974) 1021-1024.
[3] W. Bührer, R.M. Nicklow, P. Brüesch, Physical Review B 17 (1978) 3362-3370
[4] S.A. Danilkin, A.N. Skomorokhov, A. Hoser, H. Fuess, V. Rajevac and N.N. Bickulova, Journal of Alloys Compounds 361 (2003) 57-61.
[5] K. Wakamura, Solis State Ionics 171 (2004) 229-235.
[6] K. Wakamura, Physical Review B 59 (1999) 3560-3568.
[7] G. Eckold, K. Funke, J. Kalus, R.E. Lechner, Physics Letters A 55 (1975) 125-126.

# SANS Contrast Variation in Organic Magnetic Fluid of New Type

Mikhail V. Avdeev[1], Artem V. Feoktystov[1], Maria Balasoiu[1], Doina Bica[2], Ladiaslu Vékás[2]

[1]*Frank Laboratory of Neutron Physics, Joint Institute for Nuclear Research, Dubna, Russia*
[2]*Center for Fundamental and Advanced Technical Research, Timisoara, Romania*

The contrast variation technique in small-angle neutron scattering (SANS) experiments was applied to a new type of magnetic fluids based on organic non-polar carriers (benzene, cyclohexane) and stabilized by myristic acid $C_{13}H_{27}COOH$ (surfactant from a series of fatty acids). The given surfactant differs much from the classical oleic acid $C_{17}H_{33}COOH$ used usually in such kind of solvents. It is shorter by four carbon groups and does not have a specific double bond in the middle of the molecule like oleic acid. As it was recently discovered [1], despite this difference a synthesis of magnetic fluids stabilized by myristic acid is possible. In comparison with oleic acid, the given surfactant reveals a lower efficiency in respect to dispersing of the whole size-interval (1-20 nm) of magnetite particles used in the preparation. We believe it stabilizes partially this interval leaving in the carrier only a fraction of smaller particles. Nevertheless, it should be pointed out that the resulting nanofluids are as highly stable in strong magnetic field (up to 2.5 T) as the samples stabilized by oleic acid.

Scattering curves obtained at the YuMO instrument for samples with the 0.8 % volume fraction of magnetite and different relative content $\eta$ of deuterated component in the carrier (benzene) are presented in Fig.1. In Fig.2 the corresponding $p(r)$ functions (Fourier transforms of the scattering curves) obtained by the GNOM program [2] are shown. They were used to estimate reliably integral parameters of the scattering curves: intensity in zero angle $I(0)$ and visible radius of gyration $R_g$. The $\eta$-dependence of $I(0)$ satisfies well the standard quadratic behavior (Fig.3). In polydisperse and magnetic systems such as the studied fluid the intensity is not fully matched, so the residual value of $I(0)$ (here 0.13 $cm^{-1}$) in the minimum takes place. After works [3,4] we refer this point as the effective match point and use it to determine the contrast

$$\Delta\rho = \overline{\rho}_e - \rho_s , \qquad (1)$$

which is a difference between the scattering length density in effective match point, $\overline{\rho}_e$, and the

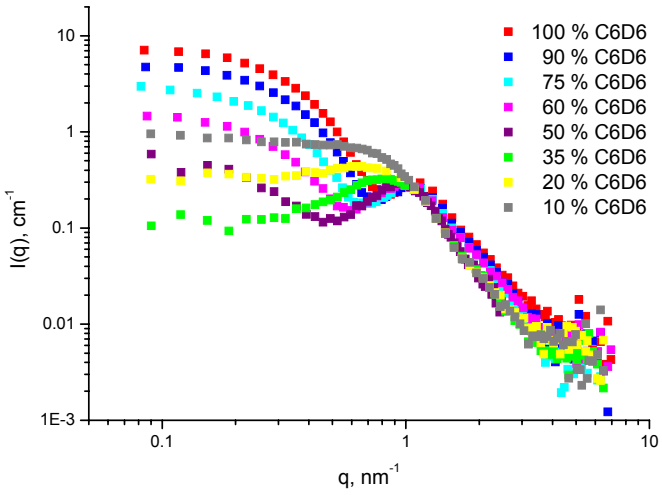


**Fig.1.** Changes in the cross-section per sample volume of the studied system as a function of relative content of the deuterated component in the solvent.

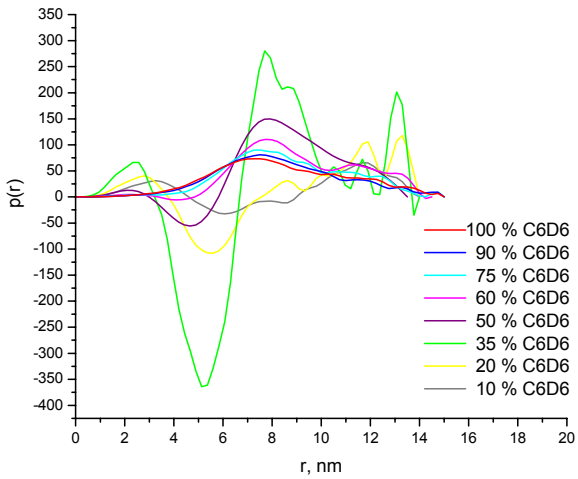


**Fig.2.** Fourier transforms of scattering curves in Fig.1 used to find integral parameters. Bimodal character of the functions reflect the core-shell organization of studied particles.

scattering length density of the solvent, $\rho_s$. One can see that the minimum in Fig.3 takes place at $\eta$ = 0.32. It is determined by the relative content of magnetite (scattering length density $\rho \sim 7 \times 10^{10}$ cm$^{-2}$) and myristic acid ($\rho \sim 0$ cm$^{-2}$) in colloidal particles of the studied fluid. This value is about two times less than the match point of the magnetic fluid with oleic acid (~ 0.6) [5], which means that the relative content of the surfactant in the given fluid is higher. We explain this fact by a significantly smaller characteristic size of nanomagnetite stabilized in the fluid with myristic acid. This is confirmed by the analysis of the $R_g$ parameter as a function of inversed contrast (Fig.4). As it was shown [4] in this case the corresponding expression takes the form:

$$R_g^2 = \left(\frac{< V_c^2 R_c^2 >}{< V_c^2 >} + \frac{A}{\Delta\rho} - \frac{B}{(\Delta\rho)^2}\right) / \left(1 + \frac{D}{(\Delta\rho)^2}\right). \qquad (2)$$

Here, $R_c$ and $V_c$ are the radius of gyration and volume regarding the particle shape; $A$, $B$, $D$ are parameters; and brackets <…> denote averaging over the particle size distribution. Equation 2 differs qualitatively from the classical expression for monodisperse multycomponent particles:

$$R_g^2 = R_c^2 + \alpha / \Delta\rho - \beta / (\Delta\rho)^2 \qquad (3)$$

with parameters $\alpha$, $\beta$. The additional parameter $D$ in Eq.2 is defined as

$$D = \frac{< (\bar{\rho} - \bar{\rho}_e)^2 V_c^2 >}{< V_c^2 >}, \qquad (4)$$

and characterizes average weighted of the size dependent mean particle scattering length density, $\bar{\rho}$.

The fit of Eq.2 to experimentally found points (Fig.4) results in the value of 4.5 nm for the characteristic radius of gyration $R_c$ for the particle shape. Assuming particles to be quasispherical one obtains 5.8 nm for the mean particle radius. After subtraction of the surfactant length (1.4 nm) we estimate the mean size as ~4.4 nm for magnetite particles in the studied fluid. It is almost two times less in comparison with the same parameter in the fluid with oleic acid (~8 nm).

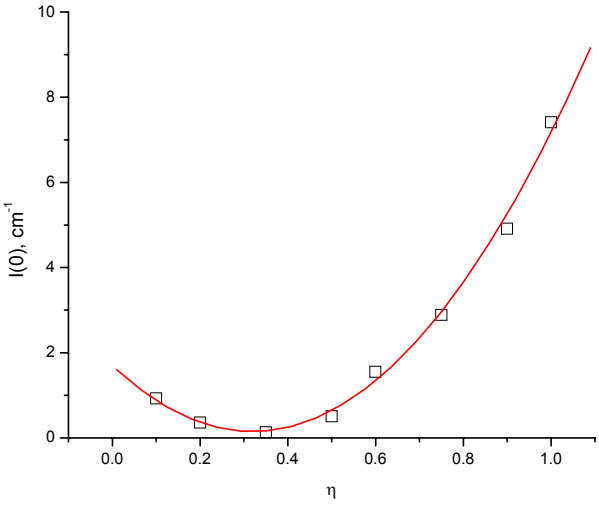


**Fig.3.** Changes in the $I(0)$ parameter during the contrast variation. Solid line is the quadratic approximation.

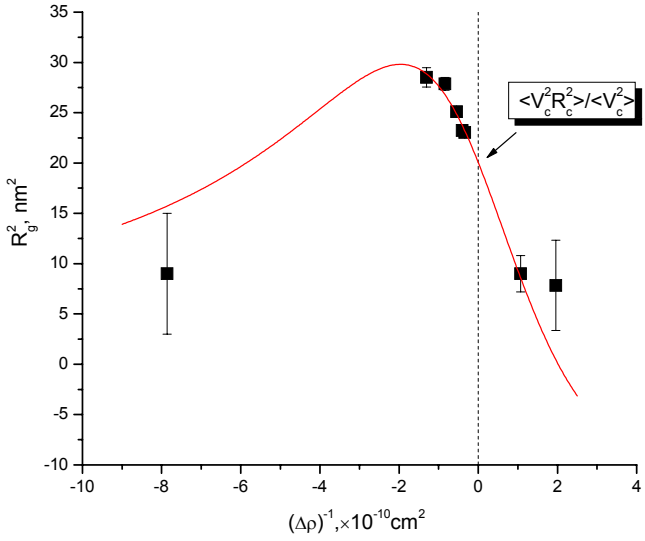


**Fig.4.** Changes in the $R_g$ parameter during the contrast variation. Solid line corresponds to the best fit of Eq.2. Resulting parameters are <V$_c^2$R$_c^2$>/< V$_c^2$> = 20.0 (4); $A$ = -9 (1); $B$ = 0; $D$ = 0.08 (3).

As one can see the $B$ parameter in Eq.2 is the analogous of the $\beta$ parameter in Eq.3, which characterizes the distance between centers of mass of different components in the particle. For spherically symmetric core-shell particles $\beta = 0$. In the general case of polydisperse particles this is not true, but despite a significant particle polydispersity in the studied fluid the resulting parameter $B$ in Fig.4 is close to zero. Probably, we deal with the compensation of effects of polydispersity and magnetic scattering in this case. Thorough analysis of this fact, as well as comparison of the $A$ parameter with the model values are in progress.

**References**


[1] M.Balasoiu, M.V.Avdeev, A.I.Kuklin, V.L.Aksenov, D.Bica, L.Vékás, D.Hasegan, Gy.Török, L.Rosta, V.Garamus, J.Kohlbrecher, *Magnetohydrodynamics* **40** (2004) 359-368

[2] D.I.Svergun, *J. Appl. Cryst.* **25** (1992) 495-503

[3] M.Balasoiu, M.V.Avdeev, V.L.Aksenov, D.Hasegan, V.M.Garamus, A.Schreyer, D.Bica, L.Vékás, *J. Mag. Mag. Mater.*, accepted (2005)

[4] M.V.Avdeev, *J. Appl. Cryst.*, submitted.

[5] B.Grabcev, M.Balasoiu, D.Bica, A.I.Kuklin, Magnetohydrodynamics **30** (1994) 156-159

# Study of the structural modification induced on the coal tar pitch by addition of single, multiwalled carbon nanotubes and nanocarbon fibers

I. Ion[a, b*], A-M. Bondar[b], Y. Kovalev[a, c], C. Banciu[b], A. Bara[b], Pasuk[b], A. Kuklin[a]

[a] Frank Laboratory of Neutron Physics, Joint Institute for Nuclear Research, 141980Dubna, Russia
[b] Carbon Materials Laboratory , National Institute for Research and Development in Electrical Engineering, 030138 Bucharest-3, Romania
[c] Skobeltsyn Institute of Nuclear Physics, Lomonosov Moscow State University, Moscow, Russia

Electromagnetic interference shielding (EMIS) is widely used for protection and stable functioning of electronic devises, as well as for human protection. Carbon composites are one of the basic materials exploited in the production EMIS [1, 2, 3]. Carbon materials show the fractal structure in the meso-scale depending on theirs origins and production process (rate and the final temperature of the heat treatment, pressure, etc.)[4]. In the current work SANS experiment, EM, OM and XRD were used to reveal the structural changes of coal tar pitch during the first carbonization.

The samples were prepared at Advanced Research Institute for Electrical Engineering Bucharest, Romania and are consisting of coal tar pitch (CTP) additivated with 1,5 % (wt.) single, multiwalled carbon nanotubes and carbon nanofibres. The mixtures were carbonized at 420, 440, $460^0$C temperatures in inert atmosphere with the purpose of studying the influence of the additives on the mesophase formation and development. The samples carbonized at $460^0$C presented suitable crystalline properties for EMIS purpose, all the sample attaining mesophase stage. The addition of nanotubes fluidized the carbonic system during the pyrolysing process and increased the temperature of mesophase formation. At this temperature, the bulk mesophase is already formed (Fig. 1a and 1b). It was observed that the sizes of crystalline isochromatic areas were strongly influenced by the size of the additive. The addition of single walled nanotubes provided the larger crystalline isochromatic areas. On the other hand, the carbon nanofibres impeded the mesophase formation at this temperature (Fig. 1c). The size and type of additive have an important effect on the mesophase formation and development.

SANS experiment was carried out on the YuMO spectrometer of the pulsed reactor IBR-2 Dubna, Russia. Determined scattering curves are presented in Fig. 2, in logarithmic coordinates the scattering curve have power-law scattering behaviour with power law exponent less than 4. The results suggest that the carbon materials present clusters characterized by the surface fractal properties. The diameters of clusters ($d=2\pi/q$) are bigger than 125 Å (which correspond to $q_{max}=0.05$ Å$^{-1}$), the upper limits cannot be determined, because are beyond the instrumental limits of the detector. The surfaces roughness is dependent of the type of the additive; it is rougher with the increasing of the additives size.

The Guinier approximation for lamellar bodies was used to calculate the thickness of the basic structural units. The plot $\ln Iq^2$ vs $q^2$ (Fig. 3) presents strait line behavior in the q range of 0.07 - 0.2 Å$^{-1}$. The thickness of basic structural units was found for all the samples to be about 8 Å. This suggests that the basic structural units consist of three-polyaromatic planar molecules stacked parallel.

We can conclude that the additive effects are small at low length scales (large q range) and became more important at large lengths scales, increasing the crystalline content in volume and quality, improve in this way the electric conductive properties of materials.

Reference.

1. Pierson H.0. Handbook of carbon, graphite, diamond, and fullerenes. Park Ridge NJ: Noyes. 1993.

2. Pasuk I., Banciu C., Bondar A.M., Rimbu G.A., Ion I., Stamatin I., Morjan I. Influence of some carbon nanostructures on the mesophase pitch development-A structural study. Romanian Reports in Physics, 2004, 56(3):320-327.
3. Rimbu G., Banciu C., Ion I., Pasuk I., Bondar A.M., Stamatin I., Morjan I., Sandu I. Proceedings of Carbon Conference,2002,Beijing, China.
4. Teixeira J. Structure and dynamics of supramolecular aggregates and strongly interacting colloids", ed. by S.H. Chen, J.S. Huang and P. Tartaglia (Kluwer, Drodecht, 1992).
*corresponded author: ionrausioana@yahoo.com; ion@nf.jinr.ru

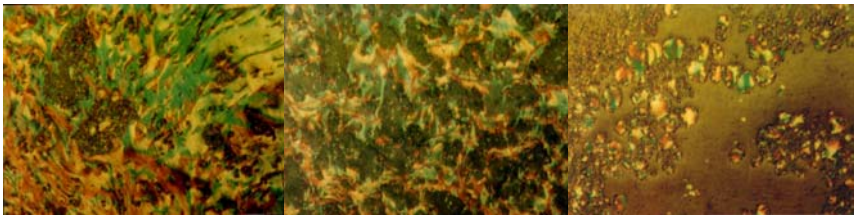

a. b. c.

Fig. 1. Optical microscopy for the samples additivated with single, multiwalled carbon nanotubes and carbon nanofibers carbonized at $460^0$C, at 300 X magnification.

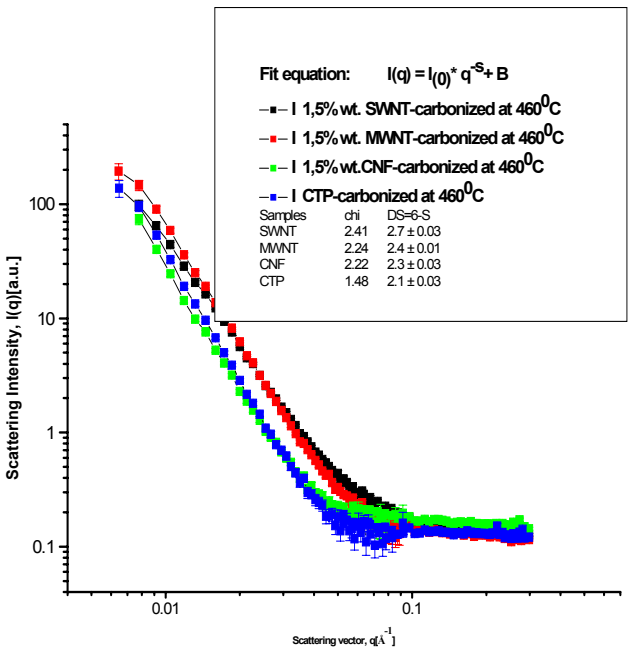


Fig. 2. Experimental scattering curves in the logarithmic scales

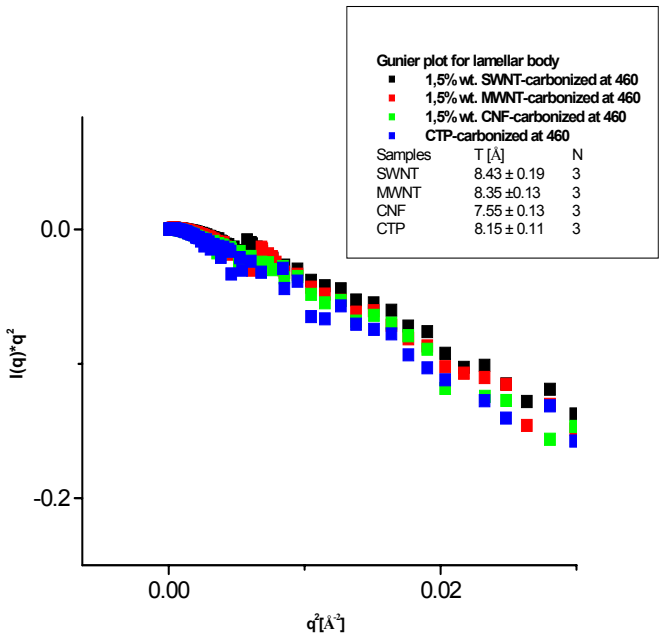


Fig. 3. Guinier approximation for lamellar bodies

# THE STUDY OF MAGNETIC ELASTOMERS BY SMALL ANGLE NEUTRON SCATTERING AND SCANNING ELECTRON MICROSCOPY

C. M. Muresan[*,#], E. M. Anitas[*], I. Bica[*], A. I. Kuklin[#], M. Balasoiu[#,&], O. Orelovitch[~], Y. Kovalev[#]

[*]*Faculty of Physics, West University of Timisoara, Romania*
[#]*Frank Laboratory of Neutron Physics - Joint Institute for Nuclear Research, Dubna, Russia*
[&]*Institute of Space Sciences, Bucharest, Romania*
[~]*Flerov Laboratory of Nuclear Reactions – Joint Institute for Nuclear Research, Dubna, Russia*

**Introduction**

Composites [1] are combinations of two or more materials with different properties. The different materials work together to produce a new material which combines all of the properties of the previously separate materials. Magnetic elastomers (ME) represent a new type of composites consisting of micro or nano-sized magnetic particles dispersed in different polymeric matrix. They are used for various technical applications such as artificial muscles, micropumps, vacuum seals and pressure seals.

**Materials**

The samples were prepared from stomaflex creme, in which were embedded nano and micro-magnetic particles: $Fe_3O_4$ (magnetite) and $Fe_2(CO)_9$ (diiron nonacarbonyl). Stomaflex creme – composition: paste – alfa omega poly(dimethylsiloxane) - $[Si(CH_3)_2O]_n$, calcium carbonate – $CaCO_3$, pigments, taste ingredients and catalyst: dibutyl tin dilaurate, benzyl silicate, pigments. Nano or microparticles foregoing bond to the polymer matrix. They are reinforced (consolidated) in the matrix behind the cross – linking of monomers. The samples were polymerized in the presence or in default of external magnetic field. The samples were investigated by Scanning electron microscopy (SEM) and Small angle neutron scattering (SANS) methods. SANS measurements were performed at the YuMO spectrometer of the IBR-2 pulsed reactor, JINR, Dubna.

**Experiments and results**

SEM images of the samples with 50 wt % $Fe_2(CO)_9$ microparticles are shown in Fig. 1. The diiron nanocarbonyl microparticles appear to be polydisperse, spherical with the mean diameter $D_m$= 2.93 μm.

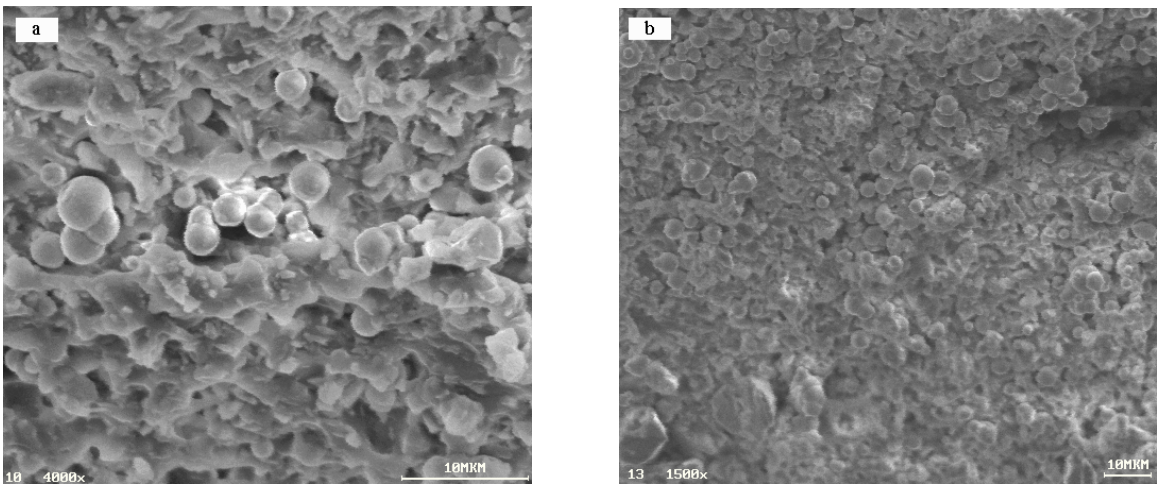


Fig. 1. a – Stomaflex creme with 50 wt % Fe2(CO)9 microparticles
b – Stomaflex creme with 50 wt % Fe2(CO)9 microparticles, polymerized in the presence of external magnetic field, B= 156,6 mT

The scattering curves from ME A and B are illustrated in Fig. 2, in logarithmic coordinates. The scattered intensity I(q) is plotted as a function of the scattering angle θ by $q = (4\pi/\lambda)\sin(\theta/2)$, where λ is the wavelength. From the Guinier plot[2], ln I(q) vs. $q^2$ of SANS ($0.0016\ Å^{-2} \leq q^2 \leq 0.0031\ Å^{-2}$), the radius of gyration $R_G$ of magnetite nanoparticles from the both magnetic elastomers where obtained, such as: in case of ME A – $R_G$ =2.37 nm, and in case of ME B – $R_G$ = 2.17 nm.

At higher q, both curves show two linear regions. When the scattering intensity I(q) follows the power law [3]:

$I(q) \sim q^{-n}$

its suggests the structure having a fractal nature. The characteristic of the fractal can be determined from n value: $1 \leq n \leq 3$ for mass fractal and $3 < n \leq 4$ for surface fractal. Fractal dimensions $d_m$ and $d_s$ for mass and surface fractals, respectively, are related to n by the following equations:

$d_m = n$ , $d_s = 2d - n$, where d is the dimension of the Euclidian space of the system considered. The fitted slope – n of -3.82 ± 0.036 for ME A suggests surface fractal with the fractal dimension of 2.18 ± 0.036, also the fitted slope –n of -3.51 ± 0.038 for ME B suggests surface fractal with the fractal dimension of 2.49 ± 0.038.

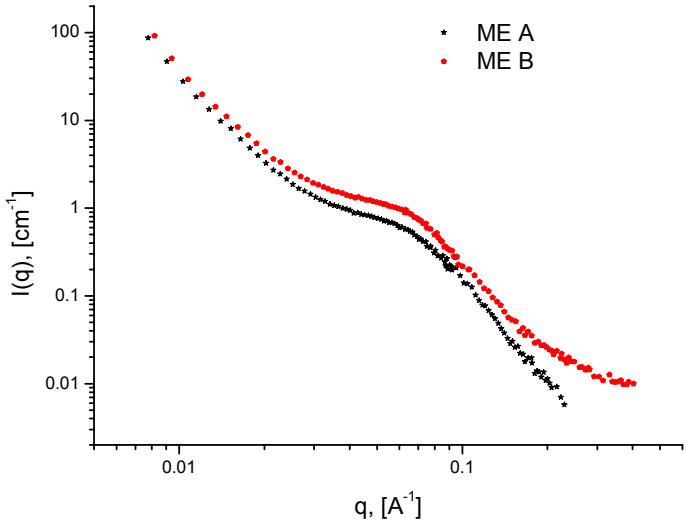


Fig. 2. SANS curves for: - ME A: stomaflex creme with $Fe_3O_4$ nanoparticles
- ME B: stomaflex creme with $Fe_3O_4$ nanoparticles, polymerized in the presence of external magnetic field

**References:**

[1]. D. Hull et all, An Introduction to composite materials , Paperback – August 13, 1996
[2]. L.A. Feigin; D.I. Svergun, in Structure Analysis by Small Angle X-ray and Neutron Scattering, G.W. Taylor (editor), Plenum, 1987
[3].Martin JE., Hurd AJ, J. Appl. Crystallography, 1987;20:61.

# Structural reorganization of mitochondrial membrane under low-amplitude swelling studied by small angle neutron scattering

**T.N. Murugova[*@], V.I. Gordeliy[@#&], A.Kh. Islamov[@], A.I. Kuklin[@], I.M. Solodovnikova[+], L. S. Yaguzhinsky[+].**

[*]Faculty of Bioengineering and Bioinformatics, Moscow State University, Russia
[@]Frank Laboratory of Neutron Physics, Joint Institute for Nuclear Research, Dubna, Russia
[#]IBI-2, Forschungszentrum Jülich 52425, IBI-2 Germany
[&]Centre for Biophysics and Physical Chemistry of Supramolecular Structures, Moscow Institute for Physics and Technology, Dolgoprudny, Russia
[+] A.N. Belozersky Institute of Physico-Chemical Biology, Moscow State University, Russia

It is well known that changes in volume of cells, organelles, bacteria stimulate specific structural reorganization in them accompanied by alterations in function of their enzymatic systems. Earlier influence of low-amplitude matrix swelling on ultrastructure of mitochondrial membrane was studied. The ultrastructure is concerned with working of the membrane enzymes. Namely under hypotonic conditions appearance of so called “dried cristae” with small gap between ctista membranes was found out in rat liver mitochondria [1,2]. This structural changes are accompanied by rise of electron transport in respiratory chain, changes in pH-regulation of potassium transport and in kinetic parameters of oxidative phosphorylation [3,4,5].

We conducted small angle neutron scattering (SANS) experiments with intact rat heart mitochondria under isotonic and hypotonic conditions. The experiments was carried out on YuMO spectrometer placed on beam 4 of pulsed reactor IBR-2 [6,7]. Mitochondria were placed in media containing 1 mM $MgSO_4 \cdot 7H_2O$, 1 mM $KH_2PO_4$, 20 mM *tris*, 10 mM *KCl*, 0.25 mM EDTA, 0.2 M sucrose (isotonic medium) and 0.058 M sucrose (hypotonic medium), pH=7.5. The temperature was 15 $^oC$.

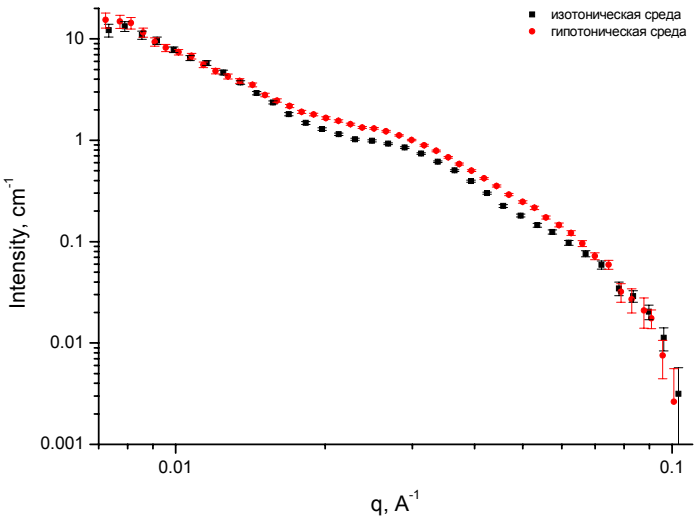


Fig. 1. Dependence of scattering intensity on scattering vector for rat heart mitochondria in isotonic and hypotonic media

The SANS curves are different for isotonic and hypotonic conditions that denotes qualitative structural reorganization in the mitochondrial membranes under the low-amplitude matrix swelling. (Fig. 1). More detailed analysis of the SANS data uncovered the presence of well-ordered structures in the mitochondria. In case of isotonic medium the mitochondrial membrane forms lamellae placing quasi parallel with each other at

particular distance equaling 195 ± 12 Å (distance between centers of the lamelae). So the scattering curve has the peak with maximum at scattering vector equals 0.032 ± 0.002 $Å^{-1}$ (Fig. 2A). In case of hypotonic conditions (low-amplitude swelling) the curve has two peaks (Fig. 2B) with maximums at

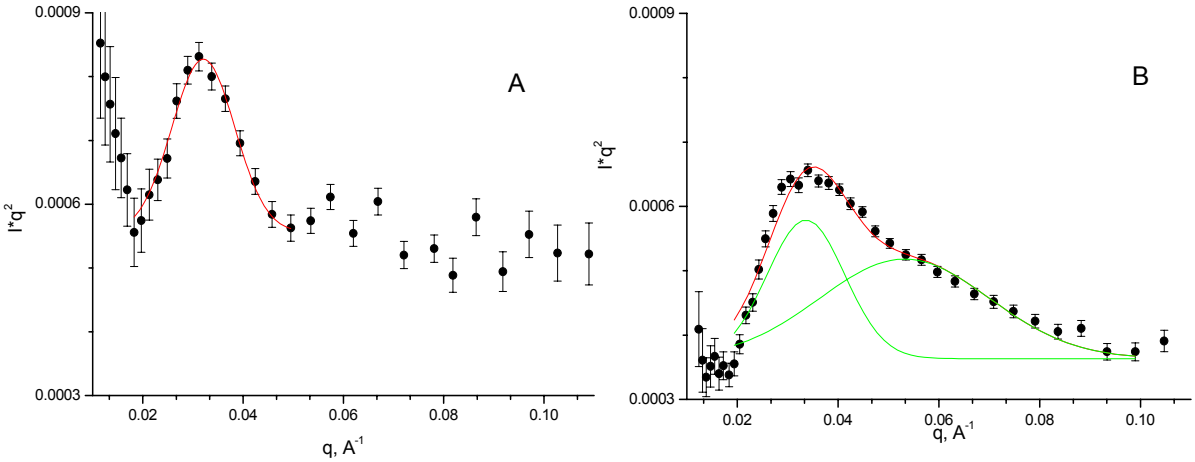


Fig. 2. Scattering intensity multiplied on Lorentz factor of plane $q^2$ against scattering vector q for rat heart mitochondria in isotonic (A) and hypotonic (B) media.

0.034 ± 0.002 and 0.053 ± 0.004 $Å^{-1}$, that corresponds to 185 ± 11 and 119 ± 9 Å respectively. That can indicate presence of lamellar structures with two characteristic distances between centers of lamellae wich equal 185 and 119 Å (for example, "dried cristae" and distance between otter and inner membranes) or formation of non-lamellar structures in mitochondria. The last assumption arises from the spacing ratio for the peaks that equals 1 : 1.6 ± 0.1, that is appropriate to non-lamellar structures such as hexagonal and cubic [8,9]. The electron microscopy will help to solve this ambiguity.

References


1. I. P. Krasinskaya, I.S. Litvinov, S.D. Zaharov, L. E. Bakeeva, L. S. Yaguzhinsky // Biochim. 1989. V. 54. №9. P. 1556-1561.
2. FLNP Annual report 2003. http://nfdfn.jinr.ru/reports/2003/index.html
3. Krasinskaya I.P., Marshansky V.N., Dragunova S.F., Yaguzhinsky L.S. // FEBS Letters. 1984. V. 167. № 1. P. 176-180
4. Garlid K.D. // Biochem. and Biophys. Res. Communs. 1978. V. 83. № 4. P. 1450-1455.
5. Brierley G.P., Jurkowitz M.S., Farooqui T., Jung D.W. // J.Biol. Chem. 1984. V. 259. № 23. P. 14672-14678.
6. Kuklin A.I., Islamov A.Kh., Gordeliy V.I. // Neutron News. 2005. V. 16. № 3. P. 16-18.
7. http://nfdfn.jinr.ru/fks/yumo/yumo.html
8. Seddon J.M. // Biochim. Biophys. Acta. 1990. V.1031. P. 1-69.
9. Lindblom G., Rilfors L. // Biochim. Biophys. Acta. 1989. V. 988. P. 221-256.

# About nucleus "superfluid-normal" state transition dynamics

A.M. Sukhovoj, V.A. Khitrov

*Frank Laboratory of Neutron Physics, Joint Institute for Nuclear Research*
*141980 Dubna, Russia*

The general form of dependence of the most reliable modern values of the level density on the investigated nucleus excitation energy points at [1,2] the presence of at least two "step-like" structures below neutron binding energy with its faster increase in between than it is predicted by a notion of a nucleus, as a system of non-interacting Fermi-particles. It means that, at least, at two excitation energies the abrupt change in the excited levels wave functions structure occurs in a nucleus. The unique factor, known by the present to be capable of providing such a change is the breaking of nucleons Cooper pairs with addition of two quasiparticles to the existing ones, as well as fast increasing the level density at increasing excitation energy.

In modern theoretical notions [3], the level density at a given nuclear excitation energy $U$, spin $J$ and parity $\pi$ is expressed through the density $\rho_{qp}$ only of the quasiparticle excitations and its vibration and rotational (for the deformed nuclei) enhancement coefficients $K_{vibr}$ and $K_{rot}$, respectively:

$$\rho(U,J,\pi) = \rho_{qp}(U,J,\pi)K_{vibr}(U,J,\pi)K_{rot}(U,J,\pi) = \rho_{qp}(U,J,\pi)K_{coll}(U,J,\pi). \qquad (1)$$

For the further analysis of the experimental data it is expedient to unite coefficients of vibration and rotational increase in the level density in the general coefficient of its collective enhancement $K_{coll}$. In the level density from the analysis [1,2] the basic contribution to its value is brought by the effect of vibration. In an examined case the effect of rotational enhancement of the level density for the deformed compound even-odd nucleus is less than the experimental data error. By the order of magnitude in a neutron binding energy range, it is expected that $K_{coll}$ value for the complete level density is [3] in an interval: $10 < K_{coll} < 100$. There is no experimental information on dependence of $K_{vibr}$ on $U$, $J$, and $\pi$. Modern theoretical ideas of this account admit a significant change in $K_{vibr}$ when changes $U$ up to the change of [4] its functional forms dependences on nucleus excitation energy. The presence [1,2] of rather reliable experimental data for the sums of radiation strength functions of dipole cascade transitions allows, basically, to solve this problem by creation of precise models of strength functions. This opportunity is caused by known distinctions in values of partial radiation width from a ratio of quasiparticle and vibration components in the structure of excited (decaying) levels. However, currently, there are no theoretical models of such level [3].

Therefore, the further analysis of the level density is possible to be carried out only within the framework of zero assumptions of $K_{coll}$ independence on the nucleus excitation energy in the interval of $\sim 0.5-3$ MeV up to $B_n$. For the first time, it allows one to receive direct experimental information on partial density of quasiparticle excitations with various number of quasiparticles in the specified excitation energy intervals for some nuclei with their masses of $40 \leq A \leq 200$.

The possibility of determining the partial level density $\rho_n$ with a given number $n$ of the excited quasiparticles for $U$ nucleus energy excitation

$$\rho_n = \frac{(J+1)exp(-(j+1/2)^2/(2\sigma^2))}{2\sqrt{(2\pi)}\sigma^3} \frac{g^n(U-E_n)^{n-1}}{((n/2)!)^2(n-1)!} \tag{2}$$

has been found by Strutinsky [5]. For the first time, he has obtained simple functional dependence of the nucleus excited states density (the second coefficient in (2)).

Practically, for comparison with the experiment [1,2] within the framework of existing [3] theoretical notions of a nucleus, it is necessary to choose value of the spin cutoff factor $\sigma = f(n, U)$ for the given Cooper pair and excitation energy, together with the energy $U-E_n$ of the excited quasiparticles. Density of single-particle levels $g$ for the presented here nuclei is known from the data on neutron resonances.

In first of the tested by us variants, the $E_n = 0.25g(\Delta_0^2-\Delta_n^2)+\delta e_n$, functional dependence suggested by A.V.Ignatjuk and Yu.V.Sokolov (see [3,4]) has been used. It is based on the idea of existence of $0.25g\Delta_0^2$ condensation energy in a nucleus at its transition from normal to superfluid state. The maximal number of decayed pairs in this variant is limited to value $N = 5$, basically, by possibilities of used fitting algorithm.

To correctly account the spin dependence of the level density is a serious problem because of the ambiguity of [3] model notions of the spin cutoff factor. In both described here variants, the functional dependence [6] suggested by Fu, has been used. The corresponding function, written in language FORTRAN77, is taken from file RIPL-2 [3] with necessary parameters. As the breaking threshold $U_{th}$ for number $N$ pair was selected only by comparing values of expression (2) with the experimental density of levels, so its value, suggested in [6], has been replaced with the best one obtained by us.

First of all, it is found out that in the representation [4] the experimental level density requires accounting for not less than 5 partial densities for its reproduction. According to the notions [5], the effect of pairing takes a share of nucleus excitation energy, which is equal to $2\Delta_0$. For five breaking nucleon pairs the total energy of pairing is equal approximately to 10 MeV for the heaviest of the nuclei that are included in the analysis. This energy is more than the neutron binding energy and, consequently, notions [4,7] seriously disagree with our experimental data.

Within the framework of notions [4] about the form of Cooper pairs correlation functions energy dependence of excited nucleus, a picture, corresponding to the basic statement [7], is observable. This statement deals with the generalized model of a superfluid nucleus – its phase-transition between superfluid and normal states (but at the essentially smaller energy of such transitions).

Model approximation of correlation function $\Delta_n$, presented in [3,4], is obtained on the base of existing experimental data with very large systematical errors. Their basic distinctive feature is that the speed of increase in the level density is smaller as compared to data of [1,2]. It is true at least for excitation energy some higher than $0.5B_n$. In this variant of model notions, at the increase in excitation energy the smooth enough change in $\Delta_n$ can provide the greater $d\rho/dU$ value only when the expression (2) accounts for five and more breaking pairs. An alternative opportunity consists in using other ideas of nucleon correlation functions of Cooper pairs in the excited nucleus.

The smaller values of $n$ can be obtained only with the more rapid decrease in $\Delta_n$, than it is predicts by [3,4], as increasing of the excitation energy $U$. And equation (2) cannot present

any other opportunity. The number of variants of the functional dependences satisfying this condition is great. In the second variant of the analysis for $E_n$ the following functional dependence has been used:

$$U - E_n = U - \Delta_0 ln[(U - U_{th})/(p\Delta_0)]. \quad (3)$$

The only ground for using such function for this purpose is a logarithmic dependence of macrosystem thermal capacity in a point of second-order phase transition on its temperature. But such dependence is shown only in an ideal case. In case of a mixture of helium isotopes, for example, the maximal thermal capacity decreases, whereas the degree of change increases at the increase of $^3$He concentration. Therefore, dependence (3) can be accepted as the utmost possible $\Delta_n$ estimation for pair number $N$ at the energy $U$ with an additional condition [5] that maximum $E_n$ value is in $E_n \leq n\Delta_0/2$. Such correction is essential only for the second breaking Cooper pair and mainly for nuclei $^{74}$Ge, $^{185}$W, $^{192}$Ir and $^{196}$Pt. If presence of systematical errors in $\rho$ is taken into account, the specified $E_n$ increase does not indicate its excessive divergence in various nuclei. It is also true for the known significant fluctuations of pairing energy of last nucleons pair.

The best value of parameter $p$ for all tested nuclei is about 2.2-2.3. Therefore, in the second of the investigated variants, the pairing influences the level density $\rho_{qp}(U, J, \pi)$ for next breaking Cooper pair only in essentially limited, as compared to [3,4], energy interval $U_{th} < U \leq U_{th} + p\Delta_0$. I. e., it is practically equal to the known value of gap width in the low-lying states spectrum of an even-even nucleus.

In the carried out variants of the analysis, the coefficient $K_{coll}$ has been accepted as independent on excitation energy $U$, spin and parity of levels and unchanging at the increase of nucleus excitation energy. Its absolute value is almost completely determined by a ratio of the experimental level density and the density of two or three quasiparticle excitations. In a case, when this value for any number $N > 1$ Cooper pairs differs by some times, such discrepancy is easily compensated by changes in $U_{th}$ within the limits of, several hundreds keV maximally.

Examples of the best approximation of the experimental data [1,2] for 4 nuclei with various parity of neutrons and protons are displayed in Fig. 1. It also shows the partial level density obtained in the first variant of the analysis. In Figs. 2-7 the similar data are presented for the most of the analyzed nuclei with partial densities obtained in the second variant of analysis.

From these data quite unequivocally follows, that:

1. The first step-like structure in level density [1,2] is caused by existence of, at least, two quasiparticles in nucleus of any type;

2. For the precise reproduction of the level density (comparable with an experimental data error) it is required to postulate the breaking from three up to five and more such pairs;

3. From the data of approximation, presented on Figs. 2-7, it is visible, that in the second variant of the analysis the experimental level density can be well reproduced at the account of only 6 or 7-quasiparticle excitations. Moreover, representation of correlation functions as (3) allows one to obtain small enough value of the level density of $n$-quasiparticle excitations, having lower energy than $U_{th}$.

4. The shell effects demonstrate itself to the maximum extent in near magic nuclei being close to $N$=82 and 126. Their exhaustive reproduction is impossible within the framework of used by us expression. More exact approximation can demand to revise the basic assumption

[5] about equidistant character of single-particle spectrum of near magic nucleus and to account [4] for shell inhomogeneities of single-particle spectrum. It may also be required to account for change in $K_{coll}$ value for different nuclei and excitation energies, not taken into account by performed analysis.

Despite of the specified ambiguity, volume and quality of the obtained [1,2] experimental data presents extremely favorable possibilities for the greatest possible development of modern models of the level density. The obtained values of the most probable parameters of the experimental data approximations can be used for $\rho$ calculation in nuclei that are relatively far from the magic ones. It may be done either directly or at interpolation of the data given by Tables 1 and 2 [8], or by using the corresponding average values. It is certainly necessary to develop new model ideas of the nucleon correlation functions energy dependence for near magic nuclei in the whole region of $E_{ex} < B_n$ and about $\rho$ vibration enhancement factor.

It is also necessary to reveal the degree with which the initial compound state structure influences on the two-step cascade intensity and to estimate the $\rho$ and $k$ systematical error connected to this circumstance.

The accumulated, up to the present, data file on two-step cascades following thermal neutron radiative capture, points to the existence of systematical discrepancy in experimentally obtained data for $\rho$ and $k$ and their model-calculated [7,9] values. Presence of significant systematical discrepancy between the experiment and theory allows one to hope on the possibility of a substantial improvement in model notions about properties of a nucleus at its excitation being lower than nucleon binding energy.

## References


[1] E.V. Vasilieva, A.M. Sukhovoj, V.A. Khitrov, Phys. At. Nucl. 64(2) (2001) 153, nucl-ex/0110017

[2] A.M. Sukhovoj, V.A. Khitrov, Physics of Paricl. and Nuclei, 36(4) (2005) 359.

[3] Reference Input Parameter Library RIPL-2. Handbook for calculations of nuclear reaction data. IAEA-TECDOC, 2002, http://www- nds.iaea.or.at/ripl2/ Handbook for Calculation of Nuclear Reactions Data, IAEA, Vienna, TECDOC-1034, 1998.

[4] A.V. Ignatyuk, Report INDC-233(L) (IAEA Vienna 1985)

[5] V.M. Strutinsky, in Proc. of Int. Conf. Nucl. Phys., Paris (1958) 617.

[6] C.Y. Fu, Nucl. Sci. Eng. 92 (1986) 440.

[7] E.M. Rastopchin, M.I. Svirin, G.N. Smirenkin, Yad. Fiz. 52 (1990)1258.

[8] A.M. Sukhovoj, V.A. Khitrov, JINR preprint E3-2005-196, Dubna, 2005.

[9] W. Dilg, W. Schantl, H. Vonach, M. Uhl, Nucl. Phys. A217 (1973) 269.

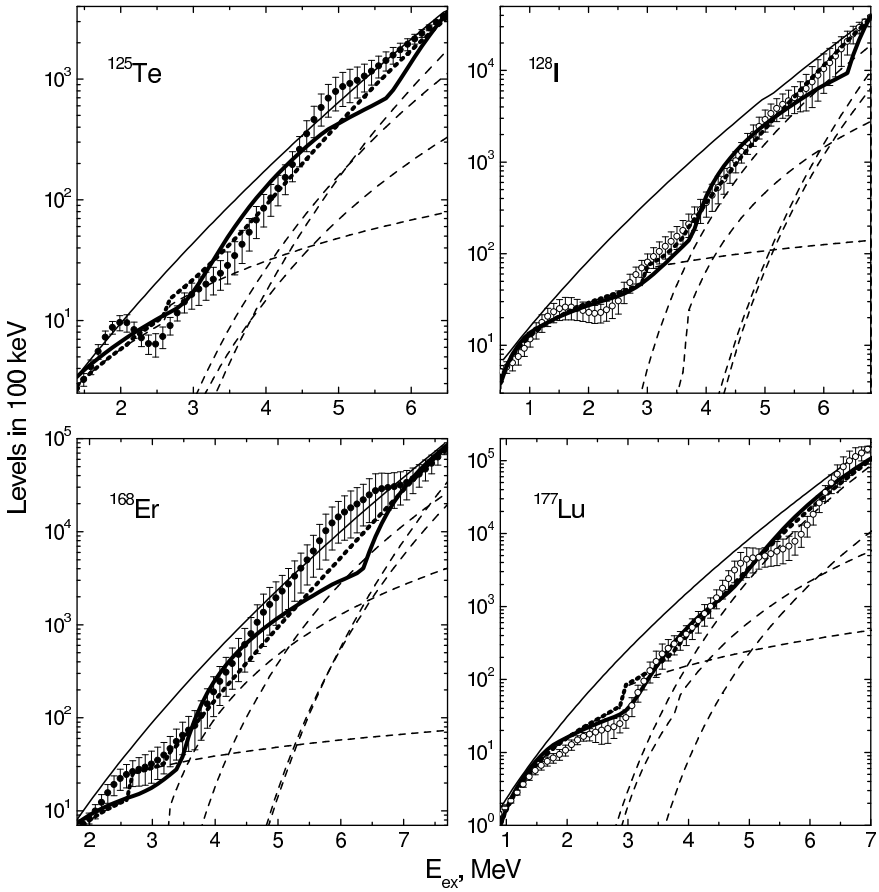


*Fig. 1. It shows examples of the experimental data on approximation for nuclei $^{125}Te$, $^{128}I$, $^{168}Er$ and $^{177}Lu$ by the partial level density in the first variant of the analysis. Full points with error bars represent the experimental data [2], open points show the data [1]. A thin dotted line indicates partial density, points display their sum. A solid line presents the sum of the partial level density from the second variant of the analysis. Thin line stands for the level density calculated within model [9].*

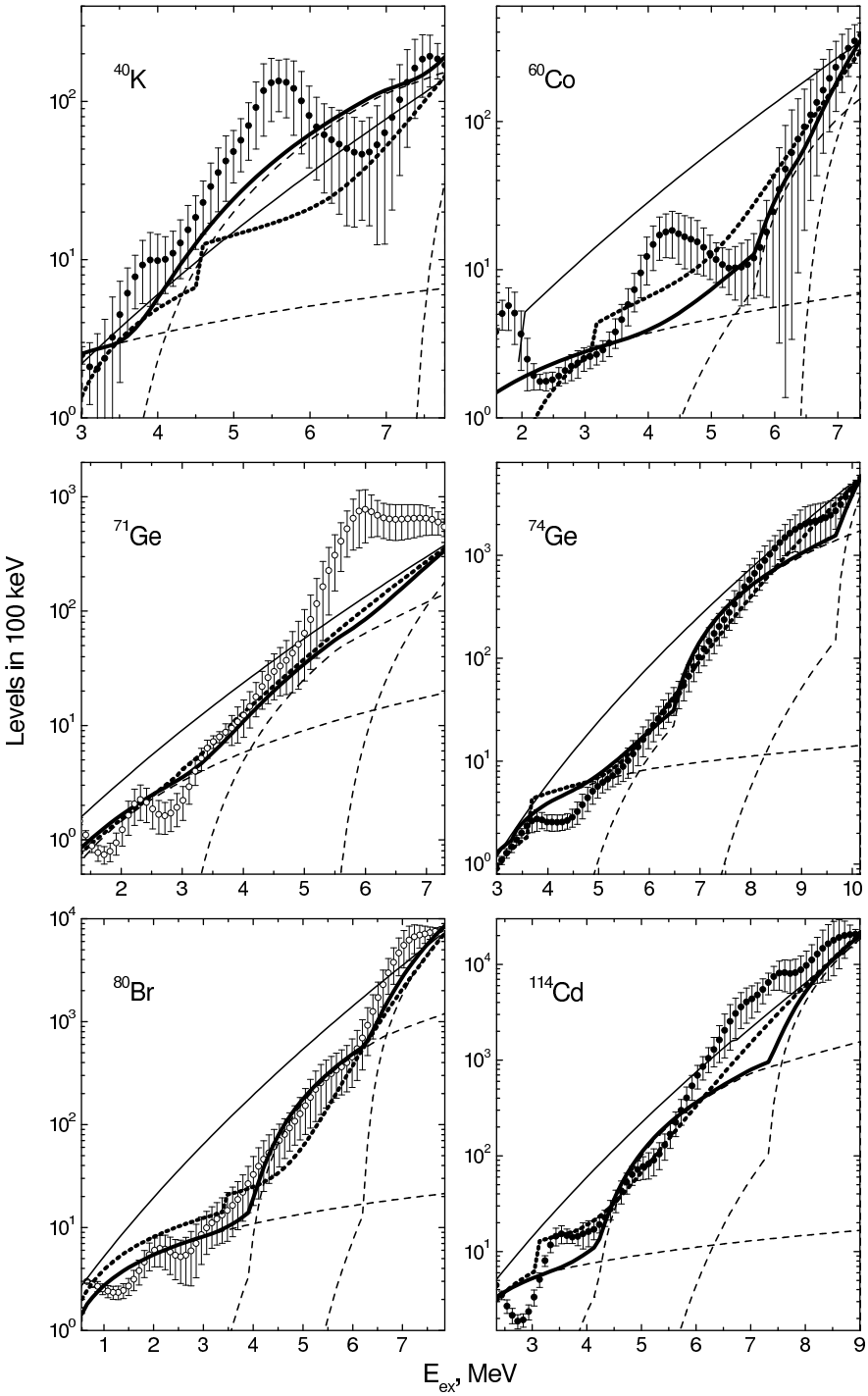


*Fig. 2.* The same as in Fig. 2 for nuclei: $^{40}$K, $^{60}$Co, $^{71,74}$Ge, $^{80}$Br, $^{114}$Cd. Here, the partial level densities are shown as obtained from the second variant of the analysis.

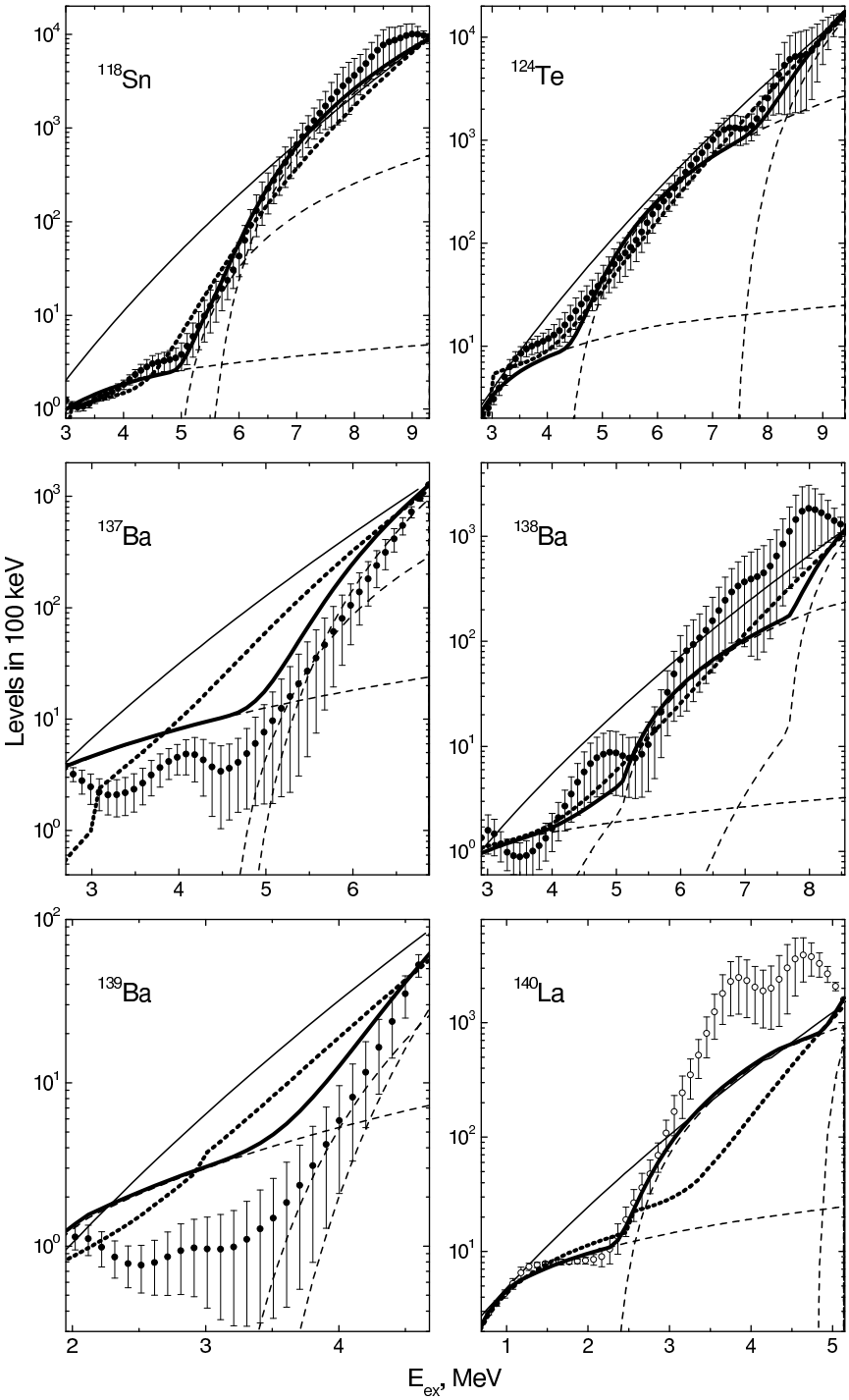


*Fig. 3.* The same as in fig. 2 for nuclei: $^{118}$Sn, $^{124}$Te, $^{137,138,139}$Ba, $^{140}$La.

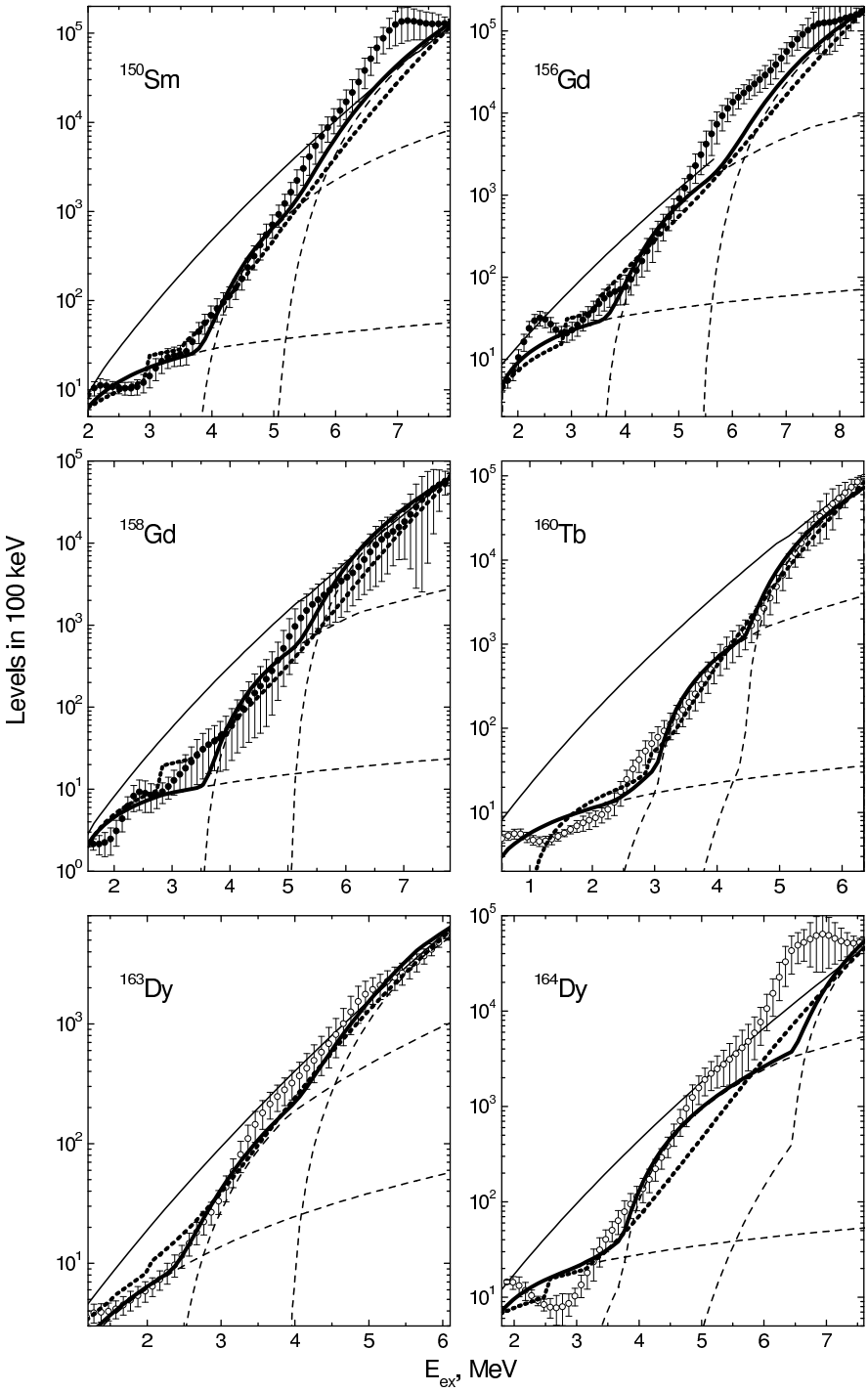


*Fig. 4. The same as in Fig. 2 for nuclei:* $^{150}Sm$, $^{156,158}Gd$, $^{160}Tb$, $^{163,164}Dy$.

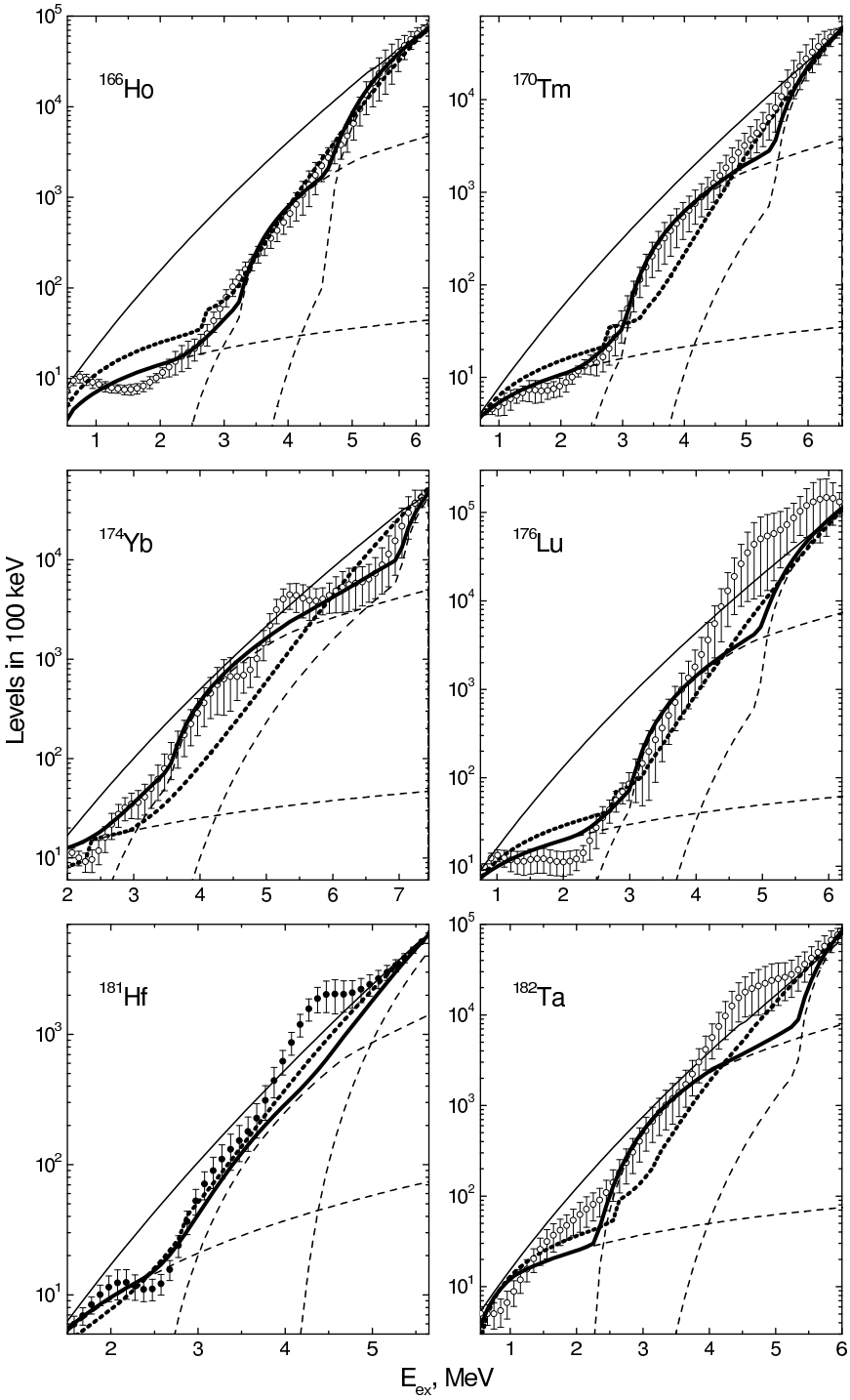


*Fig. 5.* The same as in Fig. 2 for nuclei: $^{166}$Ho, $^{170}$Tm, $^{174}$Yb, $^{176}$Lu, $^{181}$Hf, $^{182}$Ta.

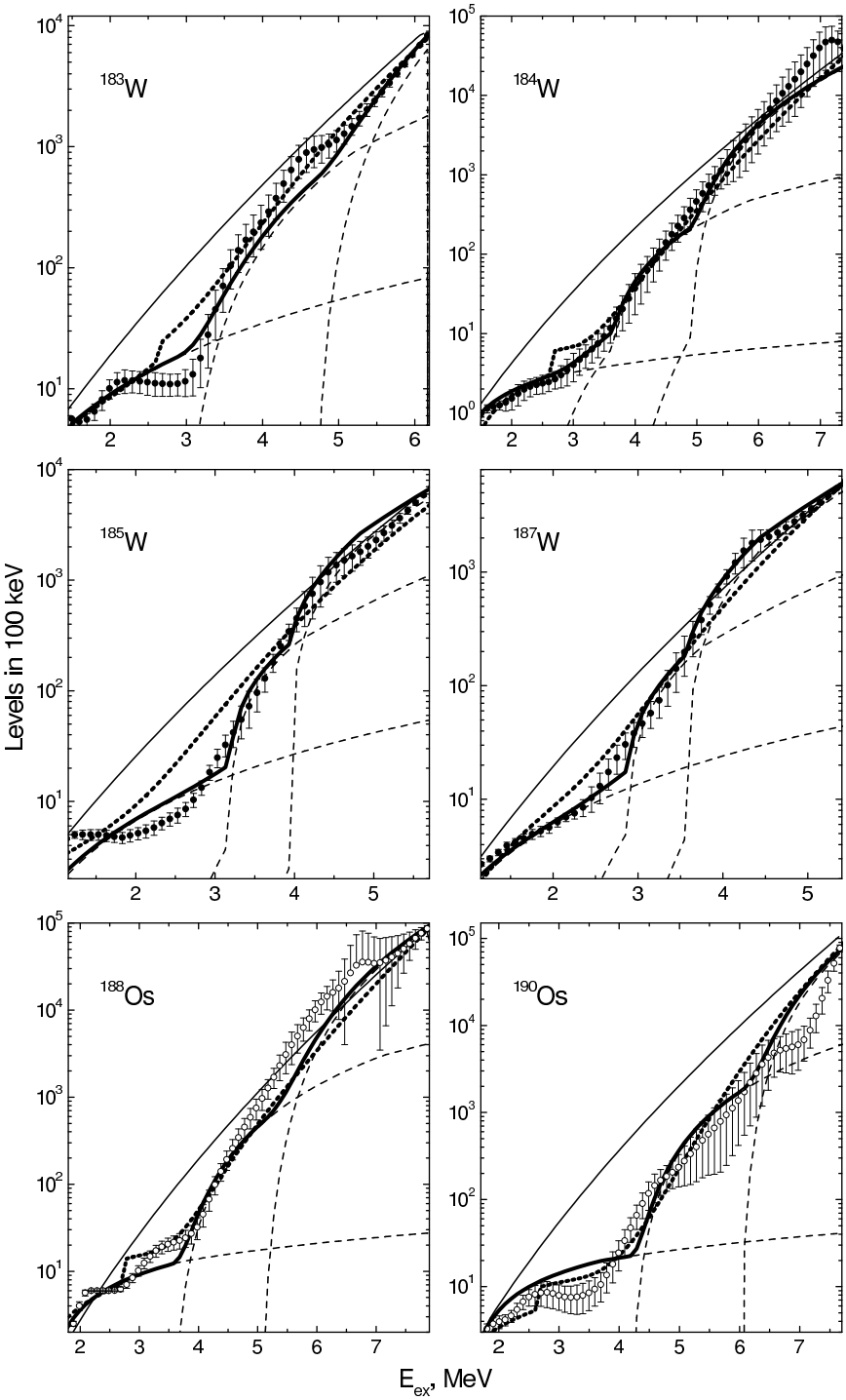


*Fig. 6.* The same as in Fig. 2 for nuclei: $^{183,184,185,187}$W, $^{188,190}$Os.

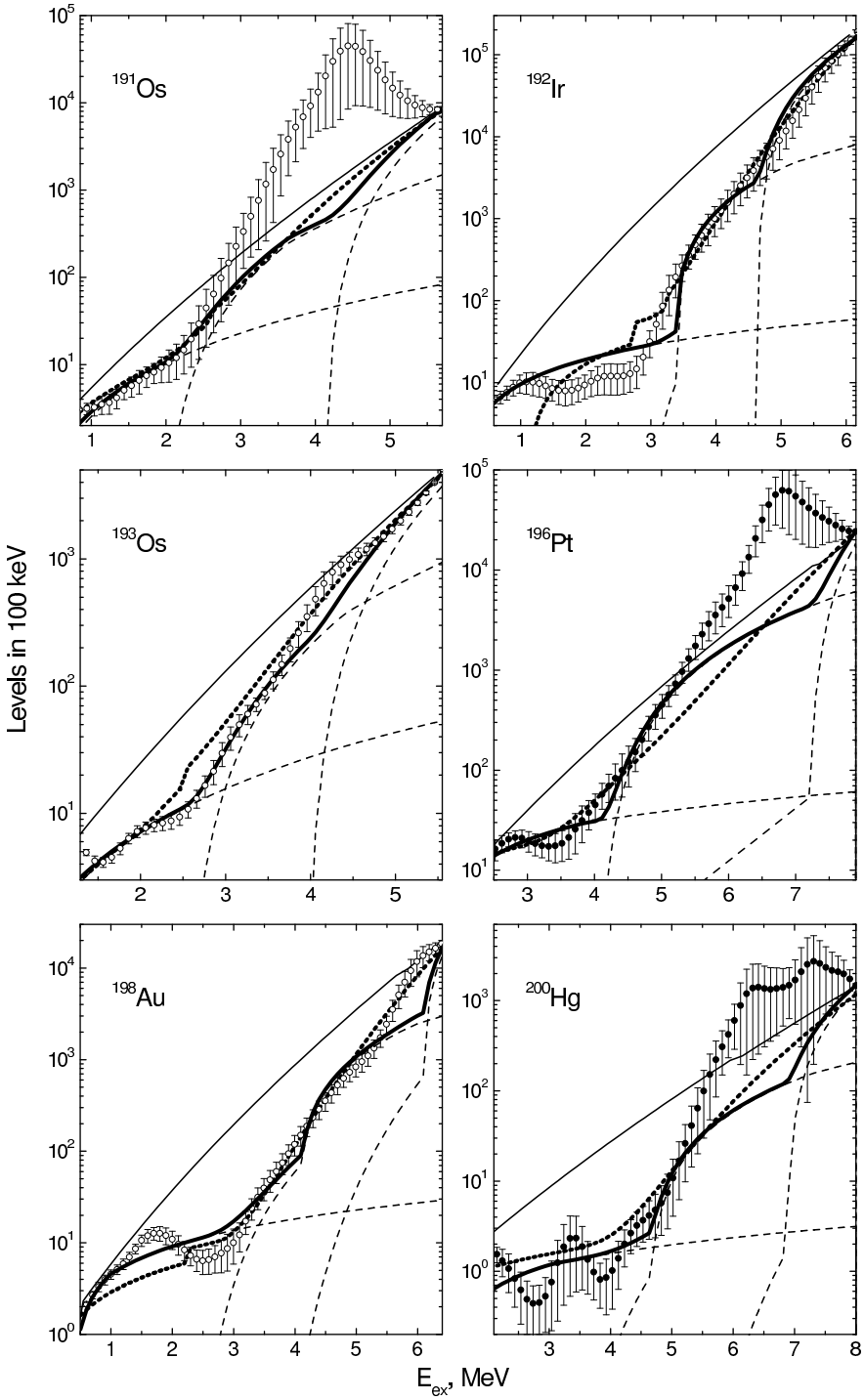


*Fig. 7.* The same as in Fig. 2 for nuclei: $^{191}$Os, $^{192}$Ir, $^{193}$Os, $^{196}$Pt, $^{198}$Au, $^{200}$Hg.

# On the possibility to estimate the n,e-scattering length from structure factors for liquid krypton.

L.V.Mitsyna, V.G.Nikolenko, S.S.Parzhitski, A.B.Popov, G.S.Samosvat

The situation with existing set of experimental values of n,e-scattering length $b_{ne}$ stimulates a search for the new approaches to experiments in order to obtain more reliable estimates of $b_{ne}$. We have demonstrated in [1, 2, 3, 4] the principle possibility to extract the $b_{ne}$ with good accuracy from the structure factor data measured for gas samples of different density for argon-36 and krypton. The proposed approach was grounded on a possibility of separation in measured angular distributions of scattered mono-energetic neutrons of the effects caused by the diffraction (depended on the gas density) and the effects related to the contribution of n,e-scattering (independent from the gas density). In present paper we have attempted to extract the n,e-scattering length from $S(q)$ obtained in [5] for seven liquid samples of krypton having similar densities. Our approach is based on two assumptions:

- The authors of [5] did not make the correction for the n,e –scattering.
- They have properly made corrections for the thermal motion of atoms in liquids.

Therefore the usual expression

$$S(q) = 1 + \frac{nC(q)}{1 - nC(q)}, \qquad (1)$$

where n is the sample density (in $10^{21}\ 1/cm^3$ units), $C(q)$ is the correlation function describing the diffraction effect, was modified to introduce in (1) the n,e-contribution in "nuclear" part (to 1) and in "diffraction" part (to $nC(q)/(1-nC(q))$)

$$S(q) = 1 + Bf(q) + \frac{nC(q)}{1 - nC(q)}[\gamma + Bf(q)]. \qquad (2)$$

Here

$$B = \frac{8\pi a_{coh} b_{ne}}{\sigma_s},$$

$f(q) = \frac{Z}{\sqrt{1 + (\frac{q}{q_0})^2}}$ is the atomic form-factor, $q_0$ is the constant calculated in Hartry's-Fok's approach ,

$$\gamma = \frac{\sigma_{coh}}{\sigma_s}.$$

We have assumed a possibility of the "phenomenological" choice of the correlation function $C(q)$ in the form

$$C(q) = (A_1 + nA_2)\exp(-A_3 q)\sin(\frac{2\pi q}{A_4 + A_5 q} + A_6) \qquad (3)$$

and during the $S(q)$ fitting procedure the values $A_1 - A_6$ are used as free fitted parameters together with $b_{ne}$ and residual normalization coefficient $C_n$. Since we could not describe the $S(q)$ by chosen function (3) with good $\chi^2$ in the region of small $q$ the analysis was restricted to the data region $q \geq 3.5 - 4\ \dot{A}^{-1}$. The MINUIT program was used for fitting procedure. The results of the joint fitting of $S(q)$ for all seven samples in the region $q \geq 4\ \dot{A}^{-1}$ (for 5068 experimental points) are:

$$C_n = 1.0010 \pm 0.0001$$
$$b_{ne} = -(1.39 \pm 0.04) \cdot 10^{-3}\ Fm \qquad \chi^2 = 3822/5068\ . \qquad (4)$$

These results are shown in Fig.1. From this figure one can see that the $S(q)$ data provide a poor information in the region of large $q$ because of their large errors. Therefore the fit was also performed excluding the $S(q)$ values in the region above $q = 14\ \dot{A}^{-1}$. In this case the fitting result was

$$C_n = 1.0016 \pm 0.0002$$
$$b_{ne} = -(1.86 \pm 0.16) \cdot 10^{-3}\ Fm \qquad \chi^2 = 3160/4089\ . \qquad (5)$$

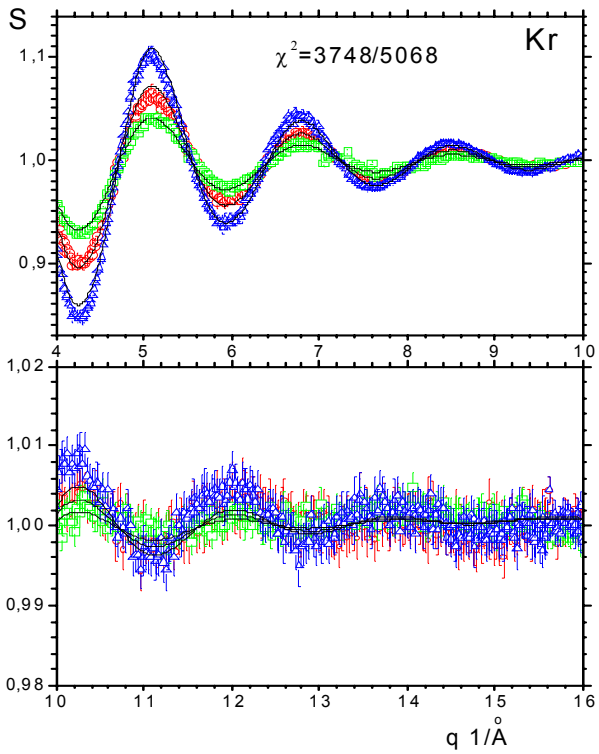


Fig.1. The joint fit of $S(q)$ for seven samples. The data only for three densities $n = 14.57 - 11.86 - 17.01$ are shown. The points – experiment, the curves – fitting result.

Independent fits for three groups of samples of close densities have given results displayed below.

A) n=14.57 – 14.47 – 14.25
$b_{ne} = -(1.37 \pm 0.07) \cdot 10^{-3}\ Fm \quad \chi^2 = 831/2172$
B) n=11.86 – 11.28
$b_{ne} = -(1.19 \pm 0.06) \cdot 10^{-3}\ Fm \quad \chi^2 = 799/1448$
C) n=17.01 – 16.83
$b_{ne} = -(1.63 \pm 0.08) \cdot 10^{-3}\ Fm \quad \chi^2 = 963/1447$

The arithmetic-mean estimate on three groups is equal to

$$b_{ne} = -(1.40 \pm 0.13) \cdot 10^{-3}\ Fm \qquad (6)$$

and agrees with the previous result (4).

In the described method of $b_{ne}$ extraction from $S(q)$ data we actually could not overcome a necessity of taking into account a correction for the effect which masks the n,e-

scattering contribution: the diffraction waves in $S(q)$. These waves exceed by many times at their maxima and minima the contribution from the n,e-scattering. The dependence of the n,e-scattering on $q$ is a monotonous function described by the form-factor $f(q)$. In order to observe a quality of diffraction correction we have extracted the contribution of the n,e-scattering for each sample after fitting by the formula (2) as

$$S_{ne}(q) = S^{\exp}(q) - \{1 - \frac{nC(q)}{1-nC(q)}(q)[\gamma + Bf(q)]\} \ , \qquad (7)$$

assuming that the contribution of $Bf(q)$ term in square brackets is negligible. The errors of $S^{\exp}(q)$ were attributed to these pseudo-experimental values. Fitting $S_{ne}(q)$ was done using the formula

$$S_{ne}(q) = C_n + \frac{8\pi a_{coh}}{\sigma_s} b_{ne} f(q) \ . \qquad (8)$$

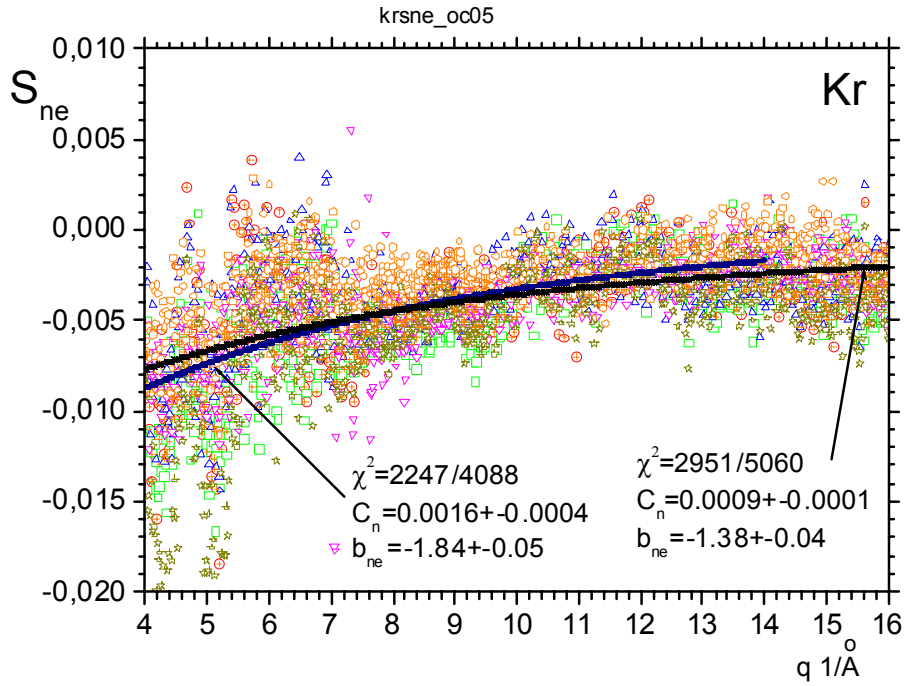


Fig.2. Joint fitting of $S_{ne}(q)$ (errors are not shown) is presented. Two fitted curves over the intervals $q = 4-16\ \dot{A}^{-1}$ and $q = 4-14\ \dot{A}^{-1}$ are shown.

In Fig.2 joint fitting $S_{ne}(q)$ for all seven samples are presented. The following result was obtained

$$\begin{aligned} C_n &= 0.0009 \pm 0.0001 \\ b_{ne} &= -(1.38 \pm 0.04)\cdot 10^{-3}\ Fm \end{aligned} \qquad \chi^2 = 2951/5060 \qquad (9)$$

In Fig.2 the fitting result is also shown when the less informative points with $q > 14\ \dot{A}^{-1}$ were excluded. In this case we obtained

$$\begin{aligned} C_n &= 0.0016 \pm 0.0004 \\ b_{ne} &= -(1.84 \pm 0.05)\cdot 10^{-3}\ Fm \end{aligned} \qquad \chi^2 = 2247/4088 \qquad (10)$$

From the observed point dispersion and the significant difference in the results (9) and (10) one should conclude that the $b_{ne}$ errors are obvious underestimated.

Unfortunately chosen function (3) for the structure factor did not allow to extract "cleanly" the diffraction contribution. Attempts to use other function for $C(q)$ with larger number of free parameters or to fit over two intervals ($\Delta q = 3.5 \div 9$ and $\Delta q = 9 \div 16$ $\dot{A}^{-1}$) did not give a positive results.

**Conclusions.**

The obtained results demonstrate the possibility of extraction of the n,e-scattering length $b_{ne}$ from $S(q)$ data for liquid krypton. The close values (4), (6), (9) in different calculation variants were obtained which reduce to the value

$$b_{ne} \approx -(1.40 \pm 0.10) \cdot 10^{-3} \ Fm .$$

However, it is impossible to guarantee unambiguity of this result as it was mentioned above: we could not completely exclude the diffraction influence; the results (5) and (10) depend on a chosen interval of $q$. Besides a correlation of values $b_{ne}$ and normalization factor $C_n$ was remaining. It is obvious that the higher accuracy of $S(q)$ data is required and it is necessity to achieve a more reliable description of diffraction effects involving for this purpose physical representations about a type of correlation function $C(q)$.

The valuable fact, in our opinion, is that the $S(q)$ data contain the n,e-scattering contribution allowing to extract the n,e-scattering length with a rather good accuracy. The present work indicates an expediency to measure the traditional angular distributions of scattered mono-energetic slow neutrons from which the structure factors for noble gases or liquids are obtained, but such measurements must be corrected for the $b_{ne}$ extraction (analysis one should start with processing of the initial intensities of scattered neutrons).

**References.**


1. L.V.Mitsyna, V.G.Nikolenko, S.S.Parzhitski, A.B.Popov, G.S.Samosvat, JINR Communication, E3-2003-183, Dubna (2003).
2. L.V.Mitsyna, V.G.Nikolenko, A.B.Popov, G.S.Samosvat, JINR Communications P3-2003-232, Дубна (2003).
3. L.V.Mitsyna, V.G.Nikolenko, S.S.Parzhitski, A.B.Popov, G.S.Samosvat, Proceedings ISINN-12, JINR E3-2004-169, 153, Dubna (2004).
4. L.V.Mitsyna, V.G.Nikolenko, S.S.Parzhitski, A.B.Popov, G.S.Samosvat, Eur.Phys.J. **C40**, 473 (2005).
5. H. Fredrikze, J.B. van Tricht, Ad A. van Well, R. Magli, P. Chieux, F. Barocchi, Phys. Rev. Lett. **62**, 2612 (1989).

# INTERACTION OF MICROALGAE *SPIRULINA PLATENSIS* WITH METALS STUDIED BY NAA AND AAS

M.V. Frontasyeva[1], S.S. Pavlov[1], N.G. Aksenova[1], E.I. Kirkesali[1], L.M. Mosulishvili[2], A.I. Khizanishvili[2], A.N. Rcheulishvili[2]

[1]*Frank Laboratory of Neutron Physics, JINR, 141980, Dubna, Russia*
[2]*Institute of Physics of Georgian Academy of Sciences, Tbilisi, Georgia*

Peculiarities of the interaction of the blue-green algae Spirulina platensis (*S. platensis*) with separate metals (Se, Cr, I, Hg) [1] have been studied earlier by epithermal neutron activation analysis (ENAA) at the IBR-2 reactor in the joint experiments with the Georgian biophysicists. Also, a combined impact of two metals (Se and Cr) on the cells of *S. platensis* in the process of their cultivation has been investigated [2]. The present study shows how the nutrient medium loading with several metals influences on the growth of *S. platensis* biomass in the process of its cultivation.

In the first case the Zaroukh nutrient medium in certain concentrations of biogenic metals (Fe (2000 μg/L), Mn (2500 μg/L), Zn (250 μg/L), Co (45 μg/L), Cu (100 μg/L), Ni (50 μg/L)) was introduced simultaneously; in the second case the toxic ones (Pb (1500 μg/L), Cr (200 μg/L), Cd (2000 μg/L), Ag (μg/L)) were introduced. Cultivation with biogenic metals was carried out for 7 days and with toxic elements – for 4 days. Samples of *S. platensis* biomass were taken for analysis every day. Moreover, a globular protein C-phycocyanin (C-PC), which is the most valuable of all the proteins of the microalgae, was extracted by a special technique from the *S. platensis* biomass after 7 and 4 days of the cultivation, respectively.

Content of the studied metals in the obtained samples has been determined by atomic absorption spectroscopy (AAS) using the Beckman-495 spectrometer. The results are given in Fig. 1, where the dynamics of accumulation of biogenic and toxic metals *by S. platensis* is observed.

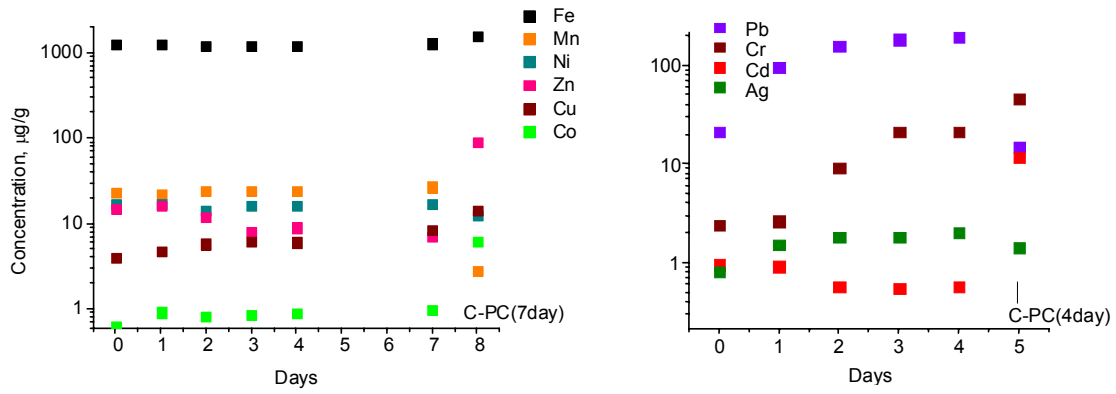


*Figure 1*

As seen from Fig. 1, at the nutrient medium loading with biogenic elements right from the start the biomass accumulates Fe most efficiently, later on its concentration remains practically unchanged. Ni, Mn and Co, which accumulate to a smaller extent, behave in much the same way as Fe. The Cu concentration increases with time, while the Zn concentration decreases. It is known from the literature that Zn and Ni compete for binding sites in macromolecules [3]. Therefore, recrease of the Zn concentration is a consequence of the fact

that Ni occupies binding sites more efficiently. For toxic metals the tendency of growth of concentrations of Pb and Cr is observed. The Cd content from the second day of cultivation decreases. Ag is bound by the cells much more intensively than Cd, though its initial concentration in the solution is by the order of three less than the Cd concentration.

For comparison of concentrations of the studied elements in the *S. platensis* biomass with their concentrations in the C-PC pharmaceuticals, concentrations of these elements for C-PC are shown in Fig. 1 (right graph). As follows from these data, the biogenic elements Fe, Zn, Co and Cu are bound more strong with the C-PC protein than Mn and Ni. As for toxic elements, Cd, Cr and Ag are bound more strong than Pb.

More elaborate multielement study of the behavior of biogenic and toxic elements in C-PC has been obtained by ENAA for the samples irradiated at the nuclear reactor of the Texas University (USA). The results of this study are presented in the Table below.

*Table*

| | **<C-PC(bio)>** | | **<C-PC(tox)>** | |
|---|---|---|---|---|
| | **ppm** | **Abs. error, ppm** | **ppm** | **Abs. error, ppm** |
| **Al** | 46 | 2 | 29 | 2 |
| **Ca** | 315 | 44 | 153 | 25 |
| **Cl** | 222 | 12 | 50 | 4 |
| **Co** | 0.34 | 0.02 | 0.13 | 0.01 |
| **Cr** | 20.1 | 0.7 | 12,8 | 0.4 |
| **Cu** | 7.7 | 0.8 | 35.9 | 1.2 |
| **Fe** | 572 | 15 | 80 | 5 |
| **Hg** | 0.024 | 0.008 | 0.047 | 0.011 |
| **K** | 1963 | 132 | 944 | 70 |
| **Mg** | 40 | 2 | 2.5 | 0.7 |
| **Mn** | 6 | 0.3 | 1.5 | 0.2 |
| **Na** | 1196 | 35 | 693 | 20 |
| **V** | 0.18 | 0.02 | 1.19 | 0.02 |
| **Zn** | 11.5 | 0.6 | 6.3 | 0.3 |

These data allow one to conclude that the content of biogenic elements in the C-PC pharmaceuticals extracted from the biomass grown in the medium with the presence of toxic elements is lower than in the medium with the presence of biogenic elements. This phenomenon could be explained by competition of metals for binding sites at the formation of bonds: metal-protein, metal-DNA protein, *etc*.

## References


1. L.M. Mosulishvili, E.I. Kirkesali, A.I. Belokobilsky, A.I. Khizanishvili, M.V. Frontasyeva, S.S. Pavlov, S.F. Gundorina. Experimental substantiation of the possibility of developing selenium- and iodine-containing pharmaceuticals based on blue-green algae *Spirulina platensis*. *Journal of Pharmaceutical and Biomedical Analysis*, 2002, 30(1), 87-97.
2. A.I. Belokobilsky, E.I. Ginturi, N.E. Kuchava, E.I. Kirkesali, L.M. Mosulishvili, M.V. Frontasyeva, S.S. Pavlov, N.G. Aksenova. Accumulation of selenium and chromium in growth dynamics of *Spirulina platensis*. *Journal of Radioanalytical and Nuclear Chemistry*, Vol. 259, № 1, 2004, p. 65-68.
3. D.R. Williams. Metals, Ligands and Cancer. *Chem. Rev*., 1972, 72, 3, 202-213.

# NAA AND AAS FOR AIR POLLUTION STUDY IN MACEDONIA

L. Barandovski[1], M.V. Frontasyeva[2], S.S. Pavlov[2],
T. Stafilov[1], V. Urumov[1]

[1]*Sts. Cyril and Methodius University, Skopje, Macedonia*
[2]*Joint Institute for Nuclear Research, Dubna, Russia*

For the first time the moss biomonitoring technique was applied to air pollution study over the entire territory of the Republic of Macedonia, in the central part of the Balkan Peninsula. This study was carried out in the framework of the International Cooperative Programme on Effects of Air Pollution on Natural Vegetation and Crops coordinated by the UNECE ICP Vegetation [1].

Mountainous and hilly relief of Macedonia, in spite of arid climate, is favorable for collecting terrestrial moss *Hypnum Cupressiforme*, *Campothecium lutescens*, and *Homolothecium Sericium*. Moss samples were collected in September-October 2002 in accordance with the sampling strategy of the European moss survey program. The sampling network included 73 sites evenly distributed over the territory of the country of 25713 sq.km. A total of 44 elements Na, Mg, Al, Cl, K, Ca, Sc, Ti, V, Cr, Mn, Fe, Co, Ni, Zn, Ga, As, Se, Br, Rb, Sr, Mo, Ag, Cd, In, Sb, I, Cs ,Ba, La, Ce, Nd, Sm, Eu, Tb, Dy, Yb, Hf, Ta, W, Au, Hg, Th, and U were determined by two complementary analytical techniques – INAA using epithermal activation at pulsed fast reactor IBR-2, FLNP JINR, Dubna, Russia, and AAS in Sts. Cyril and Methodius University, Skopje, Macedonia [2]. The large concentration range – from 10 000 ppm for Al and K to 0.001 ppm for some rare earths – was covered.

Principal component analysis distinguished among the nine factors some pointing toward natural crust, marine, and vegetation components. The other six factors reflect anthropogenic origin of trace element deposition in the Macedonian moss samples: ferrous and non-ferrous industries, oil refinery, fertilizer production and central heating stations.

Four areas are experiencing environmental stress: Veles, Skopje, Tetovo and Kavadarci-Negotino, whereas agricultural south, south-west and south-east show median European values for most of heavy metals and other element-pollutants. GIS technology (geographic information system) is used for constructing black-and-white maps based on factor scores along with colored maps of the distribution of some relevant elements for these factors over the investigated territory. Example of geographical distribution of some elements relevant to the industrial factor 2 (Ni, Zn, Se, Ag, Cd, In, Sb, Pb) is given in Fig. 1. This factor appears to be connected with the lead-zinc smelter (Pb, Zn, Cd, Sb) in Veles and ferro-nickel smelting plant (Ni and Ag) in Kavadarci. It is is also dominant further along the valley of the river Vardar flowing from Skopje toward Veles and continuing south-eastwards toward Greece. Along the river there is a highway connecting Serbia in the North with Greece in the South. Influence of the exhaust gases from cars are more present in the cities, in Skopje in particular where the concentration of cars is greatest. Indium and selenium are present practically everywhere.

Particular interest represent data on atmospheric deposition patterns of uranium in moss in the location of the uranium deposits in the Republic Macedonia (soil data) [3]. Distribution of uranium concentration in moss and soil over the examined territory is shown in Fig. 2. The appearance of the observed anomalies can be explained by the presence of the uranium minerals in some geochemical regions of Macedonia. Thus, their appearance in the western part of the country (near the city of Bitola) is due to the combustion of large amounts of coal (about 6 million tons per year) [4] in the thermo-electrical power plant in Bitola with

an air pollution from fly ash from using lignite as a fuel [5]. It should be mentioned that in the coal locality of Suvodol significant uranium minerals (plehblenda) are present [3].

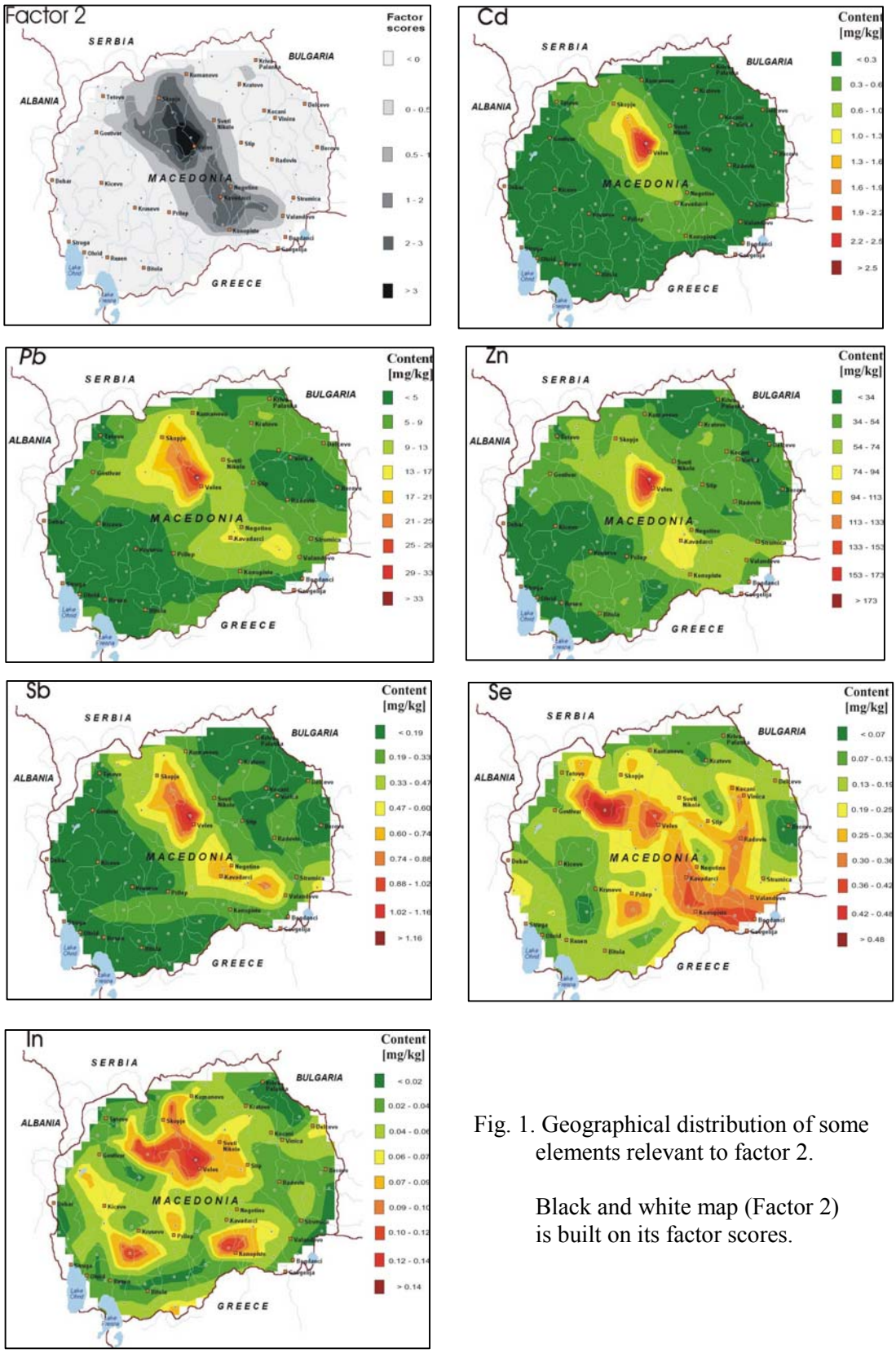


Fig. 1. Geographical distribution of some elements relevant to factor 2.

Black and white map (Factor 2) is built on its factor scores.

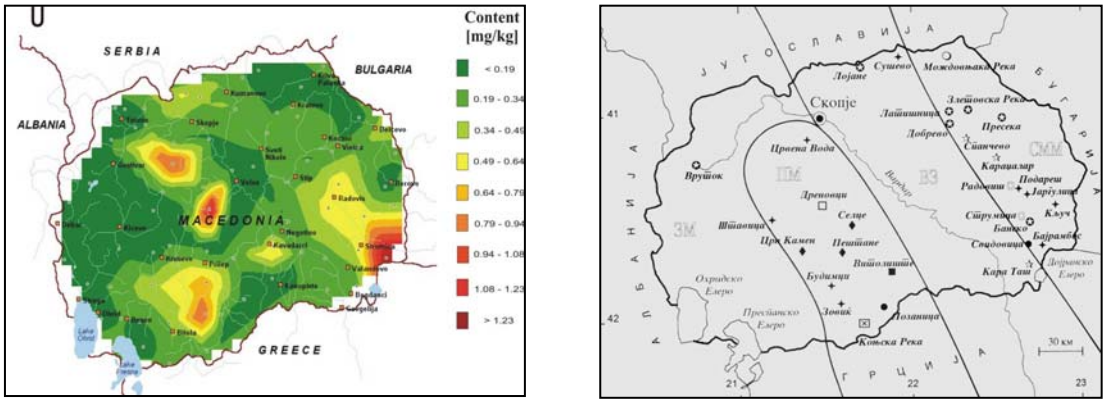


Fig. 2. Comparison of atmospheric deposition patterns determined by the moss technique and the location of the uranium deposits in Macedonia (soil data) [3].

Minerals of uranium, especially plehblenda, are very soft ones and easily could blown up into the atmosphere with dust to be later accumulated in moss growing in the surrounding area with dry and wet atmospheric depositions.

Also, the appearance of the uranium anomalies in the region of the city of Strumica (south-eastern part of the country) could be explained by the presence of significant amount of uranium minerals in the granites deposit in the geological structure of this region [3]. It is important to notify that in this region the exploitation of albitic granites (with a relatively high content of U) is taking place. During the process of drilling and milling of the ore the considerable amount of dust particles are blown into the environment.

**Acknowledgement**

Authors express their gratitude to Prof. B. Boev for discussion of the results on the uranium distribution in the Republic of Macedonia.

**References**

1. European Atlas: Heavy Metals in European Mosses: 2000/2001 Survey, UNECE ICP Vegetation. Editors: A. Buse, D. Norris, H. Harmens, P. Buker, T. Ashenden and G. Mills. Centre for Ecology & Hydrology, University of Wales Bangor, United Kingdom, March 2003, pp.45
2. L. Barandovski, M. Cekova, M.V. Frontasyeva, S.S. Pavlov, T. Stafilov, E. Steinnes, V. Urumov. Biomonitoring of atmospheric metal deposition in the Republic of Macedonia. Proceedings of the 3rd International Workshop on the Project "Anthropogenic effects on the human environment in the tertiary basins in the Mediterranean. Edts. B. Boev and T. Serafimovski, Stip, 2005, p. 5-16.
3. P. Lazarov and T. Serafimovski. Ore deposits and occurrences of energy raw materials in Republic of Macedonia, Faculty of Mining and Geology, Stip, 1997, pp. 89-91 (in Macedonian).
4. Macedonia's First National Communication Under the United Nations Framework Convention on Climate Change, Skopje, 2003, p. 31.
5. S.E. Manahan. Environmental Chemistry, Seventh Edition, Lewis Publishers, Boca Raton, Florida, 2000, p. 318.

# 5. PUBLICATIONS

## CONDENSED MATTER PHYSICS

### Diffraction


1. Aksenov V.L., Efimov V.V., Efimova E.A., Kovalev Yu.S., Mavrin B.N., Sikolenko V.V., Tiutiunnikov S.I., Shternberg A.R. Study of the influence of high-current pulsed electron beam on the CTSL 8/65/35 relaxor using the laser scanning confocal microscopy. Particles and nuclei letters, V.2, №1 [124]. p. 96-102 (2005). (in Russian).
2. Babushkina N.A., Chistotina E.A., Bobrikov I.A., Balagurov A.M., Pomjakushin V.Yu. , Kurbakov A.I., Trunov V.A., Gorbenko O.Yu., Kaul A.R., Kugel K.I. "The effect of oxygen isotope substitution on the phase diagram of nearly half-doped $R_{1-x}Sr_xMnO_3$ manganites (R=Sm, NdTb, NdEu)" J. of Phys.: Condensed Matter, 2005, v. 17, pp.1975 - 1984.
3. Balagurov A.M. "High resolution Fourier diffraction at the IBR-2 reactor" Neutron News, 2005, v.16 (3), pp.8-12.
4. Balagurov A.M., Bobrikov I.A., Pomjakushin V.Yu., Sheptyakov D.V. , Babushkina N.A., Gorbenko O.Yu., Kaul A.R. "Magnetostructural Phase Separation and Giant Isotope Effect in $R_{0.5}Sr_{0.5}MnO_3$" JETP Letters, 2005, v.82, pp.594-598.
5. Babushkina N.A., Chistotina E.A., Balagurov A.M., Pomjakushin V.Yu. , Gorbenko O.Yu., Kaul A.R., Kartavtseva M.S. "Isotope effect and cation disorder in manganites" accepted for JMMM, 2005.
6. Bikkulova N.N., Asylguzhina G.N., Skomorokhov A.N., Yadrovskiy E.L., Beskrovniy A.I., Stepanov Yu.M. Crystalline structure and ion transfer in AgCuSe. 2005. Accepted for publication in Izvestia RAN. (in Russian).
7. Bushmeleva S.N. , Pomjakushin V.Yu., Pomjakushina E.V. , Sheptyakov D.V. , Balagurov A.M. "Neutron diffraction evidence for band ferromagnetism in $SrRuO_3$" accepted for JMMM, October-2005.
8. Golosova N.O., Kozlenko D.P. Voronin V.I., Glazkov V.P., Savenko B.N. Influence of high pressure on crystalline and magnetic structure of cobaltite $La_{0.7}Sr_{0.3}CoO_3$, Fizika tverdogo tela 48, №1 p. 90-94, 2006. (in Russian).
9. Gorbenko O.Yu., Melnikov O.V., Kaul A.R., Balagurov A.M., Bushmeleva S.N., Koroleva L.I., Demin R.V. "Solid solutions $La_{1-x}Ag_yMnO_{3+\delta}$: evidence for silver doping in the A-sublattice of the perovskite manganites". Materials Science and Engineering B, 2005, v.116 (1), pp. 64-70.
10. Guskos N., Beskrovnyy A., Typek J., Ryabova N.Yu., Blonska-Tabero A., Kurzawa M., Maryniak M. Neutron diffraction study of $Zn_3Fe_4V_6O_{24}$. Journal of alloys and compounds 391 (2005) 20-25.
11. Dokukin M.E., Perov N.S., Dokukin E.B., Beskrovnyi A.I., Zaichenko S.G., Changes in the short-range order and magnetic properties of amorphous magnetic metal alloy $Fe_{78}Cu_1Nb_4B_{3.5}Si_{13.5}$, Fallowing cryogenic treatment. Phisica B 368 (2005) 267-272.
12. Efimov V.V., Efimova E.A., Khasanov S.S., Kovalev Y.S., Mavrin B.N., Pogosov A.O., Sternberg A., Tiutiunnikov S.I. / Mechanism of pulsed electron irradiation of the PLZT X/65/35 ceramics // Physics Status Solidi 2, 449 (2005).
13. Efimov V.V., Efimova E.A., Kochubey D.I., Kriventsov V.V., Kuzmin A., Sikolenko V.V., Simkin V.G., Troyanchuk I.O., Tiutiunnikov S.I. Study of $La_{1-x}Sr_xCoO_3$ (x = 0.0 ÷ 0.5) by X-ray spectroscopy of absorption and neutron diffraction. Journal "Surface. X-ray, synchrotron and neutron studies", in press (2005). (in Russian).
14. Efimov V.V., Efimova E.A., Khasanov S.S., Kochubey D.I., Kriventsov V.V., Kuzmin A., Sikolenko V., Shmakov A.N., Tiutiunnikov S.I., Troyanchuk I.O. Journal of Physics and Chemistry of Solids 2005, in press.
15. Efimov V.V., Efimova E.A., Iakoubovskii K., Khasanov S., Kochubey D.I., Kriventsov V.V., Kuzmin A., Mavrin B.N., Sakharov M., Sikolenko V., Shmakov A.N., Tiutiunnikov S.I. // EXAFS, X-ray diffraction and Raman studies of $(Pb_{1-x}Lax)(Zr0.65Ti0.35)O3$ (x = 0.04 and 0.09) ceramics irradiated by high-current pulsed electron beam // Journal of Physics and Chemistry of Solids 2005, in press.
16. Kozlenko D.P., Kichanov S.E., Voronin V.I., Savenko B.N., Glazkov V.P., Kiseleva E.A., Proskurnina N.V. Pressure induced antiferromagnetism in manganite $La_{0.75}Ca_{0.25}MnO_3$", Letters to JETP, V. 82, № 7, p. 501-505 (2005). (in Russian).
17. Kozlenko D.P., Kichanov S.E., Lee S., Park J.G., Glazkov V.P., Savenko B.N. Influence of high pressure on crystalline and magnetic structures of the frustrated antiferromagnetic $YMnO_3$", Letters to JETP, v. 82, № 4, p. 212-216 (2005). (in Russian).
18. Kozlenko D.P., Savenko B.N., Glazkov V.P., Somenkov V.A. "Neutron Scattering Investigations of Structure and Dynamics of Materials Under High Pressure at IBR-2 Pulsed Reactor", Neutron News 16, № 3, pp. 13-15 (2005).
19. Kozlenko D.P., Vonsitsky Ya.V., Glazkov V.P., Kichanov S.E., Navrochik V., Savenko B.N. Study of structural changes in pyridine nitrate under the action of low temperatures and high pressures, Crystallography, v. 50, № 1, p. 84-90 (2005). (in Russian).
20. Orlova A.I., Koryttzeva A.K., Lipatova Ye.V., Zharinova M.V., Trubach I.G., Evseeva Yu.V., Buchirina N.V., Kazantsev G.N., Samoilov S.G., Beskrovny A.I.. «New NZP-based phosphates with low and controlled thermal expansion».// Journal of Materials science letters 2005 № 40 P. 2741-2743.

21. Orlova A.I., Orlova V.A., Beskrovniy A.I., Trubach I.G., Kurazhkovskaia V.S. Synthesis and structural study of phosphates $K_2Mg_{0.5}Zr_{1.5}(PO_4)_3$, $Rb_2Mg_{0.5}Zr_{1.5}(PO_4)_3$ and $Cs_2Mg_{0.5}Zr_{1.5}(PO_4)_3$ with the structure of langbeinite mineral // Crystallography. 2005. v. 50. № 5. p. 804 – 810. (in Russian).
22. Orlova A.I., Orlova V.A., Buchirin A.V., Beskrovniy A.I., Kurazhkovskaia V.S. Cesium and its analogues rubidium, potassium in rhombohedral (of $NaZr_2(PO_4)_3$ type) and cubic (of langbeinite type) phosphates. 1. Crystal chemical investigations // Radiochemistry. 2005. V.47. № 3. p. 203-212. (in Russian).
23. Orlova A.I., Orlova V.A., Buchirin A.V., Korchenkin K.K., Beskrovniy A.I., Demarin V.T. Cesium and its analogues rubidium, potassium in rhombohedral (of $NaZr_2(PO_4)_3$ type) and cubic (of langbeinite type) phosphates. 2. Properties: behavior at heating, in water solutions and in salt melts // Radiochemistry. 2005. V. 47. № 3. p. 213-218. (in Russian).
24. Sumin V.V., Papushkin I.V. "Investigation of steels with nitrogen by thermal neutron scattering" Atomic Science and Technique: New Materials. 2004, т. 2, с. 367-376.
25. Vasilovskiy S.G., Beskrovnyi A.I., Sikolenko V.V., Aleksandrov K.S., Flerov I.N., Tressaud A., Belushkin A.V. and Balagurov A.M. Structural study of Rb2KFeF6 elpasolite by neutron diffraction method. 2005 accepted in phys. stat. sol. a.

## Textures and stresses

1. Balagurov A.M., Bokuchava G.D., Kuzmin E.S., Tamonov A.V., Zhuk V.V. "Neutron RTOF diffractometer FSD for residual stress investigation" Zeitschrift für Kristallographie, 2005, accepted for publication.
2. Balagurov A.M., Nikitin A.N., Locajicek T., Pros Z., Klima K., Vasin R.V., Papushkin I.V., Subbotin V.V., Sumin V.V. Neutron diffraction and ultrasonic measurements of elastic anisotropy of reactor graphite under uniaxial and hydrostatic loading. Submitted to Acta Geodynamica et Geomaterialia. 2005.
3. Frischbutter A., Ivankina T.I., Kern H., Nikitin A.N., Scheffzük Ch., Ullemeyer K., Walther K. Strain and texture measurements on geological samples at IBR-2 (Dubna). Physics of elementary particles and atomic nucleus. 2005 (Submitted for publication).
4. Frischbutter A., Scheffzuek Ch. & Walther K. Diffraktionsexperimente zur intrakristallinen Strainmessung mit Neutronen- und Synchrotronstrahlung an geologischen Proben. Sitzungsberichte der Leibniz-Sozietät 70, (2004) 89-108.
5. Ivankina T.I., Kern H.M. and Nikitin A.N. Directional dependence of P- and S-wave propagation and polarization in foliated rocks from the Kola superdeep well: Evidence from laboratory measurements and calculations based on TOF neutron diffraction. Tectonophysics, 2005, 407, 25-42.
6. Ivankina T.I., Klima K., Kulakovskiy A.L., Locajicek T., Morozov Yu.A., Nikitin A.N., Pros Z., Study of structure of geospace of the Kola superdeep well by ultrasonic, neutron diffraction and microstructure analysis of rocks. In Proc. «Geological-geophysical investigations in IPE RAS. 2004-2005». Publishing house of IPE RAS. 2005. (in Russian).
7. Nikitin A.N., Vasin R.N., Balagurov A.M., Sobolev G.A., Ponomarev A.V. Investigation of thermal and deformation properties of quarzite in the temperature region of polymorphous $\alpha$-$\beta$ transition by neutron diffractometry and acoustic emission. Letters to journal «Physics of elementary particles and atomic nucleus», 2005 (Accepted for publication). (in Russian).
8. Priesmeyer H.G., Bokuchava G. "Plastic Deformation in Structural Materials, investigated in situ by Neutrons and Positrons" Applied Radiation and Isotopes, 2005, accepted for publication.
9. Priesmeyer H.G., Bokuchava G. "In-situ Investigation of Plastic Deformation by Neutrons and Positrons – a Novel Approach" J. of Neutron Research, 2004, v. 12, pp. 159-163.
10. Prokoshkin S.D., Korotitskii A.V., Tamonov A.V., Khmelevskaya I.Yu. and Kartseva E.A. "In situ Investigation of the Crystal Lattice of Martensite in Binary Ti–Ni Alloys As Functions of Temperature and Stress Using the Time-of-Flight Neutron-Diffraction Method" The Physics of Metals and Metallography (Fizika metallov i metallovedenie) v. 98, p. 37, 2004.
11. Scheffzuek Ch., Walther K., Frischbutter A. & Naumann R., (2005): Residual strain and texture of an anhydrite-dolomite-specimen, sampled in the Piora-syncline (Central Switzerland). J. Struct. Geol. (Submitted for publication).
12. Scheffzuek Ch., Siegesmund S., Hoffman A. & Nikolayev D.I., (2005): Spatial and orientation dependence of internal strain in marble. Geol. Soc. London, Spec. Pub. (Submitted for publication).
13. Tamonov A.V., Sumin V.V., Balagurov A.M., Bokuchava G.D. "Studies of internal stresses in materials important for atomic science and technique" Atomic Science and Technique: New Materials. 2004, v. 2, p. 359-366.
14. Tamonov A.V., Bokuchava G.D., Shamsutdinov N.R., Schreiber J. "W/Cu composites investigation by neutron diffraction" Atomic Science and Technique: New Materials. 2004, v. 2, p. 376-382.
15. Taran Yu.V., Daymond M.R., Eifler D., Nebel T., Schreiber J. "Investigation of mechanical features of low cycle fatigue specimens of austenitic steel AISI type 321 under applied load by neutron diffraction stress analysis"

Materials Science and Technology, 2005, v.21, pp.35-45.
16. Ullemeyer K., Siegesmund S., Rasolofosaon P.N.J. & Behrmann J. H. (2005): Experimental and texture-derived P-wave anisotropy of principal rocks from the TRANSALP traverse: An aid for the interpretation of seismic field data. Tectonophysics (in press).
17. Vasin R.V., Locajicek T., Nikitin A.N., Rudaev V. Acoustic emission of rocks influenced by temperature gradients. Acta Geodynamica et Geomaterialia. 2005 (Submitted for publication).

## Inelastic neutron scattering

1. Antonov V.E., Beskrovnyj A.I., Fedotov V.K., Khasanov S.S., Sakharov M.K., Sashin I.L., Tkacz M. "Crystal structure and lattice dynamics of chromium hydrides". III Workshop of Investigations at the IBR-2 Reactor, Dubna, 2005
2. Blagoveshchenskii N.M., Morozov V.A., Novikov A.G., Savostin D.V., Savostin V.V., Shimkevich A.L. Structure of Liquid Na-Pb Alloys: Neutron-Diffraction Investigation. J. Non-Cryst. Solids, 2005 (to be published).
3. Blagoveshchenskii N.M., Morozov V.A., Novikov A.G., Savostin V.V., Shimkevich A.L., Shimkevich I.Yu. Microscopic structure of liquid lead–potassium alloys: Neutron-diffraction and molecular-dynamics investigation. Physica B, 364(2005)255.
4. Blagoveshchenskii N.M., Morozov V.A., Novikov A.G., Savostin V.V., Savostin D.V., Shimkevich A.L. Microscopic structure of liquid two-component alloy studied by neutron diffraction. Surface, 2005 (in print). (in Russian).
5. Blagoveshchenskii N.M., Morozov V.A., Novikov A.G., Savostin V.V., Shimkevich A.L. Investigation of spectrum of elementary excitations of liquid lead. Surface, 2005 (in print). (in Russian).
6. Dubovkiy O.A. Dynamic surfing – mechanism of diffusion mass carry of light atoms in constructional materials by soliton waves of oscillations of the crystalline lattices of heavy nuclei. Preprint IPPE – 3037, p.22 (2005). (in Russian).
7. Dubovskiy O.A. Analogue of the Migdal-Kon peculiarity in polariton spectrum of a two-dimensional crystal. Letters to JETP. v.81, № 10, p.603, (2005). (in Russian).
8. Dubovskiy O.A. Non-linear microdynamics of the high-amplitude oscillations and of the explosive rupture of crystalline materials. Preprint IPPE – 3056. p.20 (2005). (in Russian).
9. Dubovskiy O.A., Orlov A.V., Semenov V.A. Non-linear oscillations of crystalline atomic lattices of nuclear reactor materials near the stability threshold. Proceedings of the regional competition of scientific projects. RFBR, Publishing house "EIDAS", Kaluga, 2005, № 8, p.178. (in Russian).
10. Holderna-Natkaniec K., Jurga K., Natkaniec I., Nowak D., Szyczewski A. "Molecular dynamics of ethisterone by $^1$H NMR, IINS and quantum mechanical calculations". Chemical Physics, 37 (2005) 178-187.
11. Holderna-Natkaniec K., Natkaniec I., Jurga K., Nowak D., Szyczewski A., "Internal dynamics of norethisterone by IINS, NMR and QC methods", Solid state Phenomena, 2005 (in print).
12. Holderna-Natkaniec K., Natkaniec I., Kasperkowiak W. "Vibrational spectra of 6-benzylaminopurine by IINS and DFT methods", in: "Neutron Scattering and Complementary Methods in Investagation of Condensed Phase", Vol. 2, University of Podlasie Publishing House, Siedlce 2005, Monograph No 60, pp. 67-78.
13. Lisichkin Yu., Saharova L., Martí J., Novikov A. The temperature dependence of the generalized frequency distribution of water molecules: comparison of the neutron experiment and molecular dynamics simulation. Molecular simulation. (In press).
14. Loose A., Melnyk G., Zink N., Wozniak K., Dominiak P., Smirnov L. S., Pawlukojc A., Shuvalov L. A. "Refinement of hydrogen positions in (NH4)2SeO4", Preprint of JINR, № E14-2005-1, Dubna (2005).
15. Loose A., Smirnov L.S., Dolbinina V.V., Yakovleva L.M., Grebenev V.V. "The refinement of hydrogen positions in phase II of β-$LiNH_4SO_4$". Preprint JINR, E14-2005-133, Dubna, 2005.
16. Lushnikov S.G., Svanidze A.V., Sashin I.L. Density function of oscillatory states of lysozyme. Letters to JETP, v.82, № 1,(2005) p.31-35. (in Russian).
17. Migdal-Mikuli A., Mikuli E., Hetmanczyk L., Natkaniec I., Scisinska E., Sciesinski J., Wobel S. „Phase transitions, molecular motions, structural changes and low frequency vibrations in $[Cu(NH_3)_5](ClO_4)_2$", Chem.Phys, 317 (2005) 188-197.
18. Mikuli E., Migdal-Mikuli A., Hetmanczyk L., Natkaniec I. „Phase transitions and molecular motions in $[Zn(NH_3)_4](ClO_4)_2$ studied by infrared spectroscopy, X-ray powder diffraction and neutron scattering methods", in: "Neutron Scattering and Complementary Methods in Investagation of Condensed Phase", Vol. 2, University of Podlasie Publishing House, Siedlce 2005, Monograph No 60, pp. 43-53.

19. Morozov S.I. Investigation of the dynamics of oxygen atoms in the implantation system Ta-O". FTT, in print, reg. № 161. (in Russian).
20. Morozov S.I., Kazarnikov V.V., Kalinin I.V., Rudenko V.A., Primakov N.G., Sashin I.L. Hydrogen oscillations in the implantation phases of $Me_2(N,C)H_x$. Proceedings of the regional competition of scientific projects in the field of natural sciences. Publishing house "EIDAS", Kaluga, 2005, № 8, p.246. (in Russian).
21. Morozov S.I., Primakov N.G. Dynamics and localization of hydrogen in $TaO_{0.03}H_{0.01}$". FTT, 2005, v.47, № 7, p.1162-1164. (in Russian).
22. Natkaniec I., Holderna-Natkaniec K., Majerz I., Parlinski K. "Neutron spectroscopy of deuterated substitutes and DFT modeling vibrational spectra of methanol clusters", Chem.Phys, 317 (2005) 171-177.
23. Natkaniec I., Smirnov L.S., Shuvalov L.A. "Neutron scattering study of the dynamics of ammonium in different phases of halides of $K_{1-x}(NH_4)_xHal$ mixed Crystals", Crystallography Reports, Vol. 50, No. 2 (2005) 254-261. Translated from Kristallografiya, Vol. 50, No. 2 (2005) 287-294.
24. Pawlukojć A., Leciejewicz J., Ramirez-Cuesta A. J., Nowicka-Scheibe J. "L-cysteine: Neutron spectroscopy, Raman, IR and ab initio study", Spectrochimica Acta Part A. 61, (2005) 2474-2481.
25. Pawlukojć A., Natkaniec I., Bator G., Sobczyk L., Grech E., Nowicka-Scheibe J. "Low frequency internal modes of 1,2,4,5-tetramethylbenzene, tetramethylpyrazine and tetramethyl-1,4-benzoquinone. INS, Raman, IR and theoretical DFT studies", Spectrochimica Acta Part A, (in press).
26. Pawlukojć A., Sobczyk L. "Application of inelastic neutron scattering (INS) in studies on low frequency molecular vibration", Trends in Applied Spectroscopy, 5, (2004) 117-136.
27. Prager M., Grimm H., Natkaniec I. „Rotational tunneling of methyl groups in low temperature phases of mesitylene: potentials and structural implications". Phys. Chem. Chem. Phys., 7 (2005) 2587-2593.
28. Prager M., Pawlukojć A., Sobczyk L., Grech E., Grimm H. "Inelastic neutron scattering study of tetramethylpyrazine in the complex with chloranilic acid." J. Phys.: Condens. Matter. 17 (2005) 5725-5739.
29. Sawka-Dobrowolska W., Bator G., Sobczyk L., Grech E., Nowicka-Scheibe J. and Pawlukojć A. "Structure and vibrational spectra of 1:1 chloranilic acid (CLA)-tetramethylpyrazine (TMP) complex", Struct. Chem. 16, (2005) 281-286.
30. Skomorokhov A.N., Trots D.M., Knapp M., Bickulova N.N. and Fuess H. Structural behaviour of $\beta$-$Cu_{2-\delta}Se$ ($\delta$ = 0, 0.15, 0.25) in dependence on temperature studied by synchrotron powder diffraction. Submitted to Journal of Alloys and Compounds.
31. Skomorokhov A.N., Trots D.M., Semenov V.A., Bickulova N.N., Yadrovskiy E.L., Stepanov Yu.M., Knapp M., and Fuess H. Investigations of superionic conductor AgCuSe by inelastic neutron scattering. Submitted to journal «SURFACE». (in Russian).
32. Smirnov L.S., Natkaniec I., Kazimirov V.Yu., Dolbinina V.V., Yakovleva L.M., Shuvalov L.A. "The dynamics of ammonium in phases of mixed crystals $K_{1-x}(NH_4)_xBr$: Inelastic neutron scattering". Surface, X-ray, synchrotron and neutron studies, № 1, (2005) 3-11. (in Russian).
33. Smirnov L.S., Natkaniec I., Shuvalov L.A., Dolbinina V.V. Study of the dynamics of ammonium ions in mixed crystals $K_{1-x}(NH_4)_xCl$ by neutron scattering. Surface, X-ray, synchrotron and neutron studies, № 5 (2005) 5-11. (in Russian).
34. Smirnov L.S., Shuvalov L.A., Martiniec Sarrion M.L., Mestres L., Herrais M. Study of behavior of ammonium ion in mixed crystals $\beta$-$LiRb_{1-x}(NH_4)_xSO_4$ ($0.50 \leq x \leq 1.0$), Kristallografiya, 2005, vol. 50 (3), p. 514-524. (in Russian).
35. Titov A.N., Titova S.G., Skomorokhov A.N., Semenov V.A. Influence of Fe intercalation on phonon density of states of $TiSe_2$, FLNP Annual Report 2004, Dubna 2005, http://nfdfn.jinr.ru/reports/2004/4.pdf.
36. Krawczyk A., Mayer J., Natkaniec I., Nowina-Konopka M., Pawlukojć A., Steinsvoll O., Janik J.A. "Quasi-elastic (QENS) and inelastic neutron scattering (INS) on hexamethylbenzene." Physica B, 362, (2005) 271-277.
37. Sawka-Dobrowolska W., Bator G., Sobczyk L., Pawlukojć A., Ptasiewicz-Bąk H., Rundlöf H., Krawczyk J., Nowina-Konopka M., Jagielski P., Janik J., Prager M., Steinsvoll O., Grech E., Nowicka-Scheibe J. "Elastic, quasielastic and inelastic neutron scattering studies on the charge-transfer hexamethylbenzene-tetracyanoquinodimethane complex", J. Chem. Phys., 123 (2005) 124305.

## Reflectometry, polarized neutrons

1. Aksenov V.L. and Nikitenko Yu.V. Polarized Neutron Reflectometry at IBR-2, Neutron News, vol. 16, Issue 3, 2005, pp.19-23.

2. Aksenov V.L., Jernenkov K.N., Khaidukov Yu.N., Nikitenko Yu.V., Petrenko A.V., Proglyado V.V., Andersson G., Wappling R. Interplay between superconductivity and ferromagnetism in Fe/V multilayered structure studied by polarized neutron reflectometry, Physica B 356 (2005) 9-13.
3. Dokukin M.E., Perov N.S., Dokukin E.B., Beskrovnyi A.I., Zaichenko S.G. Changes in the short-range order and magnetic properties of the amorphous magnetic metal alloy Fe78Cu1Nb4B3.5Si13.5 following cryogenic treatment, Physica B 368/1-4 (2005) 267.
4. Jernenkov M., Lauter H., Lauter-Pasyuk V., Toperverg B., Klimko S., Gahler R. Angular encoding with Larmor precession, Physica B 357 (2005) 94-97.
5. Toperverg B.P., Lauter H.J., Lauter-Pasyuk V.V. Larmor pseudo-precession of neutron polarization at reflection, Physica B 356 (2005) 1-8.

## Small-angle neutron scattering

1. Aksenov V.L., Avdeev M.V., Tropin T.V., Priezzhev V.B., Schmelzer J.W.P. Model of aggregation in fullerene solutions, In Electronic Properties of Molecular Nanostructures-2005, edited by H. Kuzmany et al., AIP Conference Proceedings, pp. 37-40.
2. Aksenov V.L., Avdeev M.V., Tropin T.V., Priezzhev V.B., Schmelzer J.W.P. “Fullerene cluster formation in carbon disulfide and toluene”, Fullerenes, Nanotubes and Carbon Nanoclusters, accepted (2005).
3. Aksenov V.L., Avdeev M.V., Tropin T.V., Priezzhev V.B., Schmelzer J.W.P. “Cluster growth and dissolution of fullerenes in non-polar solvents”, Journal of Molecular Liquids accepted (2005).
4. Aksenov V.L., Tropin T.V., Avdeev M.V., Priezzhev V.B., Schmelzer J.W.P. «Kinetics of cluster growth in fullerene molecular solutions», Phys. Particles Nuclei, in press.
5. Aksenov V.L., Avdeev M.V., Tropin T.V., Korobov M.V., Kozhemyakina N.V., Avramenko N.V., Rosta L. Formation of fullerene clusters in the system $C_{60}$/NMP/water by SANS, Physica B, accepted (2005).
6. Avdeev M.V., Tropin T.V., Aksenov V.L., Rosta L., Garamus V.M., Rozhkova N.N. “Pore structures in shungites as revealed by small-angle neutron scattering”, Carbon, accepted (2005).
7. Avdeev M.V., Tropin T.V., Aksenov V.L. Study of cluster state of fullerenes in solutions: current status and prospects. In Proceedings of the International Workshop "Molecular Simulation Studies in Material and Biological Sciences" Ed. Kh. T. Kholmurodov, Nova Publishers: 2005.
8. Avdeev M.V., Aksenov V.L., Balasoiu M., Garamus V.M., Schreyer A., Török Gy., Rosta L., Bica D., Vékás L. «Comparative analysis of the structure of ferrofluids based on polar carriers by small-angle neutron scattering» J. Interface Colloid. Sci., in press (2005).
9. Andreeva A. S., Fomenkov A. I., Islamov A. Kh., Kuklin A. I., Filippova O. E., Khokhlov A. R., Hydrophobic Aggregation in a Hydrophobized Polyacrylic Acid Gel. Subjected to Microphase Separation, Polymer Science. 2005. Ser. A. V.47. №2. P. 194–201. (Translated from Vysokomolekulyarnye Soedineniya. 2005. Ser. A. V.47, №2. P. 338–347).
10. Balasoiu M., Vekas L., Avdeev M.V., Aksenov V.L., Khokhryakov A.A., Bica D., Hasegan D., Torok Gy., Rosta L. Use of small-angle neutron scattering in testing the stability of ferrofluids, Romanian Reports in Physics. 2005. V.57. №.2. P. 261-265.
11. Balasoiu M., Avdeev M.V., Kuklin A.I., Aksenov V.L., Bica D., Vékás L., Hasegan D., Török Gy., Rosta L., Garamus V., Kohlbrecher J. Structural studies of ferrofluids by small-angle neutron scattering, Magnetohydrodynamics 40 (2004) 359-368 (published in 2005).
12. Balasoiu M., Avdeev M.V., Aksenov V.L., Hasegan D., Garamus V.M., Schreyer A., Bica D., Vékás L. Structural organization of water-based ferrofluids with sterical stabilization as revealed by SANS, J. Mag. Mag. Mater., accepted for publication (2005).
13. Balasoiu M., Avdeev M.V., Kuklin A.I., Aksenov V.L., Hasegan D., Garamus V., Schreyer A., Bica D., Vékás L. Nuclear and magnetic structures of non-polar ferrofluids by small-angle neutron scattering, Rom. Rep. Phys., accepted for publication (2005).
14. Balasoiu M., Avdeev M.V., Kuklin A.I., Aksenov V.L., Ghenescu V., Hasegan D., Garamus V., Schreyer A., Bica D., Vékás L., Almasan V. Nuclear and magnetic structures of non-polar ferrofluids by small-angle neutron scattering, Preprint JINR E14-2005-165, (2005) (in press).
15. Ion I., Banciu C., Bondar A.-M., Pasuk I., Szekely N. K. Structural Analysis of Carbon Nanocomposite materials by SANS, Experimental report. KFKI, Budapest, Hungary.
16. Batusov Yu.A., Kovalev Yu.S., Soroko L.M. Confocal scanning microscope for nuclear photoemulsion, Preprint JINR E13-2005-69, Dubna, 2005.

17. Efremov R., Shiryaeva G., Bueldt G., Islamov A., Kuklin A., Yaguzhinsky L., Fragneto-Cusani G., Gordeliy V. SANS investigations of the lipidic cubic phase behaviour incourse of bacteriorhodopsin crystallization, Journal of Crystal Growth. 2005. V.275. P.1453–1459.
18. Fedotov G. N., Tret'yakov Yu. D., Ivanov V. K., Kuklin A. I., Islamov A. Kh., Putlyaev V. I., Garshev A.V., and Pakhomov E. I. Fractal Structures of Soil Colloids. Translated from Doklady Akademii Nauk, Vol. 404, No5, pp.638-641, 2005.
19. Fedotov G. N., Tret'yakov Yu. D., Ivanov V. K., Kuklin A. I., Islamov A. Kh., Putlyaev V. I., Garshev A.V., and Pakhomov E. I. Fractal Structures of Soil Colloids in different zone. Translated from Doklady Akademii Nauk, Vol. 405, N 3, pp.351-354, 2005.
20. Gordeliy V.I., Cherezov V. G., Teixeira J. Strength of thermal undulations of phospholipid membranes, Phys. Rev. E. 2005 72, 1-16.
21. Grudinin S.V., Büldt G., Gordeliy V., Baumgaertner A. Water Molecules and Hydrogen-Bonded Networks in Bacteriorhodopsin - Molecular Dynamics Simulations of the Ground State and the M Intermediate, Biophys. J. 2005. V.88. P.1-10.
22. Haramagatti C.R., Islamov A., Gibhardt H., Gorski N., Kuklin A., Eckold G. Pressure induced phase transitions of TTABr-micellar solutions studied by SANS and Raman spectroscopy, PCCP, 2005 (in press).
23. Ion I., Kuklin A., Kovalev Y., Bondar A.-M., Banciu C., Pasuk I. Carbon composite materials for Electromagnetic interference applications. Materials structure, Phisica B Chehia, (in press).
24. Islamov A., Haramagatti C.R., Gibhardt H., Kuklin A., Eckold G. Pressure induced phase transitions in micellar solutions (in press).
25. Khokhryakov A.O., Avdeev M.V., Andrievsky G.V., Aksenov V.L., Bulavin L.A. "Structural Organization of Colloidal Solution of Fullerene C60 in Water by Data of Small Angle Neutron Scattering". Journal of Molecular Liquids, accepted for publication (2005).
26. Kiselev M.A., Zbytovska J., Matveev D., Wartewig S., Gapienko I. V., Perez J., Lesieur P., Hoell A., Neubert R. Influence of trehalose on the structure of unilamellar DMPC vesicles. Journal of Colloids and Surfaces A: Physicochemical and Engineering Aspects. 256 (2005) 1-7.
27. Kiselev M.A., Gutberlet T., Lesieur P., Hauss T., Ollivon M., Neubert R.H.H. Properties of ternary phospholipid / dimethyl sulfoxide / water systems at low temperatures. Chemistry and Physics of Lipids. 133(2005) 181-193.
28. Kiselev M.A., Ryabova N. Yu., Balagurov A. M., Dante S., Hauss T., Zbytovska J., Wartewig S., Neubert R.H.H. New insights into structure and hydration of stratum corneum lipid model membrane by neutron diffraction. European Biophysics Journal 34 (2005) 1030–1040.
29. Kiselev M.A., Zemlyanaya E.V., Aswal V.K., Neubert R.H.H. What can we learn about the lipid vesicle structure from the small-angle neutron scattering experiment? Preprint E14-2005-93, JINR, Dubna.
30. Kiselev M.A., Zemlyanaya E.V., Aswal V.K., Neubert R.H.H. What can we learn about the lipid vesicle structure from the small-angle neutron scattering experiment? (Investigation DMPC vesicle structure by small angle neutron scattering) Physics preprint 0507140 19.07.2005, http://arxiv.org/abs/physics/0507140.
31. Kiselev M.A., Ryabova N.Yu., Balagurov A.M., Otto D., Zbytovska J., Dante S., Hauβ Th., Dobner B., Wartewig S., Neubert R.H.H. Study of the stratum corneum lipid model membranes by neutron diffraction. Proceedings of IV workshop on investigations at the IBR-2 pulsed reactor. E14-2005-80, JINR, p. 64 (2005).
32. Kiselev M.A., Kiselev A.M., Borbeli Sh., Lesieur P. Study of the ethanol penetration through a model biological membrane by small angle neutron scattering. Submitted to journal "Surface. X-ray, synchrotron and neutron studies", 2005. (in Russian).
33. Kiselev M.A., Ryabova N. Yu., Balagurov A. M., Otto D., Dante S., Hauss T., Wartewig S., Neubert R.H.H. Influence of ceramide 6 on the structure and hydration of the membrane of dipalmitoylphosphatidylcholine. Submitted to journal "Surface. X-ray, synchrotron and neutron studies", 2005. (in Russian).
34. Kiselyova O.I., Shiryaeva G.N. Efremov R.G., Gordeliy V.I., Yaminsky I.V., Yanyushin M.F., Büldt G., Yaguzhinsky L.S., Crystallization of $F_1F_0$-ATP Synthase from Chloroflexus aurantiacus, J. of Cryst. Growth. 2005. V.2. P.1447-1452.
35. Kovalev Yu.S., Kuklin A.I., Novikov A.G., Savostin V.V., Shimkevich A.L., Jadrovsky E.L. The Microstructure of Pb-K Melt from Small Angle Neutron Scattering Experiments. J. Non-Cryst. Solids, 2005 (to be published).
36. Kuklin A.I., Islamov A.Kh., and Gordeliy V.I., Two-detector System for Small-Angle Neutron Scattering Instrument, Neutron News. 2005. V.16. №3. P.16-18.
37. Lebedev D.V., Filatov M.V, Kuklin A.I., Islamov A.Kh., Kentzinger E., Pantina R., Toperverg B.P., Isaev-Ivanov V.V. Fractal nature of chromatin organization in interphase chicken erythrocyte nuclei: DNA structure exhibits biphasic fractal properties, FEBS Letters. 2005. V.579. P.1465-1468.
38. Moukhametzianov R.E., Klare J.P., Efremov R.G., Baeken C., Göppner A., Labahn J., Engelhard M., Büldt G., Gordeliy V. I., Development of the signal in sensory rhodopsin and its transfer to the related transducer, Nature. 2005. (in press).

39. Murugova T.N., Gordeliy V.I., Islamov A.Kh., Kuklin A.I., Vinogradov A.D., Yaguzhinsky L.S., Structure of membrane of submitochondrial particles studied by small angle neutron scattering, Materials structure in Chemistry, Biology, Physics and Technology. Czech and Slovak Crystallographic Association. 2005 (in press).
40. Ozerin A. N., Svergun D. I., Volkov V. V., Kuklin A. I., Gordeliy V. I., Islamov A. Kh., Ozerina L. A. and Zavorotnyuk D. S. The spatial structure of dendritic macromolecules, J. Appl. Cryst. (2005). 38, 996–1003.
41. Pasuk I., Banciu C., Bondar A.M., Rimbu G.A., Ion I., Stamatin, Morjan I., Voicu I., Sandu I. Influence of some carbon nanostructures on the mesophase pitch development. A structural study. Romanian Reports in Physics, V.56, No. 3. P. 320-327, 2004.
42. Rajewska A., Milczarek J. J., Medrzycka K., Hallmann E. SANS method study of aggregation in mixed micellar solutions of nonionic C14E7 and two cationic classic surfactants CTAB and CTACl. J. of Physical Chemistry (in press).
43. Rajewska A., Milczarek J. J., Medrzycka K., Hallmann E. Structure of the mixed micellar solutions of nonionic C14E7 with two anionic SDS and LiDS classic surfactants study by SANS method. Langmuir (in press).
44. Serdyuk I.N., Zaccai N., Zaccai J. Methods in Molecular Biophysics: Structure, Function, Dynamics. Cambridge University Press, in press (2005).
45. Soloviev A.G., Solovieva T.M., Stadnik A.V., Islamov A.Kh., Kuklin A.I. SAS: program for primary processing of small angle spectra. Version 2.4. Description and user guide, JINR Communications, Dubna, 2003. (in Russian).
46. Teterev A.Yu., Avdeev M.V., Kholmurodov M., Aksenov V.L. Organization of solvent at interface with fullerene in solutions C60/carbon disulfide by molecular dynamics simulations. In Proceedings of the International Workshop "Molecular Simulation Studies in Material and Biological Sciences" Ed. Kh.T. Kholmurodov, Nova Publishers: 2005.
47. Török Gy., Len A., Rosta L., Balasoiu M., Avdeev M.V., Aksenov V.L., Ghenescu I., Hasegan D., Bica D., Vékás L., Interaction effects in non-polar and polar ferrofluids by small-angle neutron scattering, Rom. Rep. Phys., accepted for publication (2005).
48. Zemlyanaya E.V., Kiselev M.A., Aswal V.K. Structure of the unilamellar dimyristoylphosphatidylcholine vesicles. A small-angle neutron scattering study. Journal of Computational Methods in Applied Sciences and Engineering, In press 2005.
49. Zbytovska J., Kiselev M.A., Funari S. S., Garamus V., Wartewig S., Neubert R. Influence of Ceramides [NP] and [AP] on the DMPC membrane structure. Chemistry and Physics of Lipids. 138 (2005) 69–80.
50. Zbytovska J., Kiselev M.A., Funari S. S., Garamus V., Wartewig S., Neubert R. Influence of cholesterol on the structure of stratum corneum lipid model membrane. Submitted to Chemistry and Physics of Lipids, 2005.
51. Zemlyanaya E.V., Kiselev M.A., Zbytovska J., Almasi L., Aswal V.K., Schtruns P., Wartewig S., Neubert R. Numerical analysis of the unilamellar vesicle structure on the basis of small angle neutron scattering data. Submitted to journal “Surface. X-ray, synchrotron and neutron studies”, 2005. (in Russian).

## Conferences

1. Aksenov V.L., Avdeev M.V., Kozhemyakina N.V., Tropin T.V., Priezzhev V.B., Rosta L., Korobov M.V. Formation of fullerene clusters in the system $C_{60}$/NMP/water by SANS International Conference on Neutron Scattering (ICNS-2005), Sydney, November 27 – December 2 2005.
2. Aksenov V.L., Avdeev M.V., Tropin T.V., Korobov M.V., Kozhemyakina N.V. Study of cluster formation in the systeme $C_{60}$/NMP/water by small angle neutron scattering, VII All-Russian conference: Physicochemistry of superdispersed (nano-) systems, November 22-24, 2005. (in Russian).
3. Aksenov V.L., Avdeev M.V., Tropin T.V., Priezzhev V.B., Schmelzer J.W.P. “Fullerene cluster formation in carbon disulfide and toluene”. 7$^{th}$ Biennial International Workshop: Fullerenes and Atomic Clusters IWFAC 2005, June 27 – July 1, 2005.
4. Antonov V.E., Beskrovnyj A.I., Fedotov V.K., Khasanov S.S., Sakharov M.K., Sashin I.L., Tkacz M. Crystal structure and lattice dynamics of chromium hydrides. IV Workshop on Investigations at the IBR-2 Pulsed Reactor Programme and abstracts. June 15 – 18, 2005, Dubna, Russia, p.21.
5. Avdeev M.V., Aksenov V.L., Vorobiev A.A., Balasoiu M., Rosta L., Bica D., Vekas L. Combined study of non-polar ferrofluids in bulk and interface by means of small-angle neutron scattering and neutron reflectometry, International Workshop on Reflectometry, Off-specula and GSANS scattering (ROG-2005), Villigen, October 23-27, 2005.
6. Avdeev M.V., Balasoiu M., Aksenov V.L., Garamus V.M., Schreyer A., Torok D., Rosta L., Bica D., Vekas L. Comparative analysis of the structure of sterically stabilized magnetic fluids on polar bases by small angle neutron scattering, RSNE-2005, Moscow, October 14-19, 2005. (in Russian).

7. Avdeev M.V., Tropin T.V., Aksenov V.L., Rosta L., Garamus V.M., Rozhkova N.N. Study of pore structures in shungites by small-angle neutron scattering, International Conference on Neutron Scattering (ICNS-2005), Sydney, November 27 – December 2, 2005.
8. Avdeev M.V., Tropin T.V., Priezzhev V.B., Aksenov V.L., Rosta L., Garamus V.M., Rozhkova N.N. Structural Studies of Shungites and Their Aqueous Dispersions by Small-Angle Neutron Scattering, International Nanocarbon Workshop, Hayama, Tokyo, July 29 -31, 2005.
9. Avdeev M.V., Vorobiev A.A., Vekas L., Bica D., Aksenov V.L. Study of structure of non-polar ferrofluids at the interface with silicon by neutron reflectometry, International Conference on Neutron Scattering (ICNS-2005), Sydney, November 27 – December 2 2005.
10. Balagurov A.M. "Advanced neutron scattering for nanostructures and materials science", RSNE-2005, 14 – 19 November, 2005, Moscow.
11. Balagurov A.M. "Crystal and magnetic structures of $(Nd_{1-x}Sr_x)(Mn_{1-x}Ru_x)O_3$ perovskites for x from 0.125 to 1.0", IUCr Congress, 24 – 31 September, 2005, Florence, Italy.
12. Balagurov A.M. "Mesoscopically inhomogeneous state and giant oxygen isotope effect in complex manganese oxides", RSNE-2005, 14 – 19 November, 2005, Moscow.
13. Balagurov A.M. "Spectrometers at the IBR-2 reactor after 2010", IV Workshop on investigations at the IBR-2 pulsed reactor. 15-18 June, 2005, Dubna.
14. Balagurov A.M. "Structural and magnetic oxygen isotope effects in magnetic oxides (studied by neutron diffraction)", 12th International Seminar on Neutron Scattering Investigation in Condensed Matter, Poznan, May 5 – 7, 2005.
15. Balagurov A.M. "Structural origin of the giant oxygen isotope effect in $Re_{0.5}Sr_{0.5}MnO_3$ perovskites", ICNS-2005, 27 November – 03 December 2005, Sydney, Australia.
16. Balagurov A.M., Sumin V.V. "Nuclear materials studies with FSD diffractometer", IV Workshop on investigations at the IBR-2 pulsed reactor. 15-18 June, 2005, Dubna.
17. Balasoiu M. "Water-based ferrofluids: recent results of SANS investigations", Workshop "Investigations at the IBR-2 Pulsed Reactor", June 14-15, 2005, Dubna.
18. Balasoiu M. «Interaction effects in non-polar and polar ferrofluids by small-angle neutron scattering», National Conference in Physics, CNF 2005, 13-16 septembrie 2005, Bucuresti, Romania.
19. Balasoiu M., Avdeev M.V., Aksenov V.L., Hasegan D., Garamus V., Schreyer A., Bica D., Vekas L. "Structural organization of water-based ferrofluids with sterical stabilization as revealed by SANS", Proceeding Abstracts, Moscow International Symposium on Magnetism, Moscow, Russia, June 25-30, 2005.
20. Balasoiu M., Avdeev M.V., Aksenov V.L., Hasegan D., Ghenescu V., Torok Gy., Rosta L., Bica D., Vekas L. „Structural studies of ferrofluids by small-angle neutron scattering", PLMMP 3-rd International Conference and Strategic Workshop Nanoscale Liquid Systems, Kiev, Ukraine, May 27-51, 2005, 7-12O, Abstracts Proceeding, p. 218.
21. Balasoiu M., Avdeev M.V., Aksenov V.L., Hasegan D., Ghenescu V., Torok Gy., Rosta L., Bica D., Vekas L., Garamus V., Schreyer A. "Comparative analysis of the structure of ferrofluids based on polar carriers by small-angle neutron scattering", Seminar Structural Investigations of Magnetic Fluids, Timisoara, Romania, 20 January, 2005.
22. Bickulova N.N., Asylguzhina G.N., Skomorokhov A.N., Yadrovskiy E.L., Beskrovniy A.I., Stepanov Yu.M. Ion transfer and crystalline structure of solid solutions based on cuprous selenide. 8-th International symposium «ORDER, DISORDER AND OXIDE PROPERTIES» ODPO - 2005, Sochi, September 19-22, 2005. (in Russian).
23. Bickulova N.N., Skomorokhov A.N., Beskrovniy A.I., Yadrovskiy E.L., Stepanov Yu.M., Asylguzhina G.N. Ion transfer and crystalline structure of solid solutions based on cuprous selenide. IV Workshop on Investigations at the IBR-2 Pulsed Reactor. Programme and abstracts, June 15 – 18, 2005, Dubna, Russia, p.43. (in Russian).
24. Blagoveshchenskii N.M., Loginov N.I., Morozov V.A., Novikov A.G., Puchkov A.V., Savostin V.V., Shimkevich A.L., Shimkevich I.Yu. Studies of structural-dynamic properties of liquid metals by neutron scattering. Interindustry topical conference «Thermal Physics-2005»: «Heat-hydraulic aspects of safety of NEA with reactors on fast neutrons», Obninsk, November 16 – 18, 2005 (oral report). (in Russian).
25. Blagoveshchenskii N.M., Morozov V.A., Novikov A.G., Savostin V.V., Shimkevich A.L., A study of Liquid Lead elementary excitation spectrum. IV Workshop on investigations at the IBR-2 pulsed reactor (poster).
26. Blagoveshchenskii N.M., Morozov V.A., Novikov A.G., Savostin V.V., Savostin D.V., Shimkevich A.L., Shimkevich I.Yu. Study of structure of the lithium-nitrogen melt by neutron diffraction. Interindustry topical conference «Thermal Physics-2005»: «Heat-hydraulic aspects of safety of NEA with reactors on fast neutrons», Obninsk, November 16 – 18, 2005 (oral report). (in Russian).
27. Blagoveshensky N.M., Novikov A.G., Puchkov A.V., Osawa E., Rozhkova N.N., Quasielastic neutron scattering on the aqueous nanodiamond dispersion, IV Workshop on investigations at the IBR-2 pulsed reactor, (poster).

28. Golosova N.O. “High Pressure Effects on the Crystal and Magnetic Structures of $La_{0.7}Sr_{0.3}CoO_3$” Joint 20th AIRAPT – 43rd EHPRG Conference on Science and Technology of High Pressure, June 27 – July 1, 2005, Karlsruhe, Germany.
29. Golosova N.O. “Study of Crystal and Magnetic Structures of $La_{0.7}Sr_{0.3}CoO_3$ at High Pressure”. IV Workshop on Investigations at the IBR-2 Pulsed Reactor, June 15-18, 2005, Dubna, Russia.
30. Guskos N., Beskrovnyy A., Typek J., Ryabova N.Yu., Blonska-Tabero A., Kurzawa M., and Maryniak M. Crystal structure of $Mg_3Fe_4V_6O_{24}$ studied by neutron diffraction. Workshop on Functional Materials FMA’2004, Athens, Greece, 25-30 September, 2005, p.51.
31. Hall P.J., Hall E., Hotmann S., Salacar J.I., Natkaniec I., Smirnov L.S., Ivanov A.S., Beskrovny A.I., Vasilovsky S.G., Butorin P.E. Investigation of the state of absorbed hydrogen in matters with nanocrystalline structure using elastic and inelastic incoherent neutron scattering. RSNE NANO-2005, November 14-19, 2005, Moscow. (in Russian).
32. Hołderna-Natkaniec K., Kasperkowiak W., Natkaniec I. “Vibrational spectra of 6-benzylaminopurine by IINS and DFT methods”, Polish Conference on the Neutron Scattering and Complementary Methods in the Investigations on the Condensed Phase”, Chlewiska, 5 – 9 June, 2005.
33. Hołderna-Natkaniec K., Kasperkowiak W., Natkaniec I., Mikuli E. “INS/QC Study of vibrational spectra of $N^6$benzylaminopurine and its subunits”, Investigations at the IBR-2 Pulsed Reactor, June 15 - 18, 2005, Dubna.
34. Holderna-Natkaniec K., Kasperkowiak W., Natkaniec I., Sciesinska E., Sciesinski J., Mikuli E. “The IINS, IR and DFT studies of hydrogen bonds in $N^6$-furfuryl-and $N^6$-benzyl-aminopurines”, XVIth Conference on Horizons in Hydrogen Bond Research, 30 August - 4 September, 2005, Roskilde University, Denmark.
35. Holderna-Natkaniec K., Natkaniec I., Nowak D. “IINS/QC studies of ethisterone and norethisterone”, International Conference on Neutron Scattering, ICNS2005, 27 November - 2 December, 2005, Sydney, Australia.
36. Ion I. "Advanced Nanocarbon coated nanoiron Carbon composite materials for electromagnetic interference applications – Small angle neutron scattering study". VIII Conference for Young Scientists and Specialists, 4-7, February 2005.
37. Ion I. "Carbon Composite Materials for Electromagnetic Interference Applications". 3rd Central European Training School on Neutron Scattering and COST Training School on Neutron Optics, Budapest, Hungary, April 18-23, 2005 (poster).
38. Ion I. "Structural studies of carbon composite materials by neutron techniques. Spectroscopy, Microscopy". 4th PSI Summer School on Condensed Matter Research, August 14-21, 2005. Lyceum Alpinum Zuoz, Switzerland.
39. Ion I. "Structural studies of carbon composite materials". ARM_4, New directions in Science Materials Research, 4-5 September, 2005, Constanta, Romania.
40. Ion I. "Structural studies of carbon materials by SANS-technique". Conferinta Nationala de Fizic, Bucuresti, 13-16 September, 2005, Romania.
41. Ion I. "Studies and modeling the structure of carbon materials by neutron techniques". IV Workshop on Investigations at the IBR-2 Pulsed Reactor. Dubna, Russia, 15-18 June, 2005.
42. Ivankina T.I. Marble and quartz under temperature and applied load - results of experiments using neutron time-of-flight diffraction. Workshop “Earthscience and nanoscience with neutrons at IBR-2/IBR-2M (JINR Dubna)”. Germany. GFZ Potsdam, September 5-6, 2005.
43. Ivankina T.I., Nikitin A.N., Kern H.M., Locajice T., Pros Z., Klima K. Texture and elastic anisotropy of rocks from the Kola superdeep borehole determined by neutron diffraction and ultrasonic measurements at high hydrostatic pressures and under three-axial load. XXX General Assembly of European Geophysical Union. Austria. Vienna. Geophysical Research Abstracts, vol.5, 298, 2005.
44. Jernenkov K. Spin wave of density in the structure Cr(9nm)/V(60nm). International Workshop “Hierarchy of scales in magnetic nanostructures”, May 20-22, 2005, Upsala, Sweden.
45. Jernenkov M. International Conference on Neutron Scattering (ICNS-2005), November 27 – December 2, 2005 Sydney, Australia.
46. Jernenkov M. The REMUR spectrometer on channel №8 of the IBR-2. International Workshop ROG 2005, 24-27 October 2005, PSI, Villigen, Switzerland.
47. Kalinin I., Lauter H., Puchkov A. Experimental study of zero sound and single-particle excitations in 4He, Int.conf.on Neutron Scattering (ICNS2005), Sydney, 25 Nov.-3 Dec., (poster).
48. Kalinin I.V., Novikov A.G., Puchkov A.V. The slow neutron life-time into grooved moderator of channel # 2. IV Workshop on investigations at the IBR-2 pulsed reactor, June 15 – 18, 2005, Dubna, Russia (poster).
49. Kern H., Ivankina T.I., Nikitin A.N. Propagation of longitudinal and transverse waves in textured rocks. XXX General Assembly of European Geophysical Union. Austria. Vienna. Geophysical Research Abstracts, vol.5, 312, 2005.

50. Kern H., Ivankina T.I., Nikitin A.N. Propagation of longitudinal and transverse waves in textured rocks. IV Workshop on Investigations at the IBR- 2 Pulsed Reactor. Dubna. June 15-18. 2005.
51. Khaidukov Yu.N. Standing waves in the periodic structure with non-ideal interfaces. International Workshop ROG 2005, 24-27 October 2005, PSI, Villigen, Switzerland.
52. Khokhryakov A., Avdeev M., Andrievsky G., Korobov M., Aksenov V. "Models of Structural Organization of Colloidal Particles in Aqueous Fullerene Dispersions". III International Conference “Physics of Liquids: Modern Problems and Strategic Workshop Nanoscale Liquid Systems”, Kyiv, May 27-31, 2005.
53. Khokhryakov A., Avdeev M., Andrievsky G., Korobov M., Aksenov V. "Mechanisms of Cluster Formation of Fullerene Nanoparticles in Water", Workshop on Investigations at the IBR-2 Pulsed Reactor, June 15 – 18, 2005, Dubna, Russia.
54. Khokhryakov A., Avdeev M., Tropin T., Andrievsky G., Korobov M., Aksenov V. "Models of Structural Organization of Colloidal Particles in Aqueous Fullerene Dispersions". IX Scientific confeerence of young scientists and specialists, Dubna, January 31 – February 6, 2005. (in Russian).
55. Kichanov S.E. “High Pressure Effects on Crystal and Magnetic Structure of $YMnO_3$”. IV Workshop on Investigations at the IBR-2 Pulsed Reactor, June 15-18, 2005, Dubna, Russia.
56. Kichanov S.E. “The High Pressure Powder Diffractometer on the KSSRNT”. Joint $20^{th}$ AIRAPT – $43^{rd}$ EHPRG Conference on Science and Technology of High Pressure, June 27 – July 1, 2005, Karlsruhe, Germany.
57. Kiselev M.A., Ryabova N.Yu., Balagurov A.M., Otto D., Dante S., Hauss Th., Neubert R.H.H., Wartewig S.. Influence of Ceramide 6 on the structure and hydration of multilamellar DPPC membrane. BENSC User Meeting, UMI, Berlin, September 22-23, 2005.
58. Kiselev M.A., Ryabova N.Yu., Balagurov A.M., Otto D., Zbytovska J., Dante S., Hauβ Th., Dobner B., Wartewig S., Neubert R.H.H. Study of the stratum corneum lipid model membranes by neutron diffraction. Proceedings of IV workshop on investigations at the IBR-2 pulsed reactor. Dubna, June 15-18, 2005.
59. Kiselev M.A., Ryabova N.Yu., Balagurov A.M., Otto D., Zbytovská J., Dante S., Hauβ Th., Dobner B., Wartewig S., Neubert R.H.H. Study of the stratum corneum lipid model membranes by neutron diffraction. IV Workshop on Investigations at the IBR-2 Pulsed Reactor, Programmer and abstracts. June 15 – 18, 2005, Dubna, Russia, p.64.
60. Kiselev M.A., Zemlyanaya E.V., Aswal V.K., Neubert R.H.H. What can we learn about lipid vesicle structure from the small-angle neutron scattering experiment. Program Advisory Committee for Condensed Matter Physics. April 25, 2005.
61. Kovalev Yu. SANS investigation of aggregation of nonionic surfactant NBDEO in water solutions. 3rd Central European Training School on Neutron Scattering and COST Training School on Neutron Optics, Budapest, Hungary, April 18-23, 2005.
62. Kovalev Yu.S. "Use of laser confocal microscopy in condensed matter research". PAC on Condensed Matter Physics 23-rd session, Dubna, November 14-15, 2005. (in Russian).
63. Kovalev Yu.S. "Use of laser scanning confocal microscope in condensed matter research". IV Workshop on Investigations at the IBR-2 Pulsed Reactor, June 15 – 18, 2005, Dubna, Russia.
64. Kozlenko D.P. “High Pressure Effects on Crystal and Magnetic Structures of $Pr_{1-x}Sr_xMnO_3$ Manganites (x=0.48, 0.85)”. IV Workshop on Investigations at the IBR-2 Pulsed Reactor, June 15-18, 2005, Dubna, Russia.
65. Kozlenko D.P. “Pressure-Induced Magnetic Phase Transitions in $Pr_{1-x}Sr_xMnO_3$ Manganites (x=0.48 - 0.85)”. Joint $20^{th}$ AIRAPT – $43^{rd}$ EHPRG Conference on Science and Technology of High Pressure, June 27 – July 1, 2005, Karlsruhe, Germany.
66. Kozlenko D.P. Lecture “Neutron diffraction at high pressures”, V School-seminar “Actual problems of contemporary inorganic chemistry”, November 18-22, 2005, Zvenigorod, Russia. (in Russian).
67. Lauter-Pasuk V. International conference on application of synchrotron and X-ray radiation, electrons and neutrons, November 15-18, 2005, Moscow. (in Russian).
68. Lauter-Pasuk V. New frontiers of reflectometry: 3D characterization of nano-object materials. International Workshop ROG, 2005, 24-27 October 2005, PSI, Villigen, Switzerland.
69. Loose A., Smirnov L.S., Natkaniec I., Dolbinina V.V., Yakovleva L.M., Grebenev V.V. “The ordering of ammonium in ferroelectric phase II of β-$LiNH_4SO_4$”, $13^{th}$ BENSC User Meeting, 22-23 September 2005, HMI Berlin, Germany.
70. Malenkov G.G., Natkaniec I., Smirnov L.S., Suchanov V.I. “The neutron scattering study of structural and dynamic properties of $(NH_4F)_{1-x}(H_2O)_x$ mixed crystals”. Investigations at the IBR-2 Pulsed Reactor, June 15 - 18, 2005, Dubna.
71. Mamedov T., Balasoiu M., Bica D., Duginov V.N., Gritsaj K.I., Olshevsky V.G., Petrescu C., Vekas L., Zhukov Z.A. „Magnetic properties studies of magnetite ferrofluids by □SR Spectroscopy”, PLMMP 3-rd International Conference and Strategic Workshop Nanoscale Liquid Systems, Kiev, May 27-51, 2005, 7-18O, Abstracts Proceeding, p. 223.

72. Mazitov. Investigation of nanostructural copper by inelastic scattering of slow neutrons. V National conference on application of X-ray and synchrotron radiation, electrons and neutrons to study nanomaterials and nanosystems RSNE NANO-2005, November 14-19, 2005, Moscow. (in Russian).
73. Mikuli E., Migdal-Mikuli A., Hetmanczyk L., Natkaniec I. „Phase transitions and molecular motions in $[Zn(NH_3)_4](ClO_4)_2$ studied by infrared spectroscopy, X-ray powder diffraction and neutron scattering methods", Polish Conference on the Neutron Scattering and Complementary Methods in the Investigations on the Condensed Phase", Chlewiska, 5 – 9 June, 2005.
74. Mironova G.M. Direct and inverse scenarios of phase transitions. IV Workshop on Investigations at the IBR-2 Pulsed Reactor. Programme and abstracts. June 15 – 18, 2005, Dubna, Russia, p.52. (in Russian).
75. Murugova T.N. "Investigation of the mitochondrial ultrastructure by the small angle neutron scattering method (SANS)", Russian bioenergetics: from molecules to a cell, Moscow, February 21 – 23, 2005.
76. Murugova T.N. "Structure of membrane of submitochondrial particles studied by small angle neutron scattering". 3rd Central European Training School on Neutron Scattering and COST Training School on Neutron Optics, Budapest, Hungary, April 18-23, 2005, Poster.
77. Murugova T.N. "Study of submitochondrial particles by small-angle neutron scattering". IV Workshop on investigations at the IBR-2 pulsed reactor, Dubna, Russia, June 15 -18, 2005.
78. Natkaniec I., Holderna-Natkaniec K., Johnson R.M., Majerz I., Parlinski K. "Neutron scattering and ab initio investigations of methanol and urea as examples of hydrogen bonded solids", Janiks Friends Meeting, Zakopane, July 10-15, 2005.
79. Natkaniec I., Holderna-Natkaniec K., Majerz I., Parlinski K. "Dynamics of hydrogen bonds in solid methanol investigated by neutron spectroscopy and DFT modeling of methanol clusters", 12th International Seminar on Neutron Scattering Investigation in Condensed Matter, Poznań - Ciazen, May 5 – 7, 2005.
80. Natkaniec I., Holderna-Natkaniec K., Majerz I., Parlinski K. "Dynamics of hydrogen bonds in solid methanol investigated by neutron spectroscopy and DFT modeling of methanol clusters", XVIth Conference on Horizons in Hydrogen Bond Research, 30 August - 4 September, 2005, Roskilde University, Denmark.
81. Natkaniec I., Massalska-Arodz M., Juszynska E., Hołderna-Natkaniec K., Nowak D. „The INS/DFT comparative studies of the low temperature dynamics of dimethyl butanols", International Conference on Neutron Scattering, ICNS2005, 27 November - 2 December, 2005, Sydney, Australia.
82. Natkaniec I., Shabalin E., Kulikov S., Holderna-Natkaniec K. "Comparative studies of neutron scattering and radiation properties of methane, methanol, mesitylene and water at low temperatures", 17th Meeting of the International Collaboration on Advanced Neutron Sources, April 25-29, 2005, Santa Fe, New Mexico.
83. Nikitenko Yu.N. "Magnetic state of nanostructure Fe/V in the temperature region near the point of superconducting transition". International Workshop "Hierarchy of scales in magnetic nanostructures", 20-22 May, 2005, Upsala, Sweden.
84. Nikitin A.N., Balagurov A.M., Vasin R.N., Sobolev G.A., Ponomarev A.V. Investigation of dynamics of polymorphous $\alpha$-$\beta$ transition in quarzite by neutron diffractometry and acoustic emission. Workshop on Investigations at the IBR- 2 Pulsed Reactor. Dubna. June 15-18. 2005. (in Russian).
85. Nikitin A.N., Ivankina T.I., Tareeva M.V. Plagioclase textures in amphibolites and gneisses from the Kola super deep borehole section. Workshop on Investigations at the IBR-2 Pulsed Reactor. Dubna. June 15-18, 2005. (in Russian).
86. Novikov A.G., Puchkov A.V., Osawa E., Rozhkova N.N. Quasielastic neutron scattering on the aqueous nanodiamond dispersion. Int.conf.on Neutron Scattering (ICNS2005), Sydney, 25 Nov.-3 Dec, (poster).
87. Orlova A.I., Orlova V.A., Trubach I.G., Koryttseva A.K., Beskrovny A.I., Butorin P.E., Vasilovskiy S.G. Powder Neutron Diffraction Studies for development of new phosphate materials stable under extreme conditions. IV Workshop on Investigations at the IBR-2 Pulsed Reactor. Programme and abstracts. June 15 – 18, 2005, Dubna, Russia, p.42.
88. Pawlukojć A., Natkaniec I., Bator G., Sobczyk L., Grech E., Nowicka-Scheibe J. "Low frequency internal modes of 1,2,4,5-tetramethylbenzene, tetramethylpyrazine and tetramethyl-1,4-benzoquinone. INS, Raman, IR and theoretical DFT studies", XIIIth International Conference on Molecular Spectroscopy, 13 - 18 September, 2005, Ladek-Zdroj, Poland.
89. Pomjakushin V.Yu. "Effect of oxygen isotope substitution on magnetic ordering in $(La_{1-y}Pr_y)_{0.7}Ca_{0.3}MnO_3$". ICNS-2005, November 27–December 03, 2005, Sydney, Australia.
90. Rajewska A. "Aggregation properties of aqueous solutions of nonionic classic surfactant C14E7". IV Workshop on Investigation at the IBR-2 Pulsed Reactor, 15-18 June, 2005, Dubna, Russia.

91. Rajewska A. "SANS method study of water solutions of nonionic classic surfactant C14E7". Julich Soft Matter Days, 1-4 November, 2005, Julich, Germany.
92. Rajewska A. "Structure of the micellar solutions of nonionic classic surfactant". 6-th Liquid matter Conference, 1-6 July 2005, Utrecht, The Netherlands.
93. Ryabova N.Yu., Kiselev M.A., Balagurov A.M., Otto D., Zbytovská J., Dante S., Hauss Th., Neubert R.H.H. Investigation of mixed binary phospholipids / ceramide 6 membrane structure and hydration. IV Workshop on Investigations at the IBR-2 Pulsed Reactor. Programmer and abstracts. June 15 – 18, 2005, Dubna, Russia, p.70.
94. Schreiber J., Tamonov A.V., Stuhr U. "Investigation of the residual stress distribution across hard metal plates brazed to a steel support and the effect of thermal treatment", PSI Seminar, LNS PSI, Villigen, August 30, 2005.
95. Skomorokhov A., Trots D., Semenov V., Bickulova N., Yadrovsky E.L., Stepanov Yu., Knapp M., Ovchinnikov S., Fuess H. Investigations of superionic conductor AgCuSe by inelastic neutron scattering. 8-th International symposium «Order, Disorder and Properties of Oxides» ODPO - 2005, Sochi, September 19-22, 2005, poster. (in Russian).
96. Smirnov L.S., Natkaniec I., Loose A., Wozniak K., Dominiak P., Zink N., Melnyk G., Pawlukojc A., Martinez Sarrion M.L., Mestres L., Herraiz M. "The study of crystal structure and dynamics of the $K_{2-x}(NH_4)_xSeO_4$ mixed crystals by means of neutron scattering", Investigations at the IBR-2 Pulsed Reactor, June 15 - 18, 2005, Dubna.
97. Smirnov L.S., Natkaniec I., Loose A., Wozniak K., Dominiak P., Zink N., Melnyk G., Pawlukojc A., Martinez Sarrion M.L., Mestres L., Herraiz M. "The study of crystal structure and dynamics of the $K_{2-x}(NH_4)_xSeO_4$ mixed crystals by means of x-ray and neutron scattering", 13th BENSC User Meeting, 22-23 September 2005, HMI Berlin, Germany.
98. Smirnov L.S., Reehuis M., Loose A., Hohlwein D., Hoffmann J.-H., Wozniak K., Dominiak P., Baranov A.I., Dolbinina V.V. "The crystal structure investigations of different phases of the $[Rb_x(NH_4)_{1-x}]_3H(SO_4)_2$ (neutron single crystal diffraction)", 13th BENSC User Meeting, 22-23 September 2005, HMI Berlin, Germany.
99. Svanidze A.V., Sashin I.L. and Lushnikov S.G. "Generalized Density of States of Hen Egg White Lysozyme". 3rd Central European Training School on Neutron Scattering and COST Training School on Neutron Optics, 18-23 April, 2005, Budapest, Hungary.
100. Tamonov A.V. "Residual stress investigations at FSD diffractometer", PSI Seminar, LNS PSI, Villigen, August 24, 2005.
101. Tamonov A.V. "Task Group 1: Bead-on-Plate Weld. Neutron Diffraction at FLNP (IBR-2 pulsed reactor). The Results on RSA on the TG1 sample (AISI Typ 316L) by neutrons". 7th NET Steering Meeting, Department of Materials Engineering at the Open University, Milton Keynes, UK, June 16 – 17, 2005.
102. Taran Yu.V. "Martensitic transformation in fatigued stainless steel by neutron diffraction: current status and perspectives". In: 12th International Seminar on Neutron Scattering Investigation in Condensed Matter, Poznan-Ciazen, Poland, 5-7 May 2005, Abstract book, Institute of Physics Adam Mickiewicz University, p.2-3, 2005.
103. Taran Yu.V., Daymond M.R., Oliver E.C., Schreiber J. "On-line low cycle stress rig neutron diffraction study of a martensite phase transformation in stainless steel AISI 321 ad interim high cycle fatigued". In: The 134th Annual Meeting of The Minerals, Metals and Materials Society (TMS), Symposium: Neutron Diffraction Characterization of Mechanical Behavior, San Francisco, California, USA, 13-17 February 2005, Abstract book, The TMS Meetings Department, p.347, 2005
104. Titov A.N., Skomorokhov A.N., Semenov V.A., Ovchinnikov S.G., Titova S.G., Estemirova S.Ch.and Puchkov A.V. Phonon density of states for $M_{0.25}TiSe_2$, M=Cr, Fe, Ni. IV workshop on investigations at the IBR-2 pulsed reactor, (oral report).
105. Tropin T.V., Avdeev M.V., Priezzhev V.B., Schmelzer J.W.P., Aksenov V.L. "Kinetics of cluster growth in fullerene solutions". Geilo NATO ASI 2005: Dynamics of Complex Interconnected Systems: Networks and Bioprocesses, April 11-21, 2005.
106. Tropin T.V., Avdeev M.V., Priezzhev V.B., Schmelzer J.W.P., Aksenov V.L. "Kinetics of cluster growth in fullerene solutions". IV Workshop on Investigations at the IBR-2 Pulsed Reactor, June 15-18, 2005.
107. Tropin T.V., Avdeev M.V., Priezzhev V.B., Schmelzer J.W.P., Aksenov V.L. "Kinetics of cluster growth in molecular fullerene solutions". IX Scientific conference of young scientists and specialists, Dubna, January 31 – February 6, 2005. (in Russian).
108. Trots D., Skomorokhov A., Semenov V., Ovchinnikov S., Bickulova N., Stepanov Yu., Knapp M. and Fuess H. Inelastic neutron scattering on the ternary superionic compound AgCuSe. IV workshop on investigations at the IBR-2 pulsed reactor, (poster).
109. Troyanov S.I., Natkaniec I., Ivanov A.S., Smirnov L.S., Pawlukojc A. "The study of hydrogen modes in $MH_5(PO_4)_2$, (M=Cs, $NH_4$) and $NaH_5P_2O_6$", Investigations at the IBR-2 Pulsed Reactor, June 15 - 18, 2005, Dubna.

110. Vasilovskiy S.G., Beskrovny A.I., Aleksandrov K.S., Flerov I.N. «Structural study of the $Rb_2KM^{3+}F_6$ $M^{3+}$=Fe, Ga elpasolite» \\ Solid State Physics-2005, 26-28 October, 2005, Minsk, p. 287.
111. Vasin R.V., Nikitin A.N., Locajicek T. Study of influence of temperature gradients on the properties of marble and sandstone. VI International conference «Physicochemical and petrophysical investigations in Earth sciences». Abstract book, p.12. Moscow, October 3-5, 2005. (in Russian).
112. Zlokazov V.B. "DELPHI-programs VMRIA, VACTIV, VDOMUS for the analysis of neutron spectra obtained on the IBR-2". IV Workshop on investigations at the IBR-2 pulsed reactor. 15-18 June, 2005, Dubna.

## NEUTRON NUCLEAR PHYSICS

### Experimental investigations

1. Astachova N.V., Dikoussar N.D., Maznyi N.G., Salamatin I.M., Shvetsov V.N. An Software Complex for Automation of Spectrometry, Part III: A Technique for Controlling the Sample Environment and Its Application in the Spectrometer Interactive Control Program. Instruments and Experimental Techniques. 48, No. 5 (2005) 592-598.
2. Atchison F., Van den Brandt D., Brys T., Daum M., Fierlinger P., Hautle P., Henneck R., Heule S., Kasprzak M., Kirch K., Konter J. A., Michels A., Pichlmaier A., Wohlmuther H., Wokaum A., Bodek K., Szerer U., Geltenbort P., Zmeskal J., Pokotilovski Yu. Production of ultracold neutrons from a cold neutron beam on a deuterium target. Phys. Rev. C71 (2005) 054601-054610.
3. Bondarenko V., Honzatko J., Tomandl I., von Egidy T., Wirth H.-F., Sukhovoj A. M., Malov L. A., Simonova L. I., Alexa P., Berzins J., Hertenberger R., Eisermann Y., Graw G. Low-spin mixed particle-hole structures in $^{185}$W. Nucl. Phys. A762 (2005) 167-215.
4. Bondarenko V.A., Gonzatko Ya., Li Cher, Loginov Yu.E., Malutenkova S.E., Sukhovoj A.M., Tomandl, I. Khitrov V.A. New possibilities to improve reliability of determining values of level density and radiative strength functions of dipole gamma-transitions in nuclei of any type below $B_n$. Voprosy atomnoi nauki i tehniki, Seriya Yadernye konstanty. 2004, № 2, 21-43. (in Russian).
5. Bystritsky V.M., Bystritskii Vit.M., Dudkin G.N., Gerasimov V.V., Krylov A.R., Mesyats G.A., Nechaev B.A., Padalko V.M., Parzhitsky S.S., Penkov F.M., Ratakhin N.A., Vozniak J. Study of the pd reaction at ultralow energies using hydrogen liner plazma. Yad.Fiz., 68 (11) (2005) 1839-1848.
6. Bystritsky V.M., Vozniak J. Gerasimov V.V., Dudkin G.N., Kublikov R.V., Nechaev B.A., Padalko V.M., Parzhitsky S.S., Smirnov V.S., Stolupin V.A. Scintillation detectors in experiments on plasma accelerators. Pribory i tekhnika eksperimenta, №6 (2005) 69-77. (in Russian).
7. Chernov I.P., Cherdantsev Yu.P., Sokhoreva V.V., Kobzev A.P. Study of hydrogen migration under the action of accelerated helium ions. POVERKHNOST №4, 2005г. (in Russian).
8. Frank A.I., Balashov S.N., Bondarenko I.V., Geltenbort P., Hoghoj P., Kozlov A.V., Masalovich S.V., Toperverg B.P. Resonant tunneling of UCN through the moving interference filter and experimental test of the UCN dispersion law. JINR Communication E3-2004-216.
9. Frank A.I., Geltenbort P., Kulin G.V., Kustov D.V., Nosov V.G., Strepetov A.N. UCN spectrometry at the diffraction on the moving grating. JINR Communications P3-2004-207. (in Russian).
10. Frank A.I., Geltenbort P., Kulin G.V., Kustov D.V., Nosov V.G., Strepetov A.N. Neutron diffraction on the moving grating as a non-stationary quantum phenomenon. Letters to JETP. 81 (2005) 541-545. (in Russian).
11. Granja C., Pospisil S., Chrien P.E. and Telezhnikov S.A. Levels of $^{174}$Yb populated in average resonance neutron capture. Nucl. Phys. A 757 (2005) 87-314.
12. Gundorin N.A., Zhdanova K.V., Zhuchko V.E., Pikelner L.B., Rebrova N.V., Salamatin I.M., Smirnov V.I., Furman W.I. Measurement of the delayed neutron yield at the fission of Np-237 by thermal neutrons. JINR Communications, P3-2005-171, JINR, 2005 p.7. (in Russian).
13. Ino T., Masuda Y., Kim G. N., Muto S., Skoy V. Development of $^3$He polarized neutron spin filters at KEK. Physica B 356 (2005) 109–113.
14. Jesinger P., Kopatch Yu.N., Mutterer M., Gonnenwein F., Gagarski A.M., Kalben J.V., Nesvizhevsky V., Petrov G.A., Trzaska W.H., Wollersheim H.-J., New experimental studies on the quaternary fission of 233, 235U(nth, f) and 252Cf(sf). Eur.Phys.J. A 24, 379 (2005).
15. Kozlov A.V., Frank A. I. Dynamic reflection and refraction of neutrons on the boundaries of a material with variable magnetic induction. Nuclear Physics 68 (2005) 1149-1164. (in Russian).
16. Machajdik D., Kobzev A.P., Frohlich K. Complementary of X-ray diffraction and RBS in thin film characterization. Vacuum. May 2005.

17. Masuda Y., Ino T., Jeong S.C., Muto S., Skoy V., Watanabe Y. A pulsed neutron Ramsey's method. Physica B 356 (2005) 182–186.
18. Mitchell G.E., Furman W.I., Lychagin E.V., Muzichka A.Yu., Nekhaev G.V., Strelkov A.V., Sharapov E. I., Shvetsov V.N., Chernukhin Yu.I., Levakov B.G., Litvin V.I., Lyzhin A.E., Magda E.P., Crawford B.E., Stephenson S.L., Howell C.R., Tornow W. Direct nn-Scattering Measurement with the Pulsed Reactor YAGUAR. J. Res. Natl. Inst. Stand. Technol. 110 (2005) 225-230.
19. Page Shelley A., Bowman J.D., Carlini R.D., Case T., Chupp T.E., Coulter K.P., Dabaghyan M., Desai D., Freedman S.J., Gentile T.R., Gericke M.T., Gillis R.C., Greene G.L., Hersman F.W., Ino T. and Ishimoto S., Jones G.L., Lauss B., Leuschner M.B., Losowski B., Mahurin R., Masuda Y., Mitchell G.S., Nann H., Penttila S.I., Ramsay W.D., Santra S., Seo P.-N., Sharapov E.I., Smith T.B., Snow W.M., Wilburn W.S., and Zhu H. Measurement of Parity Violation in np-Capture: the NPDGamma Experiment. J. Res. Natl. Inst. Stand. Technol. 110 (2005) 195-203.
20. Pokotilovski Yu.N. UCN anomaly and the possibility for further decreasing the neutron losses in traps. N I M A554 (2005) 356-362.
21. Pokotilovski Yu.N., Aru G.F. On the issue of ultracold neutron generation at pulsed neutron sources: Transport of very cold neutrons in the fast heated cold moderators and granular moderators. N I M A545 (2005) 355-362.
22. Seo P.-N., Bowman J.D., Gericke M., Gillis R.C., Greene G.L., Leuschner M.B., Long J., Mahurin R., Mitchell G.S., Penttila S.I., Peralta G., Sharapov E.I., and Wilburn W.S. New Pulsed Cold Neutron Beam Line for Fundamental Nuclear Physics at LANSCE. J. Res. Natl. Inst. Stand. Technol. 110 (2005) 145-148.
23. Serebrov A., Varlamov V., Kharitonov A., Fomin A., Pokotilovski Yu., Geltenbort P., Butterworth J., Krasnoshekova I., Lasakov M., Tal'daev R., Vassilijev A. Measurement of the neutron lifetime using gravitational trap and a low temperature Fomblin coating. Phys. Lett. B605 (2005) 72-78.
24. Skoy V., Masuda Y., Ino T., Muto S., Kim G.N. On the Way to Experimental Test of the Time Reversal Invariance in the Nuclear Reactions. J. Res. Natl. Inst. Stand. Technol. 110, (2005) 1-10.
25. Sukhovoj A.M., Khitrov V.A. Experimental manifestations of the effect of the assumed breaking of Cooper pairs of nucleons in nuclei of various types. EPAN 36 (4) (2005) 697-731. (in Russian).
26. Sukhovoj A.M., Khitrov V.A. Partial level density of the n-quasiparticle excitations in the nuclei of the $40 \le A \le 200$ region. JINR preprint E3-2005-196, Dubna, 2005.
27. Sukhovoj A.M., Khitrov V.A., Bondarenko V.A., Gonzatko Ya., Tomandl I. Cascade gamma-decay of $^{183}$W compound state: possibilities of development of new methods of the experimental study of properties of a heavy nucleus below $B_n$. Izv. RAN. Ser. fiz. 69 (5) (2005) 648-657. (in Russian).
28. Sukhovoj A.M., Khitrov V.A., Li Cher, Pluiko V.A. Level density and radiative strength functions of cascade gamma-transitions at the decay of $^{114}$Cd and $^{124}$Te compound states. Izv. RAN. Ser. fiz. 69 (5) (2005)641-647. (in Russian).
29. Sukhovoj A.M., Khitrov V.A., Li Cher. Experimental grounds of the necessity to specify model notions about the cascade gamma-decay of compound state of complex nucleus. Nuclear Physics 68 (9) (2005) 1568-1582. (in Russian).
30. Telezhnikov S.A., Granja C., Honzatko H.T., Kralik M., Montero-Cabrera M.-E. and Pospisil S. Primary gamma transitions in $^{174}$Yb in neutron capture at isolated resonances. Nucl. Phys. A 763 (2005) 1-44.
31. Vesna V.A., Gledenov Yu.M., Nesvizhevskiy V.V., Petukhov A.K., Sedyshev P.V., Soldner T., Zimmer O., Shulgina E.V. Detection of P-odd effect of triton escape in the reaction $^{6}$Li(n,$\alpha$)$^{3}$H. Letters to JETP. 82 (8) (2005) 519-523. (in Russian).

## Theoretical investigations

1. Bunatian G.G. Standard Model Treatment of the Radiative Corrections to Neutron beta-Decay. Journal of Research of the National Institute of Standard and Technology. 110 (4) (2005) 319.
2. Ignatovich V.K., Shabalin E.P. Neutron albedo. JINR Communications. P4-2005-107, Dubna, 2005. (in Russian).
3. Korneev D.A., Ignatovich V.K., Yaradaykin S.P., Bodnarchuk V.I. Specular reflection of neutrons from potentials with smooth boundaries. Physica B: Physics of Condensed Matter. 364/1-4 (2005) 99-110.
4. Lednicky R., Lyuboshitz V.L., Lyuboshitz V.V. Effect of relativistic spin rotation on two-particle spin composition. PEPAN 35 (7) (2004) pp. 93-99.
5. Lyuboshitz V.L., Lyuboshitz V.V. Correlations of polarizations of two photons. PEPAN 2005 (in press).
6. Lyuboshitz V.L., Lyuboshitz V.V. Lifetime and path-length of the virtual particle. Phys. At. Nucl. 68 (3) (2005) 524-527.
7. Lyuboshitz V.L., Lyuboshitz V.V. Strangeness conservation and pair correlations of neutral kaons with close momenta produced in inclusive multiparticle processes. PEPAN Let. 2006 (in press).
8. Radu F., Leiner V., Wolff M., Ignatovich V.K., Zabel H. Quantum State of Neutrons in Magnetic Thin Films. Phys. Rev. B 71 (2005) 214423.

## Applied investigations


1. Coşkun Mahmut, Frontasyeva M.V., Steinnes E., Çotuk A.Y., Pavlov S.S., Coşkun Münevver, Sazonov A.S., Çayır A., Belivermis M. Atmospheric deposition of heavy metals in Thrace Region studied by analysis of moss (Hypnum cupressiforme). Bulletin of Environmental Contamination and Toxicology 74 (1) (2005) 201-209.
2. Culicov O.A., Mocanu R., Frontasyeva M.V., Yurukova L., Steinnes E. Active moss biomonitoring applied to an industrial site in Romania: relative accumulation of 36 elements in moss-bags. Environmental Monitoring and Assessment. 108 (2005) 229-240.
3. Demkina S.V., Frontasyeva M.V., Coşkun Mahmut, Coşkun Münevver, Steinnes E. ENAA and AAS for analysis of surface soil: example from the Thrace Region, Turkey. Submitted to FLNP Annual Report 2004 (CD version), Dubna, 2005.
4. Duliu O.G., Culicov O.A., Radulescu I., Cristea C., Vasiu T. Major, trace and natural radioactive elements in bituminous coal from Australia, Romania, Russia, South Africa and Ukraine: a comparative investigation. Journal of Radioanalytical and Nuclear Chemistry. 264 (2005) 525-536.
5. Dutov A.G., Komar V.A., Shipilo V.B., Shipilo N.V., Azarko I.I., Frontasyeva M.V., Pavlov S.S. Influence of synthesis conditions and irradiation on physical properties of spontaneous crystalline diamonds. Diamond and Related Materials. 14 (2005) 1678-1682.
6. Ermakova E., Frontasyeva M.V. and Steinnes E. Use of ENAA to study metal pollution in the vicinity of thermal power plants in Central Russia. Submitted to FLNP Annual Report 2004 (CD version), Dubna, 2005.
7. Frontasieva M.V., Pavlov S.S., Dutov A.G., Komar V.A., Shipilo V.B., Shipilo N.V., Azarko I.I. Neutrons for styding synthesis of fine crystalline diamonds. Submitted to FLNP Annual Report 2004 (CD version), Dubna, 2005.
8. Frontasyeva M. V., Pavlov D. F. and Pavlov S. S. Epithermal neutron activation analysis for freshwater ecosystem monitoring: the Rybinsk Reservoir case study. Submitted to FLNP Annual Report 2004 (CD version), Dubna, 2005.
9. Frontasyeva M.V., Cilicov O.A., Dinescu L., Pantelica A. and Mocanu R. Retrospective review and future prospects of Russian-Romanian studies in Life Sciences using INAA at the IBR-2 reactor in Dubna. Ovidius University Annals of Chemistry. 16 (1) (2005) 76-80.
10. Frontasyeva M.V., Gundorina S.F., Gorbunov A.V., Lyapunov S.M., Okina O.I. NAA and AAS for studying elemental content of staple foodstuffs in Central Russia. Submitted to FLNP Annual Report 2004 (CD version), Dubna, 2005.
11. Frontasyeva M.V., Krmar M., Radnovic D., Steinnes E. Trace element contamination around a copper smelter complex in Bor Region (Serbia) studied by moss biomonitoring. The 18th Task Force Meeting of the United Nations Economic Commission for Europe (UNECE) ICP Vegetation, 1-4 February, 2005, Almeria, Spain.
12. Frontasyeva M.V., Steinnes E. Distribution of 35 elements in peat cores from ombrotrophic bogs studied by epithermal neutron activation analysis. Journal of Radioanalytical and Nuclear Chemistry. 265 (1) (2005) 11-15.
13. Gorbunov A.V., Liapunov S.M., Okina O.I., Frontasyeva M.V., Gundorina S.F. Seasonal changes of trace element content in vegetative organs of trees. Environmental Chemistry, St. Petersburg 14 (4) (2005) 258-265. (in Russian).
14. Gorbunov A.V., Liapunov S.M., Okina O.I., Frontasyeva M.V., Gundorina S.F. Assessment of human organism's intake of trace elements from staple foodstuffs in Central regions of Russia. In press, Environmental Chemistry, St. Petersburg. 2005. (in Russian).
15. Gorelova S.V., Ermakova E.V., Kolotev E.P., Nizovskiy S., Pestsov G.V., Frontasyeva M.V. Peculiarities of accumulation of macroelements and trace elements by daikon samples. Bulletin of Tolstoy TSPU. № 2. Tula, 2005, p. (in Russian).
16. Grodzinska K., Szarek-Lukaszewska G., Frontasyeva M.V., Pavlov S.S., Gudorina S.F. Multielement concentration in mosses in the forest influenced by industrial emissions (Niepolomice Forest, South Poland) at the end of 20th century. Polish Journal of Environmental Studies 14 (2) (2005) 171-178.
17. Mosulishvili L.M., Belokobylskiy A.I., Khizanishvili A.I., Kirkesali E.I., Frontasyeva M.V., Aksenova N.G. Application of neutron activation analysis to investigate accumulation and adsorption of mercury by Spirulina platensis biomass. Ecological chemistry, Saint-Petersburgh. 14 (2) (2005) 104-109. (in Russian).
18. Oprea C. Multivariate analysis of environmental data by SPSS. Environment & Progress 3 (2005) 285-290.
19. Oprea C., Cadar D. Strategical orientation towards clean energy production in accordance with environmental protection. The Modern Science and Energy XXIV (2005) ISBN 973-656-897-0, 66-72.
20. Oprea C., Curuia M., Filip S., Baluta A., Gergely I., Paraipan M. Development of a methodology on critical loads for trace metals in soils and surface waters. ANALE. Seria Geografie. 4 (2005) 5 p.

21. Oprea C., Filip S., Baluta A., Pater P., Fener M., Istvan G., Teusdea A., Costea M. Environmental pollution assessment around a medium industrial city: the case study of Oradea, Bihor, Romania. Environment & Progress 3 (2005) 273-278.
22. Oprea C., Kobzev A.P., Filip S., Burca I., Tentis M., Cadar D., Pater P. Biomonitoring of atmospheric pollution in Transylvania. Public health and risk factors. Revue de Cytologie et Biologie végétales-Le Botaniste 28 (s. i) (2005) 439-444.
23. Oprea C., Oprea I. A. Aspects of the method of receiving of nuclear energy by electronuclear methods and transmutation of radioactive waste. The Modern Science and Energy XXIV (2005) 62-65.
24. Pavlov D.F., Frontasyeva M.V., Pavlov S.S., Pankratova Yu. Distribution of trace elements in freshwater ecosystem compartments of man-made Rybinsk Reservoir (Central Russia) using epithermal neutron activation analysis. Ovidius University Annals of Chemistry. 16 (1) (2005) 72-75.
25. Tsibakhashvili N.Ya., Frontasyeva M.V., Kirkesali E.I., Aksenova N.G., Kalabegishvili T.L., Murusidze I.G., Mosulishvili L.M., Holman H.-Y.N. Epithermal neutron activation analysis of Cr(VI)-reducer basalt-inhabiting bacteria. Submitted to Analytical Chemistry (USA), 2005.

## Reports at Schools and Conferences

1. Abbondanno U. et al. The n_TOF facility at CERN: Performances and first results. In Proc. Int. Conf. on Nuclear Data for Science and Technology. Santa Fe, 26.09 - 01.10.04, part 1. Ed. Haight R. C., Chadwick M. B., Kawano T. and Talou P. p.p. 724-729C.
2. Aerts G. et al. Measurement of the $^{232}$Th neutron capture cross-section at the CERN n_TOF facility. In Proc. Int. Conf. on Nuclear Data for Science and Technology. Santa Fe, 26.09 - 01.10.04, part 1. Ed. Haight R. C., Chadwick M. B., Kawano T. and Talou P. p.p.1470-1473
3. Barandovski L., Cekova M., Frontasyeva M. V., Pavlov S. S., Stafilov T., Steinnes E., Urumov V. Biomonitoring of atmospheric metal deposition in the Republic of Macedonia. Proceedings of the 3rd International Workshop on the Project "Anthropogenic effects on the human environment in the tertiary basins in the Mediterranean. Edts. Boev B. and Serafimovski T., Stip, 2005, p. 5-16.
4. Cano-Ott D. et al. Measurements at n_TOF of the neutron capture cross-section of Minor actinides relevant to the nuclear waste transmutation. In Proc. Int. Conf. on Nuclear Data for Science and Technology. Santa Fe, 26.09 - 01.10.04, part 1. Ed. Haight R. C., Chadwick M. B., Kawano T. and Talou P. p.p. 1442-1445.
5. Domingo-Pardo C. et al. New measurement of the capture cross-section of Bismuth and Lead isotopes. In Proc. Int. Conf. on Nuclear Data for Science and Technology. Santa Fe, 26.09 - 01.10.04, part 1. Ed. Haight R. C., Chadwick M. B., Kawano T. and Talou P. p.p. 1521-1324
6. Furman W., Cennini P., Ketlerov V. et. al. High-Resolution Study of $^{237}$Np Fission Cross-Section from 5 eV to 1 MeV. In Proc. Int. Conf. on Nuclear Data for Science and Technology. Santa Fe, 26.09 - 01.10.04, part 1. Ed. Haight R. C., Chadwick M. B., Kawano T. and Talou P. p.p. 1039-1042
7. Gorelova S.V., Gins V.K., Ermakova E.V., Pestsov G.V., Frontasyeva M.V. Sort specifity of element accumulation from soil in diakon. Proc. of the VI International symposium «New and non-traditional plants and prospects of their usage». Volume III. M., 2005, p. 75-78. (in Russian).
8. Hambsch F.-J., Oberstedt S., Kornilov N., Varapai N. and Zeinalov Sh. Improved Data Applying the Digitization Technique to Nuclear Experiments, The 11th International Conference on Acquisition Information Systems Analysis and Synthesis: ISAS 2005 and The 2nd International Conference on Cybernetics and Information Technologies, Systems and Applications: CITSA 2005. July 14 - 17, 2005 in Orlando, Florida, USA.
9. Hambsch A.-J., Oberstedt S., Kornilov N., Varapai N. and Zeinalov Sh. Digitization technique in fission of $^{252}$Cf. FISSION 2005. 3rd International Workshop on Nuclear Fission and Fission Product Spectroscopy, 11-14 May 2005, Chateau de Cadarache, Saint Paul Paul lez Durance, France
10. Kadmensky S.G., Lyuboshitz V.V., Tchuvil'sky Yu.M. Self-consistent weak nucleon potential for various sets of weak meson-nucleon constants within the generalized Fermi-liquid theory. Report at XVI International School on Nuclear Physics, Neutron Physics and Nuclear Energy – Varna-2005 (Varna, Bulgaria, September 19–26, 2005); Abstracts of the International School Varna-2005, pp. 24-25 (2005); to be published in the journal "Transactions of the Bulgarian Nuclear Society" – Proceedings of the International School Varna-2005, 2006 (in press).
11. Kadmensky S.G., Lyuboshitz V.V., Tchuvil'sky Yu.M. Testing various sets of weak meson-nucleon constants by theoretical construction and calculation of weak P-odd terms in the nucleon-nucleus interaction. Poster presentation at V International Conference on Non-Accelerator New Physics. NANP'05 (Dubna, June 20–25, 2005); allocated on the NANP'05 web site (address: http://nanp.dubna.ru/docs/lyuboshitz.pdf).

12. Lednicky R., Lyuboshitz V.L., Lyuboshitz V.V. Effect of the relativistic spin rotation for one-particle and two-particle spin states. Proceedings of XXXVII and XXXVIII PNPI Winter Schools "Physics of Atomic Nucleus and Elementary Particles". Saint-Petersburg, 2004, pp. 366-389.
13. Lyuboshitz V. L., Lyuboshitz V. V. On the coherent inelastic processes at collisions of hadrons and γ-quanta with nuclei at ultrarelativistic energies. Poster presentation at the 18-th International Conference on Ultrarelativistic Nucleus-Nucleus Collisions. Quark Matter 2005 (Budapest, Hungary, August 4–9, 2005); accepted for publication in the journal "Heavy Ion Physics" (Acta Physica Hungarica A) – QM'2005 Poster Session Proceedings.
14. Lyuboshitz V. L., Lyuboshitz V. V. Pair correlations at small relative momenta in nuclear and particle physics. Proceedings of XXXVII and XXXVIII PNPI Winter Schools "Physics of Atomic Nucleus and Elementary Particles", Saint-Petersburg, 2004, pp. 390-430.
15. Lyuboshitz V. L., Lyuboshitz V. V. Pair correlations of neutrons produced in nuclear fission. Proceedings of XII International Seminar on Interaction of Neutrons with Nuclei. ISINN-12 (Dubna, May 26 –29, 2004), JINR E3-2004-169, Dubna, 2004, pp. 323-331.
16. Lyuboshitz V.L., Lyuboshitz V.V. Coherent inelastic processes on nuclei at ultrarela-tivistic energies. Report at the Conference of Nuclear Physics Department of Russian Academy of Sciences, dedicated to the 60-th anniversary of ITEP – NPD2005 (ITEP, Moscow, December 5–9, 2005); to be submitted to " Yadernaya Fizika " – Proceedings of the NPD2005 Conference.
17. Lyuboshitz V.L., Lyuboshitz V.V. On the correlations of polarizations in the system of two photons. Report at XI Advanced Research Workshop on High Energy Spin Physics. DUBNA-SPIN-05 (Dubna, September 27 – October 1, 2005), allocated on the DUBNA-SPIN-05 web site (address: http://thproxy.jinr.ru/diastp/spin05/270905_Lyuboshitz.pdf); Abstracts of DUBNA-SPIN-05, JINR E1,2-2005-119, Dubna, 2005, p.17; accepted for publication in Proceedings of DUBNA-SPIN-05 (Dubna, 2006).
18. Lyuboshitz V.L., Lyuboshitz V.V. On the Coulomb dissociation of relativistic nuclei and hypernuclei with small binding energies. Proceedings of XVIII International Workshop on High Energy Physics and Quantum Field Theory. QFTHEP'2004 (Saint-Petersburg, Peterhof, Russia, June 17 – 23, 2004), 2005 (in press).
19. Lyuboshitz V.L., Lyuboshitz V.V. Polarization effects in the reactions $p + {}^3He \to \pi^+ + {}^4He$, $\pi^+ + {}^4He \to p + {}^3He$ and verification of the consequences of quantum-mechanical coherence for the correlation tensor. Proceedings of the 16-th International Spin Physics Symposium. SPIN2004 (Trieste, Italy, October 10 – 16, 2004), World Scientific, New Jersey – London – Singapore, 2005, pp. 251-254.
20. Lyuboshitz V.L., Lyuboshitz V.V. Spectrum of relative momenta of the neutron and proton at deuteron peripherical breakup in the limit of very low momentum transfer. Report at XIII International Seminar on Interaction of Neutrons with Nuclei. ISINN-13 (Dubna, May 25–28, 2005); Abstracts of ISINN-13, JINR E3-2005-48 , Dubna, 2005, p.41.
21. Lyuboshitz V.L., Lyuboshitz V.V. Strangeness conservation and pair correlations of neutral kaons with close momenta in inclusive processes. Poster presentation at the 18-th International Conference on Ultrarelativistic Nucleus-Nucleus Collisions. Quark Matter 2005 (Budapest, Hungary, August 4–9, 2005); to be published in the journal "Nukleonika" QM'2005 Poster Session Proceedings (in press).
22. Lyuboshitz V.L., Lyuboshitz V.V. Strangeness conservation and structure of pair correlations of neutral kaons with low relative momenta in inclusive processes. Proceedings of XVII International Baldin Seminar on High Energy Physics Problems. ISHEPP-XVII (Dubna, September 27 – October 2, 2004), Dubna, 2005 or 2006 (in press).
23. Lyuboshitz V.L., Lyuboshitz V.V. The nucleon charge transfer reaction $n + p \to p + n$ at zero angle and the role of spin effects. Report at XI International Conference on Elastic and Diffractive Scattering. EDS'05 (Blois, France, May 15–20, 2005), allocated on the EDS'05 web site (address: http://lpnhe-theorie.in2p3.fr/TRANSPARENTS/Lyuboshitz.pdf); Proceedings of the EDS'05 Conference, 2006 (in press).
24. Lyuboshitz V.L., Lyuboshitz V.V. The process of Coulomb dissociation of weakly bound relativistic nuclei and hypernuclei within the two-cluster model. Report at VIII International Workshop "Relativistic Nuclear Physics – from Hundreds MeV to TeV". RNP-2005 (Dubna, May 23–28, 2005); Proceedings of the International Workshop RNP-2005, Dubna, 2006 (in press). Also presented at HEP2005 – International Europhysics Conference on High Energy Physics (Lisbon, Portugal, July 21–27, 2005).
25. Magli R., Mitsyna L.V., Nikolenko V.G., Parzhitski S.S., Popov A.B., Samosvat G.S. Neutron-electron scattering length deduced from neutron diffraction experiment on noble gas $^{36}Ar$. XIII International Seminar on Interaction of Neutrons with Nuclei, Dubna, May 25-28, 2005, 8 pages (in press).
26. Mitsyna L.V., Nikolenko V.G., Parhitski S.S., Popov A.B., Samosvat S.G. New method to extract the neutron-electron scattering length. The European Physical Journal C 40 (2005) 473-477.
27. Moreau et al. Measurement of capture cross-sections of $^{90,91,92,94,96}Zr$ isotopes at n_TOF. In Proc. Int. Conf. on Nuclear Data for Science and Technology. Santa Fe, 26.09 - 01.10.04, part 1. Ed. Haight R. C., Chadwick M. B., Kawano T. and Talou P. In Proc. Int. Conf. on Nuclear Data for Science and Technology. Santa Fe, 26.09 - 01.10.04, part 1. Ed. Haight R. C., Chadwick M. B., Kawano T. and Talou P. p.p. 880-883.

28. Mosconi M. et al. Neutron capture cross-section for the Re/Os clock. In Proc. Int. Conf. on Nuclear Data for Science and Technology. Santa Fe, 26.09 - 01.10.04, part 1. Ed. Haight R. C., Chadwick M. B., Kawano T. and Talou P. p.p. 1335-1338
29. Oprea A.I., Gledenov Yu. M., Oprea C., Sedyshev P. V., Sedysheva M. V. Evaluation of the cross section in the (n,α) reaction with fast neutrons. ISINN-12. Neutron Spectroscopy, Nuclear Structure, Related Topics. (Dubna: JINR, 2004) E3-2004-169, 205 – 208
30. Oprea A.I., Gledenov Yu.M., Khuukhenkhuu G., Oprea C., Sedyshev P.V., Sedysheva M.V., Szalanski P.J. Evaluation of the forward-backward coeffitient in the $^{14}N(n,p)^{14}C$ reaction. ISINN-12. Neutron Spectroscopy, Nuclear Structure, Related Topics. (Dubna: JINR, 2004) E3-2004-169, 201 - 204
31. Oprea A.I., Oprea C., Gledenov Y.M., Sedyshev P.V. Calculation of angular correlations in the $^{14}N(n, p)^{14}O$ reaction up to 1 MeV neutron energy region. Proceedings of the ISINN-14, 2005, 7 p (in press).
32. Oprea C., Burca I., Cupsa D., Telcean I., Tomulescu I., Tentis M., Radoviciu E., Teusdea A., Cadar D., Gergely I., 2005. Monitoring of pollution and biodiversity in Crisuri Basin by ecotourism. XXXV ESNA Congress, University of Picardie Jules Verne, 29 August – 2 September, Amiens, France, Revue de Cytologie et Biologie végétales, 11 p. (in press).
33. Oprea C., Cadar D., Candea D., Ozunu A., 2005. Retrospective study of environmental pollution with heavy metals in the Copsa Mica – Medias region, Proceedings of the ISINN-14, 8 p (in press).
34. Oprea C., Chernenko L.P., Cios M. and Oprea I.A., 2005. The influence of magnetoactivated water on plants. University of Picardie Jules Verne, 29 August – 2 September, Amiens, France, Revue de Cytologie et Biologie végétales, 20 p. (in press).
35. Oprea C., Filip S., Mitrut T., Gergely I., Baluta A., Oprea I. A., Cadar D. Geochemical studies applied to the exploration of water quality in the Crisuri Basin. Proceedings of the ISSIN-14, 2005, 8 p (in press).
36. Oprea C., Kobzev A. Analytical Methods Based on Ion Beams. Summer Student Practice in JINR Fields of Research, JINR University Centre, Dubna, 12 July – 4 August 2005, publication on CD - ROM.
37. Oprea C., Kobzev A.P., Buzguta V., Oprea I. A., Szodorai F., Cadar D. Determination of trace heavy metals in human teeth using PIXE. Proceedings of the ISINN-14, 8 p (in press).
38. Oprea C., Kobzev A.P., Filip S., Burca I., Tentis M., Cadar D., Pater P., 2005. Biomonitoring of atmospheric pollution in Transylvania public health and risk factor. XXXV ESNA Congress, University of Picardie Jules Verne, 29 August – 2 September, Amiens, France, Revue de Cytologie et Biologie végétales, 16 p. (in press).
39. Oprea Cristiana, Nicolescu Carmen, Loghin Vasile, Gorghiu Gabriel, Hussain Aziz Saleh, Szalansky Pavel Jan, 2005. Modeling the human health and environmental impacts status at Targoviste city area using neural network algorithms. Conference Integration of the New EU Member Countries into the GMES Programme, 12-14 December 2005 – Warsaw, Poland, 10 p, publication on CD – ROM.
40. Oprea Cristiana, Sedysheva Milana, Oprea Ioan Alexandru, Sedyshev Pavel, Loghin Vasile, Gorghiu Gabriel, Nicolescu Carmen, Busuioc Gabriela, Muratoreanu George, Hussain Aziz Saleh, Szalansky Pavel Jan, 2005. Analysis of the pollution agents through neural network algoritms. Conference Integration of the New EU Member Countries into the GMES Programme, 12-14 December 2005 – Warsaw, Poland, 8 p, publication on CD – ROM.
41. Popov Yu.P., Gledenov Yu.M., Sedyshev P.V., Andrzejewski J., Szalanski P., Perekrestenko A.D., Goncharenko O.N. Surprising resonances in the $^{147}Sm(n,\alpha)^{144}Nd$ reaction. ISINN-12. Neutron Spectroscopy, Nuclear Structure, Related Topics. (Dubna: JINR, 2004) E3-2004-169, 95 - 101
42. Sharapov E.I., Furman W.I., Lychagin E.V., Muzichka A.Yu., Nekhaev G.V., Strelkov A.V., Shvetsov V.N., Chernukhin Yu.I., Kandiev Ya.Z., Levakov B.G., Litvin V.I., Lyzhin A.E., Mitchell G.E., Crawford B.E., Stephenson S.L., Howell C.R., Tornow W. An approach to the spatial-temporal analysis of the n-n collision rate in the YAGUAR experiment. XIII International Seminar on Interactions of Neutrons with Nuclei. (submitted to ISINN-XIII), JINR, Dubna, 2005.
43. Szalanski P., Marganiec J., Gledenov Yu.M., Sedyshev P.V., Oprea A., Brozowski R., Wasilewski M. Neutron sources in massive stars – important topics during hydrogen, helium, and carbon burning. ISINN-12. Neutron Spectroscopy, Nuclear Structure, Related Topics. (Dubna: JINR, 2004) E3-2004-169, 450 – 455
44. Tishchenko V.G., Kopatch Yu.N., Mutterer M., Gönnenwein F., Gagarski A.M., Jesinger P., von Kalben J., Kojouharov I., Lubkiewics E., Mezentseva Z., Nesvizhevsky V., Petrov G.A., Schaffner H. , Scharma H., Speransky M., Trzaska W.H., Wollersheim H.-J. Recent Multi-Parameter Studies on Particle-Accompanied Fission of $^{252}Cf(sf)$ and $^{235}U(n_{th},f)$. XIII International Seminar on Interaction of Neutrons with Nuclei, Dubna, May 25-28, 2005 (in press).
45. Zeynalov Sh., Furman V. and Hambsch F.-J. Investigation of mass-TKE distributions of fission fragments from the $^{235}U(n,f)$-reaction in resonances", ISINN-13, 23-26 June 2005, Dubna, Russia

## NEUTRON SOURCES


1. Baranov I.M., Voronin I.I., Ermilov V.G., Kulagin E.N., Kulikov S.A., Melikhov V.V., Pushkar R.G., Ro Du Min, Shabalin D.E., Shabalin E.P.. Investigation of the process of radiolytic hydrogen outlet out of an experimental element of the cold moderator on solid mesitylene. JINR Communications, P3-2004-212. (in Russian).
2. Idelchik I.E.. Reference book on hydraulic resistances. M., (in Russian). Mashinostroenie, 1975, 560 p. (in Russian).
3. Malkov M.P., Danilov I.B., Zeldovich A.G., Fradkov A.B.. Reference book on physicotechnical fundamentals of cryogenics. M., Energoatomizdat, 1985, 432 p. (in Russian).
4. Rogovaia I.A., Kaganer M.G.. Journal of Phys. Chem., 1961, v. 4, No 11, p. 2135-2136. (in Russian).


## DEVELOPMENT AND CREATION OF ELEMENTS OF NEUTRON SPECTROMETERS FOR CONDENSED MATTER INVESTIGATIONS


1. Levchanovski F., Gebauer B., et al. Data acquisition boards for high-rate neutron delay line detectors with 2D position and time resolution. IV Workshop on Investigations at the IBR-2 Pulsed Reactor, Dubna, June15-18, 2005: Book of Abstracts, JINR E-14-2005-80, p. 79.
2. Gebauer B., et al. Development of very high rate and resolution time-of-flight area detectors for pulsed neutron sources in DETNI. IV Workshop on Investigations at the IBR-2 Pulsed Reactor, Dubna, June15-18, 2005: Book of Abstracts, JINR E-14-2005-80, p.71
3. Kirilov A., et al. Control system Sonix+: main features and experience of use. IV Workshop on Investigations at the IBR-2 Pulsed Reactor, Dubna, June15-18, 2005: Book of Abstracts, JINR E-14-2005-80, p. 74.
4. Belushkin A., et al. 2D Position-sensitive detector for thermal neutrons. XX Int. Symposium on Nuclear Electronics and Computing, Varna, Bulgaria, September 12-18, 2005: Book of abstracts, JINR E 10,11-2005-122, p.15.
5. Drozdov V., Kuzmin E., Zhuk V. Detector electronics for FSD diffractometer. XX Int. Symposium on Nuclear Electronics and Computing, Varna, Bulgaria, September 12-18, 2005: Book of abstracts, JINR E 10,11-2005-122, p.19-20.
6. Kirilov A., et al. Control system Sonix+ for neutron spectrometer REMUR. XX Int. Symposium on Nuclear Electronics and Computing, Varna, Bulgaria, September 12-18, 2005: Book of abstracts, JINR E 10,11-2005-122, p. 27.
7. Kirilov A., et al. Sonix+ - the new instrument control software at the IBR-2. http://Ins00.psi.ch/nobugs2004/paper00020.pdf
8. Kirilov A. Script interpreter in the Python environment – a new approach (in press).
9. Chernikov A.N., Zhuravlev V.V., Ulianov V.A., Trunov V.A., Bulkin A.P., Kolkhidashvili M.R. Shaft cryostat for powder diffraction of neutrons based on the closed cycle refrigerator for operation in the range 6-300 K, JINR Communications, P8-2005-23, Dubna, 2005. (in Rlussian).
10. Trofimov V.N., Chernikov A.N., Vdovin V.F., Perminov V.G., Vystavkin A.N. Optical cryostat with a sorption $^3$He refrigerator, JINR Communications, P8-2005-41, Dubna, 2005. (in Russian).

# 6. PRIZES

***JINR Prizes:***

**In Experimental Physics Research*:***

Second Prize:

*A.M.Sukhovoj, V.A.Khitrov. "Experimental model-free determination of main parameters of cascade gamma-ray of compound nuclei from the region 39<A<201"*

**In Applied Physics Research*:***

Second Prize:

*A.M.Balagurov, G.D.Bokuchava, E.S.Kuz'min, V.V.Sumin, A.V.Tamonov, Yu.V.Taran, J.Schreiber."Neutron Fourier diffractometry to study internal mechanical stresses in industrial bulky products and new advanced materials"*

Encouraging Prize:

*I.Natkaniec, A.Pawlukojc, K.Holderna-Natkaniec, A.Szyczewski, I.Majerz, K.Parlinski. "Neutron spectroscopy and quantum-chemical simulation of hydrogen bonds and dynamics of biologically active molecules"*

***FLNP Prizes*:**

**In Nuclear Physics**:

First Prize:

*Yu.N.Pokotilovsky. "Investigation of low-temperature liquid fluoropolymers for coating UCN trap walls and their application for measuring neutron lifetime"*

Second Prize:

*A.I.Frank, G.V.Kulin, D.V.Kustov. "Neutron diffraction on a moving grating as a nonstationary phenomenon"*

Third Prize:

*Yu.N.Kopatch. "New experimental studies of quaternary fission of $^{233,235}U(n_{th},f)$ and $^{252}Cf(sf)$"*

**In Condensed Matter Physics**:

First Prize:

*A.M.Balagurov, I.A.Bobrikov, V.Yu.Pomyakushin. "Magnetic structural phase separation and giant isotope effect in $R_{0.5}Sr_{0.5}MnO_3$"*

Second Prizes:

*D.P.Kozlenko, S.E.Kichanov, B.N.Savenko. "High pressure effect on crystal and magnetic structures of frustrated antiferromagnet $YMnO_3$"*

*M.A.Kiselev, N.Yu.Ryabova, A.M.Balagurov. "New data in the structure and hydration of model lipid membranes of outer layer of the skin (stratum corneum) by the neutron diffraction method"*

Third Prize:

*D.A.Korneev, V.K.Ignatovich, S.P.Yaradaikin, V.I.Bodnarchuk. "Specular neutron reflection from potentials with diffuse interfaces"*

**In Applied and Methodical Physics:**

First Prize:

*A.M.Balagurov, G.D.Bokuchava, E.S.Kuz'min, V.V.Sumin, A.V.Tamonov. "Neutron Fourier diffractometry for studies of reactor materials"*

***I.M.Frank Stipend:***

**In Nuclear Physics:**

*G.V.Kulin*

**In Condensed Matter Physics:**

*K.N.Zhernenkov*

**In Methodical Investigations:**

*A.V.Tamonov*

# 7. SEMINARS

| Date | Authors | Title |
|---|---|---|
| 13.01.05 | M.Litvak<br>(IKR RAN) | Study of Mars nuclear radiation on the basis of data registered by the Russian device HEND installed on board of the space vehicle 2001 Mars Odyssey |
| 12.05.05 | E.P.Shabalin<br>(FLNP JINR) | On the construction of new pulsed neutron source in the Rutherford Laboratory (England) |

# 8.1. STRUCTURE OF LABORATORY AND SCIENTIFIC DEPARTMENTS

**Directorate:**
Director:
A.V.Belushkin
Deputy Directors:
N.Popa
V.N.Shvetsov
Scientific Secretary:
V.A.Khitrov

**Reactor and Technical Departments**
Chief engineer: V.D.Ananiev
**IBR-2 reactor**
Chief engineer: A.V.Vinogradov
**Department of IREN**
Head: V.G.Pyataev
**IBR-30 booster + LUE-40 Group**
Head: S.A.Kvasnikov
**Mechanical maintenance division**
Head: A.A.Belyakov
**Electrical engineering department**
Head: A.A.Yakovlev
**Design bureau**
Head: A.A.Kustov
**Experimental workshops**
Head: A.N.Kuznetsov

**Scientific Departments and Sectors**
**Condensed matter department**
Head: V.L.Aksenov
**Nuclear physics department**
Head: Yu.N.Kopatch
**Department of IBR-2 spectrometers complex**
Head: A.V.Belushkin

**Administrative Services**
Deputy Director: S.V.Kozenkov
Secretariat
Finances
Personnel

**Scientific Secretary Group**
Translation
Graphics
Photography
Artwork

## CONDENSED MATTER DEPARTMENT

| Sub-Division | Title | Head |
|---|---|---|
| **Diffraction sector. Head: A.M.Balagurov** | | |
| Group No.1 | HRFD | V.Yu.Pomjakushin |
| Group No.2 | DN-2 | A.I.Beskrovnyi |
| Group No.3 | DN-12 | B.N.Savenko |
| Group No.4 | NSVR | A.N.Nikitin |
| Group No.5 | SKAT | Ch.Scheffzük |
| **Small-angle neutron scattering group. Head: V.I.Gordeliy** | | |
| **Neutron optics sector. Head: V.L.Aksenov** | | |
| Group No.1 | REMUR | Yu.V.Nikitenko |
| Group No.2 | REFLEX | V.I.Bodnarchuk |
| Group No.3 | BIOPHYSICS INVESTIGATIONS | I.N.Serdyuk |
| **Inelastic scattering group. Head: I.Natkaniec** | | |

## NUCLEAR PHYSICS DEPARTMENT

| Sub-Division | Title | Head |
|---|---|---|
| **Sector 1. Correlation γ-spectroscopy and development of experimental installations. Head: N.A.Gundorin** | | |
| **Sector 2. Polarized neutrons and nuclei. Head: Yu.D.Mareev** | | |
| Group No.1 | Polarized nuclear targets | Yu.D.Mareev |
| Group No.2 | Thermal polarized neutrons | M.I.Tsulaya |
| **Sector 3. Neutron activation analysis. Head: M.V.Frontasyeva** | | |
| Group No.1 | Analytical | M.V.Frontasyeva |
| Group No.2 | Experimental | S.S.Pavlov |
| **Group No.2** | **Neutron spectroscopy** | **Yu.N.Kopatch** |
| **Group No.3** | **Nuclear fission** | **Sh.S.Zeinalov** |
| **Group No.5** | **Proton and α-decay** | **Yu.M.Gledenov** |
| **Group No.6** | **Properties of γ-quanta** | **A.M.Sukhovoy** |
| **Group No.7** | **Neutron structure** | **V.G.Nikolenko** |
| **Group No.8** | **Ultra-cold neutrons** | **A.V.Strelkov** |
| **Group No.9** | **Neutron optics** | **A.I.Frank** |
| **Group No.11** | **Theory** | **V.K.Ignatovich** |
| **Group No.12** | **Electrostatic generator-5** | **I.A.Chepurchenko** |

## DEPARTMENT OF IBR-2 SPECTROMETERS COMPLEX

| Sub-Division | Title | Head |
|---|---|---|
| Group No.1 | Scintillation detectors | E.S.Kuzmin |
| Group No.2 | Gaseous detectors | Ts.Panteleev |
| **Sector No.1** | **Electronics** | **V.I.Prikhodko** |
| Group No.1 | Analog electronics | A.A.Bogdzel |
| Group No.2 | Digital electronics | V.F.Levchanovsky |
| Group No.3 | Software | A.S.Kirilov |
| Group No.4 | Local network | G.A.Sukhomlinov |
| Group No.5 | Technology | A.B.Melnichuk |
| **Sector No.2** | **Spectrometers** | **A.P.Sirotin** |
| Group No.1 | Development of spectrometer elements | A.P.Sirotin |
| Group No.2 | Sample environment | A.N.Chernikov |

## 8.2. USER POLICY

In 2005 the experimental activity at the IBR-2 spectrometers went according to the users' program elaborated in 2004. A short description of this program can be found in the previous annual report and in a detailed form on the laboratory web site: http://nfdfn.jinr.ru/ibr-2/index.html .

A number of 256 experiments were performed, 193 with normal access (reviewed applications) and 63 (~25%) with fast access. From these experiments only 27% were performed by the laboratory staff, the rest of 73% by users from outside. The distribution of experiments on instruments and countries is shown in the following table.

| | HRFD | DN-12 | DN-2 | SCAT | NERA | DIN-2PI | KDSOG-M | REMUR. | YuMO | Total |
|---|---|---|---|---|---|---|---|---|---|---|
| FLNP | 11 | 4 | 14 | | 2 | 2 | 3 | 8 | 24 | 68 |
| Russia | 16 | 2 | 25 | 10 | 2 | 5 | 6 | | 18 | 84 |
| Germany | | 1 | | 6 | 1 | 2 | 2 | 2 | 14 | 28 |
| Romania | 2 | | 2 | | | 2 | | | 15 | 21 |
| Poland | | 1 | 5 | | 7 | | 2 | | 4 | 19 |
| Czech R. | | 3 | 1 | 6 | | | | | 2 | 12 |
| Belarus | 2 | 2 | 1 | | | | | | | 5 |
| Slovakia | | | 1 | | | | | | 4 | 5 |
| Ukraine | | | 3 | | | | | | | 3 |
| Hungary | | | | | | | | 2 | | 2 |
| France | | | | | | | | 2 | | 2 |
| Belgium | | | | | | | | 2 | | 2 |
| KPDR | | 2 | | | | | | | | 2 |
| Switzerland | | | | | | | 1 | | | 1 |
| Latvia | | | | | | | | 1 | | 1 |
| U.S.A. | | | | | | | | | 1 | 1 |
| Total | 31 | 15 | 52 | 22 | 12 | 11 | 14 | 17 | 82 | 256 |

## 8.3. MEETINGS AND CONFERENCES

***In 2005, FLNP organized the following meetings:***

| | | | |
|---|---|---|---|
| 1. | International Seminar dedicated to 90-th Anniversary of F.L.Shapiro | April 5-6 | Dubna |
| 2. | Workshop "Investigations in Giant Pulses of Thermal Neutrons at Pulsed Reactors and in Traps of Big Accelerators" | April 27-29 | Dubna |
| 3. | XIII International Seminar on Interaction of Neutrons with Nuclei (ISINN-13) | May 25-28 | Dubna |
| 4. | IV Workshop on Investigations at the IBR-2 Pulsed Reactor | June 15-17 | Dubna |
| 5. | SAD International Workshop | June 27-28 | Dubna |
| 6. | IAEA Technical Cooperation Workshop "Investigation of Health Effects on Children from the Consumption of Food Growth in Industrially Contaminated Areas" | November 14-16 | Dubna |

***In 2006, FLNP will organize the following meetings:***

| | | | |
|---|---|---|---|
| 1. | XIV International Seminar on Interaction of Neutrons with Nuclei (ISINN-14) | May 24-27 | Dubna |
| 2. | V Workshop on Investigations at the IBR-2 Pulsed Reactor | June 15-17 | Dubna |
| 3. | International Seminar "Crystallography at High Pressures" | September 28-October 1 | Dubna |
| 4. | International Workshop on Small-Angle Neutron Scattering, dedicated to the 7-th Anniversary of Yu.M.Ostanevich | October 5-7 | Dubna |

## 8.4. COOPERATION

**List of Visitors from Non-Member States of JINR in 2005**

| Name | Organization | Country | Dates |
|---|---|---|---|
| O.Steinsvoll | Institute for Energy Technology, Kjeller | Norway | 14.01-30.01 |
| V.Lauter | ILL, Grenoble | France | 15.01-26.01 |
| H.-J.Lauter | ILL, Grenoble | France | 15.01-26.01 |
| F. Tanczico | KFKI RIPNP, Budapest | Hungary | 19.01-29.01 |
| M. Major | KFKI RIPNP, Budapest | Hungary | 19.01-29.01 |
| L.Bottyan | KFKI RIPNP, Budapest | Hungary | 19.01-29.01 |
| L.Barandovski | Univ. Saints Cyril &Methodius, Skopje | Macedonia | 22.01-22.03 |
| O.Kuzmnovska | Univ. Saints Cyril &Methodius, Skopje | Macedonia | 22.01-22.03 |
| M.Anikin | SUNY Health, Brooklyn | USA | 23.01-24.01 |
| D.Temyakov | SUNY Health, Brooklyn | USA | 23.01-24.01 |
| K.Walther | Potsdam Geological Research Centre | Germany | 31.01-18.02 |
| A. Frischbutter | Potsdam Geological Research Centre | Germany | 31.01-11.02 |
| H.-J.Lauter | ILL, Grenoble | France | 05.02-18.02 |
| V.Lauter | ILL, Grenoble | France | 05.02-18.02 |
| D.Trots | Darmstadt Technical University | Germany | 13.02-26.02 |
| K.Ullemeyer | Freiburg University | Germany | 22.02-05.03 |
| E. Klementyev | Munich University | Germany | 22.02-25.02 |
| M.Frager | Juelich Res. Center | Germany | 13.03-27.03 |
| A.Ioffe | Juelich Res. Center | Germany | 14.03-17.03 |
| H.-J.Schreiber | Inst. Of Non-Destructive Insp.Methods | Germany | 15.03-19.03 |
| M.Anicic | VINCA INS, Belgrade | Serbia&Montenegro | 01.04-30.11 |
| H.-J.Schreiber | Inst. Of Non-Destructive Insp.Methods | Germany | 12.04-15.04 |
| K.Ullemeyer | Freiburg University | Germany | 13.04-19.04 |

| | | | |
|---|---|---|---|
| H.-J.Lauter | ILL, Grenoble | France | 22.04-30.04 |
| V.Lauter | ILL, Grenoble | France | 22.04-30.04 |
| K.Walther | Potsdam Geol. Res. Center | Germany | 24.04-06.05 |
| A.Frischbutter | Potsdam Geol. Res. Center | Germany | 24.04-06-05 |
| G.Fioni | CEA, Saclay | France | 25.04-27.04 |
| D.Ridikas | CEA, Saclay | France | 25.04-27.04 |
| G.Pepy | LLB, Saclay | France | 27.04-04.05 |
| V.Sikolenko | HMI, Berlin | Germany | 07.05-22.05 |
| M. Major | KFKI RIPNP, Budapest | Hungary | 17.05-24.05 |
| F. Tanczico | KFKI RIPNP, Budapest | Hungary | 17.05-24.05 |
| Guohui ZHANG | Inst. of Heavy Ion Physics, Beijing | China | 24.05-14.06 |
| K.-M.Sjoestroem | Swedish Educational Broadcasting Company, Stockholm | Sweden | 24.05-27.05 |
| Jan-Aake Toivo Wallenius | Swedish Educational Broadcasting Company, Stockholm | Sweden | 24.05-27.05 |
| Niclas Juho JENSEN | Swedish Educational Broadcasting Company, Stockholm | Sweden | 24.05-27.05 |
| B.Gebauer | HMI,Berlin | Germany | 15.06-20.06 |
| D.Trots | Darmstadt Technical University | Germany | 20.06-24.06 |
| M.Hayn | Heidelberg University | Germany | 10.07-29.10 |
| V.Layec | ENSTA, Paris | France | 16.07-17.08 |
| K.Walther | Potsdam Geol. Res. Center | Germany | 18.07-20.07 |
| A.Ioffe | Juelich Res. Center | Germany | 18.07-20.07 |
| K.Walther | Potsdam Geol. Res. Center | Germany | 15.08-26.08 |
| L.Cser | KFKI RIPNP, Budapest | Hungary | 02.09-09.09 |
| I.Gladkih | KFKI RIPNP, Budapest | Hungary | 02.09-09.09 |
| C.-J.Broeders | Karlsruhe Res. Center | Germany | 14.09-16.09 |
| J.-U.Knebel | Karlsruhe Res. Center | Germany | 14.09-16.09 |
| G.Granget | CEA, Saclay | France | 14.09-16.09 |
| W.Gudowski | RUT, Stockholm | Sweden | 14.09-16.09 |
| D.Sheptyakov | PSI, Villigen | Switzerland | 08.10-12.10 |
| K.Ullemeyer | Freiburg University | Germany | 10.10-21.10 |
| A.Frischbutter | Potsdam Geol. Res. Center | Germany | 12.10-21.10 |
| H. Rajashekara | Goettingen University | | 16.10-29.10 |
| V.Kozhevnikov | University of Louvain | Belgium | 23.10-24.10 |
| S.Lindert | Leipzig University | Germany | 23.10-28.10 |
| W.Gudowski | RUT, Stockholm | Sweden | 06.11-09.11 |
| G.Pepy | LLB, Saclay | France | 06.11-17.11 |
| K.Walther | Potsdam Geol. Res. Center | Germany | 08.11-18.11 |
| H.-J.Lauter | ILL, Grenoble | France | 16.11-19.11 |
| U.Kroner | Freiburg University | Germany | 05.12-16.12 |
| E.-R.Hilscher | Freiburg University | Germany | 05.12-16.12 |
| K.Ullemeyer | Freiburg University | Germany | 11.12-20.12 |
| V.Kozhevnikov | University of Louvain | Belgium | 12.12-16.12 |

## 8.5. EDUCATION

The objective of the FLNP educational program is the training of specialists in the field of neutron methods for condensed matter and nuclear physics research. The students of neutron diffraction department of MSU and the students of the MSU Interfaculty Center «Structure of Matter and New Materials» do their diploma works in FLNP. At the Center the students from the Chemical Faculty of MSU, Higher College of Materials Sciences of MSU, Tula State University, Tver State University and other universities of Russia and JINR Member States do their course works.

In June, September and February of 2005 a school and practical work on condensed matter with neutrons were organized.

In February the practical work for the students of neutron diffraction division of Physical Department of MSU was organized.

From the 3$^{d}$ to the 9$^{th}$ of June the Summer School for the students of MSU, IATP (Obninsk), SSPI (Sterlitamak), N-NSU (Niznii Novgorod) and so on (29 students and PhD students) was held.

In September there was practical work for students of Technical University – "Ural Polytechnical Institute (UPI)", and students from Kostroma (KSU).

## 8.6. PERSONNEL

**Distribution of the Personnel per Department as of 01.01.2006**

| Theme | Departments | Main staff |
|---|---|---|
| -1036- | Nuclear Physics Department | 58 |
| -1031- | Condensed Matter Physics Department | 43 |
| -1052- | IBR-2 Spectrometers Complex Department | 38 |
| -0993- | IREN Department | 8 |
| -0851- | IBR-2 Department | 47 |
| | Mechanical and Technical Department | 46 |
| | Electric and Technical Department | 30 |
| | Central Experimental Workshops | 36 |
| | Nuclear Safety Group | 4.5 |
| | Cold Moderator Group | 8 |
| | Design Bureau | 7 |
| | FLNP infrastructure: | |
| | Directorate | 9 |
| | Services and Management Department | 22 |
| | Scientific Secretary Group | 6 |
| | Supplies Group | 3 |
| **Total** | | **365.5** |

**Personnel of the Directorate as of 01.01.2006**

| Country | People |
|---|---|
| Armenia | 1 |
| Bulgaria | 1 |
| Vietnam | 1 |
| Germany | 1 |
| Georgia | 2 |
| KPDR | 4 |
| Kazakstan | 1 |
| Macedonia | 1 |
| Mongolia | 3 |
| Poland | 5 |
| Romania | 9 |
| Russia | 29 |
| Ukraine | 7 |
| **TOTAL** | **65** |

## 8.7. FINANCE

**Financing of the FLNP Scientific Research Plan in 2005 (th. USD)**

| No. | Theme | Financing plan, $ th. | Expenditures For 9 months, $ th. | In % of FLNP Budget |
|---|---|---|---|---|
| I | Condensed matter physics<br>-1031-<br>-0851-<br>-1052- | 4772,3<br>2684,2<br>1154,2<br>933,9 | 4513,5<br>2438,0<br>1249,4<br>826,1 | 94,6<br>90,8<br>108,2<br>88,5 |
| II | Neutron nuclear physics<br>-1036-<br>-0993- | 1202.9<br>868.0<br>334.9 | 1455.4<br>1081.0<br>374.4 | 121.0<br>124.5<br>76.0 |
| III | Elementary particle physics<br>-1007- | 6.1 | 29.7 | 486.8 |
| IV | Relativistic nuclear physics<br>-1008- | 44.9 | 28.6 | 63.7 |
| **V** | **TOTAL:** | **6026.2** | **6027.2** | **100.0** |

***International Seminar on Interactions of Neutrons With Nuclei***

*The opening ceremony of the Seminar. FLNP Director A.V.Belushkin.*

*Working moment of the Conference (Conference hall).*

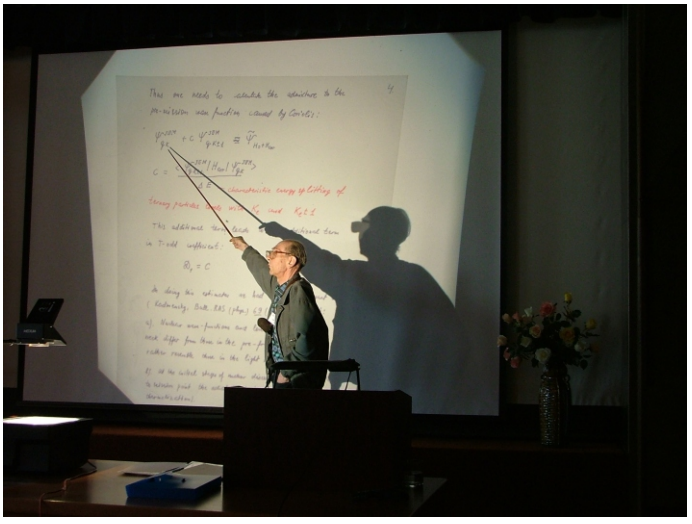

*Discussion on UCN experiments. V.Ye.Bunakov's report.*

*Discussion on UCN experiments.*
*Ye.V.Lychagin, A.Yu.Muzychka,*
*V.V.Nesvizhevsky, K.K.Protasov.*

*Group of scientists of the Neutron*
*Activation Analysis Sector.*

*Barbecue.*

## *IBR-30 reactor dismantling*

*A.I.Grudinin and V.K.Pokrovsky place a transport block with an assembly onto a shielding container.*

*G.N.Pogodaev, V.D.Denisov and A.I.Babayev discuss a plan of dismantling the core in the dosimetry room.*

*A.I.Babayev, S.V.Kulikov and A.I.Grudinin: measurement of radiation doze on the surface of the transport block with an assembly.*

*V.G.Pyataev chooses a position to extract the next assembly from the reactor core.*

*V.G.Pyataev and V.D.Denisov place the transport block onto a universal device.*

*V.D.Denisov extracts a fuel assembly from the core.*

*Shielding containers to transport the IBR-30 spent fuel.*

*FLNP collective in the IBR-30 reactor hall after the completion of the core dismantling works: V.I.Klopov, A.I.Babayev, V.I.Furman, A.V.Sokolov, I.S.Yarovoy, V.K.Pokrovsky, V.D.Denisov, A.V.Belushkin, G.N.Pogodaev, V.N.Zelenov, S.V.Kulikov, A.I.Grudinin.*